OXIDE DISPERSED CERAMIC COMPOSITES - THEIR FRACTURE TOUGHNESS AND HARDNESS CHARACTERISTICS

A THESIS

Submitted in partial fulfilment of the requirements for the award of the degree of

DOCTOR OF PHILOSOPHY

in

METALLURGICAL AND MATERIALS ENGINEERING

by

KUNTAL MAITI

DEPARTMENT OF METALLURGICAL AND MATERIALS ENGINEERING
INDIAN INSTITUTE OF TECHNOLOGY ROORKEE
ROORKEE-247 667 (INDIA)

OCTOBER, 2010

INDIAN INSTITUTE OF TECHNOLOGY ROORKEE
ROORKEE

CANDIDATE'S DECLARATION

I hereby certify that the work which is being presented in the thesis entitled **OXIDE DISPERSED CERAMIC COMPOSITES - THEIR FRACTURE TOUGHNESS AND HARDNESS CHARACTERISTICS** in partial fulfilment of the requirements for the award of the degree of Doctor of Philosophy and submitted in the Department of Metallurgical and Materials Engineering of the Indian Institute of Technology Roorkee, Roorkee is an authentic record of my own work carried out during a period from January, 2006 to October, 2010 under the supervision of Dr. Anjan Sil, Professor, Department of Metallurgical and Materials Engineering, Indian Institute of Technology Roorkee, Roorkee.

The matter presented in the thesis has not been submitted by me for the award of any other degree of this or any other Institute.

Kuntal Maiti

(KUNTAL MAITI)

This is to certify that the above statement made by the candidate is correct to the best of my knowledge.

Anjan Sil

(Anjan Sil)
Supervisor

Date: 11/10/2010

The Ph.D. Viva-Voice Examination of Mr. **KUNTAL MAITI**, Research Scholar, has been held on 9/5/2011

Anjan Sil

Signature of Supervisor

P. P. 9.5.11

Signature of External Examiner

Abstract

Ceramics are well known for their high relative hardness, high stiffness, chemical inertness and high temperature withstanding capacity. These abilities make such materials of great interest in demanding applications, such as in heat engines, turbines, automotive as well as aeronautical components. It is hoped that not only can the performance of these components be improved by low weight, high operating temperature properties of the ceramics, but also that their length of use can be increased. Incredibly low wear rates of ceramic materials is a great benefit to many applications. However, currently it is not possible to take full advantage of these properties due to the fact that ceramics generally have low fracture toughness. This is due to the nature of the bonds in the materials i.e. ionic and covalent, which prevents plastic deformation as dislocation movement is extremely limited.

The present thesis aims at exploring and investigating fracture toughness and hardness characteristics of oxide dispersed Al_2O_3 based ceramic composites with a view to assess their suitability in the application of structural ceramics. The microstructural and grain morphological relationship with mechanical properties i.e. fracture toughness and hardness of the ceramic composites prepared has been investigated through this work.

The presentation in the thesis is divided in the following seven chapters:

The ***Chapter 1*** provides an introductory overview of the rationale behind the selection of the problem and the objectives of the research work carried out.

Chapter 2 present an overview of literature covering structure, toughening mechanisms, role of microstructural and morphological factors of Al_2O_3 and the relation of the mechanical properties with microstructural features. The related literature on ZrO_2 dispersed Al_2O_3 system and effect of rare earth elements doping in Al_2O_3 have also been discussed.

Chapter 3 describes the sample preparation and the different techniques applied to characterize the samples for their density determination, fracture toughness and hardness determinations, phase identification and microstructural observations.

Chapter 4 describes the preparations of only Al_2O_3 ceramics for investigation on their microstructural relationship with fracture toughness and hardness characteristics. In order to investigate the rare earth doped ceramic composites, the effect of microstructural variations on the fracture toughness characteristics of only Al_2O_3 has been studied initially. For this purpose the samples were prepared by solid state sintering at different temperatures of 1500°, 1600° and 1700 °C for various soaking times of 3, 6, 9 and 12 hr. These different sintering schedules have resulted in the variations of grain size, grain size distribution and grain shape. The fracture toughness of all the sintered samples have been determined by using (i) Indentation method and (ii) Single edge precracked beam (SEPB) method separately. The observation on the sample surface after indentation to witness the mode of crack propagation and examination of fracture surfaces generated by SEPB method have been related to grain size distribution by way of histograms and grain shape variation by calculating aspect ratio of the grains. For hardness characteristics the measured hardness data of the samples have been examined by fitting them into Hall Petch equation which shows the variation of hardness with square root of the average diameter of the grain size. Indentation size effect (ISE) and Reverse indentation size effect (RISE) have been discussed.

Chapter 5 present a systematic investigation on the variation of Y_2O_3 doping levels into Al_2O_3 matrix along with the densification and fracture toughness characteristics, to find an optimum doping level. The optimum level of doping has been found to be 1000 ppm Y_2O_3.

Chapter 6 present the investigations on rare earths (Y and La) doped (singly and simultaneously) ZrO_2 dispersed Al_2O_3 composites for fracture toughness characteristics and their relationship with the microstructure developed. The rare earth doping in ceramics has been extensively exploited in the fields of magnetic ceramics, electronic ceramics, dielectric materials and optical properties applications. However the reported investigations on rare earth doped ceramics for structural application are limited. A few studies on rare earth doped structural ceramics reported are for development of creep resistant materials which show

grain boundary segregation of rare earth elements. Improvement in wear resistant of ceramic material by rare earth doping has also been reported. However the study presented in this chapter aims at investigating the role of rare earth elements dopants on fracture toughness of the ZrO_2 dispersed Al_2O_3 composites. The fracture toughness of Y doped Al_2O_3 – ZrO_2 composites and (Y+ La) doped Al_2O_3 – ZrO_2 composites are found consistently uniform for the samples sintered at all the three temperatures of 1500°, 1600° and 1700°C, compared to Al_2O_3 – ZrO_2 and La doped Al_2O_3 – ZrO_2 composites for which the fracture toughness has been found lower with samples sintered at 1700°C for 6, 9 and 12 hr. The phase analysis from the XRD results of Y doped Al_2O_3 – ZrO_2 and (Y+ La) doped Al_2O_3 – ZrO_2 composites sintered at 1700°C for 6 hr reveals that the formation of major second phases $Zr_{0.88}$ $Y_{0.12}O_{1.94}$ and $Zr_{0.935}Y_{0.065}O_{1.968}$ respectively. Whereas $Al_{0.18}Zr$ $_{0.82}O_{1.91}$ and $Al_{0.01}$ $Zr_{0.99}O_{1.99}$ are formed in the Al_2O_3 – ZrO_2 and La doped Al_2O_3 – ZrO_2 composites sintered at 1700°C for 6 hr as major second phases. The location of such phases, which has also been determined by point scanning method in EDS analysis. Therefore it may be predicted that the second phase Zr-Y-O present both in Y doped Al_2O_3 – ZrO_2 and (Y+ La) doped Al_2O_3 – ZrO_2 composites with slightly different stoichiometric compositions, play an important role for the material to show higher fracture toughness. The investigation on the nano sized ZrO_2 dispersion in Al_2O_3 shows the development of larger grain size and higher fracture toughness compared to the cases of pure Al_2O_3 and micron sized ZrO_2 dispersed Al_2O_3.

Chapter 7 presents the major conclusions of the work and suggested future scope.

List of Publications

Reviewed Journals

1. **Kuntal Maiti** & Anjan Sil, "Relationship between fracture toughness characteristics and morphology of sintered Al_2O_3 ceramics", **Ceramics International, 36 (2010) 2337.**
2. **Kuntal Maiti** & Anjan Sil, "Relationship of R-curve with microstructure of alumina ceramics", **Journal of Ceramic Processing Research (In press)**
3. **Kuntal Maiti** & Anjan Sil, "Preparation of rare earth doped alumina ceramics, their hardness and fracture toughness determination", **Indian Journal of Engineering & Materials Science, 13, 2006, 443.**
4. **Kuntal Maiti** & Anjan Sil, "Microstructural relationship with fracture toughness of undoped and (Y + La) rare earth's doped Al_2O_3-ZrO_2 ceramic composites", **Ceramics International** (under review).
5. Debajyoti Mohanty, Anjan Sil, **Kuntal Maiti,** "Development of input output relationships for self-healing Al_2O_3/SiC ceramic composites with Y_2O_3 additive using design of experiments", **Ceramics International** (Under review)

Conferences

6. **Kuntal Maiti** & Anjan Sil, "Al_2O_3-SiC ceramic composites and their fracture toughness characteristics", Proceedings of MR-09 Held in IIT Mumbai,8-9th May, 2009.
7. **Kuntal Maiti** & Anjan Sil , "Preparation of SiC dispersed Al_2O_3 ceramic composites and studies their fracture toughness", Proceedings of 63rd Annual Technical Meeting of The Indian Institute of Metals,Kolkata,India,16-17 November,2009.
8. Gurpreet Singh,Anjan Sil, **Kuntal Maiti**, Priti Singh,Sudipto Ghosh, "Synthesis and characterization of the doubly doped lithium manganese oxide spinel" Proceedings of International conference on Nanotechnology and technology in chemistry, health environment and energy, NATCHEE 2010, January 7-9,2010.
9. **Kuntal Maiti** & Anjan Sil, "Preparation of Nano and micron sized ZrO_2 dispersed Al_2O_3 ceramic composites and study their mechanical properties", Proceeding on

International conference on nano science and Technology, ICONSAT-2010,I.I.T.Bombay, Powai, India, 17-20 February, 2010.

10. **Kuntal Maiti**, Anjan Sil, Niranjana A.P. "Fabrication and mechanical properties of nano-and micron-sized Al_2O_3/ZrO_2 composites" , Proceedings of International Conference on Advancement of Nanoscience and Nanotechnology (ICOANN-2010), Alagappa University, Karaikudi, Tamil Nadu, March 1-3, 2010.
11. **Kuntal Maiti** & Anjan Sil, "Synthesized and properties of Y_2O_3 doped Al_2O_3 ceramic" Proceedings of 3rd National Symposium for Materials Research Scholars (MR-2010), I.I.T.Bombay, Powai, India, 6-8 May,2010.
12. **Kuntal Maiti** and Anjan Sil, "Synthesis and mechanical properties of nano-and micron-sized Al_2O_3/ZrO_2 composites", Proceedings of International Conference on Fundamental & Applications of Nano Science & Technology, (ICFANT-2010), Jadavpur University, Kolkata – 700032, West Bengal, India. December 9-12, 2010 (accepted for presentation).
13. **Kuntal Maiti** & Anjan Sil, "Preparation of nano- and micron–sized ZrO_2 dispersed Al_2O_3 ceramic composites and study their hardness and fracture toughness" Proceedings of Materials Science & Technology 2010 conference & Exhibition to be held In Houston, Texas, USA, October 17-21, 2010 (accepted for presentation).

Manuscripts submitted

14. **Kuntal Maiti** & Anjan Sil, " Preparation of Nano and micron sized ZrO_2 dispersed Al_2O_3 ceramic composites and study their mechanical properties", **International Journal of Nanoscience**
15. **Kuntal Maiti** & Anjan Sil, "Fabrication and mechanical properties of nano-and micron-sized Al_2O_3/ZrO_2 composites", **Journal of Nanoparticle Research**
16. **Kuntal Maiti** & Anjan Sil, "Preparation of nano- and micron–sized ZrO_2 dispersed Al_2O_3 ceramic composites and study their hardness and fracture toughness", **Ceramic Transactions**

Manuscript prepared

17. **Kuntal Maiti** & Anjan Sil, "Effect of sintering temperature and soaking time period on the preparation of Al_2O_3 ceramics and their hardness characteristics (to be communicate)

Acknowledgement

"Ra.Sa."

I take this opportunity to express my deep sense of gratitude and profusely thank my guide Professor **Anjan Sil**, Department of Metallurgical and Materials Engineering, Indian Institute of Technology Roorkee, Roorkee for his excellent guidance and painstaking efforts in carrying out this work. His invaluable and prompt remarks at the time of manuscript are especially appreciated. The thought provoking discussions I had with him and his valuable suggestions make my association with him memorable.

I would like to give my special thanks to Professor **Subrata Ray**, Department of Metallurgical and Materials Engineering, Indian Institute of Technology Roorkee, Roorkee. His helpful attitudes have contributed significantly in this thesis as well as my personal life.

I am immensely indebted to Professor P.K.Ghosh, Head, Department of Metallurgical and Materials Engineering, Indian Institute of Technology Roorkee, Roorkee. It is my pleasure to thanks Professor S.K.Nath, Professor Satya Prakash, Professor P.S.Mishra, Department of Metallurgical and Materials Engineering, Indian Institute of Technology Roorkee, Roorkee. I would like to thank to Dr.B.K.Mishra, Department of Mechanical and Industrial Engineering,IIT Roorkee, for valuable suggestions. I would like thank Dr.D Basu, CGCRI, Kolkata for allow me to use Isostatic press.

I would like to thank the people at University of Cambridge, Dr. Kevin Knowles and Samantha with whom the discussion on subject was very fruitful. Visit in the Inorganic microstructure group at Department of Materials Science and Metallurgy, University of Cambridge, was a fruitful and memorable trip of my life. I would like thanks to Robert Stern for helping in all possible ways to carry out the experimental work in Gordon Lab, University of Cambridge.

Friends play a special role at different stages of life. I would like to thank some of my friends who helped me in reaching the writing stage of Ph.D. thesis. I would like to thank Dr. Dipendu Bhunia, Dr. Goutam Ghosh, Dr. Vikash Narayan, Dr. Sushant, Dr. Vipin Chawla, Dr. Amit

Chawla, Mr. Sudipto Haldar, Rajendra Prasad, Raja Ram Prasad, Manoranjan, Ghanaraja, Banshi Prasad, Mr. Mukesh, Rajen, Hetal, Paresh, Dr. Rajib Sarkar, Dr. Arya, Mr. Manjeet Singh Goyat,Debesh, Bidhan encouraged me to achieve the required work.

I am very much thankful to my hostel mates, Malay Jana, Chanchal, Suman Chandra and Tapas Bhattacharya for their moral supports and their loving feelings. Although I spend very less time with them but it was really memorable at the end specially Chanchal's photography, Suman's joking attitude and Malay or Tapas hot temper attitude.

Laboratory mates play a crucial role in the race of Ph.D. thesis and they always share the two sides of a coin, happiness and sadness. I would like to thank my laboratory mates Dr.Manoj Kushwaha, Dr. Gurpreet Singh, Kuldeep Rana, Priti Singh, Vinay Pratap Singh, Paroma, Ashutosh, Sanjeeb, Anup, Shubham, Pankaj, Soumya, Niranjana, Rajni, Rajeev and Malay Jana. During this time period discussion with Gurpreet helped me to solve some conceptual problems. At the time of M.Tech, Kuldeep was the alone guy to work with me in the lab. Morning work with Gurpreet were beneficial sometimes. Malay admitted me to the hospital were really beneficial. I cannot summarize my words for these four lab mates.

I would also like to thank technicians who worked with me as friends, Mr. Dhanprakash, Mr. Bidya, Mr. Barma, B.D.Sharma.

I cannot thank enough to my parents, sister, brother and their in-law families. Their endless support and great love made me strong and confident. Special thanks to my close heart Sangu who was with me in my sweet and bitter time during my entire Ph.D period.

I would like to thanks Ministry of Human Research Development (MHRD) and Department of Science and Technology (DST), **Government of India** for financial support.

Contents

Page Number

Candidate's declaration

Abstract *I*

List of Publications *V*

Acknowledgement *VII*

Contents *IX*

List of Figures *XVII*

List of Tables *XXIV*

Chapter 1 Introduction 1

1.1 Classification of ceramics 4

1.2 Application of ceramics 6

1.3 The ceramic market 9

1.4 Overview of thesis 10

Chapter 2 Literature Review 12

2.1 Background and crystal structure of Al_2O_3 14

2.2 Toughening mechanisms for brittle materials 16

2.2.1 The role of residual stresses 16

2.2.2 Microcracking 18

2.2.3 Crack deflection and branching 20

2.2.4 Crack bridging 21

2.2.5 Crack pinning 22

2.2.6 Phase transformation 23

2.3 Al_2O_3-based ceramics 23

2.4 Al_2O_3 composites 27

2.4.1 Second phase particle in Al_2O_3 28

2.4.2 Mechanical properties of Al_2O_3 composites 29

2.4.3 The effect of rare earth elements doping 30
2.4.4 Doped Al_2O_3 31
2.4.4.1 Y_2O_3 doped Al_2O_3 33
2.4.4.2 Phase diagram of Al_2O_3 - Y_2O_3 40
2.4.4.3 Properties of Al_2O_3 and Y_2O_3 42
2.4.5 ZrO_2 doped Al_2O_3 43
2.4.5.1 Solubility of ZrO_2 in Al_2O_3 44
2.4.5.2 Phase diagram of Al_2O_3 - ZrO_2 45
2.4.5.3 ZrO_2 toughened Al_2O_3 46
2.4.5.4 Rare earth doped Al_2O_3 – 5 wt% ZrO_2 51
2.4.5.5 Phase diagram of ZrO_2 –Y_2O_3 52
2.5 Summary 54
Chapter 3 Experimental *56*
3.1 Sample preparation 58
3.1.1 Raw material 58
3.1.2 Powder preparation 58
3.1.3 Binder preparation and addition 59
3.1.4 Green sample preparation by compaction 59
3.2 Sintering 60
3.2.1 Importance of sintering 61
3.2.2 Types of sintering 61
3.2.3 Sintering variables 61
3.2.4 Heating schedule 62
3.3 Density measurement 62
3.4 Polishing 62
3.5 Hardness measurement 64
3.6 Measurement of fracture toughness 66
3.6.1 Indentation method 66
3.6.2 Single edge precracked beam (SEPB) test method 69
3.6.2.1 Test fixture schematic 69

3.6.2.2 Measurement of fracture toughness 69
3.7 Characterization techniques 70
3.7.1 Microstructural investigations by field emission scanning electron microscope (FESEM) 70
3.7.2 X-Ray diffraction analysis 72
3.7.3 Atomic force microscope (AFM) 74
3.8 Sample nomenclature 74
Chapter 4 Microstructure, hardness and fracture toughness of Alumina (Al_2O_3) 77
4.1 Introduction 79
4.2 Characterization of raw materials 80
4.2.1 XRD analysis of green compacted sample 80
4.2.2 EDS analysis of powder 82
4.2.3 Comparison of density of the sample compacted by isostatic pressing and uniaxial pressing methods 82
4.2.4 Sintering of ceramics 83
4.3 Physical properties of Al_2O_3 84
4.4 Analysis of microstructure 86
4.4.1 Effect of sintering temperature and soaking time on microstructure of Al_2O_3 samples 86
4.4.2 Grain size histogram of the sintered Al_2O_3 samples 93
4.5 Effect of mechanical properties of Al_2O_3 sintered at different temperatures for different soaking time period 94
4.5.1 Hardness of the sintered Al_2O_3 samples 94
4.5.1.1 Effect of soaking time period on hardness 95
4.5.1.2 Effect of grain size on hardness 96
4.5.1.3 Reverse Indentation Size Effect 98
4.5.1.4 Proportional Specimen Resistance Model 101
4.5.2 Fracture toughness of the sintered Al_2O_3 samples 103
4.5.2.1 Effect of sintering temperature on the fracture toughness 103

4.5.2.2 Effect of grain size on the fracture toughness 106
4.5.2.3 Correlation of fracture toughness with mode of crack propagation 107
4.5.2.4 Microstructures of the fracture surfaces 109
4.5.2.5 Grain size histograms and there correlation with fracture toughness 111
4.5.2.6 Correlation of fracture surface roughness with the fracture toughness 111
4.5.2.7 R- curve behavior of Al_2O_3 samples 112
4.5.2.8 Fracture toughness of Al_2O_3 measured by Single-edge precracked beam method 118
4.6 Summary 120
Chapter 5 Microstructure, hardness and fracture toughness of Y_2O_3 doped Al_2O_3 ceramic composites 121
5.1 Effect of sintering temperature and soaking time on physical properties of Al_2O_3 –Y_2O_3 composites 123
5.2 Microstructure analysis 126
5.2.1 Microstructure of Y_2O_3 doped Al_2O_3 sample 126
5.2.2 Grain size histogram 129
5.3 Effect of mechanical properties of A and AY samples sintered at 1500°C for different soaking time periods 130
5.3.1 Hardness of the sintered sample 130
5.3.1.1 Effect of soaking time on hardness 130
5.3.1.2 Effect of grain size on the hardness of the sample 131
5.3.2 Fracture toughness of the sample 132
5.3.2.1 Effects of soaking time period on fracture toughness of A and AY samples 132
5.3.2.2 Effects of Y_2O_3 on the fracture toughness of A and AY samples 133
5.3.2.3 Correlation of fracture toughness with mode of crack path 134

5.4 XRD analysis 134
5.5 Comparison of Indentation method (IM) and SEPB method for the calculation of fracture toughness 136
5.6 Mechanical properties of 1000 ppm Y $(NO_3)_3$ $6H_2O$ doped Al_2O_3 ceramic composites 136
5.7 Summary 138
Chapter 6 Microstructural changes with single and double rare earth doped $Al_2O_3 - ZrO_2$ composites and their fracture toughness 139
6.1 Introduction 141
6.2 Physical properties of Al_2O_3–5wt% ZrO_2 composites 141
6.3 Analysis of microstructure of AZ samples 144
6.3.1 Microstructure of sintered AZ samples 144
6.3.2 Grain size histogram plots for the AZ samples 149
6.4 Effect of mechanical properties of AZ sample sintered at different temperature for various soaking time periods 151
6.4.1 Hardness of the sintered AZ samples 151
6.4.1.1 Effect of sintering temperature on hardness of the samples 151
6.4.1.2 Effect of soaking time period on hardness 152
6.4.1.3 Effect of grain size on hardness 152
6.4.2 Fracture toughness of the sintered AZ samples 154
6.4.2.1 Effect of sintering temperature on the fracture toughness of AZ samples 154
6.4.2.2 Effect of grain size on the fracture toughness 155
6.4.2.3 Correlation of fracture toughness with mode of crack propagation 156
6.4.2.4 Microstructures of the fracture surfaces 158
6.4.2.5 Grain size histograms and fracture toughness 159
6.4.2.6 Comparison of the fracture toughness data obtained by Indentation method and SEPB method 159
6.5 Al_2O_3 – 5wt%ZrO_2 composites doped with rare earth elements 160

6.5.1 Al_2O_3 – 5wt%ZrO_2 composites doped with 1000 ppm $Y(NO_3)_3$ $6H_2O$ 161
6.5.1.1 Physical properties of Al_2O_3 – 5wt% ZrO_2 –$Y(NO_3)_3$ $6H_2O$ composites 161
6.5.1.2 Analysis of microstructure of AZY samples 163
6.5.1.2.1 Microstructure of sintered AZY samples 163
6.5.1.2.2 Grain size histogram of the sintered AZY samples 164
6.5.1.3 Effect of mechanical properties of AZY sample sintered at different temperatures for various soaking time periods 166
6.5.1.3.1 Hardness of the AZY samples 166
6.5.1.3.1.1 Effect of sintering temperature on hardness 166
6.5.1.3.1.2 Effect of soaking time period on hardness 166
6.5.1.3.1.3 The effect of grain size on the hardness through Hall Petch Equation 167
6.5.1.3.2 Fracture toughness of the sintered AZY samples 168
6.5.1.3.2.1 Effect of sintering temperature on the fracture toughness 168
6.5.1.3.2.2 Effect of grain size on the fracture toughness 169
6.5.1.3.2.3 Correlation of fracture toughness with mode of crack propagation 170
6.5.1.3.2.4 Comparison of fracture toughness data obtained by Indentation method and SEPB method 171
6.5.2 Al_2O_3 – 5wt% ZrO_2 composites doped with 1000 ppm $La(NO_3)_3.6H_2O$ 172
6.5.2.1 Physical properties of Al_2O_3 –5 wt%ZrO_2 – $La(NO_3)_3.6H_2O$ composites 172
6.5.2.2 Analysis of microstructure of AZL samples 175
6.5.2.2.1 Microstructure of sintered AZL samples 175
6.5.2.2.2 Grain size histogram of the sintered AZL samples 177
6.5.2.3 Effect of mechanical properties of AZL samples sintered at different temperature for various soaking time periods 178

6.5.2.3.1 Hardness of the AZL samples 178
6.5.2.3.1.1 Effect of sintering temperature on hardness 178
6.5.2.3.1.2 Effect of soaking time period on hardness of the sample 178
6.5.2.3.1.3 The effect of grain size on the hardness through Hall Petch Equation 179
6.5.2.3.2 Fracture toughness of the sintered AZL samples 180
6.5.2.3.2.1 Effect of sintering temperature on the fracture toughness 180
6.5.2.3.2.2 Effect of grain size on the fracture toughness 182
6.5.2.3.2.3 Fracture toughness with mode of crack propagation and fracture surface 183
6.5.2.3.2.4 Comparison of fracture toughness data obtained by Indentation method and SEPB method 183
6.5.3 Al_2O_3 – 5wt% ZrO_2 composites doped with 1000 ppm $Y(NO_3)_3.6H_2O$ –1000 ppm La $(NO_3)_3.6H_2O$ 184
6.5.3.1 Physical properties of Al_2O_3 – 5 wt% ZrO_2 –1000 ppm $Y(NO_3)_3.6H_2O$ – 1000 ppm La $(NO_3)_3.6H_2O$ composites 185
6.5.3.2 Analysis of microstructure of AZYL samples 187
6.5.3.2.1 Microstructure of sintered AZYL samples 187
6.5.3.2.2 Histograms of grain size data of the sintered AZYL samples 188
6.5.3.3 Effect of mechanical properties of AZYL samples sintered at different temperatures for various soaking time periods 189
6.5.3.3.1 Hardness of the AZYL samples 189
6.5.3.3.1.1 Effect of sintering temperature on hardness 189
6.5.3.3.1.2 Effect of soaking time period on hardness 189
6.5.3.3.1.3 The effect of grain size on the hardness through Hall Petch Equation 190
6.5.3.3.2 Fracture toughness of the sintered AZYL samples 191

6.5.3.3.2.1 Effect of sintering temperature on the fracture toughness 191
6.5.3.3.2.2 Effect of grain size on the fracture toughness 193
6.5.3.3.2.3 Correlation of fracture toughness with mode of crack propagation 193
6.5.3.3.2.4 Microstructure of the fracture surfaces 194
6.5.3.3.2.5 Comparison of fracture toughness data obtained by Indentation method and SEPB method 195
6.6 Comparison of physical properties and mechanical properties of A, AZ, AZY, AZL and AZYL samples 196
6.6.1 Physical properties 196
6.6.2 XRD patterns 199
6.6.3 Mechanical properties 203
6.7 Nano size ZrO_2 dispersed Al_2O_3 ceramic 204
6.7.1 Physical properties 205
6.7.2 Microstructural analysis 206
6.7.2.1 Effect of micron and nano sized ZrO_2 powder dispersion on microstructure of Al_2O_3-ZrO_2 samples 206
6.7.2.2 Grain size histogram of Al_2O_3 and Al_2O_3- ZrO_2 207
6.7.3 Mechanical properties 208
6.7.4 Microstructure of fracture surface 209
6.8 Summary 210
Chapter 7 Conclusions and suggestions for future work 212
7.1 Studies on the Al_2O_3 ceramics 214
7.2 Studies on Y_2O_3 doped Al_2O_3 materials 216
7.3 Studies on Al_2O_3 – 5 wt% ZrO_2, Y, La doped (singly and simultaneously) Al_2O_3 - 5 wt % ZrO_2 216
7.4 Suggestions for future work 218
References 219

List of Figures

Figure Number	Figure Description	Page Number
1.1	Development of the US market for advanced ceramics from the year of 2000 to 2015 (Rodel, 2009)	9
2.1	(a) Arrangement of aluminum ions and holes between two layers of oxide ions. Large open circles represent underlying oxide ions, small open circles represent holes, and small filled circles represent aluminum ions. The upper layer of oxide ions is not shown. Basal hexagonal cell vectors and directions are shown (b) distribution of aluminum ions and holes on the simple hexagonal lattice. The smallest rhombohedral cell which correctly describes the positions of the cations is shown along with the corresponding hexagonal cell vectors (Kronberg, 1957).	14
2.2	A fibre in a matrix when the thermal expansion coefficient of the fibre is greater than that of the matrix (a) at the fabrication temperature, (b) at room temperature without constraining the fibre and matrix to remain in contact and (c) at room temperature when contact between the fibre and the matrix is retained. (d) Illustrates the stress condition in the fibre in the case of (c).	17
2.3	A fibre in a matrix when the thermal expansion coefficient of the fibre is smaller than that of the matrix (a) at the fabrication temperature, (b) at room temperature when the fibre and matrix are hypothetically not constrained to retain a common interface and (c) at room temperature when a common interface between the fibre and the matrix is retained. (d) Illustrates the stress condition in the fibre in the case of (c).	18
2.4	Microcracking toughening mechanism: (a) thermal residual stress field alone and (b) combination of the thermal stresses and the applied	19

	stresses causing microcracking in a process zone in front of a macrocrack.	
2.5	Toughening by crack branching or deflection: (a) a crack deflected along the interface and (b) a crack deflected by connecting to microcracks.	21
2.6	Toughening by crack bridging: (a) a crack in a matrix with no fibres and (b) a crack bridged by fibres.	22
2.7	Crack front pinned by fibre (Xia & Langdon, 1994).	23
2.8	SEM fractographs of (a) undoped Al_2O_3 and (b) rare earth (Yb) doped Al_2O_3.	35
2.9	SEM micrographs showing the crack propagation in Al_2O_3–SiC composites (a) without dopants and (b) with dopant 800 ppm RE element.	36
2.10	Al_2O_3 - Y_2O_3 phase diagram (Warshaw and Roy, 1959).	41
2.11	Phase diagram of the Al_2O_3–ZrO_2 system (Levin and McMurdie, 1975)	46
2.12	A schematic representation of the ZrO_2 phase transformation	47
2.13	Schematic representation of interaction between crack and transformation zone	48
2.14	Phase diagram of ZrO_2 – Y_2O_3 (Scott, 1975)	53
3.1	Changes of particle shape during compaction of the powder	59
3.2	Time - temperature profile for sintering operation	62
3.3	Optical micrographs of sintered samples (a) unpolished surface (b) unpolished surface with indentation impression.	63
3.4	Optical micrograph of (a) polished and unpolished regions of the surface and (b) indentation in polished sample	64
3.5	Optical microscope with computer Axiovert 200 MAT (ZEISS)	66
3.6	Crack formation from the indent	67
3.7	Schematic diagram of three point bend test	69
3.8	Notch generated on samples	69
3.9	Sketch showing the working of a Scanning Electron Microscope	72

3.10	(a) Photograph of the XRD unit (Bruker AXS D8 Advance diffractometer) and (b) schematic diagram of beam path.	74
3.11	Flow diagram for formulation of problem	76
4.1	XRD patterns of Al_2O_3 powder used and α- Al_2O_3	80
4.2	SEM micrograph and EDS spectra of as received Al_2O_3 powder	82
4.3	Porosity vs. sintering temperature for Al_2O_3 samples sintered for the soaking time period of 12hr.	84
4.4	Weight loss of Al_2O_3 sample as a function of soaking time period for the samples sintered at 1500°C, 1600°C and 1700°C.	84
4.5	SEM micrograph of green compacted Al_2O_3 powder	87
4.6	SEM micrograph of Al_2O_3 powder compact sintered at 1500°C for (a) 3hr, (b) 6 hr, (c) 18 hr and (d) 24hr	88
4.7	SEM micrograph of Al_2O_3 compact sintered at 1600°C for (a) 3hr, (b) 9 hr and (c) 12 hr	89
4.8	SEM micrographs of Al_2O_3 sintered at 1700°C for (a) 3h and (b) 12 hr	90
4.9	Average grain size vs. soaking time period for the samples sintered at (a) 1500°C, (b) 1600°C and (c) 1700°C for different soaking time periods.	92
4.10	Grain size histograms for the samples of (a) A_9^{1500}, (b) A_{18}^{1500}, (c) A_9^{1600}, (d) A_9^{1700}	94
4.11	Hardness of Al_2O_3 samples sintered at (a) 1500°C, (b) 1600°C and (c) 1700°C as a function of soaking time period.	95
4.12	Grain size dependent hardness of Al_2O_3 ceramics	97
4.13	Hardness of the Al_2O_3 samples sintered at 1500°C for soaking time of (a) 6hr, (b) 12hr (c) 18hr and (d) 24hr, as a function of indentation load.	99
4.14	Hardness vs. indentation load for the sample sintered at 1600°C for (a) 3hr and (b) 12 hr.	100
4.15	Hardness vs. indentation load of sintered sample at 1700°C for (a) 3hr, (b) 6hr, (c) 9hr and (d) 12hr	101
4.16	P/L vs L plots for the Al_2O_3 ceramic samples sintered at (a)1500°C for	102

	3hr, (b) 1500°C for 18hr, (c) 1600°C for 3hr and (d) 1700°C for 3hr.	
4.17	Fracture toughness of the Al_2O_3 ceramics sintered at 1500°C ,1600°C and 1700°C as a function of average grain size	107
4.18	Vickers's indentation with crack in the Al_2O_3 samples sintered 1600°C for 3hr	108
4.19	SEM micrograph of Al_2O_3 sample sintered at (a)1500°C for 3hr, (b) 1600°C for 3hr.	108
4.20	SEM micrograph of Al_2O_3 sample sintered at 1700°C for 3hr	109
4.21	SEM micrograph of fracture surface of Al_2O_3 sample sintered at (a) 1500°C for 3hr, (b) 1500°C for 18hr, (c) 1600°C for 3hr and (d) 1700°C for 3hr	110
4.22	Fracture toughness vs fracture surface roughness of the samples sintered at 1500°C, 1600°C and 1700°C.	111
4.23	Fracture toughness vs. average length of the crack in the Al_2O_3 ceramics sintered at 1500°C for (a) 3hr, (b) 6hr,(c) 9hr,(d) 12hr,(e) 18hr and (f) 24hr.	115
4.24	Fracture toughness vs. average length of the crack in the Al_2O_3 ceramics sintered at 1600°C for (a) 3hr,(b) 6hr,(c) 9hr and (d) 12hr.	116
4.25	Crack extension resistance of Al_2O_3 ceramics sintered at 1700°C for (a) 3hr,(b) 6hr, (c) 9hr and (d) 12hr	117
5.1	SEM micrograph of (a) A, (b) A1Y, (c) A5Y and (d) A15Y sintered at 1500°C for the soaking time period of 6hr	127
5.2	Grain size histograms of the samples (a) A_6^{1500}, (b) $A1Y_6^{1500}$, (c) $A5Y_6^{1500}$ and (d) $A15Y_6^{1500}$	129
5.3	Hardness of A and AY samples as a function of soaking time period	130
5.4	Fracture toughness of A and AY samples containing different Y_2O_3 contents sintered at 1500°C for the soaking time period of 12hr	133
5.5	SEM micrograph of A1Y sample sintered at 1500°C for 6hr	134
5.6	X-ray diffraction pattern of (a) $A1Y_9^{1500}$, (b) $A5Y_9^{1500}$, (c) $A10Y_9^{1500}$ and (d) $A15Y_9^{1500}$	135

5.7	SEM micrograph of 1000 ppm $Y(NO_3)_3.6H_2O$ doped Al_2O_3 ceramic composites sintered at 1500°C for 12hr	137
6.1	EDS spectra of as received ZrO_2 powder	142
6.2	Weight loss as a function of soaking time of sintering the AZ samples at 1500°C, 1600°C and 1700°C	143
6.3	Linear shrinkage as a function of soaking time period for the samples sintered at (a) 1500°C, (b) 1600°C and (c) 1700°C	144
6.4	SEM micrograph of composite samples (a) AZ_3^{1500}, (b) AZ_{12}^{1500} with EDS spectra	146
6.5	SEM micrograph of (a) AZ_3^{1600}, (b) AZ_{12}^{1600} composite samples	147
6.6	SEM micrograph of (a) AZ_3^{1700}, (b) AZ_{12}^{1700} composite samples	147
6.7	Grain size histograms for the samples of (a) AZ_3^{1500}, (b) AZ_{12}^{1500}.	149
6.8	Grain size histograms for the samples (a) AZ_3^{1600}, (b) AZ_{12}^{1600}	150
6.9	Grain size histograms for the samples of (a) AZ_3^{1700}, (b) AZ_{12}^{1700}	150
6.10	Variation of hardness of the AZ samples with sintering temperature for a soaking time period of 3hr	151
6.11	Hardness of the AZ samples as a function of soaking time period	152
6.12	Grain size dependent hardness of AZ ceramic composites	153
6.13	Plot of fracture toughness with grain size of the AZ samples	156
6.14	SEM micrograph of AZ samples sintered at (a)1500°C , (b) 1600°C and (c) 1700°C for the soaking time period of 6hr	157
6.15	SEM micrographs of fracture surface of (a) AZ_3^{1500}, (b) AZ_6^{1600}, (c) AZ_3^{1700} and (d) AZ_{12}^{1700}	158
6.16	Weight loss for sintering of AZY samples sintered at (a) 1500°C, (b) 1600°C and (c) 1700°C for different soaking times	162
6.17	SEM micrographs of the samples (a) AZY_6^{1500}, (b) AZY_6^{1600} ,(c) AZY_3^{1700} with EDS and (d) AZY_6^{1700}	164
6.18	Grain size histograms of the sample (a) AZY_6^{1500}, (b) AZY_6^{1600}, (c) AZY_3^{1700} and (d) AZY_6^{1700}	165
6.19	Variation of hardness of the AZY samples with sintering temperature	166

	samples sintered at 1500°C for different soaking time periods	
5.5	Hardness and grain size of the A and AY samples sintered at 1500°C for different soaking time periods	131
5.6	The fracture toughness of the A and AY samples sintered 1500°C for the different soaking time periods	132
5.7	Fracture toughness of the A and AY samples measured by SEPB and indentation methods	136
5.8	Hardness and fracture toughness of Y $(NO_3)_3$ $6H_2O$ doped Al_2O_3 sample sintered at 1500°C for 12 hr	137
6.1	Relative density of AZ samples sintered at 1500°C, 1600°C and 1700°C for different soaking time periods.	143
6.2	Average grain size, grain size range and grain size difference of AZ samples sintered at 1500°C, 1600°C and 1700°C for different soaking time periods	148
6.3	Hardness, fracture toughness and grain size of the AZ samples sintered at 1500°C, 1600°C and 1700°C for different soaking time periods	155
6.4	Comparison of the fracture toughness data obtained by Indentation method and SEPB method	160
6.5	Relative densities of AZY samples sintered at 1500°C, 1600°C and 1700°C for different soaking time periods	161
6.6	Linear shrinkage of AZY samples sintered at 1500°C, 1600°C and 1700°C for different soaking time periods	163
6.7	Grain size, hardness and fracture toughness of AZY samples sintered at 1500°C, 1600°C and 1700°C	169
6.8	Comparison of fracture toughness determined by Indentation method and SEPB method	172
6.9	Density of AZL samples sintered at 1500°C, 1600°C and 1700°C for different soaking time periods	173
6.10	Hardness and fracture toughness of the AZL samples sintered at different temperatures	181
6.11	Comparison of fracture toughness determined using Indentation	184

method and

6.12 Relative densities of Al_2O_3 samples sintered at 1500°C, 1600°C and 1700°C for different soaking time periods 185

6.13 Hardness, fracture toughness and grain size of AZYL samples sintered at 1500°C, 1600°C and 1700°C 192

6.14 Comparison of fracture toughness measured by Indentation method and SEPB method 196

6.15 Fracture toughness and hardness of the A, AZ, AZY, AZL and AZYL samples sintered at different temperatures and soaking time periods 204

6.16 Density, shrinkage and grain size of A, AMZ and ANZ sintered at 1500°C for 3 hr, 6hr and 9hr 205

6.17 Fracture toughness and hardness of A, AMZ and ANZ samples sintered at 1500°C for 3 ,6 and 9hr 208

Chapter 1

Introduction

Chapter 1

In the past the word 'ceramics' meant porcelain, brick and other traditional products which were chiefly fabricated from clay, feldspar and silica. A ceramic is traditionally defined as an inorganic, nonmetallic solid that is prepared from powder materials. They are fabricated into products through application of heat and sometimes heat and pressure, and these products display characteristic properties i.e. high hardness, strength and brittleness as well as low electrical conductivity. Ceramics are typically crystalline in nature and are compounds formed between metallic and nonmetallic elements such as aluminum and oxygen (aluminum oxide, Al_2O_3), calcium and oxygen (calcium oxide, CaO), silicon and nitrogen (silicon nitride, Si_3N_4).

One of the major challenges for the materials scientists and engineers is to cope with the growing demands for long lasting and reliable materials, which work in different extreme environments for a range of industries from electronics and communication to chemical and structural industries, power generation to distribution, ground transportation to aerospace and household to fashion design etc. Ceramic materials, white and black, in the form of monoliths, hetrostructured and composites are the obvious solutions to all these problems. Tremendous progress has been made in the technology development, manufacturing and commercialization of some of these materials all over the world. However, significant challenges still remain to further develop and improve the properties of these materials, especially in the areas where reliable performance at high temperatures is critical. The research is aimed at providing developed ceramic composites.

Al_2O_3 have been used is in industry as, for example, cutting tools, spark plug insulators, and sodium vapor lamp housings due to their excellent mechanical, electrical, chemical and thermal properties (Dorre and Hubner, 1984). Al_2O_3 has been investigated since 1907, when a patent was issued for refining Al_2O_3 ceramic. However, commercialization of these products developed much later, in the 1920s and 30s, at which time high-temperature furnace materials were manufactured. Sintering of Al_2O_3 powder with the addition of MgO as sintering aid was developed. Essentially pure Al_2O_3 (>99.5%) has been utilized since the early 1970s as an implant material, especially for artificial joint

prostheses (mostly hip) and teeth because of its excellent biocompatibility and its good mechanical properties (particularly friction and wear) (Dorre and Hubner, 1984). However, it has a much lower tensile strength than compressive strength due to its brittleness (i.e., it cannot undergo plastic deformation like metals and plastics). These characteristics limit its use to compressive loading applications.

Depending on their method of formation, ceramics can be dense or lightweight. Ceramics can also be formed to serve as electrically conductive materials or insulators. Some ceramics, like superconductors, also display magnetic properties. They are also more resistant to high temperatures and harsh environments than metals and polymers. Ceramic composite have been used as brakes of the U.S. Air Force F-16, on the space shuttle, Airbus airline fleet, B7474-400, etc (Lie, 2005).

1.1 Classification of ceramics

Ceramics are broadly classified into two group namely traditional ceramics and advanced ceramics.

The examples of traditional ceramics are the following:

- Structural clay products (brick, sewer pipe, roofing and wall tile, etc.)
- White wares (dinnerware, floor and wall tile, electrical porcelain, etc.)
- Refractory (brick and monolithic products used in metal, glass, cements, ceramics, energy conversion, petroleum, and chemicals industries)
- Glasses: flat glass (windows), container glass (bottles), pressed and blown glass (dinnerware), glass fibers (home insulation), and advanced/specialty glass (optical fibers)
- Abrasives: natural (garnet, diamond, etc.) and synthetic (silicon carbide, diamond, fused alumina, etc.) abrasives are used for grinding, cutting, polishing, lapping, or pressure blasting of materials)
- Cements (for roads, bridges, buildings, dams, etc.)

The advanced ceramics are like:

- Structural (wear parts, bio ceramics, cutting tools, and engine components)
- Electrical (capacitors, insulators, substrates, integrated circuit packages, magnets and superconductors)

- Coatings (engine components, cutting tools, and industrial wear parts)
- Chemical and environmental (filters, membranes, catalysts, and catalyst supports)

The atoms in ceramic materials are held together by chemical bonds. The two chemical bonds for ceramic materials are covalent and ionic. Covalent and ionic bonds are much stronger than in metallic bonds that is why ceramics are brittle and metals are ductile. Compared to metals the ceramic compounds have higher melting temperatures, Young's moduli and hardness, lower densities, electrical and thermal conductivities. Engineering ceramics which are used in thermal and structural applications require high temperature resistance, high hardness and chemical inertness. Applications that exploit thermal and structural properties of ceramics, commonly include cutting tool inserts, wear resistant components, ballistic armor, heat exchangers, burner tubes, prosthetics, dental implants, heat engine components, thermal barrier coatings etc. The manufacturing of aeronautical and automobile engine parts that are light and resistant to corrosion and high temperatures owes a lot on ceramic materials. Table 1.1 shows the comparisons of the properties of metal and ceramics.

Table 1.1 Comparison of properties of metals and ceramics.

Material	Density (g/cm^3)	Room temperature strength (MPa)	Vickers hardness ($kg\ mm^{-2}$)	Thermal conductivity (W/m °C)	Fracture toughness $MPa\ m^{1/2}$
Various sintered SiC materials	3.2	340-550 (flexure)	2500-2790	85	3.0-3.5
Various sintered Si_3N_4 materials	2.7-3.2	205-690 (flexure)	2000	17	4.0-6.0
Transformation toughened Zirconia	5.8	500-1250 (flexure)	1300-1635	1.7	6.5-15.0
Alumina	3.9	300-600 (flexure)	1100-3000	30	3.5-4.0
Steels (4100, 4300, 8600, and 5600 series)	7.8	1035-1380 (tensile yield)	450-650	43	44-66
Aluminum alloy	2.5	415-895 (tensile yield)	100-500	140-225	33-44

1.2 Application of ceramics

In the following machine parts the use of ceramic materials instead of steel has shown a great promise in technology.

Cutting tools

Ceramics have demonstrated capability as cutting tools, especially in competition with carbon steel-high speed steel as inserts for metal turning and milling operations. The advantage of ceramics compared with other material is retention of high hardness, strength, and chemical inertness at higher temperatures. This permits use of the ceramics at much higher machining speeds than can be tolerated by other materials. However, the ceramics have lower toughness, and have only been used successfully in the limited operations of turning and milling.

Bearings

High-performance ceramic bearings have been developed for military applications such as missiles. The primary candidate material is hot pressed silicon nitride. Silicon Nitride (Si_3N_4) ceramic bearings are 30% lighter and 40% stronger than steel. Ceramic balls are 60% lighter, 50% stiffer, 70% smoother, and much harder than steel balls (Quantum Precision Group, 2007). Ceramic balls have 100 times better rolling contact fatigue life in comparison to all steel ball bearings. Ceramics bearing last as much 5 times longer than the conventional bearings. They have an incredible maximum spin rating of 300,000 rpm under load. Ceramics offer resistance to low-temperature corrosion, high-temperature stability, low density, and the ability to operate for a moderate length of time with little or no lubrication.

Bioceramics

Bioceramics, or ceramics for medical applications such as dental or orthopedic implants, represent a major market opportunity for ceramics in the future. Bioceramics represent the largest segment with 2005 sales estimated at $1.5 billion and this is expected to become double or triple in the next decade. Ceramics could account for 25 to 30 % of this market. Bioceramics may be grouped into three categories: nearly inert, surface-active (semi inert), and resorbable (non inert). Nearly inert ceramics can be implanted in the body without

toxic reactions. These materials include alumina, silicon nitride-based ceramics, transformation-toughened zirconia, and transformation-toughened alumina.

Heat exchangers

Ceramic heat exchangers are cost-effective because they can use waste heat to reduce fuel consumption. Heat recovered from the exhaust of a furnace is used to preheat the inlet combustion air so that additional fuel is not required for this purpose. Ceramic systems have the potential to reduce fuel consumption by more than 60% (Johnson and Rowcliffe, 1986). Ceramic heat exchangers may be used in a variety of settings, including industrial furnaces, combined heat and power, gas turbine engines, and fluidized bed combustion. Sintered silicon carbide and various aluminosilicates have been used in low-pressure heat exchangers because of their thermal shock resistance; however, the service temperature of these materials is currently limited to under 1204°C. As long as low fuel prices persist, this could delay the widespread implementation of ceramic heat exchangers for waste heat recovery. In recent years, increasing fuel prices have generally increased this sense of urgency.

Heat engines

The advantages of using ceramics in advanced heat engines have been widely publicized. These include increased fuel efficiency due to higher engine operating temperatures, more compact designs, and reduction or elimination of the cooling system. Ceramics are being considered in three general categories: 1) discrete components such as turbocharger rotors in metal reciprocating engines; 2) coatings and monolithic hot section components in advanced diesel designs; and 3) all-ceramic gas turbine engines. Some analysts have predicted that components for heat engines will be the largest area of growth for structural ceramics over the next 25 years.

Military applications and production

Production of ceramics for military applications is projected to expand. Near-term growth is expected for armor, radomes and infrared windows, bearings for missiles, and rocket nozzles (carbon-carbon composites and ceramic-coated carbon-carbon composites). New applications are likely to be laser mirrors, gun barrel liners, rail gun components, and turbine and diesel engine components.

Diesel engines

There are several levels at which ceramics could be incorporated in diesel engines. The first level involves a baseline diesel containing a ceramic turbocharger rotor and discrete ceramic components. The second level adds a ceramic cylinder and piston, and eliminates the cooling system; the ceramic used at this level would provide high-temperature strength, rather than thermal insulation. The third level would use ceramics for thermal insulation in the hot section as well as in the exhaust train. The fourth level would use advanced minimum friction technology to improve the performance of the engine. These four levels place different demands on the ceramic materials. Levels one and two require a low-cost, high-strength material, but without insulating properties; sintered silicon nitride or silicon carbide would be possibilities here. It has been suggested that level two represents the best compromise for light-duty ceramic diesels such as those in automobiles (Katz, 1985). Diesel engines generally produce a high level of particulate emissions. The higher operating temperatures of the adiabatic diesel could reduce emissions or permit emission control devices to operate more efficiently. The market for ceramics could also be affected by the fact that one major candidate for diesel emission control is a ceramic particle trap. Recent work at Ford Motor Co. also showed a 5 – 9% increase in fuel efficiency in an uncooled test engine fitted with ceramic inserts, compared to the baseline water-cooled design.

Automotive gas turbines

The primary advantage of using ceramics in turbines is the ability of operating the engine at turbine inlet temperatures up to about 1371°C which is higher compared to super alloy designs for which the operation is limited to about 1038°C without cooling. This temperature difference translates into an increased thermal efficiency from about 40 percent to nearly 50%. Power increases of 40% and fuel savings of around 10% have been demonstrated in research engines containing ceramic components. Other potential advantages include reduced engine size and weight, reduced exhaust emissions, and the capability to burn alternative fuels, such as powdered coal (Mason and McLean, 1984).

Space shuttle and aeronautical

Ceramics are increasingly being used in commercial and military aircraft as well as space shuttles and their equipment. Ceramic applications include thermal protection systems

in rocket exhaust cones, insulating tiles for the space shuttle, engine components and ceramic coatings that are embedded into the windshield glass of many airplanes. Ceramics are used as heat shields for fire protection and thermal insulation in aircraft and space shuttles because they resist heat, are lightweight and do not corrode. Other significant characteristics include high melting temperatures, hardness, light weight and chemical inertness. Presently, ceramics are being tested for use in ceramic engine components of airplanes. The results expected will be lighter engines with increased fuel efficiency.

1.3 The ceramic market

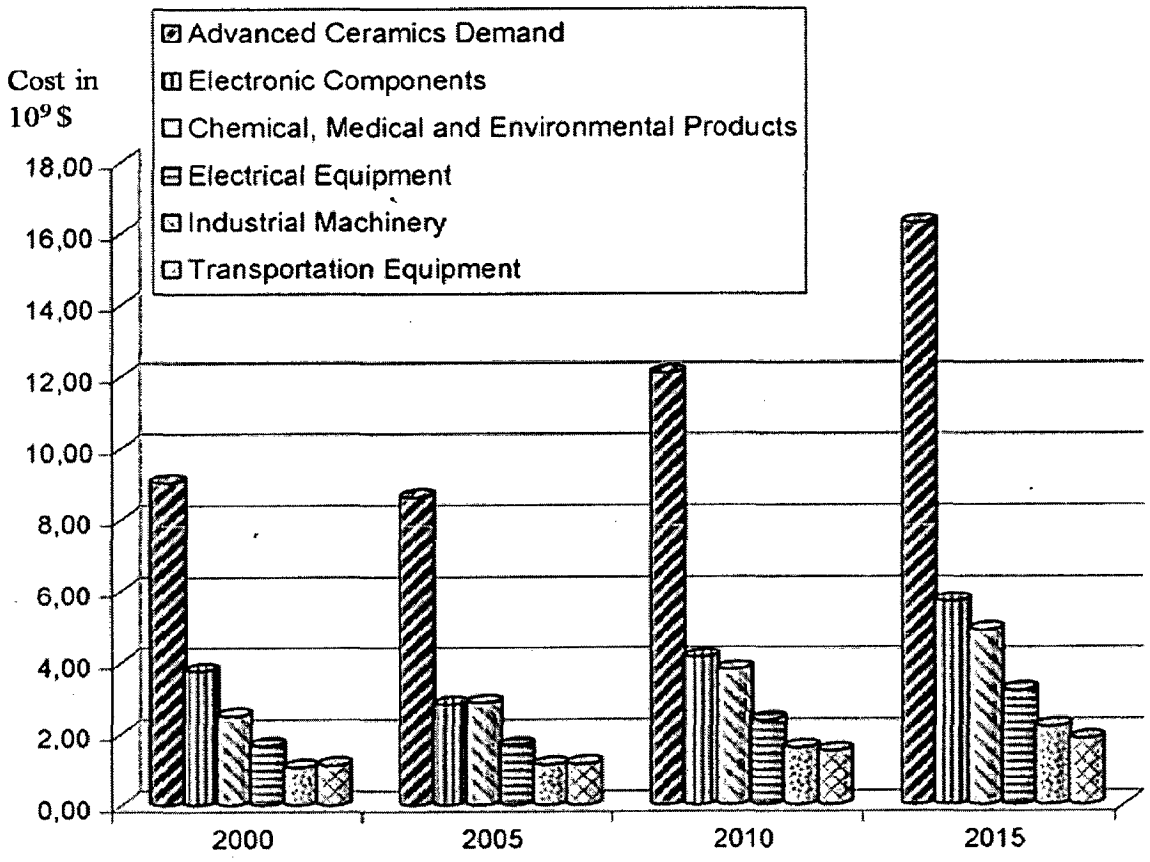

Fig.1.1 Development of the US market for advanced ceramics from the year of 2000 to 2015 (Rödel et al., 2009)

Fig.1.1 gives the expected growth of the US market upto 2015, indicating that all sectors will exhibit a continuous growth. Demand for advanced ceramics in the U.S. is forecast to increase 3.5% per year to over $12.6 billion in 2012.

1.4 Overview of thesis

Ceramics posses different advantageous properties compared to metals. But low fracture toughness restricts the use of ceramics in various applications. So it is important to focus on fracture toughness enhancement in ceramics, therefore in the present study it has been chosen to improve the fracture toughness in the ceramic material.

Most of the research work related to structural ceramics has been carried out on the whisker and fiber reinforced ceramic matrix composites (CMCs) (Song et al., 1999, Thouless and Evans, 1988). Whiskers and fiber manufacturing is time consuming and requires careful control during the processing (in some cases the direction of the fibres or whiskers is also important). In the case of particulate composites, particulate manufacturing is relatively easy and fast. Use of ball milling makes it easy to reinforce the particulate into ceramic composites and homogeneous mixing is possible. Depending upon the required strength of the composite it is easy to vary the size of particulate. Particulate composites require lower sintering temperature compared to whisker composites for which high temperature is required. The issue on improving fracture toughness in the ceramics has been investigated by considering the preparation of particulate composites.

Al_2O_3 is by far the most basic compound for technical ceramics, because Al_2O_3 exhibits versatile applications such as in cutting tools, friction and wear, refractory, electrical and electronics, optics, biomedical, jewelry, etc (Castel, 1990). Chemical and thermal stability, relatively good strength, thermal and electrical insulation characteristics combined with availability in abundance have made Al_2O_3 attractive for engineering applications. However, the brittleness of the material (Al_2O_3) limits its potential applications. The present study aims primarily at improving the fracture toughness of Al_2O_3-based ceramics prepared in the form of oxide dispersed ceramics matrix composites. The dispersoids chosen are rare earth oxides and elements.

Microstructural and morphological factors play a leading role in the emergence of properties of ceramic materials. It is known that the fracture toughness of Al_2O_3 is enhanced by the presence of elongated grains or second phase(s) present which promote crack deflection and/or crack bridging (Becher, 1991). A combination of large, elongated grains

and intergranular fracture results in significant grain bridging in the coarse grained materials, causing higher fracture toughness. For monolithic Al_2O_3, only coarse grains and grains having high aspect ratio can produce an improvement in fracture toughness. Residual stress, that generates due to thermal expansion anisotropy of Al_2O_3 and is dependent on grain size. This residual stress influences the fracture toughness of Al_2O_3 ceramics. The present study is an effort to improve the fracture toughness of Al_2O_3 by preparing Al_2O_3 based composites using rare earth elements as dopants. The rare earth elements are introduced by way of their nitrate form or rare earth oxides (West et al., 2004, Rani et al., 2004). A small amount (2000 ppm as per phase diagram of $Al_2O_3 - ZrO_2$) of ZrO_2 addition into the Al_2O_3 results in the formation of solid solution which promotes the densification characteristics of the Al_2O_3-based composite (Levin and McMurdie, 1975). Therefore for the preparation of dispersed composites the ZrO_2 added Al_2O_3 i.e. Al_2O_3-ZrO_2 system has been prepared separately. Investigations on Al_2O_3 matrix, ZrO_2 dispersed Al_2O_3 matrix and rare earth elements such as oxide or nitrate doped Al_2O_3–ZrO_2 composites have been made systematically for microstructural, phase, hardness and fracture toughness characterizations.

In order to fulfill the objective, two types of single rare earths Yttrium, Y and lanthanum, La doped and one type of rare earths (Y + La) co-doped Al_2O_3–5 wt% ZrO_2 ceramic composites were prepared. The influence of the sintering temperature and the soaking period on the microstructural and the fracture toughness characteristics of undoped Al_2O_3 and Al_2O_3 – 5 wt% ZrO_2 and rare earths doped Al_2O_3-ZrO_2-based ceramic composites was investigated.

Chapter 2

Literature review

Chapter 2

2.1 Background and crystal structure of Al_2O_3

Al_2O_3 is produced from bauxite by Bayer process. Bauxite (hydrated aluminum oxide) and native corundum (aluminum oxide mineral) are the main sources of high-purity Al_2O_3. Aluminium oxide (Al_2O_3) exists in many forms, α, χ, η, δ, κ, θ, γ, ρ which arise during the heat treatment of aluminium hydroxide or aluminium oxyhydroxide. The most thermodynamically stable form is α-Al_2O_3. The α-Al_2O_3 has a corundum structure which can be described as a slightly distorted hexagonally closed packed (HCP) sublattice of oxygen anions, with two out of three octahedral interstices are filled with Al^{+3} cations in an ordered fashion (Kronberg, 1957).

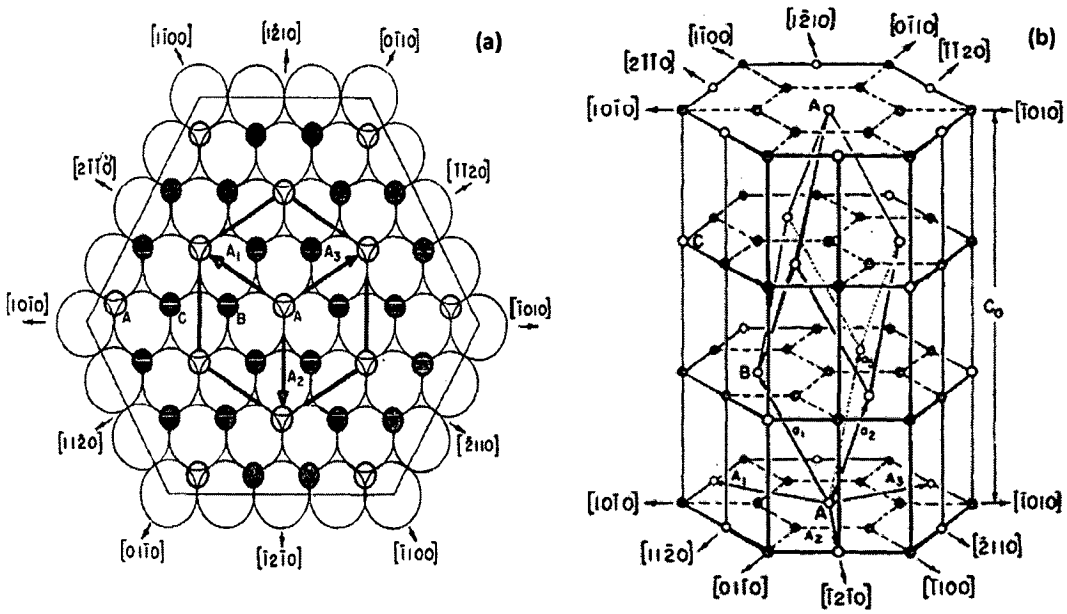

Fig. 2.1 (a) Arrangement of aluminum ions and holes between two layers of oxide ions. Large open circles represent underlying oxide ions, small open circles represent holes, and small filled circles represent aluminum ions. The upper layer of oxide ions is not shown. Basal hexagonal cell vectors and directions are shown (b) distribution of aluminum ions and holes on the simple hexagonal lattice. The smallest rhombohedral cell which correctly describes the positions of the cations is shown along with the corresponding hexagonal cell vectors (Kronberg, 1957).

Fig.2.1 (a) illustrates the normal structural distribution of aluminum ions on the mesh, and furthermore shows that the arrangement of filled and empty interstices is an ordered one. Fig. 2.1(b) shows the normal distribution of cations on this simple lattice. Two-thirds of the octahedral interstices are seen to be occupied, and one-third remains vacant. Fig.2.1 shows the hexagonal lattice representation of the α - Al_2O_3 crystal structure viewed from two different orientations (Kronberg, 1957). Because of the varying number of anion-cation bonds which would be broken when fracture takes place on different crystallographically oriented surfaces, Al_2O_3 shows a high degree of anisotropy in surface energy. The presence of secondary phases and segregating elements at the grain surfaces influence the grain morphology.

Al_2O_3 is a popular material used in industries, since it has some excellent properties, such as high strength, high hardness and high corrosion resistance. However, it still has problems of lack of toughness and low reliability thereby preventing it from wider applications. Many researchers, therefore, have tried to increase its toughness and reliability by making Al_2O_3-based composites. Conventionally, there are two methods for making ceramic composites, i.e., adding fibre (or short fibre), or adding particle for reinforcement. Experiments have shown that fibre enhances the toughening behaviour of the material. However, it is difficult to prepare fully densified fibre reinforced ceramic composites. The particle reinforced ceramic composite, on the other hand, can be sintered to a fully densified ceramic body, yet the mechanical properties of such composites are not as good as of the fibre reinforced ceramic composites. In general, the process of making particle reinforced ceramic composites is more convenient and less expensive than that of fibre/whisker reinforced ceramic composites. For example, the sintering temperature for Al_2O_3 composite is lowered from 1850°C for Al_2O_3 / SiCw (whisker) composites to 1400°C for Al_2O_3 /Cr_3C_2p (particles) composites. The ceramic whiskers or short fibres are more likely carcinogenic in nature, resulting in less acceptable compared to ceramic particles. Moreover, the cost of the ceramic particles is appreciably less than that of ceramic fibres / whiskers. This is also another consideration for particle reinforced ceramic composites have wider applications. To improve the fracture toughness in Al_2O_3 ceramics second phase is introduced in it and thus developed Al_2O_3 particulate composite shows higher fracture toughness

compared to pure Al_2O_3 ceramics (Tuan et al., 2002). The following toughening mechanisms are applicable to improve the fracture toughness of Al_2O_3 material. In the field of advanced ceramics especially for optical, magnetic properties, the performance of the ceramics was greatly improved by addition of rare earth (RE) oxides which act as additive, stabilizer and sintering aid (Guanming et al., 2007).

2.2 Toughening mechanisms for brittle materials (Xia and Langdon, 1994)

A ceramic material consists of an assemblage of grains, grain boundary phases, pores and likely isolated inclusions or cracks. These microstructural features represent a range in the size of flaws. If the sample is loaded in uniform tension, fracture will initiate at the largest flaw in the gauge section. Assume that, start at zero load and increase the load slowly until reaches to the critical stress for the largest flaw. Below the critical stress in elastic deformation, the energy is stored within the volume of the material. At the critical stress crack propagation initiates corresponding to the critical size of the crack. The stored energy available is concentrated at the tip of the new crack and drive the crack through the material medium resulting eventually in catastrophic brittle failure of the material. In order to avoid such fracture (by brittle mode), there is a need to design ceramic microstructure that will either allow the material to withstand the concentratation of stored energy at the crack tip or to delocalize (spread out) the energy (Richerson, 2005).

2.2.1 The role of residual stresses

A ceramic composite consists of a matrix, which is of ceramic material, and reinforcing elements which are ceramics also, thus two phases are involved. There is usually a mismatch between the two phases in terms of their structural, mechanical and / or physical properties. The difference in thermal expansion coefficients and elastic moduli of the two phases are pertinent to the toughening and strengthening characteristics in the composites. In addition, interfaces are introduced into the matrix and the strength of these interfaces plays an important role in dictating the operating toughening mechanisms and the effectiveness of the second phase to contribute to strengthening behaviour. The different thermal contractions shown by the second phase and the matrix phase gives rise to residual stresses when the

composite is cooled down from the fabrication temperature. If the coefficient of thermal expansion of the reinforcing phase (fibres or particulates) is greater than that of the matrix, the field of residual stresses in the matrix consists of circumferential compression and radial tension and the fibre is in axial tension, as shown in Fig. 2.2. Conversely, when the coefficient of thermal expansion of the reinforcing phase is less than that of the matrix, circumferential tensile stresses and radial compressive stresses are created in the matrix so that the fibre is then in axial compression, as shown in Fig, 2.3. Such a stress field, for example, was detected in the system of an Al_2O_3 matrix with SiC whiskers using neutron diffraction (Majumdar et al., 1988). Some second phases undergo a martensitic transformation which involves volumetric changes when the composite is cooled. This also leads to stresses in the matrix and the process may be utilized for toughening the material. The most prominent example of the latter process is found in Zirconia toughened ceramics (ZTC).

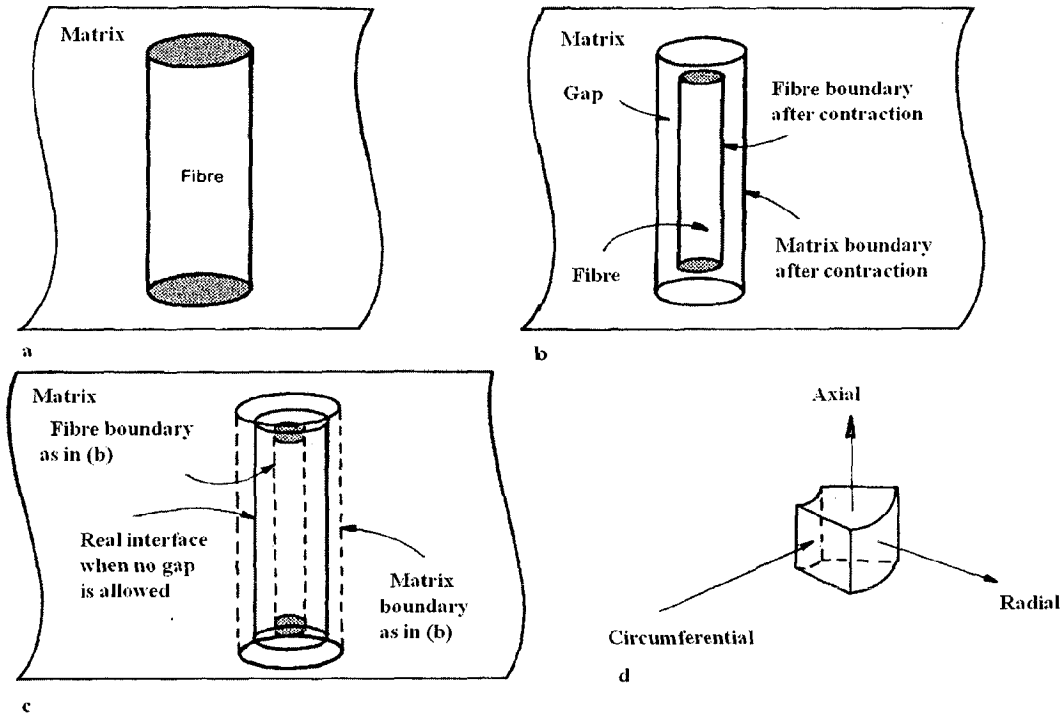

Fig. 2.2 A fibre in a matrix when the thermal expansion coefficient of the fibre is greater than that of the matrix (a) at the fabrication temperature, (b) at room temperature without constraining the fibre and matrix to remain in contact and (c) at room temperature when contact between the fibre and the matrix is retained. (d) Illustrates the stress condition in the fibre in the case of (c).

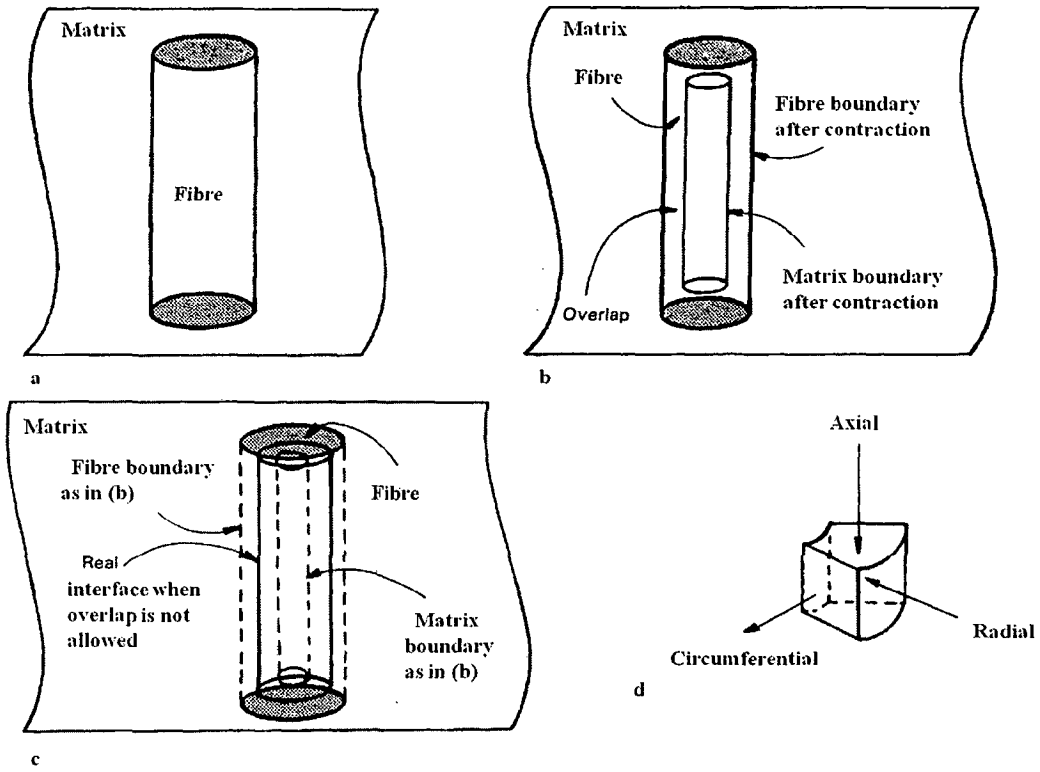

Fig. 2.3 A fibre in a matrix when the thermal expansion coefficient of the fibre is smaller than that of the matrix (a) at the fabrication temperature, (b) at room temperature when the fibre and matrix are hypothetically not constrained to retain a common interface and (c) at room temperature when a common interface between the fibre and the matrix is retained. (d) Illustrates the stress condition in the fibre in the case of (c).

2.2.2 Microcracking

As already noted, a misfit between the thermal expansion coefficients of the matrix and the fibre introduces a stress field in the matrix. Such stresses can produce spontaneous microcracks if the residual stresses are sufficiently large (Davidge and Green, 1968). However, the preferred situation in toughening is to create a stress field that will not produce cracks without the application of a superimposed extrinsic stress field. In this way microcracks are present only at the vicinity of the tip of a macrocrack where a stress concentration is available, thereby forming a process zone (Evans, 1976). Using this procedure the stress intensity at the crack tip is reduced and the toughness is therefore increased. The principle of this mechanism is shown schematically in Fig. 2.4, where σ is the applied stress. The energy dissipated in generating microcracks is used primarily to create

new surfaces. The increase in fracture energy of the primary crack is expected to be directly proportional to the surface energy of the microcracks, the volume fraction of second-phase particles or fibres producing the microcracks and the size of the process zone (Rice, 1981). Under a fixed residual stress field there is a critical fibre or particle size above which the fibre or particle will develop spontaneous microcracks (Davidge and Green, 1968). Thus, in order to increase the number of fibres or particles contributing to the toughening, it is necessary to keep the fibres or particles below this critical size. In practice, analysis indicates that maximum toughening necessitates having a narrow distribution of particle sizes close to the critical size (Evans and Faber, 1981). The microcracks thus formed reduce the elastic modulus within the process zone. This serves to lower the near-crack tip stress intensity factor and thus to shield the crack tip from the applied stress field (Huchinson, 1987). If not controlled, however, excessive microcracks may also lead to a decrease in fracture toughness (Han et al., 1992). In addition, the main crack may be deflected or it may branch due to the presence of these microcracks, and this provides the potential for additional toughening.

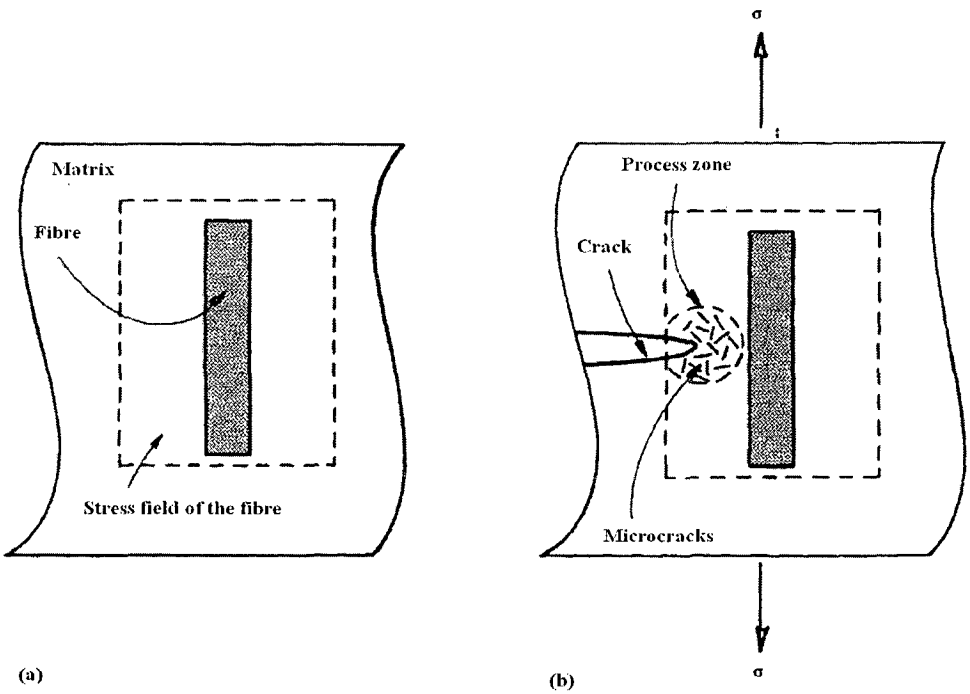

Fig. 2.4 Microcracking toughening mechanism: (a) thermal residual stress field alone and (b) combination of the thermal stresses and the applied stresses causing microcracking in a process zone in front of a macrocrack.

2.2.3 Crack deflection and branching

The direction of a crack extension / propagation may change when the crack comes across an obstacle such as a second phase particle or a fibre. There are several possible situations, as illustrated schematically in Fig. 2.5. In practice, this deviation in direction means that the crack travels a longer path and the stress intensity at the crack tip is reduced since the plane of the crack is no longer perpendicular to the tensile axis. In the case of fibre reinforcement, the crack may be deflected to extend along the interface between the fibre and the matrix, as shown in Fig. 2.5(a), and this facilitates fibre pull-out which is another toughening mechanism. The microcracks ahead of the crack tip may also attract the crack and thereby cause it to deflect, as shown in Fig. 2.5(b). Crack branching results when the crack bi-furcates into more than one direction. In general, a crack propagates perpendicular to the tensile axis and parallel to the compressive stress. This means that a residual stress field may also deflect the crack. For example, a particle having a thermal expansion coefficient higher than the matrix has around it a radial tension and a hoop compression. Such a stress field produced by a particle in the plane of a crack may deflect the crack and forces it to travel around the particle (Wei and Becher, 1984). In addition to crack deflection, the compressive stress field at a distance from the particles also contributes to enhancing toughness in such a system (Taya et al., 1990). The treatment of crack deflection has been developed theoretically (Faber and Evans, 1983) and examined experimentally (Faber and Evans, 1983a). It has been concluded that a rod-shaped second phase with a high aspect ratio is the most effective in enhancing toughness. The toughness is also improved by increasing the volume fraction of the second phase, but it is independent of the size of the second phase. The most important contribution to toughening by deflection comes from a twist after an initial tilt of the crack front (i.e. the crack front is deflected off the original plane, followed by its rotation around the axis perpendicular to the fracture plane). Such a crack-deflection mechanism of toughening was recently modified to include microstructural parameters such as volume fraction, shape, size, orientation and distribution of the second-phase particles (Pezzotti, 1993).

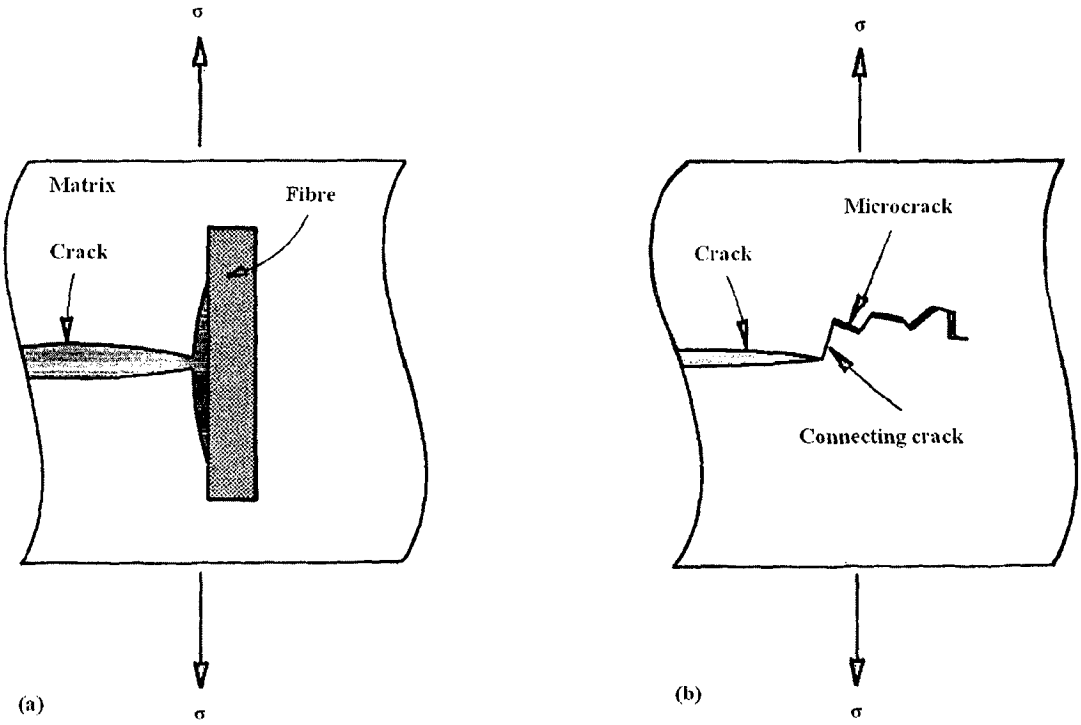

Fig. 2.5 Toughening by crack branching or deflection: (a) a crack deflected along the interface and (b) a crack deflected by connecting to microcracks.

2.2.4 Crack bridging

In the crack bridging mechanism, shown schematically in Fig. 2.6, the crack front passes beyond the reinforcing fibres but the fibres remain intact and bridge the fracture surfaces in the wake of the crack. The open displacement of the crack is then limited and this makes further propagation of the crack difficult. Several theoretical analyses of the bridging process have been proposed (Evans and McMeeking, 1986, Becher et al., 1988, Campbell et al., 1990). The toughness of the composite is improved by increasing the strength, the diameter and the volume fraction of the reinforcements. An important factor is to prevent damage to the fibres by passage of the crack. This requires either partial debonding of the fibres from the matrix at the crack tip or a high strength for the fibres. Contributions from bridging by large matrix grains have also been reported (Becher et al., 1991). Experimental evidence for crack bridging (Ruhle et al., 1987) indicates that debonding of the fibres occurs along the interfaces. Whisker bridging has also been observed in situ (Rodel et al., 1991).

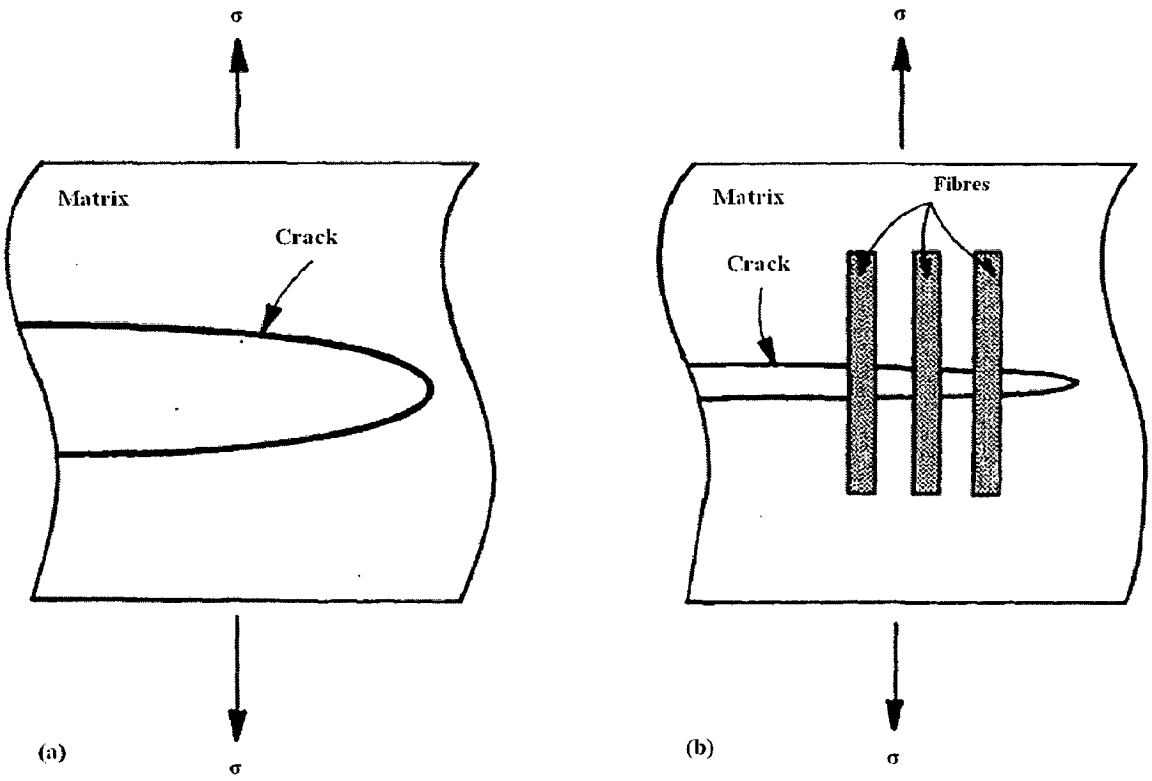

Fig. 2.6 Toughening by crack bridging: (a) a crack in a matrix with no fibres and (b) a crack bridged by fibres.

2.2.5 Crack pinning

Unlike crack bridging, where a crack tip passes beyond a reinforcing fibre, crack propagation may be stopped due to crack pinning effect by the fibres or particles. A model has been developed by the researchers (Lange, 1970) where the increase in fracture energy is attributed to the bowing out of the crack front between the fibres or particles, as illustrated in Fig. 2.7. It is clear that this mechanism demands a strong reinforcement as well as a good interface so that the fibres or particles can act as barriers. The spacing between the reinforcements must be small compared to the crack size in order for this mechanism to be effective.

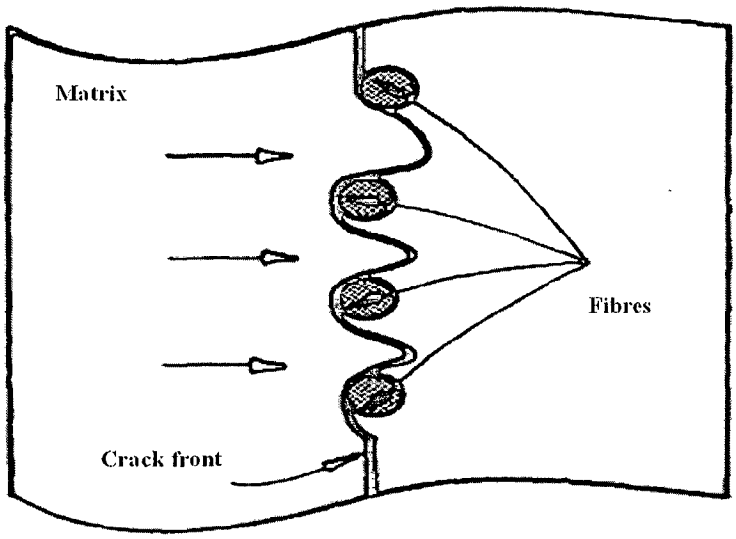

Fig. 2.7.Crack front pinned by fibre (Xia & Langdon, 1994)

2.2.6 Phase transformation

Due to phase transformation of second phase particle the volume change occurs which results in the increase in fracture toughness. Due to change in the volume stress field is generated which creates resistance to crack propagation. The crack front experiences the compressive stress and consequently the fracture toughness of the material increases.

2.3 Al_2O_3-based ceramics

The science governing the strength and fracture of structural ceramics was developed from a mostly empirical topic in 1965 into a mature discipline that now sets the standards in the field of mechanical behavior.

The field of engineering ceramics (structural ceramics) is much more limited in volume than functional ceramics. Monolithic ceramics are inherently brittle, making them highly sensitive to process and service related flaws. Due to their low fracture toughness, monolithic ceramics are prone to catastrophic failure and thus may be unsuitable for engineering applications that require high reliability (Miller and Liaw, 2000). Microstructural and morphological factors play leading roles in the emergence of properties of ceramic materials (Wu et al., 2001, Wang et al., 2001). Important factors such as powder processing route, sintering temperature, sintering rate and time, grain boundary chemistry, and so on, which govern the evolution of

desired properties, must be well understood and amenable to manipulations. Differences in the processing environment and sources of raw materials have also contributed significantly to disparities in results obtained from similar experiments (Wang et al., 2001).

For monolithic Al_2O_3, only coarse grains and grains having high aspect ratio can produce an improvement in fracture toughness (Kovar et al., 2000, Xu et al., 2005). This is because only crack bridging and crack deflection mechanisms can be activated; longer and larger particles can bridge and deflect cracks more effectively. However, the improvement of fracture toughness by elongated or coarse grains suffers from a trade-off. Kovar et al. correlated the fracture toughness with grain size and shape distributions. They have reported the fracture toughness values of Al_2O_3 is about 5 $MPam^{1/2}$ (Kovar et al., 2000). A combination of large, elongated grains and intergranular fracture results in significant grain bridging in the coarse grained materials causing higher fracture toughness. Sintering is one of the most important processes for the production of ceramic materials. Almost all the ceramic materials are made through the powder processing route, and also a variety of components used in modern technology undergoes sintering as one of the production steps. During the sintering of a powder compact, densification and grain growth occur simultaneously (Shaw, 1989). It has been recognised that the relationship between densification and grain growth must be assessed in order to understand and control the sintering process. Several mechanisms are involved in the densification of a sintered powder compact. For high temperature sintering of fine grained materials, it is well accepted that diffusional mechanisms dominate the sintering process. It is also noted that the dominant path for diffusion is usually along the grain boundary (Kingery et al., 1960). Ma (Ma, 1997) verified that the sintering mechanism for pure Al_2O_3 ceramics is interface reaction dominated when grain size is less than 3 μm and indicated that the constitutive model for interface reaction proposed by Cocks (Cocks, 1994) accurately describes the sintering process. He et al. (He and Ma., 2001) reported the relationship between densification and grain growth in Al_2O_3 ceramics by way of control in sintering. They reported the increase in grain size with the increase in density of the sample.

Flinn et al. showed that fracture strength depends on the pores size. The specimens failed predominantly due to unidentified surface flaws. This reveals the requirement of careful steps in the process of ceramic materials, so as to avoid flaws that significantly determine materials

behavior. This is a major reason for the wide scatter in properties recorded for ceramics (Flinn et al., 2000).

Hotta et al. also carried out similar investigation and they have shown that the fracture strength is governed significantly by small inclusions of a coarse or an agglomerated mass within a sintered body and the fracture strength decreases as the size of the coarse mass increases. All fractures were reported to originate from the coarse particles. However, the fracture toughness was not found to vary with the size of the coarse particles, showing that particle agglomeration is more detrimental than pores as they degrade fracture strength. Therefore, effective methods of avoiding agglomeration of mass and inclusion of coarse particle must be used for samples preparation (Hottaa et al., 2005).

Olszyna et al. reported that the density of the Al_2O_3 sample can be controlled by particle size distribution. They developed a model to improve the density of Al_2O_3 with particle size distribution (Olszyna et al., 1997).

Hardy and Green showed that it is possible to increase the flexural strength, modulus, and fracture toughness of porous Al_2O_3 by increasing the dwell time at a fixed sintering temperature below 1050°C because significant densification begins beyond or above this temperature. Increasing the dwell time leads to an increase in neck growth by surface diffusion, and hence an increase in mechanical resistance with only by densifications (Hardy and Green, 1995).

The role of microstructure on the mechanical properties of Al_2O_3 is now well established. Like most other ceramics, the strength of Al_2O_3 is determined by a critical flaw in the material which is commonly proportional to the grain sizes. Therefore, the strength is high when the micro- structure (grain size) of the Al_2O_3 is fine and homogeneous. In this case, however, the fracture toughness of the material is generally low (Chantikul et al., 1990). The fracture toughness of ceramic materials, including Al_2O_3, increases when large elongated or platelike grains are randomly dispersed in a fine-grained matrix. During the fracture process, these large grains resist crack propagation effectively, like whiskers or platelets do in composite materials (Harmer et al., 1992, Riu et al., 2000, Chen and Chen, 1992).

Tani el al. reported the fracture toughness of Al_2O_3 ceramics decreases sharply with increasing grain size. Fully dense Al_2O_3 ceramics without additives were fabricated by high

pressure hot-pressing, and their average grain size ranges from 6.2 to 60.11 μm. But the grain size upto 20 μm the fracture toughness increases with increasing grain size (Tani et al., 1986).

Teng et al. reported the fracture toughness of nano and micron size Al_2O_3 based ceramics. They have shown the slight improvement in fracture toughness in the nano Al_2O_3 compared to micron size Al_2O_3. Crack deflection, micro cracking and intergranular crack propagation are the toughening mechanisms in nano sized Al_2O_3 (Teng et al., 2007, Janbey et al., 2001, Kumar et al., 2002).

Bennison and Lawn, developed a model which allows for quantitative predictions as to how the toughness and strength characteristics of ceramics depend on microstructural variables such as grain size and shape, grain boundary energy, level of internal stress and sliding friction coefficient. As mentioned by Bennison and Lawn, due to anisotropy in crystallographic and thermal properties of Al_2O_3, some grains in the Al_2O_3 matrix are subjected to compression and act as bridges. The remaining grains, subjected to tension, are considered as making up the constitutive matrix. The bridging grains, wedged in the microstructure by this internal compressive stress, lead to an increase in fracture toughness as the crack grows (Bennison and Lawn, 1989).

Tomaszewski et al. (Tomaszewski et al., 2000a) reported that the fracture toughness of Al_2O_3 ceramics strongly increases with the increase of Al_2O_3 grain size and have shown that the decrease in grain size reduces the grain bridging as well as residual stress. Al_2O_3 samples with average grain size ranging from 2.6 to 67.4 μm were prepared by sintering at 1500°C - 1900°C for 1 - 20h in high vacuum. They have shown the grain bridging increases with increasing the grain size. Crystallographic and thermal expansion mismatch between adjacent grains during cooling involved residual stresses in these ceramics. Residual stress, which generates due to thermal expansion anisotropy of Al_2O_3 is dependent on grain size. This residual stress influences the fracture toughness of Al_2O_3 ceramics (Tomaszewski et al., 1999, Fett and Munz, 1992).

Koyama et al. reported that the effects of grain morphology and grain size on the mechanical properties, bending strength, fracture toughness, fracture energy and crack extension resistance. They also reported an equation to measure the fracture energy by using the value

of fracture toughness and Young's modulus of the material. They reported that the fracture toughness of Al_2O_3 ceramics with equiaxed and platelet grains increases with increasing grain size, but the toughness of ceramics with platelet grains was higher and increased up to 6.6 MPa $m^{1/2}$ with the increase in grain size. According to them fracture toughness depends, not only for grain size but also on morphology of the material (Koyama et al., 1994).

Li et al. used Al_2O_3 nanoparticles to strengthen and toughen porous Al_2O_3. They reported over a 50% increase in fracture strength and fracture toughness by 2 wt% addition of Al_2O_3 nanoparticles. The use of an entirely nanoscale Al_2O_3 powder significantly enhances the fracture strength, but only nominal improvements are achieved for fracture toughness. This is so because nanoparticles result in a more refined microstructure and grain boundary strengthening, necessary for high strength. But fracture toughness is enhanced by coarse grains or those with a high aspect ratio, which Al_2O_3 nanoparticles lack (Teng et al., 2007, Li et al., 1991, Silva et al., 1994, Ighodaro and Okoli, 2008).

Rao et al., shows the properties like fracture toughness and hardness of α-Al_2O_3 sintered at different temperatures. Al_2O_3 sintered at higher temperature (more than 1700 °C) and in higher temperature abnormal grain growth occurs in the final stage of sintering which affects the mechanical properties (Taylor et al., 1976). They have shown relative density increases with increasing temperature. They used 3-point bending test method with a 30 mm span and cross head speed of 0.5 mm min^{-1}. In each sample a notch was cut with 0.1 mm width and about 1.5 mm depth. They have shown the fracture toughness and hardness of sintered sample are 5.7 MPa $m^{-1/2}$ and 18.5 GPa respectively. Intercrystalline cracking occurs in coarse grained ceramics due to thermal expansion anisotropy which may affect the fracture toughness of the sample. Grain size is about 10 μm in the sample sintered at 1600 °C (Rao et al., 2000).

2.4 Al_2O_3 composites

Many studies have focused on particulate dispersed $A1_2O_3$ composites in order to improve mechanical properties both at room temperature and high temperature (Harmer et al., 1992, Evans, 1990). The brittle nature of ceramics, including Al_2O_3, has prompted many investigations to explore a variety of approaches to enhance their mechanical properties with respect to strength, fracture toughness and high temperature performance. The mechanical

properties of ceramics can be improved by the incorporation of various reinforcing second phases which control the microstructure (e.g. suppression of grain growth, control of grain morphology) and improve toughening (through deflection, microcracking, grain bridging). In particulate reinforced composites, the mechanical properties can be improved through controlling the microstructure of the matrix (Green, 1982). For Al_2O_3 based composites, it can be expected that the morphology of Al_2O_3 grains influences the mechanical properties, thus, the microstructural control of composites is very important. Jang et al., reported the grain growth in Al_2O_3 ceramics is known to occur with increase in sintering temperature. They suggest that second phase of particulates effectively suppresses grain growth at high temperature, resulting in increased homogeneity by inhibiting the abnormal grain growth in Al_2O_3 (Jang et al., 1995).

2.4.1 Second phase particle in Al_2O_3

It has been documented that the addition of small amount of metal oxide will sensitively change the mechanical properties of oxide ceramics. Recent studies have shown that rare earth oxides such as of Y, La and Lutetium (Lu) improve the high temperature tensile and compressive creep resistance of Al_2O_3 ceramics. The followings are the purposes for introduction of second phase particle in the matrix:

- Sinterability can be enhanced with dopants.
- Dopants control particle rearrangement.
- Dopants permit sintering at lower temperature.
- Dopants are used to control grain growth or achieve final density high.
- Segregation of dopants at the grain boundary weakens the interface which helps to deflect the crack and fracture toughness of the material gets modified.
- Segregation of dopants change the conductivity as well as strength compared to the undoped materials.

To fulfill the above purposes, the second phase has been choosen by considering the followings parameters:

- Young's modulus
- Thermal expansion coefficient

- Bond strength between matrix and second phase particle
- Particle size difference between the matrix and the second phase
- Particle shape

2.4.2 Mechanical properties of Al_2O_3 composites

Chae et al., (Chae et al., 1993) report that the densification of Al_2O_3-TiC composites by incorporating Y_2O_3. They observed very small amount of Y is effective in aiding the densification. They sintered the samples at 1600 °C and 1700 °C. Y was added at concentrations of 0.07, 0.35, 0.7 and 3.5 wt%. The addition of more than 0.35 wt% sintering aid decreased density and increased apparent porosity of the sintered material. They have shown that the specimen without Y has porous microstructure whereas specimen containing 0.35 wt% Y shows dense microstructure. They report that the pores are either present in the green compact or formed by the reaction between Al_2O_3 and TiC. The materials were expected to coarsen by a process analogous to Ostwald ripening which proceeds through the interconnected network of pores where large pores grow and small ones disappear (Lange, 1984).

Louet et al. (Louet et al., 2008) report the effect of small addition (500 – 2000 ppm) of silica on densification and microstructural evolution in ultrapure Al_2O_3. They sintered samples at 1600°C and 1700 °C for 2 hr with heating and cooling rate of 300 °C h^{-1}. They have shown silicon also goes to the grain boundary. In lower temperature (1000 – 1200 °C) sintering is controlled by a volumetric diffusion mechanism while between 1200 and 1270 °C sintering is controlled mainly by the diffusion in grain boundary. Segregation of cations (Ca, Ti, Mn and Si) in the vicinity of the Al_2O_3 grain boundaries has been observed (Monceau et al., 1995, Wang et al., 1999). This segregation of cations was reported by energy dispersive spectroscopy (EDS) results. At higher temperature silica allowed the formation of intergranular liquid phase which enhances densification in doped samples and also leads to an abnormal grain growth in the final stage of sintering.

Li et al. reported the mechanical propertics of Al_2O_3/BN composites where BN is in nano size dispersion. From scanning electron microscopy (SEM) study they observed that nano sized BN is dispersed within Al_2O_3 grain as well as in grain boundary. It was found that the

Vickers hardness of the composites decreases with increasing BN content. The samples were sintered at 1600 – 1800 °C. Fracture toughness measured by the single edge precracked beam (SEPB) method using a rectangular bar (3x4x25 mm^3) with span of 20 mm and a crosshead speed of 0.5 mm min^{-1}. The hardness of this composite is 8.10 GPa. Thermal expansion mismatch between Al_2O_3 matrix and the BN results in higher fracture toughness by forming weak interface (Li et al., 2002).

Miyahara et al. studied the fracture toughness of Al_2O_3 ceramics sintered at 1600 °C by following different techniques viz. Bridge indentation (BI), Fatigue precrack (FP), Controlled surface flaw (CSF), Chevron notch (CN). They have investigated the effect of grain size on the fracture toughness. They established the correlation between fracture toughness and grain size of the sample through measuring the fracture toughness by different techniques.

They have shown fracture toughness increases gradually with increasing grain size in FP, CSF and BI method and fracture toughness is high for sample having small grains using CN method. Swanson et al. reported that the grain bridging is the main mechanism for R-curve behaviour (Swanson et al., 1987). The large grain size results in larger bridging length and consequently in higher crack growth resistance (Miyahara et al., 1994).

Ji and Yeomans, reported the increase in fracture toughness of monolithic Al_2O_3 by introducing nano sized chromium (Cr). They have shown the improvement of fracture toughness from 3.6 to 4 MPa $m^{1/2}$. The fracture mode changes for monolithic Al_2O_3 from intergranular fracture to transgranular mode for the nanocomposites (Mula et al., 2009, Ji and Yeomans, 2002).

2.4.3 The effect of rare earth elements doping

The rare earth elements are good surface active elements and can have the effect of improving the wetting property of Al_2O_3 composites, reducing the melting point of Al_2O_3 ceramic composites (Yang et al., 2009), purifying the interface between different phases of Al_2O_3 composites (Xu et al., 2006) and strengthening the grain boundary of Al_2O_3 (Buban et al., 2006).

2.4.4 Doped Al_2O_3

In the present study presureless sintering has been used for the densification. But for the pressureless sintering high temperature (>1750 °C) is required to achieve near full densification of the material (Baron et al., 2002). Pressureless sintering requires the use of sintering aids such as CeO_2, MgO, Y_2O_3, etc, for full densification at a temperature of about 1500°C (Pillai et al., 2004, Wang et al., 1988). Y_2O_3 reduces the sintering temperature of Al_2O_3 to 1500°C while the use of MgO and CeO_2 the sintering of Al_2O_3 is done at about 1600°C. The use of dopants allows pressureless sintering of the doped composites to be carried out at much lower temperatures and this affects the microstructure, particularly grain size.

The ultimate properties of a material depend on the microstructures developed during sintering. Usually, undoped Al_2O_3 is very difficult to sinter to theoretical density. The major factors which hinder the densification are abnormal grain growth and pore detachment from the grain boundaries during boundary migration, which effectively leaves the pores permanently trapped inside the grains (Powers and Glaeser, 1998). Small amounts of dopants, such as MgO, can improve the densification and microstructural development of Al_2O_3 (Coble, 1961). Dopants can alter the boundary, lattice and surface diffusivities, leading to a change in boundary and pore mobilities. They can create drag forces on boundary motion by segregating to grain boundaries and, when segregation increases, they can pin the grain boundaries, thus inhibiting growth. If the solute concentration at the grain boundary is too high, it becomes oversaturated and a new phase is formed (Gruffel and Carry, 1993). Bae and Baik have shown that impurities, even at levels of <30 ppm, can have significant effect on ceramic system (Bae and Baik, 1993). It was also observed that a small amount of Y_2O_3 could induce exaggerated grain growth in the composite which can be controlled. Pillai et al. shows the grain boundary of Al_2O_3 enriched by high atomic number element (Yttrium) (Pillai et al., 2004). The main factors which control the solubility of solute in a solvent include: (1) the elastic strain due to the difference in atomic sizes (ionic radius of Al^{3+} is 0.5 Å and that of Y^{3+} is 0.93 Å), and (2) the mismatch between crystallographic structures of the two equilibrium phases (the electronic charge associated with each species is the same in this case) (Gruffel and Carry, 1993). In the Y_2O_3- Al_2O_3 system, the presence of Y^{3+} is reported at

the grain boundaries (Li and Kingery, 1985, Bender et al., 1980) and at the free surfaces (Lagrange et al., 1987). Cawley and Halloran evaluated the solubility limit of Yttrium in Al_2O_3 to be 10 ppm by mass at 1600°C (Cawley and Halloran, 1986). Hence, the remaining Yttrium migrates to the grain boundaries. During sintering, the grain boundary solute content increases due to the diminution of the area of grain boundary per unit volume. When the solubility limit at the grain boundaries (which is higher than the bulk) is reached, the boundaries become oversaturated and, if grain growth continues. Yttria can not be accommodated in solid solution at the grain boundaries and therefore forms a separate phase. It is well known that grain boundary segregation strongly affects the macroscopic properties of both metallic and ceramic polycrystalline materials. The difference in the atomic sizes between the solute and solvent and the mismatch between the crystallographic structures of the two equilibrium phases limit the solubility of the solute in the solvent, i.e. these two factors are responsible for grain boundary segregation. In ceramics, in addition to the elastic strain and the crystallographic mismatch, (Yan et al., 1983) different electronic charge associated with each species and space charge effects can also affect the solubility limit and contribute to solute segregation. Two main approaches have generally been applied to treat grain boundary segregation phenomena such as thermodynamic, where an analogy with surface adsorption is applied (Hondros and Seah, 1977), and atomistic, where the effect of solute addition on the structure of the grain boundary, or the reverse, is investigated by numerical calculations (Sutton and Vitek, 1982, Hashimoto et al., 1984). Then a model regrouping these two main approaches has been proposed (Nowoski et al., 1990). Cook and Schrott report the effect of the mean grain size on the segregation of calcium in Al_2O_3 (Cook and Schrott, 1988). Sickafuss and Sass reported that the second phase in metals affects the structure of grain boundary (Sickafuss and Sass, 1987).

In the case of Al_2O_3, segregation of many elements has been reported at the free surfaces of monocrystals (Baik et al., 1985, Baik and White, 1987) as well as at the grain boundaries in polycrystals (Bender et al., 1980). For grain boundary segregation, Li and Kingery (Li and Kingery, 1985) concluded that it is controlled by an elastic strain effect rather than a charge effect. This conclusion seems valid whether or not the valence state of the solute cations is the same as that of the Al ions (3+). In the case of yttrium (Y) doping in

Al_2O_3, solute and solvent cations have the same valence state. Consequently, it can be assumed that the strain effect is responsible for segregation and that there is no charge effect and / or modification of the defect concentration when Y is added to Al_2O_3. In this system, segregation has been reported to take place at the grain boundaries (Bender et al., 1980) and at the free surfaces (McCune et al., 1986).

For single crystal, calculations have shown that segregation of Y at the free surfaces is related to the crystallography of the surface (Mackrodt and Tasker, 1989). This low solubility of Y in Al_2O_3 (10 ppm weight of Y) is due to rather high defect formation energy as deduced from ab-initio calculations by Ching et al.. They have shown chemical bonding of Y into the Al_2O_3 (Ching et al., 1997). In polycrystalline Al_2O_3, precipitates of yttrium garnet are formed at the grain boundaries (McCune, et al., 1986, Lagrange et al., 1987, Nanni et al., 1976). Y is isovalent to Al^{3+} and its ionic radius (r=0.93 Å) is larger than that of Al^{3+} (r=0.51 Å).

2.4.4.1 Y_2O_3 doped Al_2O_3

It has been proved that, strength and toughness of some structural ceramics can be improved greatly by adding rare earth (RE) oxides as stabilizer, sintering aids to reduce sintering temperature and production costs. RE oxides also play an important role in functional ceramics, such as semiconductor sensors, magnetic ceramics, microwave dielectric and piezoelectric ceramics etc (Guanming et al., 2007). Different amount of Y_2O_3 can reduce sintering temperature and increase mechanical properties (Anthony et al., 2005). In Al_2O_3, doping with Y affects properties related to grain boundary phenomena such as diffusion (Lagrange et al., 1987, Nanni et al., 1976). Gruffel and Carry reported the effects of grain size and microstructure by varying the Y concentration in Al_2O_3. They varied the concentration of Y_2O_3 upto 1500 ppm by weight (Gruffel and Carry, 1993).

The presence of RE cations at grain boundaries is well known to reduce both the grain growth kinetics and densification rate at a given temperature and consequently results in materials with very different microstructures (i.e. variation in grain size and porosity distribution) (West et al., 2007).

Chronologically, Y is firstly described as a possible beneficent doping element for Al_2O_3 in a 1968 US patent. The authors claimed that the perfect additive Y content is 0.05 wt%. It is further stated that Al_2O_3 containing Y can attain the density of 3.99 gm/cc and have excellent mechanical properties (Wolkodoff and Weaver, 1968, Korinek et al., 2002). In mid 1970s, US patents by Japanese teams proposed the range of 0.05–0.5 wt % Y_2O_3 as an optimum for improvement of the properties (Kobayashi and Kameno, 1974, Kobayashi and Kaneno, 1975). Basically sintering is controlled by diffusion process and the addition of Y_2O_3 increases the diffusion rate in Al_2O_3 and hence the mobility of the vacancies increases. This increase in mobility should improve the plasticity of the Al_2O_3 (Delaunay et al., 1980).

Fang et al. reported the densification rate of doped and undoped Al_2O_3. They used 1000 ppm Y and 1000 ppm La as the dopants in Al_2O_3. It is postulated that these large RE cations, which segregate to the grain boundaries in Al_2O_3, block the diffusion of ions along grain boundaries, leading to reduced grain-boundary diffusivity. In addition, doping with Y and La decreases grain growth during sintering. The morphology of Y doped Al_2O_3 sample consists of equiaxed grains with almost-spherical pores situated at grain boundaries (Fang et al., 1997).

Rani et al. reported (Rani et al., 2004) that effect of RE dopants on mechanical properties of Al_2O_3. The fracture toughness is found to increase with sintering temperature and grain size. The RE ions offer remarkable improvement in toughening of Al_2O_3 ceramics at all the sintering conditions over that in the undoped Al_2O_3 samples. A noticeable morphological modification was observed in the samples sintered at higher temperature. Due to the preferential segregation of the RE ions to basal planes (0001) in Al_2O_3 grain boundary (Atlay and Gulgun, 2003), there is a tendency of anisotropic elongated grain growth which enhances the fracture toughness. Especially Al_2O_3 doped with Er and La attained high fracture toughness of about 7.0 MPa $m^{1/2}$ for the samples sintered at a temperature above 1600 °C. This is due to formation of anisotropic elongated grains, which can result in crack bridging and crack deflection. Xu et al. reported the elongated grain shows higher fracture toughness than equiaxed grain (Xu et al., 2005).

West et al. reported (West et al., 2007) the effect of RE element segregation at the grain boundary, on mode of fracture in Al_2O_3. The magnitude of the grain growth retardation

depends on the particular rare earth species, and increases with increasing ionic radius of cations (Yb <Gd < La). This dependence is consistent with the RE cations blocking Al^{3+} diffusion pathways at grain boundaries. RE doping results in an increased proportion of intergranular fracture in the doped ceramics compared to that in the undoped material of similar grain size. West et al. reported the generation of thermal stresses with increasing grain size which results in grain boundary cracking. The maginitude of this thermal stress reduces with decreasing grain size, which may improve the fracture toughness. The undoped Al_2O_3 sample shows less intergranular fracture compared to the RE doped Al_2O_3 samples as shown in the Fig.2.8.

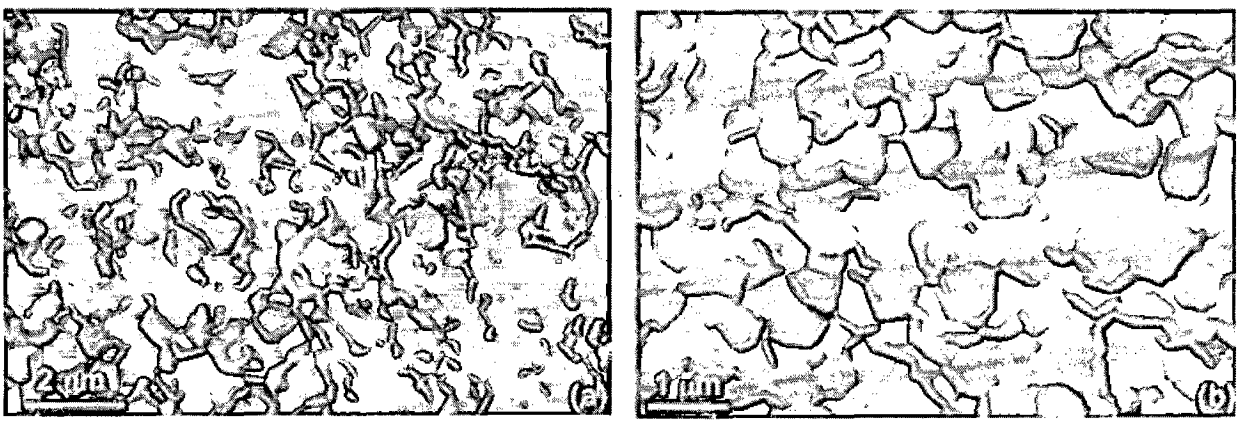

Fig.2.8 SEM fractographs of (a) undoped Al_2O_3 and (b) rare earth (Yb) doped Al_2O_3.

Muchtar and Lim examined the change in fracture mode with the increase in grain size in pressureless sintered Al_2O_3. They reported a transition from intergranular to transgranular fracture mode as the grain size is increased. They varied the grain size between 0.5 and 4.5 μm. It is further noted that for the specimens having submicron sized grains fracture intergranularly. On the other hand, for the specimens having micron sized grains, there is mixture of transgranular and intergranular fractures, with the proportion of transgranular fracture increasing with the increase in grain size. They reported, for the submicron grains the fracture toughness of the sample is relatively load independent. Samples having larger grain size (20 - 80 μm) show higher fracture toughness due to the

grain bridging mechanism. They reported the fracture toughness of Al_2O_3 is 3.9 MPa $m^{1/2}$ (Muchtar and Lim, 1998).

Deng et al. reported (Deng et al., 2004, Deng et al., 2003) the effect of RE element on grain boundary bonding in Al_2O_3–5 vol.% SiC composites. It was found that doping of 800 ppm different RE (Y^{3+}, Nd^{3+} and La^{3+}) leads to fracture-mode change from transgranular in dopant-free composites to intergranular in rare-earth doped composites. Boundary chemistry analyses showed that rare-earth ions and Si^{4+} ions (dissolve from the SiC particle surfaces) segregated at the Al_2O_3 grain boundaries and resulted in a weak grain boundary bonding. Fig.2.9 shows the crack propagation in dopant free Al_2O_3 – 5 vol.% SiC composites and RE doped composite. The intergranular fracture in RE doped composite significantly increases the crack deflection, compared to the dopant-free composite.

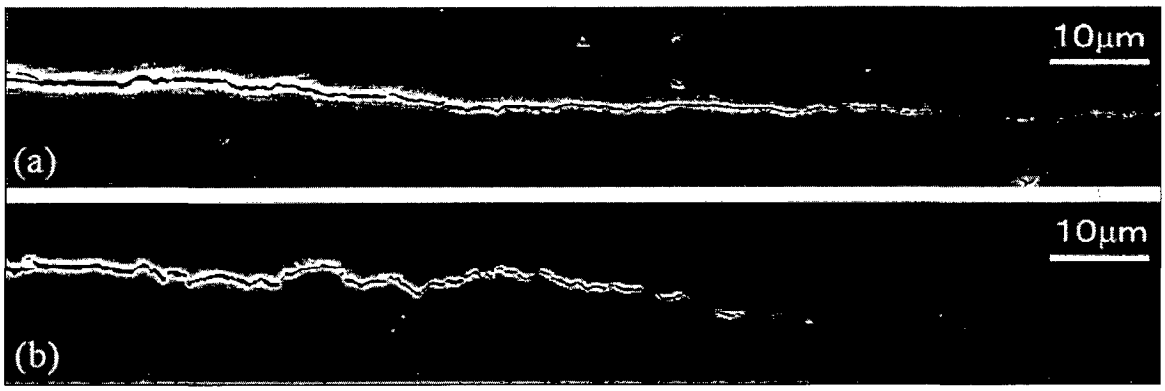

Fig.2.9 SEM micrographs showing the crack propagation in Al_2O_3–SiC composites (a) without dopants and (b) with dopant 800 ppm RE element.

Cho et al. reported (Cho et al., 2002) that oversized (relative to the size of the cation in the matrix) rare-earth dopant ions such as Y^{3+}, Nd^{3+}, and La^{3+} segregate to grain boundaries and reduce the tensile creep rate of α-Al_2O_3 by 2-3 orders of magnitude. It has been speculated that these dopant ions can modify the grain boundary structure in Al_2O_3 by promoting the formation of special grain boundaries. They have also shown that the dopants segregate at the grain boundaries, driven by their large size (radius) mismatch between the dopant ions (Y^{3+}: 0.89 Å, Nd^{3+}: 0.99 Å, La^{3+}: 1.06 Å), and the host Al^{3+} (0.51 Å) (Loudjani et al., 1993). It was suggested by Cho et al. that the observed reduction in creep rate resulted from a 'site-blocking' effect of oversized ions segregated at selected grain boundary

diffusion paths. Cho et al. found that doping of 450–1000 ppm Y^{3+}, La^{3+} and Lu^{3+} in Al_2O_3 reduces the creep rate approximately by two orders of magnitude. The segregation of rare earth element to the grain boundary strongly influences the creep rate of the ceramic material. They have shown the controlling of microstructure by varying dopant level. The rare earth elements Y and La retard the grain growth (Cho et al., 1997).

Hooker et al. reported the effect of single and double rare earth oxide in terms of sintering behavior, density and grain size. They report the Y^{3+} and Gd^{3+} go to the Al_2O_3 grain boundary. The rare earth oxide doped sample attains higher density even at lower sintering temperature but sintering at higher temperature the densification is almost same in doped and undoped Al_2O_3 samples. From the grain size point of view the doped sample sintered at lower temperature shows larger grain size than the undoped sample. However a reverse trend is found for the samples sintered at higher temperatures. The results were presented for 500 ppm Y in Al_2O_3 (Hooker et al., 2001).

Boutz et al. reported fracture toughness of yttria ceria tetragonal zirconia polycrystals (Y, Ce-TZP) as a function of grain size and ceria content. They showed fracture toughness increases with increasing grain size (Boutz et al., 1995).

Park and Yoon reported the abnormal grain growth in Al_2O_3 by changing the sintering temperature. Dislocation and other surface defects can influence the growth behaviour. They have shown that MgO influences the abnormal growth in Al_2O_3 (Park and Yoon, 2002).

Arato et al. reported that the apparent density is increased with the increase in temperature. They reported that the modulus of elasticity, hardness, and fracture toughness are increased with the increase in apparent density. They correlated these mechanical properties with the apparent density (Arato et al., 1995).

Chonghai reported the effect of microstructure especially the interface microstructure on the physical and mechanical properties of rare earth element doped Al_2O_3/(W,Ti)C ceramic composite. Rare earth materials help to make different types of interfaces and boundaries in the ceramic composites. The residual stresses and microcracking improve the mechanical properties of the ceramics (Chonghai, 2006). Rare earth element Y strengthens and toughens the Al_2O_3/(W,Ti)C ceramic composite to yield good mechanical properties (Chonghai, 2004).

West el al. reported the grain boundary segregation of rare earth element in Al_2O_3 ceramics. They used different characterization techniques to show the grain boundary segregation. To improve mechanical properties porosity and other defects must be avoided thus controlled sintering is required. Undoped Al_2O_3 grain growth control is difficult and controlled grain growth is possible by RE doping, which inhibits the grain growth by reducing the diffusivity of cations at grain boundary (West et al., 2004).

Xihua et al. reported the RE doping results in an increased proportion of intergranular fracture relative to the undoped material having similar grain size. This is due to the RE dopant, which segregates to the grain boundary reducing grain boundary cohesion. The fracture toughness increases up to the certain content of RE element and decreases thereafter with increasing the RE content. The fine and homogeneous grain structure improves the fracture toughness of the samples (Xihua et al., 2008).

Xu has reported the development of advanced RE (Y) reinforced Al_2O_3/(W,Ti)C ceramic composite materials and their microstructure, mechanical properties and the cutting performance. The improvement in fracture toughness of this material has been viewed through the formation of the complex RE compounds which increase the binding strength of the interfaces. As a result crack propagation resistance is enhanced resulting in improved fracture toughness. Excessive amount of Y results in the increase in the grain size and its inhomogeneous distribution. This causes the decrease in the mechanical properties (Xu, 1998).

Korinek et al. reported the Y doping induces modifications of the microstructural features and properties of polycrystalline Al_2O_3. Experimental and calculated results on Y grain boundary (GB) segregation are first described by them. They reported the role of Y on the overall microstructure, GB structure, GB defects and grain growth. During the grain growth, the GB Y content increases until GBs are saturated with Y and precipitation of yttrium aluminium garnet $Y_3Al_5O_{12}$ (YAG) compound occurs (Gulgun et al., 1999). An interesting result is that the transition from GB segregation to precipitation at GBs depends only on the grain size, whatever the thermomechanical history of the material has. The grain sizes for which the transition occurs have been determined for different Y is concentrations (2.3 μm for 225 ppm Y/Al and 0.8 μm for 676 ppm Y/Al). The toughness of polycrystals displaying

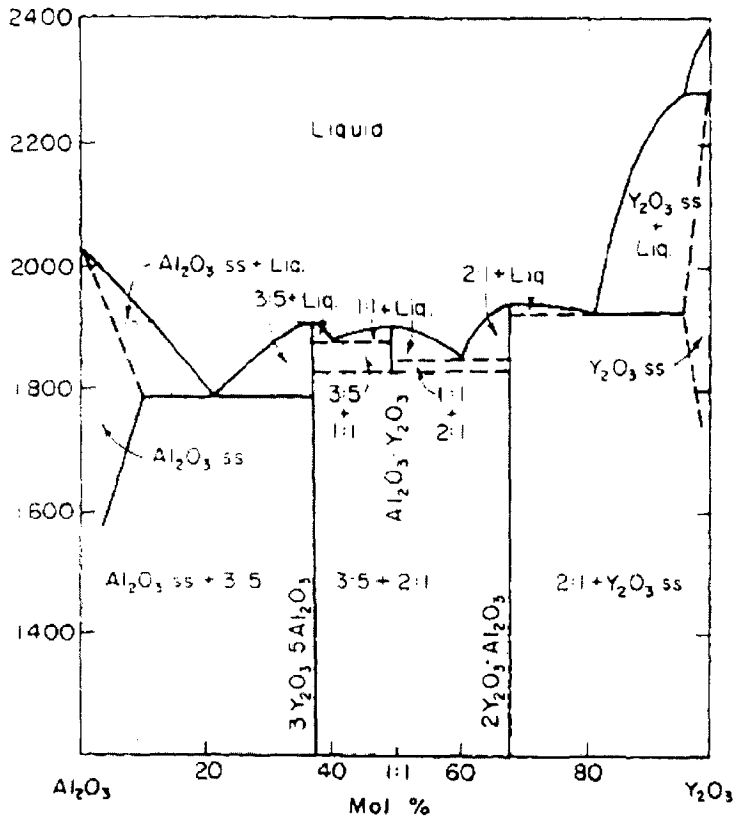

Fig. 2.10 Al_2O_3 - Y_2O_3 phase diagram (Warshaw and Roy, 1959).

The composite Al_2O_3 - Y_2O_3 has three different phases: yttrium aluminum monoclinic, $Y_4Al_2O_9$ (YAM), yttrium aluminum perovskite, $YAlO_3$ (YAP) and yttrium aluminum garnet, $Y_3Al_5O_{12}$ (YAG) (Duk et al., 2002).

Lo and Tseng studied phase development in the Al_2O_3–Y system synthesized by sol–gel method and the formations of YAG, YAP and YAM were observed in the XRD analysis (Lo and Tseng., 1998).

Y in the Al_2O_3 matrix has been transformed to YAP, YAG and YAM. Initially, YAM and YAP are formed, the formation of YAG occurs after prolonged heat treatments at temperatures around 1600°C. The formation of YAG, YAP and YAM promotes bonding between Al_2O_3 and Y_2O_3, which also contributes to the improvement of the mechanical properties of the composite (Kinsman et al., 1994).

Hongzhi et al., (Hongzhi et al., 2001) prepared Al_2O_3–5 vol% YAG composites and reported that the bending strength and the fracture toughness are 604 MPa and 5.0 MPa $m^{1/2}$,

respectively. The formation of YAG in the Al_2O_3 matrix improves the mechanical properties of composite (Kumar et al., 2007).

2.4.4.3 Properties of Al_2O_3 and Y_2O_3

Dieter (Dieter, 1988) explained the strengthening mechanisms of the dispersion of soft particles in the hard matrix. The dislocation can cut and deform the soft particles, however, the particles cannot be easily sheared due to the strengthening mechanisms such as coherency strains, stacking fault energy, ordered structure, modulus effect, interfacial energy and lattice friction stress effect. Due to these strengthening mechanisms, an additional expenditure of energy is required, in order to propagate the crack through the particles. Kim et al. (Kim et al., 1997) described the strengthening mechanism of compressive thermal residual stresses. These stresses are developed due to the difference in thermal expansion coefficient and elastic modulii of matrix and particles and they reduce the stress intensity factor at the crack tip. These stresses are formed around the dispersed particles (Awaji et al., 2002). The thermal residual stresses depend on the thermal expansion coefficients of the particle and the matrix. These thermal residual stresses are of sufficient magnitude to generate lattice defects such as dislocations around the particle even in ceramic materials. Thermal residual stresses are likely to be developed due to the differences in thermal expansion coefficients and young moduli of Al_2O_3 and Y_2O_3. These residual stresses influence in the pinning of crack propagation initiated in the matrix by reducing the stress intensity factor at the crack tip (Ohji et al., 1998). So, the addition of Y particle in the Al_2O_3 matrix introduces particulate toughening effect and increases the fracture toughness of the composite (Kumar et al., 2007).

Voytovych et al., reported the grain growth and densification of α-Al_2O_3, doped with varying amounts of Y (0 to 3000 ppm of Y) sintered in air at 1450°C, 1550°C and 1650°C. They reported that the Y doping inhibited densification and coarsening at 1450°C, but had very little effect at 1550°C and no effect at 1650°C. Y is known to have a very low solubility limit in α-Al_2O_3 and segregates to the grain boundary. They have shown the lower grain size in doped Al_2O_3 compared to undoped Al_2O_3 through micrograph. The doping label of 1000 ppm Y shows the higher relative density (Voytovych et al., 2002).

Progrion et al., reported the effect of microstructural changes and the reason of grain growth with abnormal grain growth (AGG) or with uniform grains in Y (150 ppm) doped Al_2O_3. They developed a mathematical model to correlate the geometrical parameters of the powder and green bodies in correlation with the porosity in sintering compacts (Pogrion et al., 2004). Dudkin et al., reported that the function of Y in the RE aluminate. For the mixing of Y_2O_3 as a sintering aid into the ceramic materials, two models have been proposed to explain the sintering action of Y_2O_3. In one model, Y_2O_3 enters into reaction with one or several components of the ceramic mixture to form solid solutions. In the other model, Y is segregated onto the surface of the ceramic grain, which prevents the transfer of the main material through the intergranular interface (Dudkin et al., 2004).

Hah et al., reported the mechanical properties of highly purified α-Al_2O_3 (>99.5%) as a function of dopant concentration from 0-1500ppm Y_2O_3 and mean grain size from 0.49 to 1.44 μm. In pure Al_2O_3, Vickers indentations produce subsurface cracks detected by Nomarski interference contrast microscopy. No such cracks are formed in the Y-doped materials. The hardness is higher when mean grain size is small. The higher amounts of Y dopant generate precipitates of yttrio-garnet in the grain boundaries and increase the fracture toughness. They have reported that the effect of grain size and dopant on fracture toughness. They established a relationship between hardness and mean grain size which follows a modified Hall-Petch equation and have also shown that this equation is independent of Y doping (Hah et al., 1995)

2.4.5 ZrO_2 doped Al_2O_3

All of these mechanisms essentially redistribute stress at the crack tip and increase the energy needed to propagate a crack through the composite material, thereby resulting in toughening improvement. Particulate toughening is commonly adopted to strengthen the ceramic–ceramic composites (Dutta, 2001). It has been well-documented that the addition of a small amount of metal oxide will sensitively change the mechanical properties of oxide ceramics (Riu et al., 2000).

The introduction of ZrO_2 into Al_2O_3 as a sintering aid has long been practiced for densification of Al_2O_3 (Cahnoon and Christensen, 1956). The introduction of a small amount

(1000 to 2000 ppm) of ZrO_2 into Al_2O_3 as a sintering aid allows the formation of a solid solution which promotes the densification process by the introduction of lattice defects (Wang and Stevens, 1989). In contrast, the microstructures of zirconia toughened alumina (ZTA) are characterized by the presence of the two distinct phases (monoclinic and tetragonal), which do not react with each other to form a solid solution (Levin and McMurdie, 1975). The toughening of Al_2O_3 by dispersing ZrO_2 particles was first encouraged by the development of the partially stabilized ZrO_2 (PSZ) (Garive et al., 1975). The presence of ZrO_2 grains in the Al_2O_3 matrix as a discrete second phase enables the former to behave in an intrinsic manner, that is, to undergo the tetragonal to monoclinic transformation or to be retained as the metastable tetragonal form during cooling of the composites from the fabrication temperatures. It is the volume expansion and shear strain associated with the tetragonal to monoclinic transformation that result in toughening in these composites, along with other mechanisms such as stress-induced transformation toughening, microcracking toughening, compressive surface stresses and crack deflection (Wang and Steven, 1989).

2.4.5.1 Solubility of ZrO_2 in Al_2O_3

The rules following which the second element (solute) dissolves into matrix (solvent) are as follows: 1) The atomic radii of solute and solvent must differ by no more than 15% i.e. % difference = $((r_{solute} - r_{solvent}) / r_{solvent}) \times 100 \leq 15\%$. The ionic sizes of Al and Zr are 0.53 Å and 0.72Å respectively and therefore the %difference is 38%, showing the probability of substitutional solid solution formation in Al_2O_3- ZrO_2 system is very low. 2) The crystal structure of solute and solvent should be same. But in the present study, ZrO_2 has different crystal structure from room temperature to high temperature so chances of substitutional solid solution is less. 3) Electronegativity difference between the elements should be minimum. But in the present study, electronegativity difference is not low so chances to the formation of solid solution is low.

Zhao et al. (Zhao et al., 2008) reported the toughening mechanisms of ZrO_2 toughened Al_2O_3 composite ceramics. They have reported that the nano ZrO_2 containing composite provides better mechanical properties than micron size ZrO_2 containing composites. Tetragonal phase transforms to monoclinic phase ($t \rightarrow m$) when the grain overcomes the binding force around

it. The binding force increases with the increase in Al_2O_3 content, so phase transition t→m becomes difficult. ZrO_2 phase transition is controlled by three factors: (1) binding force of matrix, (2) grain size of ZrO_2, (3) chemical free energy of the t and m phases. With the increase of ZrO_2 content and particle size, tetragonal phase (t) becomes unstable and is transformed into monoclinic phase (m) easily. ZrO_2 grains play a different role in toughening of Al_2O_3 ceramics. It is supposed that ZrO_2 grain diameter is d, critical grain diameter producing phase transition is d_c and critical grain diameter inducing microcracks is d_m. When $d>d_c$, stress-induced phase transformation plays a toughening role, when $d_m<d<d_c$, residual stress plays a toughening role, and when $d<d_m$, microcrack toughening occurs (Wu, 2006). In this experiment, to every inequality as above, there are some grains in ceramics meeting it, so mechanical properties of ZrO_2 toughened Al_2O_3 composite ceramics is improved by composite toughening mechanism. They have reported that for the nano ZrO_2 composite, stress induced ZrO_2 phase transformation toughening is the main toughening mechanism. In addition, to second phase, majority of the grains meet the inequality $d<d_m$, so microcracks toughening is also one of the toughening mechanisms.

2.4.5.2 Phase diagram of Al_2O_3 - ZrO_2

The introduction of small amount of ZrO_2 as an additive into the Al_2O_3 results in the formation of solid solution as can be seen in the Al_2O_3–ZrO_2 phase diagram given in Fig.2.11 (Levin and McMurdie, 1975, Zhou et al., 2003). This solid solution promotes the densification of the Al_2O_3- ZrO_2 based composites by the introduction of lattice defects.

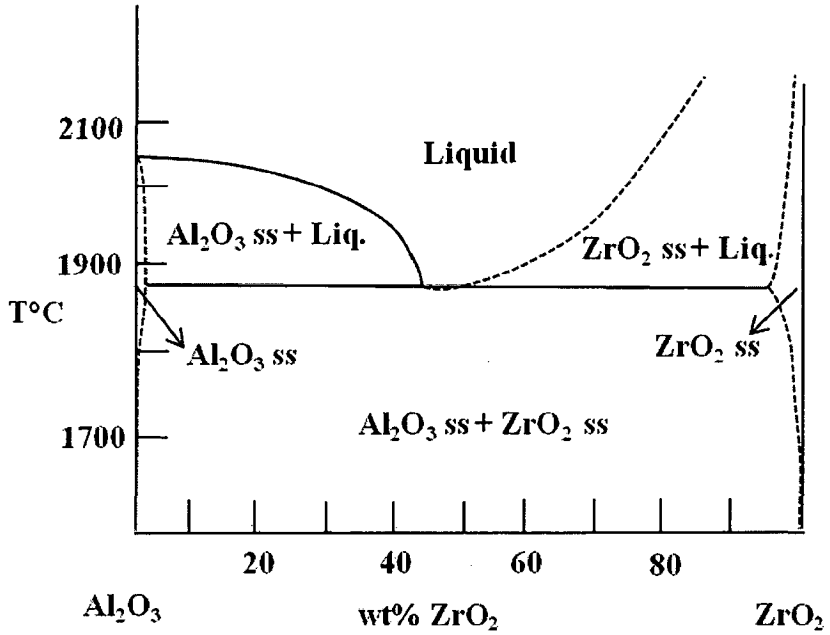

Fig.2.11 Phase diagram of the Al_2O_3–ZrO_2 system (Levin and McMurdie, 1975)

Majumdar et al., reported that the density of the Al_2O_3–ZrO_2 composites decreases slightly with the increase of ZrO_2 contain, indicating that the presence of ZrO_2 particles prohibits the densification of Al_2O_3 matrix. Although the solubility of ZrO_2 in Al_2O_3 is as low as ~ 2000 ppm, the presence of Zr^{4+} solute can slow down the densification of Al_2O_3 (Majumdar et al., 1993, Tuan et al., 2002). Sharma proposed an equation to measure the density in composites. The changes in density occur in composites due to the thermal mismatch between the matrix and reinforcement. The model proposed would be useful to predict the density of the composites as well as the mechanical properties of the composites (Sharma, 2003).

2.4.5.3 ZrO_2 toughened Al_2O_3

The martensitic phase transformation which occurs in ZrO_2 is most widely used for toughening of Al_2O_3. ZrO_2 undergoes several phase transformations upon cooling from the melt. At least three crystallographic modifications exist, which possess cubic (c), tetragonal (t) and monoclinic (m) symmetry and are stable at high, intermediate and low temperatures respectively as shown below:

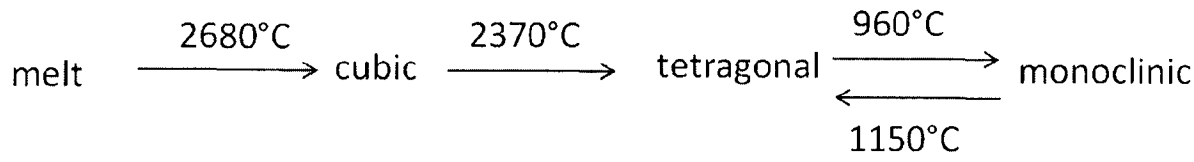

This transformation is the source of toughness in ZrO_2-containing ceramics (Evans and Cannon, 1986, Green et al., 1989, Heuer and Hobbs, 1981). The t → m phase transformation (Fig. 2.12) involves a set of transformation strains that increase the volume and change the shape of the particle/grain.

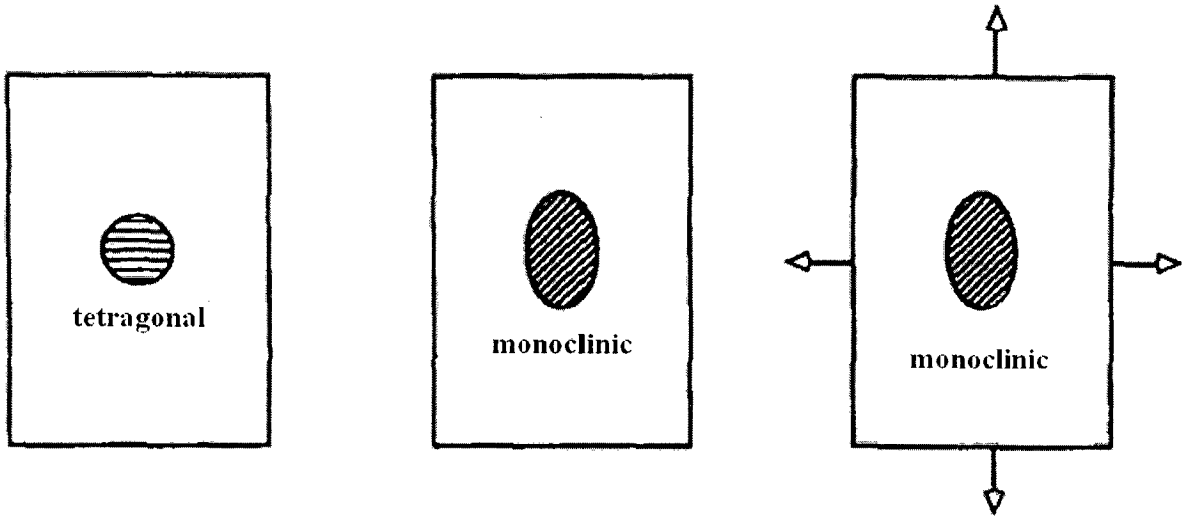

Fig. 2.12 A schematic representation of the ZrO_2 phase transformation

Isolated grains invariably transform provided that the nucleation conditions are satisfied. However, for grains embedded in a matrix, strain energy changes tend to oppose the transformation. Then, for the transformation to proceed, the system has to be supercooled to sufficiently increase the chemical driving force. The retention of t-ZrO_2 to room temperature can be controlled by several microstructural and chemical factors, such as grain size and alloy content.

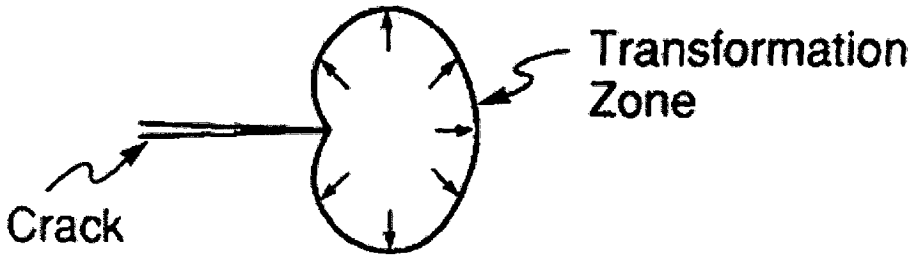

Fig. 2.13 Schematic representation of interaction between crack and transformation zone

Fig 2.13 shows the crack tip facing the transformation zone which helps to deflect the crack and increase the traveled crack path thereby improving the fracture toughness of the material. Evans et al., considered that cracks can be deflected by localized residual stress fields which are developed as a result of phase transformation, thermal expansion mismatch or by the fracture of a second phase. The deflection results in a degree of toughening dictated by the reduced force on the deflected portion of the propagating crack. For the deflection by a second phase in the matrix, the parameters which have been shown to influence the toughening include volume fraction, particle morphology and aspect ratio of the second phase (Evans and Cannon, 1986, Faber and Evans, 1983). The phase transformation, which is accompanied by a volume expansion (~ 4%) and shear strain (-~ 6%), will provide a compressive stress which acts to reduce and eventually stop the propagation of the crack, necessitating extra work for further crack propagation. Microcracks in ZrO_2-toughened ceramic materials can be subdivided as residual microcracks and stress induced microcracks. The residual microcracks are due to the volume expansion and shear strain associated with the t $\rightarrow$ m transformation which takes place on cooling from the sintering temperature (Claussen, 1976). The stress induced microcracks are those caused by the volume expansion and shear strain associated with the subsequent stress-induced transformation during fracture process. It is considered that residual stresses are required for the formation of stress-induced microcracks, however, the magnitude of the stresses is insufficient to cause spontaneous microcracks. Thus when the external stress and the tensile stress associated with the t $\rightarrow$ m transformation are linearly superimposed on the residual stresses, microcracks will be induced (Wang and Stevens, 1989).

Moraes et al. (Moraes et al., 2004) reported that the Al_2O_3 – ZrO_2 composite is a promising candidates for biomaterial application due to biocompatibility and mechanical properties that combine high flexural strength with a high fracture toughness. They varied the ZrO_2 content between 5 and 80 wt % in Al_2O_3 and examined the physical as well as mechanical properties in the system. The uniaxially compacted samples sintered at 1600°C and the fracture toughness of this sintered sample measured by using ASTM C-1421. They used different equations for measuring the fracture toughness. They have shown the presence of porosity decreases the fracture toughness by the reduction of the resistance area and by the effect of stress concentration at the pores. Peras and Dauknis have established analytically the dependence of strength of a ceramic material on its porosity. The weibull parameter (m) affects the relation of porosity and strength (Peras and Dauknis, 1971).

Basu and Sarkar reported the mechanical properties of Al_2O_3 and Al_2O_3 – ZrO_2 composite. They have shown the improvement of fracture toughness in Al_2O_3 – ZrO_2 ceramic composites compared to monolithic Al_2O_3. They reported the fracture toughness of Al_2O_3 – 15 vol% ZrO_2 ceramic composite is 5.7 MPa $m^{1/2}$. They measured the fracture toughness by using Anstis equation and measured the crack length generated from the corner of the Vickers indentation (Basu and Sarkar, 2001).

Chou et al., (Chou et al., 2009) reported the coefficients of thermal expansion (CTE) and internal residual strains in metal reinforced ceramic matrix composites. They have reported the formation of thermal residual stress that is induced in the particle reinforced ceramic composites. The residual stress is attributed to the mismatch in the CTEs between the matrix and the second phase. They proposed the following equation

$$P = \frac{(\alpha_m - \alpha_p) \cdot \Delta T \cdot E_m}{[(1+\nu_m)/2] + [(1-2\nu_p) \cdot E_m/E_p]} \qquad (2.1)$$

where the subscripts p and m refer to the particle and matrix, respectively, and E, α, and ν are the elastic modulus, thermal expansion coefficient, and Poisson's ratio, respectively. Eq. (2.1) indicates that, when the value of either ΔT or (α_m – α_p) is negative, a hydro-static compression will occur in the particles; or else hydrostatic tension appears. A second phase with a greater coefficient of thermal expansion than the matrix produces tangential

compressive stress in the matrix near the particle/matrix interface and diverts the crack around the particle. A second phase with a lower coefficient of thermal expansion than the matrix induces tangential tensile stress in the matrix causing the crack to deflect towards the particle (Faber and Evans, 1983).

Daguano et al., reported that the mechanical properties of ZrO_2 with 20 wt% Al_2O_3 ceramic composites. They investigated the influence of sintering time on the microstructural characteristics and mechanical properties of ZrO_2 –Al_2O_3 composites. They sintered the samples at 1600 °C and report the variation on hardness with soaking time periods. Hardness variation of the samples is 15.00 to 13.10 GPa and fracture toughness is 8 MPa $m^{1/2}$ which makes this materials suitable for bioapplications, such as dental implants. Addition of Al_2O_3 increases hardness in ZrO_2 – Al_2O_3 composites. The grain size of Al_2O_3 increases with increasing soaking time period. They developed an equation for the determination of the thermal residual stress between ZrO_2 matrix and the Al_2O_3 reinforcement (Daguano et al., 2007).

Shin et al., reported the contribution of the two toughening mechanisms, e.g. stress-induced phase transformation and micro cracking by measuring the fracture toughnesses of Al_2O_3 -15 vol% ZrO_2 composites with similar microstructures and elastic properties but different m-ZrO_2 contents. The measured fracture toughness reflected a combination of the two toughening mechanisms. The grain size of ZrO_2 influences the change in fracture toughness of the Al_2O_3 – ZrO_2 samples (Shin et al., 1999).

Haldar et al. reported the effects of Y with sintering temperature for fracture toughness of mullite-zirconia composite. They sintered the samples at 1500°C and 1600°C for 2 hr. They also showed how Y affects physical, mechanical properties and microstructural features. They report that the Y helps in grain growth as the sintering temperature increases. Exaggerated grain growth is responsible for higher porosity as the temperature increases. But undoped samples show downtrend in porosity with an increase in sintering temperature (Haldar et al., 2002). Rajendran and Rossell, reported that the addition of ZrO_2 enhances the sintering kinetics as well as fracture strength of mullite ($3Al_2O_3.2SiO_2$) (Rajendran and Rossell, 1991).

Zhao et al., show a new way, named the thermit combustion induced ceramic rapid-

solidification process to prepare Al_2O_3/ZrO_2 ceramic composites. This process yields rod shaped eutectic grains which help to improve fracture toughness following grain bridging, crack deflection and crack shielding toughening mechanisms. They report different fracture toughness of Al_2O_3/ZrO_2 composite (Zhao et al., 2006).

Zhao et al., reported improvement in the fracture toughness of Al_2O_3 matrix ceramics reinforced with ZrO_2 composite. It has been determined that toughening of ceramics is obtained by the action of multiple toughening mechanisms involving reinforcement-induced toughening by ZrO_2, deflection-induced toughness, stress-induced transformation toughening, transformation-induced microcrack toughening and crack-bridging toughening (Zhao et al., 2005, Ray et al., 2000). Basu et al. has reported the fracture toughness of Y stabilized tetragonal ZrO_2 polycrystalline (Y-TZP) and Y-free commercial ZrO_2-20 wt% Al_2O_3. They reported the almost double fracture toughness in Y-TZP than the commercial ZrO_2-20 wt% Al_2O_3 ceramic. Transformation toughening mechanism is the toughening mechanism to increase the fracture toughness in Y-TZP. They also proposed a simple root to develop the fracture toughness of TZP-Al_2O_3 composites. They have reported the fracture toughness of 10 MPa $m^{1/2}$ (Basu et al., 2004). Zhou et al., report that the fracture toughness of Al_2O_3 and ZrO_2 nanocomposites for hip replacement. They varied ZrO_2 from 0 to 20 wt% for making composites and sintered the samples by varying the temperature from 1300 to 1500 °C. They have shown increase in density with increase in sintering temperature by removing pores from the compacts and enhancing diffusion. They report the decrease of hardness with increasing ZrO_2 content. Fracture toughness of Al_2O_3 – ZrO_2 increases upto a certain wt% of ZrO_2 then after it decreases. The maximum fracture toughness is 8.4 MPa $m^{1/2}$, hardness is only higher in Al_2O_3 (Zhou et al., 2008).

2.4.5.4 Rare earth doped Al_2O_3 – 5 wt% ZrO_2

ZrO_2 has characteristic of multi-phase transformation, it is of monoclinic at room temperature, tetragonal at intermediate temperature and cubic at high temperature. There is an obvious change in volume when ZrO_2 crystal transforms, thus the scope of direct use of ZrO_2 is limited. ZrO_2, should be treated to acquire crystal stability so as to prevent ZrO_2 ceramics from cracking during heating or cooling procedure. Research showed that the addition of other oxide with cation radius similar to Zr^{4+} ionic radius played a role of

inhibiting phase change and stabilizing ZrO_2 crystal. At first, CaO, MgO were often chosen as a stabilizer, along with research development. It is noticed that rare earth oxides are better stabilizer for inhibition of ZrO_2 phase change. The rare earth oxides, such as Y_2O_3, Nd_2O_3, and CeO_2 are mainly used as additives in ZrO_2 ceramics, as they have higher solubility in ZrO_2. The radius of Y^{3+}, Nd^{3+} and Ce^{3+} is close to that of Zr^{4+}, which makes these ZrO_2 - rare earth oxides solid solution with crystal structure of monoclinic, tetragonal and cubic system. Along with adding different types and quantities of the rare earth oxides, ZrO_2 structural ceramics of high performance can be prepared, such as fully stabilized zirconia ceramics (FSZ), partially stabilized zirconia ceramics (PSZ), tetragonal zirconia ceramics (TZP). The addition of rare earth oxides not only inhibits phase transformation of ZrO_2 ceramics, but also increases the bending strength and fracture toughness, so ZrO_2 ceramics with rare earth addition have been widely used as a new type structural ceramics only after Al_2O_3 ceramics. A kind of toughened ZrO_2 ceramics with improved performance compared with traditional Al_2O_3, Si_3N_4 ceramics can be prepared by adding RE-stabilized ZrO_2 (Daniel et al., 2001, Agrawal et al., 1989).

The main applications of ZiO_2 toughened Al_2O_3 (ZTA) are cutting tools and rocket nozzles (Biswas and Chaudhuri, 1999, Dhas and Patil, 1994). ZTA materials have also received increased attention as implant materials, structural materials, and cutting tools in metal-working and paper cutting (Basu et al., 2004). Wang et al. reported the Y-doping was achieved by adding an yttrium nitrate (99.999%). They analyzed the Y and ZrO_2 doped ultra high purity Al_2O_3 indicates that dopants at the level of 100 ppm are mainly segregated to the Al_2O_3 grain boundary (Wang et al., 1999).

2.4.5.5 Phase diagram of ZrO_2 –Y_2O_3

The electronegetivity difference of Al and Y is higher so there is very less chance for Y to diffuse into Al_2O_3.

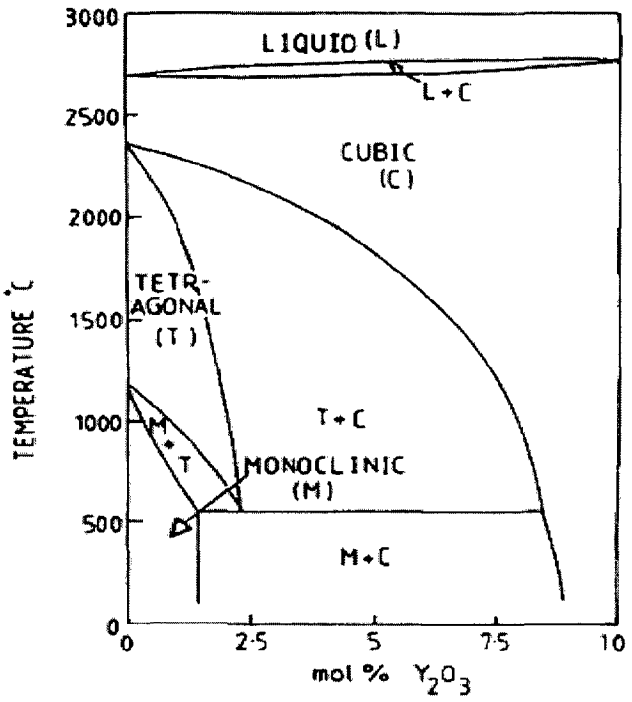

2.14 Phase diagram of $ZrO_2 - Y_2O_3$ (Scott, 1975).

The phase transformation temperature from t ⟶ m can be suppressed by doping with Y_2O_3 in the Al_2O_3 - ZrO_2 (Heuer and Hobbs, 1981). The small amount of Y_2O_3, the stabilizing agent for ZrO_2 (Fig. 2.14), prohibits the grain growth of Al_2O_3 (Tuan et al., 2002). Though the ionic charge of Y is the same as that of Al, the Y ion is much larger than the Al ion (0.89 Å vs. 0.52 Å) (Kingery et al., 1960). Large Y ions tend to segregate at the grain boundaries of Al_2O_3, thus reducing elastic strain energy (Cho et al., 2000). Although the solubility of Y in Al_2O_3 is extremely low (<10 ppm), (Cawley and Halloran, 1986) large Y ions can block the diffusion of ions along grain boundaries, leading to reduced densification and grain growth rates.

Tomaszewski et al. reported that fracture toughness of layered Al_2O_3 - 50 % Y-ZrO_2 composite. The sample were compressed by using isostatic press and sintered at 1600 °C temperature. They reported the fracture toughness of 7.11 MPa $m^{1/2}$ of the composite and reason of the increase in fracture toughness is crack deflection. Formation of stress due to the difference in thermal expansion coefficient of Al_2O_3 and ZrO_2 may deflect the crack (Tomaszewski et al., 2000). Moreno and Yoshimura, reported that the ternary diagram of Y-

ZrO_2 and Al_2O_3. There is high mutual solid solubility between ZrO_2 and Y phases, while Al_2O_3 shows very little solubility. They used Raman spectroscopy for the structural study of Y-ZrO_2 solid solution (Moreno and Yoshimura, 2004).

Zhou et al., has shown that the large amount of Y content helps to grain growth. Pure ZrO_2 with a monoclinic structure is very brittle, a suitable addition of phase-stabilizing oxides resulting in retention of the tetragonal phase to room temperature leads to a marked increase of strength and fracture toughness (Zhou et al., 1992).

2.5 Summary

Alumina (Al_2O_3) is by far the most basic compound for technical ceramics, as it exhibits applications in diverse areas such as cutting tools, friction and wear, refractories, electrical and electronics, optics, biomedical, jewelry, etc. However, it still has problems with lack of toughness and low reliability preventing it from being used in wider applications. There are some mechanisms to improve the fracture toughness these are crack deflection, crack bridging, microcracking, crack pinning and transformation toughening etc. Initially researchers tried to develop the fracture toughness in ceramic by self-reinforcing. They developed the microstructure of the ceramics by changing the sintering parameters like temperature and soaking time period. In 1960 Kingery tried to develop the densified ceramics. The distribution of grain size in the sample helps to improve the fracture toughness of the ceramics. Researchers have developed large grains which help to follow the grain bridging mechanism. The elongated grain helps to follow the crack deflection mechanism. Larger grains generate residual stress in the sample which also improves the fracture toughness in ceramics. But they also found that there is limitation of grain size range upto which fracture toughness of ceramic will increase then it will decrease. It is also reported that the increase in grain size increases the density of the materials. To restrict the grain growth second phase has been incorporated in to the matrix. Second phase (Y) goes to the grain boundary of matrix to restrict the grain growth. The formation of weak interface between Y and Al_2O_3 grain boundaries is also one of the reasons to incorporate Y into the matrix (Al_2O_3). The weak interfaces force the crack path to pass through the weak interface, which follows the crack deflection mechanism. Thus the path traveled is also more which helps to improve the fracture toughness. In this study it has been attemped to incorporate Y upto

and $La(NO_3)_3.6H_2O$ to the slurries of the Al_2O_3–5wt% ZrO_2. The rare earth doped samples were prepared in the systems of Al_2O_3 – 5 wt% ZrO_2 – 1000 ppm $Y(NO_3)_3.6H_2O$, Al_2O_3 – 5 wt% ZrO_2 – 1000 ppm $La(NO_3)_3.6H_2O$ and Al_2O_3 – 5 wt% ZrO_2–1000 ppm $Y(NO_3)_3.6H_2O$ – 1000 ppm $La(NO_3)_3.6H_2O$, which are denoted briefly in this thesis as A, AZ, AZY, AZL and AZYL respectively (Deng et al., 2003). The different powders of required quantities for each system were dispersed in distilled water by the ultrasonication method which deagglomerates the powders. The sonication was done for 6hr for each system. The deagglomerated powders were mixed for 36 hr using magnetic stirrer. The powder mixtures were then dried at 100°C for 12hr. The dried mixture was further ground lightly in a mortar and pestle.

3.1.3 Binder preparation and addition

The polyvinyl alcohol (PVA) was used as binder. The solid PVA crystal is slowly dissolved in distilled water by heating for the binder preparation. The binder PVA (3-5 % by weight) was added to the different powder mixture systems prepared and mixed thoroughly. This process was continued until the granulation of powder was achieved. The binder provides some lubrication during pressing and gives adequate strength for handling, inspection to the pressed parts (Basu and Sarkar, 2001).

3.1.4 Green sample preparation by compaction

The required quantity of the powder was used to achieve the desired thickness of the sample. The granulated powder was compacted in the form of rectangular bar having dimension of 3 x 5 x 45 mm^3, uniaxially in a hydraulic press at different loads ranging between 7.5x 10^4 and 22.5x 10^4 N. The dried mixtures were also pressed in the form of cylindrical pellets (diameter ~ 20mm and thickness 2.8 mm). All samples were weighed and dimensions were measured to study the linear shrinkage and density measurements (Lee et al., 1988).

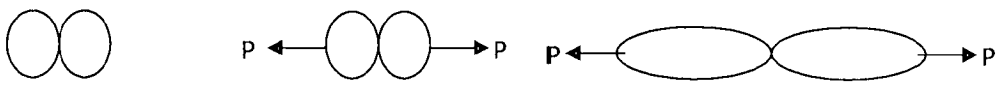

1. Initial condition 2.Force Applied 3.Bond stretched after compaction

Fig.3.1 Changes of particle shape during compaction of the powder.

Fig.3.1 shows schematically the changes in particle shape during compaction of the powder. During the application of the force the energy is stored in the pellets and is later utilized during the sintering. So the compaction load plays a role in sintering.

3.2 Sintering

Sintering is the primary method for converting loosely bonded powder compact into a dense ceramic body. Sintering is a method for making objects from powder, by heating the material in a sintering furnace below its melting point (solid state sintering) until its particles adhere to each other. Sintering is traditionally used for manufacturing ceramic objects, and has also found uses in such fields as powder metallurgy. Sintering commonly refers to the process involved in heat treatment of powder compacts at elevated temperature $T > 0.5\ T_m$ (Barsoum, 1997). The successful sintering usually results in dense polycrystalline solid. The principal goal of sintering is the reduction of the compacts porosity. The sintering process is usually accompanied by other changes within the material, some desirable and some undesirable. The properties of the materials, which undergo change are the following:

1. Strength, elastic modulus
2. Hardness and toughness
3. Electrical and thermal conductivity
4. Permeability of gases and liquid
5. Average pore size and shape
6. Distribution of pore size and shape

Temperature is very important to control the sintering process, since grain-boundary diffusion and volume diffusion rely heavily upon temperature, the size and distribution of particles of the material, the materials composition, and often the sintering environment to be controlled. Microstructure is very important for the mechanical property of the material. Sintering aims to achieve the desired microstructure through control of sintering variables. Microstructural control means the control of grain size, sintered density, and distribution of

other phases including pores. In most cases, the final goal of microstructural control is to prepare a fully dense body with a fine grain structure.

3.2.1 Importance of sintering

The densification of particulate powder compact is technically referred as sintering. Sintering is essentially the removal of pores between the starting particles, combined with growth of particles and strong bonding between adjacent particles.

3.2.2 Types of sintering

There are two types of sintering, solid state sintering and liquid state sintering. In solid state sintering grain coarsening and densification occur. Sintering involves consolidation of the powder compact by diffusion on an atomic scale. Moisture and organic constituents of the green body are first burned away and then, at the temperature range at which diffusion process occurs, matter moves from the particles into the void spaces between the particles, causing densification and resulting in shrinkage of the part. In solid state sintering densification is achieved through changes in particle size and shape, without rearrangement or presence of liquid. In case of liquid state sintering, the liquid that is present at sintering temperature aids densification. Grain rearrangement occurs in the initial stage followed by a solid precipitation stage.

3.2.3 Sintering variables

The major variables which determine sinterability and the sintered microstructure of a powder compact may be divided into two categories, material variables and process variables. The variables related to raw materials (material variables) include chemical composition of powder compact, powder size, powder shape, powder size distribution, degree of powder agglomeration, etc. These variables influence the powder compressibility and sinterability (densification and grain growth). The other variables involved in sintering are mostly thermodynamic variables, such as temperature, time, atmosphere, pressure, heating and cooling rate (West, 1984).

Solid state sintering was carried out at 1500°C, 1600°C and 1700°C. The green compacts in the form of rectangular bar were sintered at 1500°C for different soaking time periods of 3hr, 6hr, 9hr, 12hr, 18hr, 24hr and 36 hr. At the 1600°C and 1700°C sintering

temperatures the samples were soaked for 3hr, 6hr, 9hr and 12hr. Soaking time was varied in order to study the effect of soaking time on density variation, bond strength, fracture load and fracture toughness.

3.2.4 Heating schedule

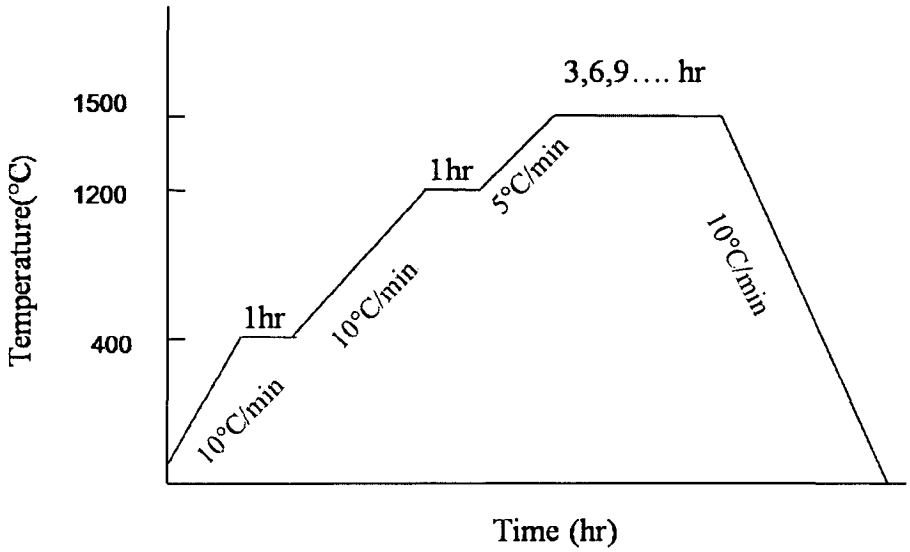

Fig. 3.2 Time - temperature profile for sintering operation

The graph shows the heating cycle for sintering at 1500°C. The sintering has been done using a high temperature furnace. The rates of heating as well cooling used in the sintering process are shown in the Fig. 3.2.

3.3 Density measurement

The density of sintered samples is a very critical parameter and much care must be made during the measurement. The theoretical density of the composites was calculated using the rule of mixtures. The density of all the samples was measured following Archimedes principle using water as an immersion medium. Using values of density of Al_2O_3, ZrO_2 and Y_2O_3 as 3.97, 5.60 and 5.01 g cm^{-3} respectively, the theoretical densities (ρ_t) for each composition were calculated.

3.4 Polishing

The surface of a metallographic specimen is prepared by various methods of grinding,

polishing, and etching. Polishing is also a crucial step for microscopic observations on ceramic samples. Metallographic specimen preparation included cutting, mounting, grinding, polishing and cleaning. The specimens were cut using precision diamond cutter. The specimen was then hot mounted in bakelite powder at 130°C in a hydraulic mounting press. The mounted specimens were then prepared by mechanical grinding and polishing method for microstructural observations.

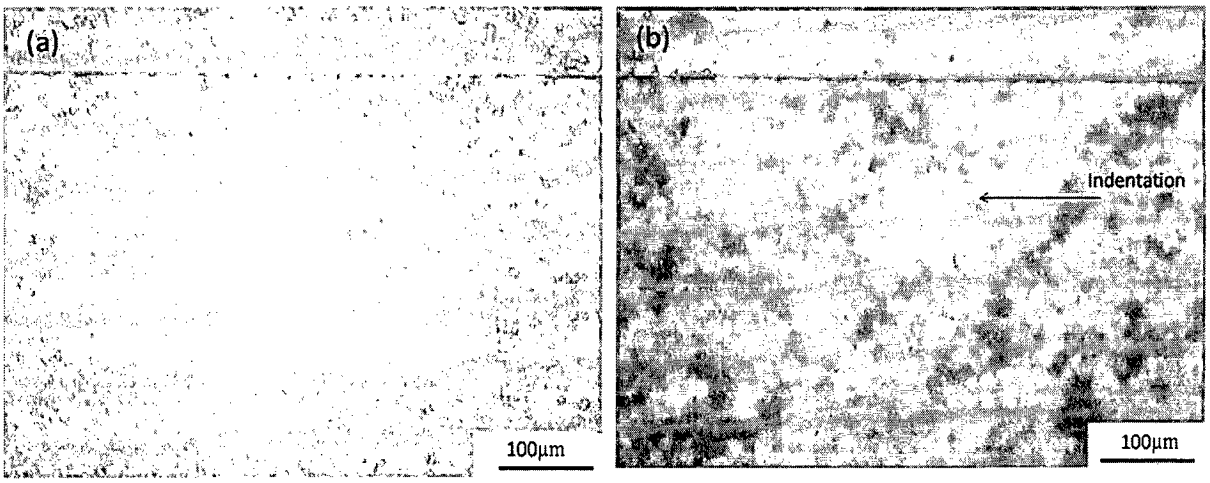

Fig.3.3 Optical micrographs of sintered samples (a) unpolished surface (b) unpolished surface with indentation impression.

Fig.3.3 (a) shows the unpolished surface of only Al_2O_3 sample after sintering at 1500°C. Fig.3.3 (b) shows the optical micrograph of the sample surface with indentation impression on the unpolished sample. In the Fig.3.3 (b) indentation is not visible which was not desirable to measure the indentation size of the sample. To overcome the problem the samples were ground using silicon carbide (SiC) paper in sequence of # 120, # 220, # 320 mesh sizes to have smooth surface finish. The samples after ground, polished with diamond pastes of two different grades of 6 and 3 μm sizes to get the surface to the level of near mirror finish.

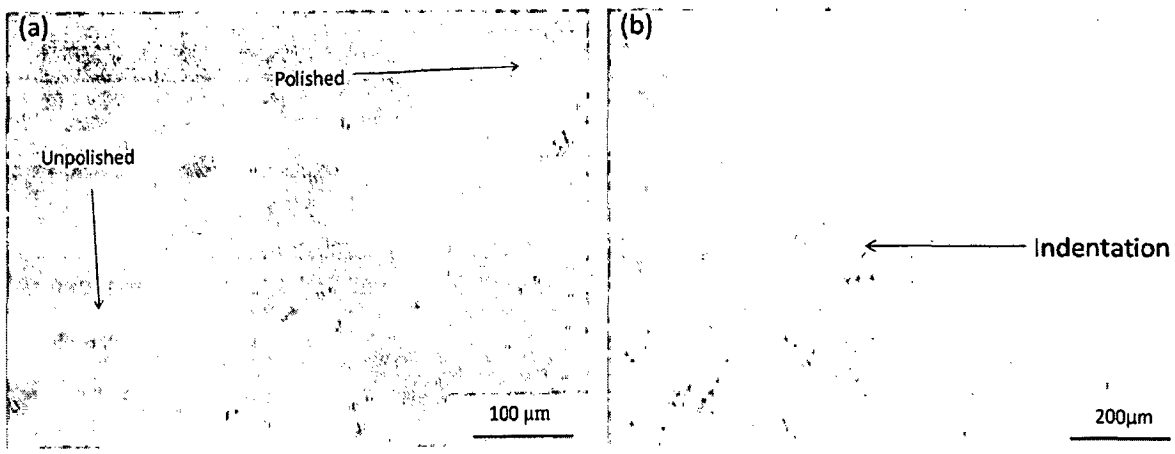

Fig.3.4. Optical micrograph of (a) polished and unpolished regions of the surface and (b) indentation in polished sample.

Fig.3.4 (a) shows the difference between the polished and unpolished surface areas of only Al_2O_3 samples. Fig.3.4 (b) shows the indentation mark on the polished area on the sample surface. Note that the indentation is much clears now, permitting accurate size measurement.

3.5 Hardness measurement

Hardness is a key attribute of ceramics. There are many pitfalls, controversies, new developments and some time surprises in the measurement of ceramic hardness. The hardness of ceramic is important for characterizing ceramic cutting tools, wear and abrasive parts, optical lens glasses, ballistic armor, molds and dies, valves and seals (Clinton and Morrell, 1987). Hardness characterizes the resistance of ceramics to deformation, densification, displacement and fracture. Densification is very important because it relates to micro porosity that is often present in sintered ceramics. The micro fracture and shear fracture under an indentation are also important. Hardness is usually measured with conventional micro indentation hardness machine using Knoop or Vickers diamond indentation. The Vickers hardness test has received fairly wide acceptance for research work. Polished samples in the form of pellet are mounted on Vickers indentation and then at different loads indentations are taken. Vickers indentation makes use of square base diamond pyramid as indenter. The angle between the two opposite faces of the indenter is 136°. The

microindentation (Yount, 2006). Vickers microindentation is specifically considered because it uses a sharp indenter that produces well-defined cracks. It has been reported that the fracture toughness values obtained with a Vickers indenter are independent of indentation load used (Gong et al., 2002). Cracks produced via Vickers indentation were first recognized as a potential fracture toughness evaluation technique by Palmqvist in 1962 (Palmqvist, 1962). Since then, many researchers have improved the initial work relating to the crack growth from Vickers indentation in brittle materials to fracture toughness. These cracks have been divided into two systems, classic median / radial (halfpenny) and Palmqvist cracks. The variables 'L', 'c' and 'a' are noticed in the Fig.3.6. The variable 'L' indicates the length of the diagonal of the indent. The variable 'a' indicates the length of crack from the tip of the indent to its termination in the material. The variable c is the sum of 'a' and 'L'/2 which is shown in Fig.3.6.

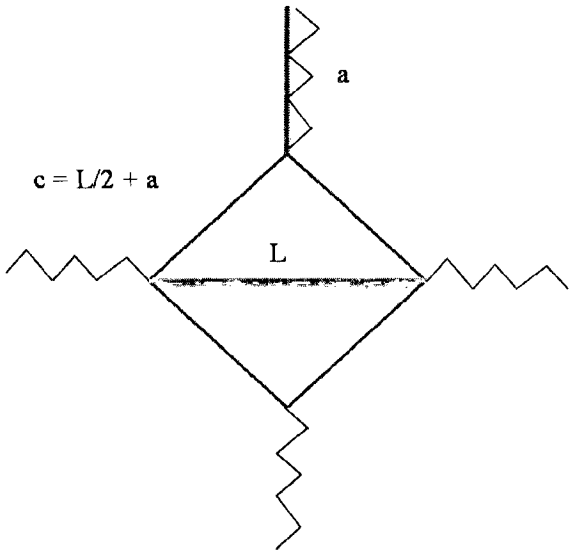

Fig. 3.6 Crack formation from the indent

There is not just one formula to determine fracture toughness from indentation, because the testing conditions and material response play important roles in determining toughness (Glandus et al., 1991). There are also some discrepancies between K_{IC} values determined by indentation techniques and those determined through more conventional methods. Proposed reasons for these differences include the dependence of crack geometry on the (i) applied

indentation load and (ii) microstructure of the sample, and the effects of some non-ideal indentation deformation/fracture behavior (lateral cracking, sub-critical growth of cracks, or phase transformation due to indentation) (Gong, 1999). Equations have been developed and refined to calculate fracture toughness, and more than 20 semi-empirical relationships have been proposed (Yount, 2006). These relationships can be classified into some general groups.

In the first group, fracture toughness is determined using the radial crack length and indentation load. Equilibrium equation for well-developed half-penny cracks were described by Lawn and Marshall (Lawn and Marshall, 1979) to be

$$K_{IC}\beta_o = P/c^{3/2} \tag{3.3}$$

where P is the applied load, c is crack length from the center of the indentation to the crack end, and β_o is an empirical value to account for geometry and is often set equal to 7 for a Vickers indenter. This equation is load independent because for any load applied the corresponding crack length will yield the correct fracture toughness value.

In the second group of equations, the hardness and diameter of the indenter are taken into consideration in order to account for plasticity necessary to remove stress singularities (stress at crack tip) at the indenter tip. For load-dependent materials tested with a Vickers indenter, Evans and Charles (Evans and Charles, 1976) determined this equation to be

$$K_{IC} = 0.016\, H_V\, L^2 / c^{3/2} \tag{3.4}$$

Where, H_V is the Vickers hardness. If the toughness of the material being tested is load independent, then Eq.3.1 can be substituted for $H_V L^2$ in Eq.3.4, and the equation becomes Eq.3.3.

Finally according to Anstis et al., the elastic modulus is taken into consideration by inserting the ratio $(E/H)^{0.5}$. For load-dependent materials the equation becomes (Anstis et al., 1981)

$$K_{IC} = 0.016\, (E/H_V)^{1/2}\, P / c^{3/2} \tag{3.5}$$

Where, E is the elastic modulus of the sample (Haldar et al., 2002, Basu et al., 2004, Yount, 2006).

3.6.2 Single edge pecracked beam (SEPB) test method

Bend tests are often employed to evaluate fracture toughness of materials because of ease of sample preparation and localization of stress. The tests are often conducted in three-point or four-point mode with fairly complex equation for calculating fracture toughness (Bowman, 2004).

3.6.2.1 Test fixture schematic

Fig. 3.7 shows the schematic view of three point test fixture. The samples were prepared following ASTM standard (ASTM C 1421). The outer span S_o of the test specimen was 20 mm. The cross head speed was kept 0.5mm/minute.

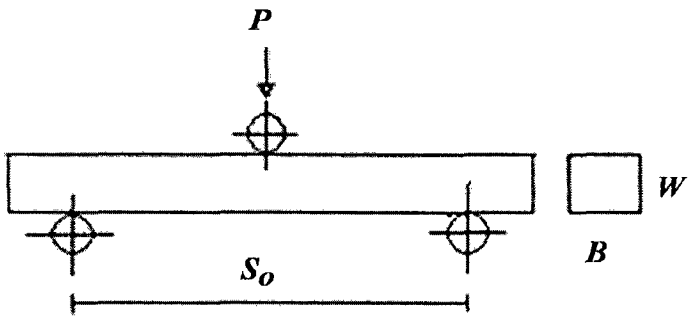

Fig.3.7 Schematic diagram of three point bend test

3.6.2.2 Measurement of fracture toughness

As discussed earlier fracture toughness was evaluated by Single-Edge Precracked Beam (SEPB) test method using three-point bending test with the help of following formula (ASTM C-1421). The Fig.3.8 shows the notched sample of the SEPB. The precrack length is between $0.2W$ and $0.30W$, where W is the test specimen height (Quinn et al., 2003).

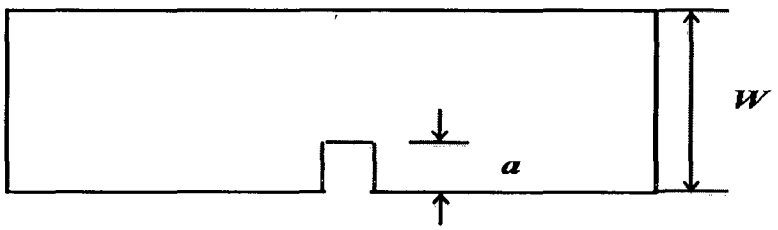

Fig. 3.8 Notch generated on samples

For the three point bend test, the fracture toughness by SEPB method is calculated as,

$$K_{Ipb} = g\left[\frac{P_{\max} S_o 10^{-6}}{BW^{3/2}}\right]\left[\frac{3(a/W)^{1/2}}{2(1-a/W)^{3/2}}\right] \quad (3.6)$$

Where,

$$g = g(a/W) = \frac{1.99-[a/W][1-(a/W)][2.15-3.93(a/W)+2.7(a/W)^2]}{1+2(a/W)}$$

g = Geometric correction factor which is function of *a/W* ratio

a = Notch length or pre-crack length

W = Thickness of sample

P_{max} = Load at fracture

S_o = Span between lower rollers

B = Breadth of sample

3.7 Characterization techniques

Both the microstructures and chemical compositions of the ceramics were analyzed by following techniques.

3.7.1 Microstructural investigations by field emission scanning electron microscope (FESEM)

Morphology, size distribution and other microstructural properties of the particles play a crucial role in determining the physical and chemical properties of the various materials (Sanyal et al., 2002, Carty and Senapati, 1998). Therefore microstructural properties of the materials for different compositions have been studied by using FESEM. In FESEM the electrons liberated from a field emission source and are accelerated in a high electrical field gradient. Within the high vacuum column these primary electrons are focused and deflected by electronic lenses to produce a narrow scan beam that bombards the object resulting in emission of secondary electrons from the object. These secondary electrons are registered by a detector which produces electronic signals. These signals are amplified and transformed to an image that can be seen on a monitor. There are two classes of electron emission source, which are thermionic emitter and field emitter. The emitter type is the main

difference between the Scanning Electron Microscope (SEM) and the Field Emission Scanning Electron Microscope (FESEM). Thermionic Emitters use electrical current to heat up a filament; the two most common materials used for filaments are Tungsten (W) and Lanthanum Hexaboride (LaB_6). When the heat is enough to overcome the work function of the filament material, the electrons can escape from the material. Thermionic sources have relatively low (i) brightness, (ii) evaporation of cathode material and (iii) thermal drift during operation. Field Emission is one way of generating electrons that avoids these problems. A Field Emission Gun (FEG) also called a cold cathode field emitter, does not heat the filament. The emission is reached by placing the filament in a high electrical potential gradient. The FEG is usually a wire of Tungsten (W) fashioned into a sharp point. The significance of the small tip radius (~ 100 nm) is that an electric field can be concentrated to an extreme level, becoming so high that the work function of the material is lowered and electrons can leave the cathode easily. In order to make the sample's surface conducting a thin (1.5 - 3.0 nm) layer of gold coating was applied on the surface. Further on, objects must be able to sustain the high vacuum and should not alter the vacuum, for example by losing water molecules or gasses. The coated samples were mounted on a holder which was inserted through an exchange chamber into the high vacuum part of the microscope and anchored on a moveable stage. The secondary electron emission detector (scintillator) is located at the rear of the object holder in the chamber. A schematic in Fig. 3.9 shows the working of a scanning electron microscope. When the primary beam bombards the surface of an object, secondary electrons are emitted from the object surface. The secondary electrons, which are attracted by the Corona, strike the scintillator fluorescent mirror that produces photons. The location and intensity of illumination of the mirror vary depending on the properties of the secondary electrons. The signal produced by the scintillator is amplified and transduced to a video signal that is fed to a cathode ray tube in synchrony with the scan movement of the electron beam. The contrast in the real time image that appears on the screen reflects the structure on the surface of the object. Parallel to the analog image, a digital image is generated which can be further processed.

The microstructural investigations of the samples in the present study were

carried out using FEI QUANTA 200 F models of FESEM. Samples were glued onto the sample holder with the help of both sided tape.

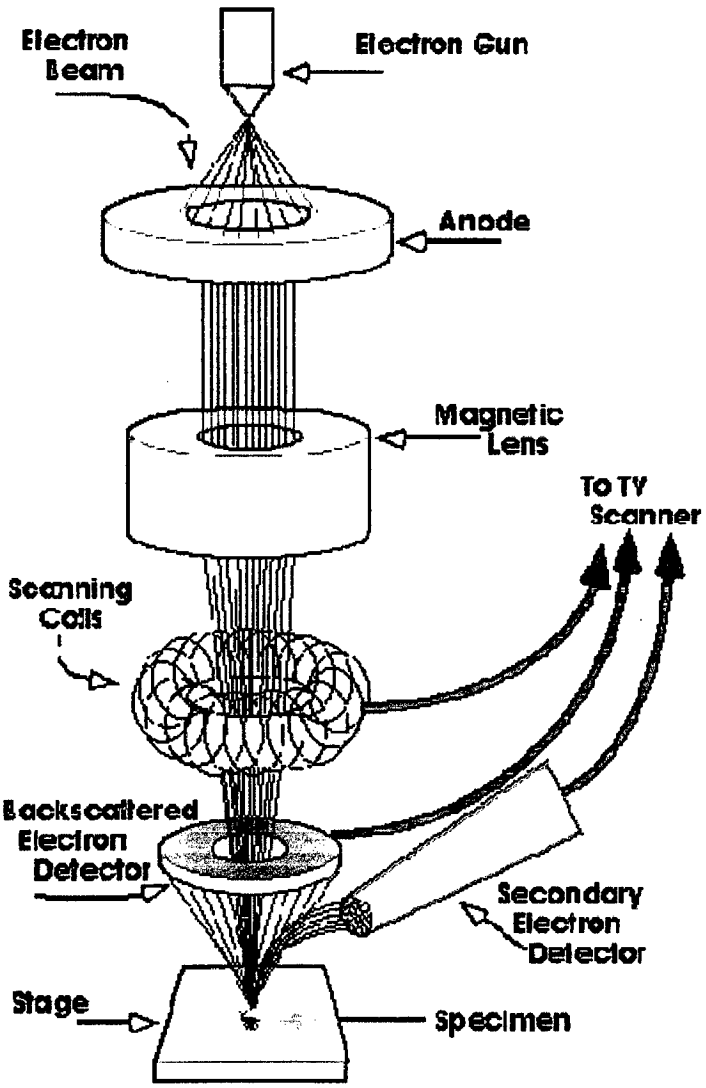

Fig. 3.9 Sketch showing the working of a Scanning Electron Microscope

3.7.2 X-Ray diffraction analysis

The sintered samples were subjected to X-ray diffraction study using X-ray diffractometer D8 Advance, Bruker AXS, Karlsruhe, Germany. The photograph of the equipment is shown in Fig.3.10(a). Scanning in the 2θ range of 10 - 90° using CuK_{α} radiation

is done and nickel filter is used. The step size and dwell time were suitably adjusted in order to obtain the good signal to noise ratio. The working principle of the presently used XRD unit is relatively simple. The specimen is rotated at constant angular speed in such a way that, as the angle of incidence of primary beam changes, the detector moves about the specimen at twice the angular speed. The diffraction angle (2θ) is thus always equal to double the glancing angle (θ). The beam path is shown in the Fig. 3.10(b). Whenever the Bragg condition, $2d\sin\theta = n\lambda$, is satisfied, the incident X-ray beam is diffracted at the specimen and reaches the detector. Where n is an integer, λ is the wavelength of incident wave, d is the spacing between the planes in the atomic lattice. The detector converts the X-ray quanta into electron pulses, which are recorded. Bruker D8 Advance diffractometer uses NaI scintillation counter as a detector. It can detect the diffracted radiations in the wavelength ranging from 0.5 to 3 Å. The monochromators are used to suppress the undesired portions of radiation. To restrict the irradiated specimen area, aperture diaphragm is arranged between the tube and the specimen as shown in Fig.3.10 (b). The second aperture diaphragm shields the strong scattered radiation of the first aperture diaphragm. The resolution depends upon the detector diaphragm. The scattered radiation diaphragm is used to suppress undesired scattered radiation. The essential condition which must be met if diffraction is to occur is given as

$$n\lambda = 2d \sin \theta$$

where n is the order of diffraction; it may take on any integral value consistent with $\sin \theta$ not exceeding unity and is equal to the number of wavelengths in the path difference between the rays scattered by adjacent planes. Therefore for a fixed value of λ and d, there may be several angles of incidence at which diffraction may occur. Phase analysis of the various samples was done using X'pert High Score plus software.

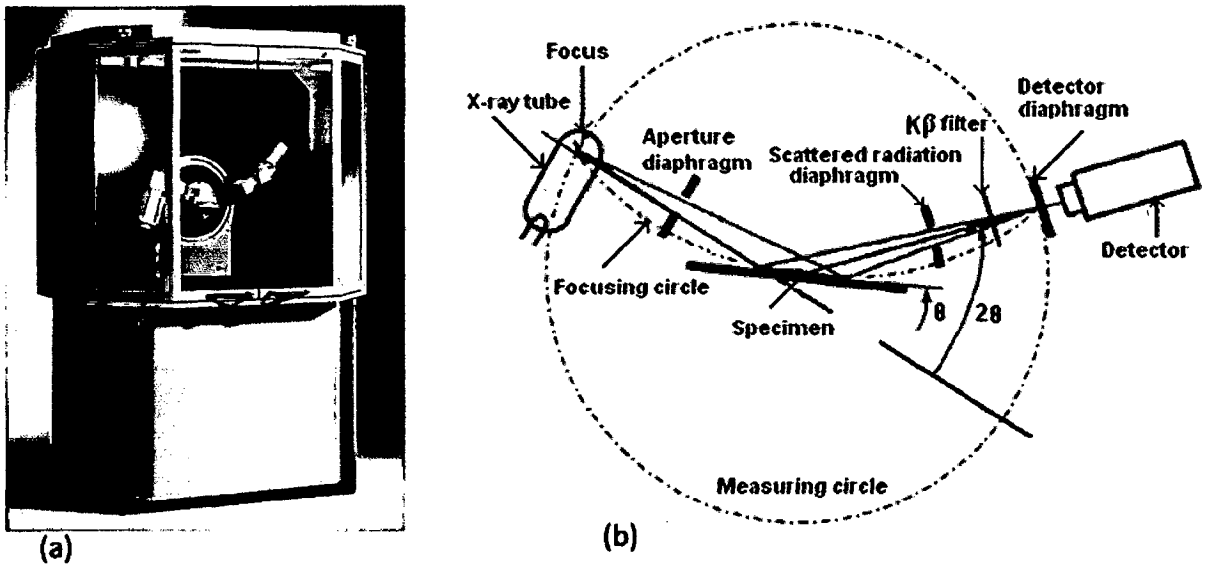

Fig.3.10 (a) Photograph of the XRD unit (Bruker AXS D8 Advance diffractometer) and (b) schematic diagram of beam path

3.7.3 Atomic force microscope (AFM)

The Atomic Force Microscope (AFM) or scanning force microscope (SFM) is a very high-resolution (0.01 nm) type of scanning probe microscope. Unlike traditional microscopes, the AFM does not rely on electromagnetic radiation such as photon or electron beams to create an image but is based on the interactive forces called the van der Waals force between the sample and the probe tip. It does not require vacuum environment or any special sample preparation, and can be used in either an ambient or liquid environment. For the present work, Atomic Force Microscope (NT-MDT Ntegra) has been used for the measurement of roughness of the fracture surface of the sample.

3.8 Sample nomenclature

Table 3.1 shows the identification of samples prepared with different composition of ZrO_2, $Y(NO_3)_3.6H_2O$ and $La(NO_3)_3.6H_2O$ in Al_2O_3. Throughout this report, the following nomenclature has been used for pure oxides and composites. The letter A stands for Al_2O_3, AZ represents Al_2O_3 - 5wt% ZrO_2 system, AZY represents Al_2O_3 - 5wt% ZrO_2 - 1000ppm $Y(NO_3)_3.6H_2O$ system, AZL represents Al_2O_3 - 5wt% ZrO_2 - 1000ppm $La(NO_3)_3.6H_2O$

system, AZLY represents Al_2O_3 - 5wt% ZrO_2 - 1000 ppm $Y(NO_3)_3.6H_2O$ - 1000ppm $La(NO_3)_3.6H_2O$. As shown in Table 3.1, for reference.

Table 3.1 Composition of the different Al_2O_3 - based ceramics

Sample identification	ZrO_2 (wt %)	Y_2O_3 (ppm)	$Y(NO_3)_3.6H_2O$ (ppm)	$La(NO_3)_3.6H_2O$ (ppm)
A	-	-	-	-
A1Y		1000		
A3Y		3000		
A5Y		5000		
A10Y		10000		
A15Y		15000		
AZ	5	-	-	-
AZY	5	-	1000	-
AZL	5	-	-	1000
AZYL	5	-	1000	1000

The sintering parameters i.e. temperature (°C) and soaking time period (hr) used are specified in the sample notations as superscript and subscript respectively e.g. $A_{t(hr)}^{T(C)}$. For example A_3^{1500} represents the pure Al_2O_3 sample sintered at 1500°C and soaked for 3 hr and AZ_3^{1500} represents the Al_2O_3 – 5wt% ZrO_2 ceramic composite sintered at 1500°C and soaked for a time period of 3 hr.

A flowchart sumarising the sample preparation and characterization is shown in Fig. 3.11 for clarity.

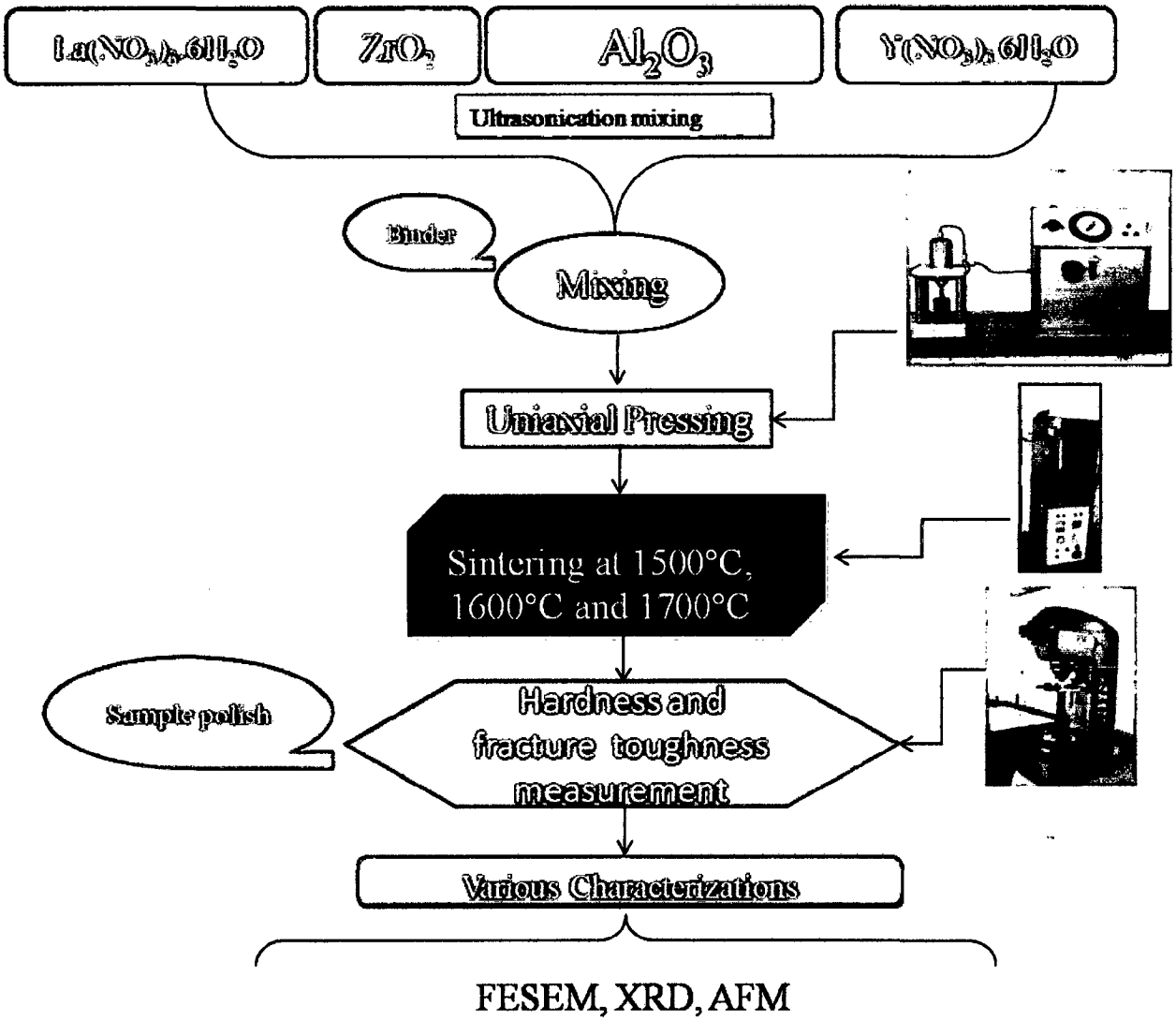

Figure 3.11 Flow diagram for formulation of problem

Chapter 4

Microstructure, hardness and fracture toughness of Alumina (Al_2O_3)

Chapter 4

4.1 Introduction

The most widely used ceramic material is Al_2O_3. One can say that Al_2O_3 is for a ceramist what iron is for a metallurgist and, to pursue the analogy further, that the Al_2O_3 – SiO_2 phase diagram is as important for ceramics as the iron-carbon phase diagram is for metals (Boch and Niepce, 2007).

Al_2O_3 has been chosen in the present study as a matrix of the ceramic composites for the following reasons. Al_2O_3 has several useful applications which have been discussed earlier in the chapter 1. Besides that the Al_2O_3 has the following advantageous properties:

- High compression strength
- High hardness
- Resistant to abrasion
- Resistant to chemical attack by a wide range of chemicals even at elevated temperatures
- Resistant to thermal shock
- High degree of refractoriness
- High dielectric strength
- High electrical resistivity even at elevated temperatures
- Low neutron capture cross section
- Raw material readily available with reasonable price

Chemical and thermal stability, relatively good strength, thermal and electrical insulation characteristics combined with availability in abundance have made Al_2O_3, an attractive material for engineering applications. Al_2O_3 has several allotropic forms but only the α- Al_2O_3 which has confirmed through XRD, is considered here. In its crystal structure the oxygen ions are in hexagonal close-packed (HCP) arrangement with aluminum ions occupied in the two third of the octahedral sites. Al_2O_3 does not deviate much from stoichiometry but even small level of impurity can influence high temperature diffusion rates greatly. Al_2O_3 has a melting temperature of about 2072°C, but impurities and alloying

elements from secondary phases that can melt at considerably lower temperatures (Auerkari, 1996).

Microstructural and morphological factors play leading roles in the emergence of properties of ceramic materials. For monolithic Al_2O_3, grains with the combination of smaller, larger sizes and high aspect ratio can produce an improvement in fracture toughness. This is because crack bridging and crack deflection mechanisms can be activated.

4.2 Characterization of raw materials

4.2.1 XRD analysis of green compacted sample

The most thermodynamically stable form is α- Al_2O_3 among the others forms of Al_2O_3. The γ-Al_2O_3 phase is stable up to 900°C but by heating above this temperature it converts into α-Al_2O_3 through a series of polymorphic transformations γ→δ → θ →α- Al_2O_3 (Kaplyanski et al., 1998).

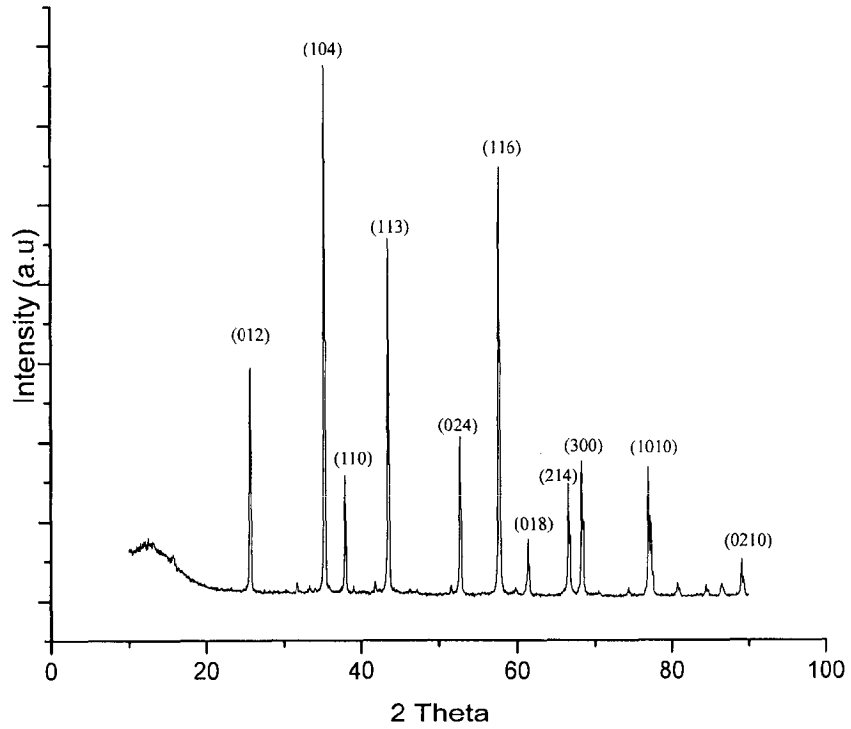

Fig.4.1 XRD patterns of Al_2O_3 powder used and α- Al_2O_3.

According to the XRD studies the parameter, such as observed peak maximum position is matched with α-Al_2O_3 (ICSD file No: 01-071-1683) peaks which has been given in Table 4.1 (Feret et al., 2000, Ishizawa et al., 1980). The sample was scanned between 2θ = 10 and 90° with an angular step of 0.02° and the dwell time for every step is 0.1 second.

Table 4.1 Comparison of as received Al_2O_3 and reported α-Al_2O_3 major XRD reflection

D (Å)		Relative Intensity		(hkl)		Angle 2θ (Cu $K_{\alpha 1}$)	
As received Al_2O_3 powder	α- Al_2O_3	As received Al_2O_3 powder	α- Al_2O_3	As received Al_2O_3 powder	α- Al_2O_3	As received Al_2O_3 powder	α- Al_2O_3
3.477	3.48	66.8	45	012	012	25.597	25.59
2.549	2.551	100.0	100.0	104	104	35.168	35.14
2.377	2.379	45.2	21	110	110	37.818	37.78
2.083	2.083	94.6	66	113	113	43.392	43.36
1.738	1.740	46.2	34	024	024	52.596	52.55
1.600	1.601	89.5	89	116	116	57.535	57.52
1.403	1.405	33.4	23	214	214	66.585	66.55
1.372	1.374	50.5	27	300	300	68.291	68.20
1.238	1.234	15.0	10.8	1010	1010	76.897	76.87
1.098	1.099	6.2	5.6	0210	0210	89.045	89.04

4.2.2 EDS analysis of powder

Chemical composition of the raw material was determined by EDS analysis of the powder.

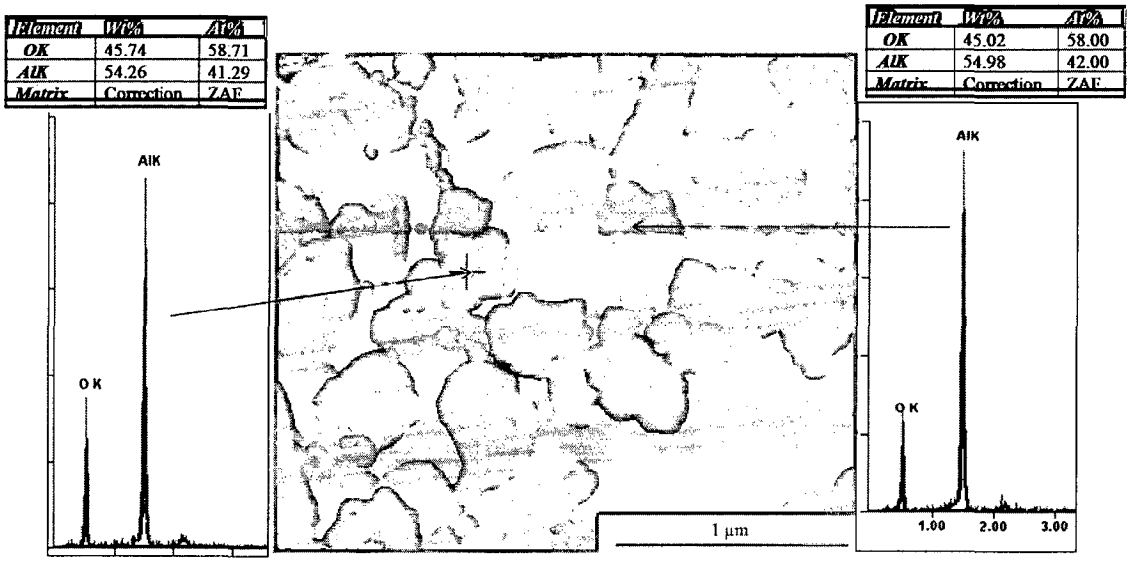

Fig.4.2 SEM micrograph and EDS spectra of as received Al_2O_3 powder.

Fig.4.2 shows the EDS of as received powder. It can be seen from the elemental analysis results at two different points on the microstructure that the atomic ratio between Al and O is close to 2:3 which is ideal for the Al_2O_3. It can also be observed that the signals from other elements are practically non-existent or negligibly low. Therefore the purity of the powder used is justified.

4.2.3 Comparison of density of the sample compacted by isostatic pressing and uniaxial pressing methods

The granulated powder was compacted in the form of rectangular bars and cylindrical pellets, uniaxially using a hydraulic press at different loads ranging between 7.5x 10^4 and 22.5x 10^4 N. A few green compacted samples were pressed by using isostatic press at a load of 150 MPa. Table 4.2 shows the density values of green compacted Al_2O_3 samples pressed by using uniaxial and isostatic press. The results show that the green density of Al_2O_3 increases with increasing load used in the uniaxial press. The samples compacted with the load between 15 x 10^4 N to 22.5 x 10^4N show the identical green density and sintered density

for both uniaxially and isostatically pressed samples. Therefore the samples for further investigations were prepared using uniaxial pressing method.

Table 4.2 Density of green compact Al_2O_3 samples prepared using uniaxial and isostatic pressing.

Compaction load, uniaxial (10^4 N)	Green density (gm/cc)		Density of sintered sample (gm/cc)	
	Uniaxially pressed sample	Isostatically pressed sample	Uniaxially pressed sample	Isostatically pressed sample
7.5	2.22	2.27	3.66	3.83
10	2.28	2.44	3.69	3.86
12.5	2.27	2.34	3.72	3.86
15	2.47	2.50	3.89	3.92
17.5	2.48	2.54	3.91	3.91
20	2.50	2.51	3.91	3.92
22.5	2.53	2.56	3.92	3.93

4.2.4 Sintering of ceramics

Sintering of ceramic materials is the method involving the heating the green compact ceramic powdered sample to a high temperature (below the melting point of the material) at which the material of one particle starts diffusing to another neighbouring powder particles. The decrease in porosity of the sample, caused by the sintering, is determined by the level of the porosity in the green compact, sintering temperature and soaking time period. The Fig.4.3 shows the porosity of Al_2O_3 samples sintered at 1200°C, 1300°C, 1400°C, 1500°C, 1600°C and 1700°C for the soaking time period of 12hr. The porosity lavels found in the sintered samples are approximately 40%, 27%, 1.5%, 1.25% and 1.25% at the sintering temperatue of 1200°C, 1400°C, 1500°C, 1600°C and 1700°C respectively. Porosity and density of the ceramics are important for their applications related to mechanical properties. The samples sintered at 1500°C and higher temperatures show desirable density suitable for the good

mechanical properties. The change of grain size and shape at different sintering temperature and for different soaking time periods influences to change the fracture toughness of the samples.

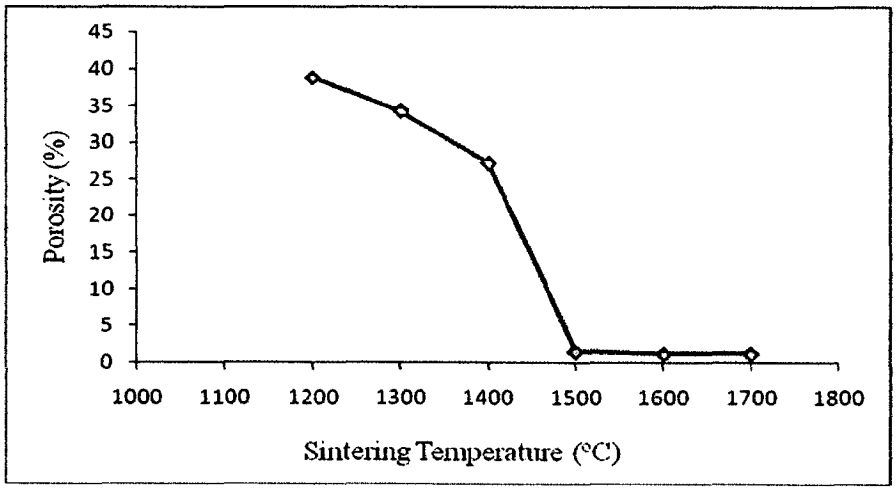

Fig.4.3 Porosity vs. sintering temperature for Al_2O_3 samples sintered for the soaking time period of 12hr.

4.3 Physical properties of Al_2O_3

4.3.1 Weight Loss

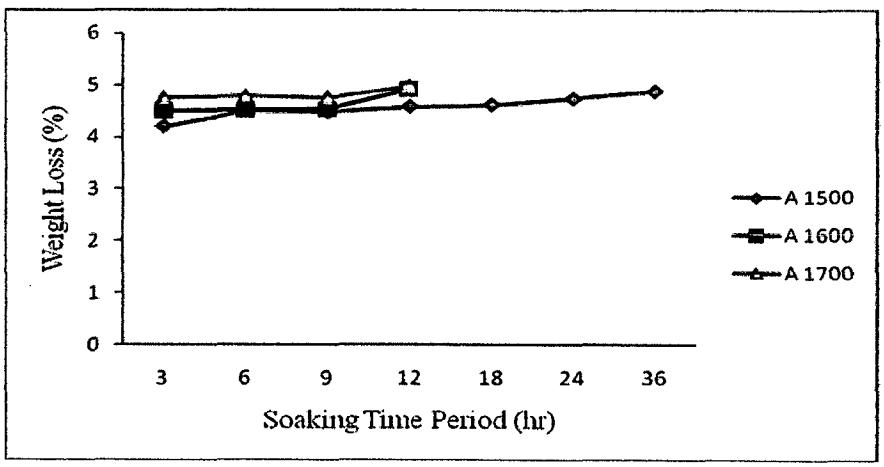

Fig.4.4 Weight loss of Al_2O_3 sample as a function of soaking time period for the samples sintered at 1500°C, 1600°C and 1700°C.

Weight loss of the samples has been estimated from the weight measurement of the samples before and after sintering. The nomenclatures A1500, A1600 and A1700 in the graph represent the Al_2O_3 sintered at 1500°C, 1600°C and 1700°C respectively. Fig.4.4 shows that the weight loss increases slightly with increasing soaking time period. The samples sintered at 1600°C show the weight loss almost remains same with increasing soaking time period. The samples sintered at 1700°C also show there is no change in weight loss with increasing soaking time period. The samples sintered at 1600°C and 1700°C shows the identical weight loss with increasing soaking time periods. Weight loss has occurred due to the loss of water molecules, organic binder and formation of volatile matters. The chemical reactions promoting weight loss are endothermic solid-gas reactions occurring on the powder surface (Hue et al., 1997).

4.3.2 Density

Table 4.3 Density of Al_2O_3 samples sintered at 1500°C, 1600°C and 1700°C for different soaking time periods.

Temperature (°C)	1500°C				1600°C				1700°C			
Soaking time (hr)	3hr	6hr	9hr	12hr	3hr	6hr	9hr	12hr	3hr	6hr	9hr	12hr
Density (gm/cc)	3.84	3.89	3.91	3.91	3.90	3.91	3.91	3.92	3.90	3.92	3.93	3.92
Relative density (%)	96.72	97.98	98.49	98.49	98.24	98.49	98.49	98.74	98.24	98.74	98.99	98.74

Table 4.3 shows the absolute density and relative density values of the Al_2O_3 samples sintered at 1500°C, 1600°C and 1700°C for different soaking time periods. The density was determined by Archimedes principle as described in the Chapter 3. The table shows that the absolute density and the relative density of the sample vary with the variation of the sintering

temperature and the soaking time periods. The samples sintered at 1500°C for the soaking time period of 3hr show lower density and relative density than that of the samples sintered at 1600°C and 1700°C for which the density and relative density are almost identical. The densification occurs with reducing pore volume. Grain growth of the samples sintered at higher temperature leads to better grain to grain connectivity and lower porosity (Durrani et al., 2006).

4.3.3 Linear shrinkage

Table 4.4 Linear shrinkage of Al_2O_3 samples in rectangular shape sintered at 1500°C, 1600°C and 1700°C for different soaking time periods.

Temperature (°C)	1500°C				1600°C				1700°C			
Soaking time (hr)	3	6	9	12	3	6	9	12	3	6	9	12
Linear shrinkage (%)	13.19	13.41	13.54	13.3	13.6	13.59	13.53	13.6	13.7	13.6	13.71	13.6

The Table 4.4 shows that the linear shrinkage of the samples sintered at 1500°C, 1600°C and 1700°C for different soaking time periods. The linear shrinkage of the sintered samples remains almost same for all the sintering temperatures. The shrinkage of the samples depends on the some factors like compaction pressure sintering condition and composition. The occurrence of densification increases the shrinkage. The occurrence of densification increases the shrinkage. Shrinkage is the most apparent physical change to take place when a green ceramic compact is fired. The linear shrinkage of Al_2O_3 is about 20% and dimensions may vary by up to ±1% (Smallman and Bishop, 2002).

4.4 Analysis of microstructure

4.4.1 Effect of sintering temperature and soaking time on microstructure of Al_2O_3 samples

Microstructure of the sintered Al_2O_3 is largely dependent on the sintering temperature and soaking time.

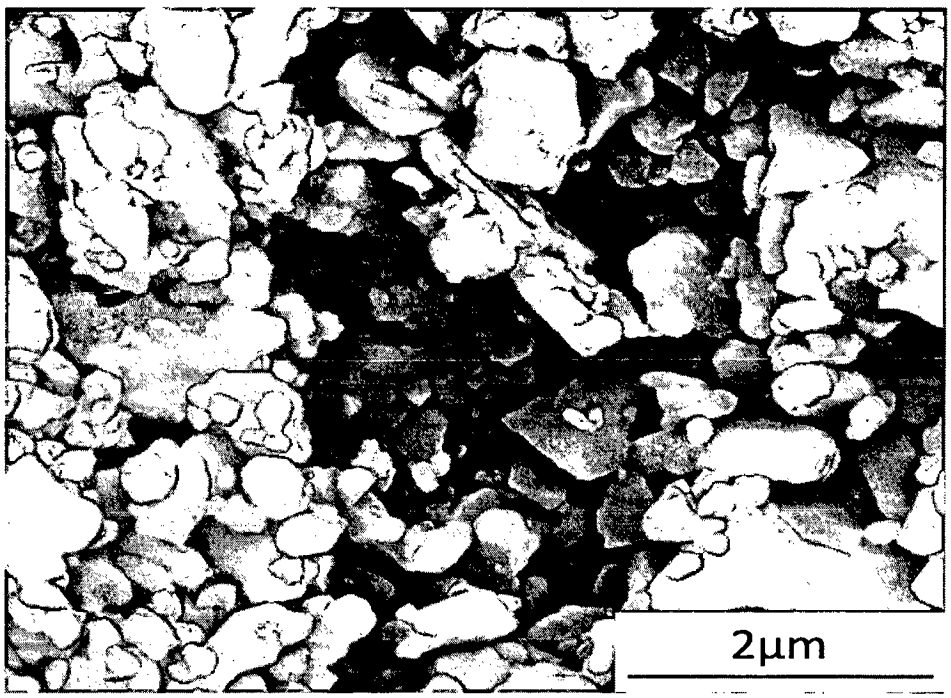

Fig.4.5 SEM micrograph of green compacted Al_2O_3 powder.

Fig.4.5 is the micrograph of green compact of Al_2O_3 powder. This micrograph has been shown to provide a basis of comparing the microstructural changes in the sample with sintering temperature and soaking time periods. The lenticular surface area between the particles seen in the green compact gradually vanishes as the samples are sintered for more and more soaking time. The surface feature (Fig.4.6) of the samples sintered for 18 and 24 hrs show patch like appearance for a few grains which appear to have grown extensively. Although the intervening or intergranular spaces between the largely grown grains are filled with smaller grains.

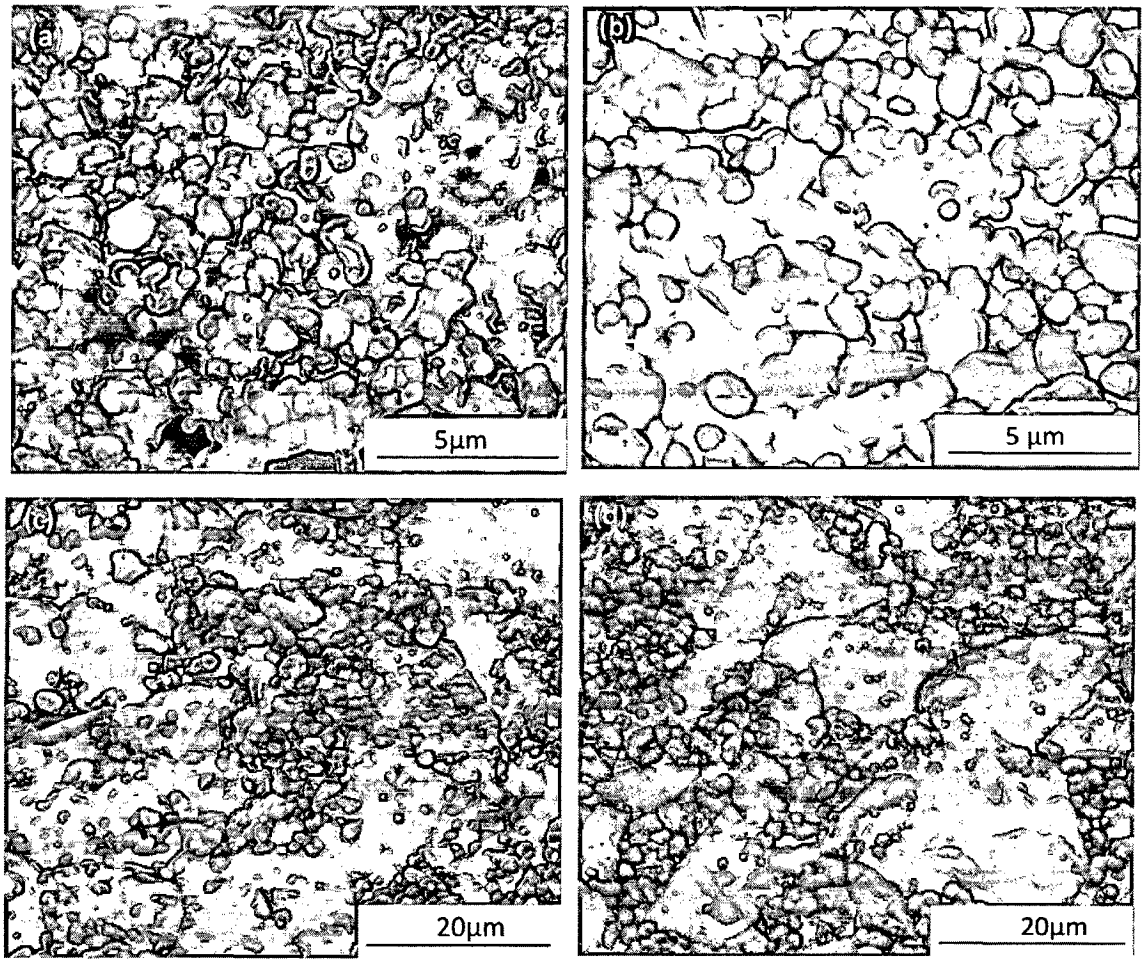

Fig.4.6 SEM micrograph of Al_2O_3 powder compact sintered at 1500°C for (a) 3hr, (b) 6 hr, (c) 18 hr and (d) 24hr.

Fig.4.6(a,b,c,d) show the SEM micrographs of Al_2O_3 samples sintered at 1500°C for four different soaking time periods of 3hr, 6hr, 18hr and 24hr. The micrographs in Fig.4.6 show the increase in average grain size with the increase in soaking time period. The estimated grain sizes are given in Table 4.5. As evident from the micrographs, the samples consist of grains having varied sizes. The grains in the Fig. 4.6(a) are smaller and have almost rounded shape. It can be observed from the Fig.4.6(a) that at some regions the grains tend to join together to give rise to larger grains. The estimated grain size varies between 0.22 and 1.29μm giving an estimated average grain size of 0.688 μm.

Fig.4.6(b) shows that the average grain size is slightly bigger than that in Fig.4.6(a). The grains are of mixed sizes. The smaller grains are of rounded shape and relatively larger grains appear to be of elongated. The range of grain size is 0.33-1.91μm and the average grain size is 0.837 μm. In Fig.4.6(c) and (d), the occurance of exaggerated grain growth is evident. The larger grains are seen to have been developed from a number of smaller grains joined preferentially by surface diffusion process. The larger grains are also seen surrounded by a number of well separated smaller grains. The average grain sizes are 4.81 and 4.93 μm for A_{18}^{1500} and A_{24}^{1500} samples respectively. As can be observed from Table 4.5, that exaggerated grain growth occurs in the samples sintered at 1500°C for a soaking time period of 18 hr, 24 hr, 36 hr. Therefore a large grain size difference is resulted in all the samples sintered at 1500°C and soaking for 18, 24 and 36hr.

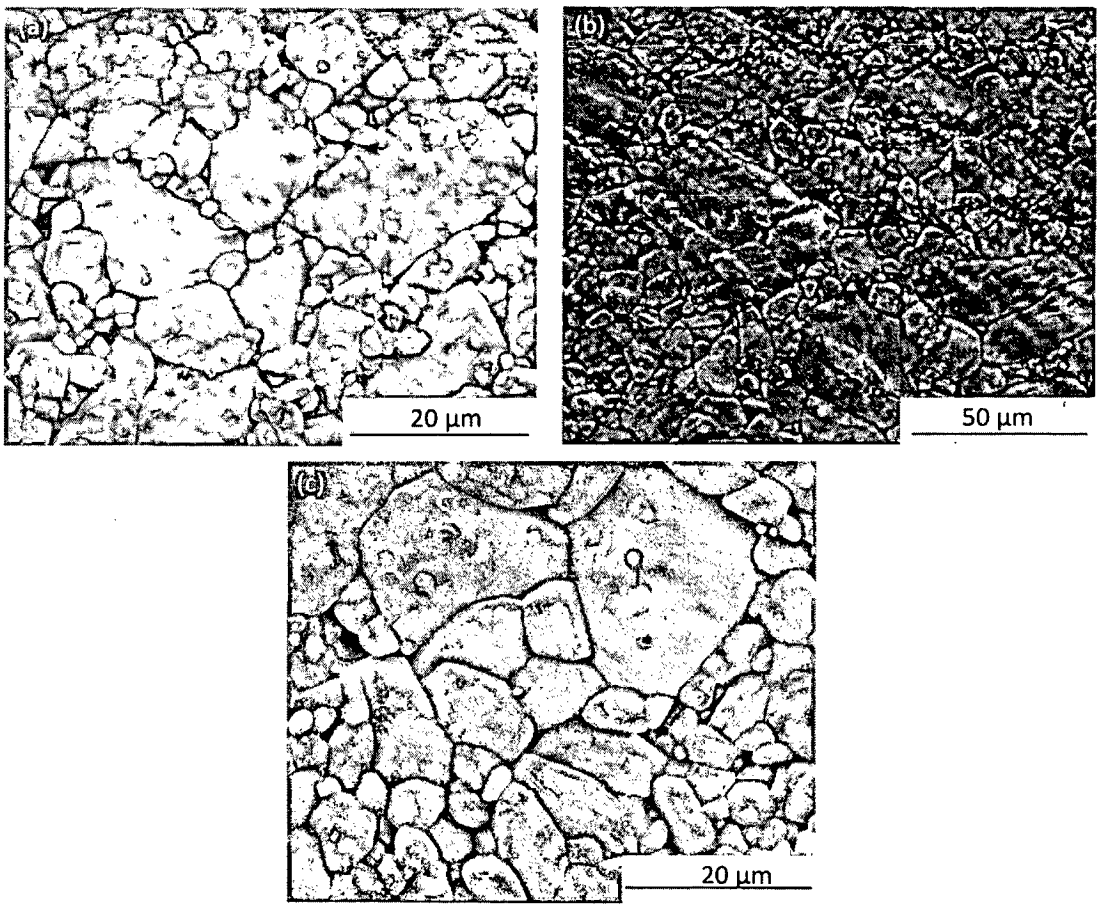

Fig.4.7 SEM micrograph of Al_2O_3 compact sintered at 1600°C for (a) 3hr, (b) 9 hr and (c) 12 hr.

Fig.4.7 ((a) - (c)) show the SEM micrographs of Al_2O_3 samples sintered at 1600°C for the soaking time periods of 3hr, 9hr and 12hr. The average grain size increases with increasing soaking time period. The average grain size and the grain size range in the samples sintered at 1600°C are larger compared to that in the samples sintered at 1500°C for identical soaking time period. It can be seen from the Fig.4.7 that the microstructure consists of thin grain boundaries compared to that in the samples sintered at 1500°C. Fig.4.7(a) shows the combination of smaller and larger grains with a size variation lying in the range of 1.52 to 21.44μm with an average grain size of 5.35μm. Fig. 4.7(b) shows the larger and smaller grains with a few larger grains having high aspect ratio and this microstructure is suitable to offer crack bridging as one of the possible mechanisms for the enhancement in fracture toughness, which has been discussed later (in the section 4.5.2.1). In Fig 4.7(c) the grain size has rather a wide range of variation from 2.80 to 25.80μm giving rise to an average grain size of 6.07μm. As the micrographs show multimodal distribution of grain size, the detailed variation in the grain size of the samples prepared has been worked out in the form of histograms in all the cases. A few of such histograms are presented in Fig.4.10.

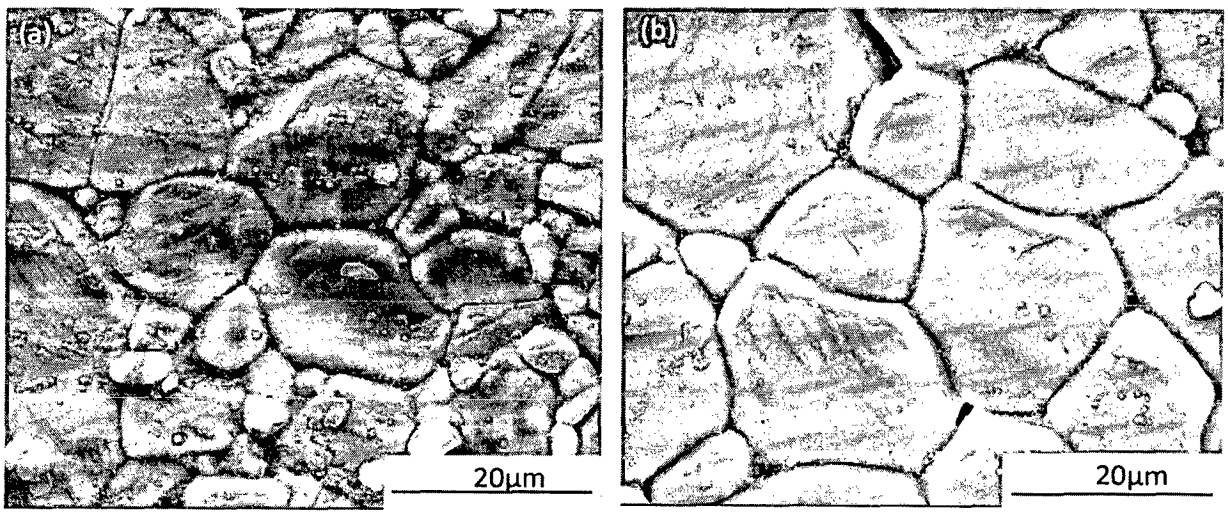

Fig.4.8 SEM micrographs of Al_2O_3 sintered at 1700°C for (a) 3h and (b) 12 hr.

Fig.4.8((a) – (b)) show the SEM micrographs of Al_2O_3 samples sintered at 1700°C for 3hr and 12hr respectively. Fig.4.8(a) shows that the grains are of equiaxed and polygonal type. The range of grain size is 2.99 - 26.39μm and the average grain size is 7.30μm. Fig.4.8(b)

shows that majority of the grains are larger and equiaxed. The range of grain size is 4.31-41.21μm and the average grain size is 17.11 μm.

Table.4.5 Average grain size, grain size range and grain size difference of pure Al_2O_3 samples sintered at 1500°C, 1600°C and 1700°C.

Sample	Average grain size (d) (μm)	Grain size range (μm)	Grain size difference (μm)
A_3^{1500}	0.688	0.22-1.29	1.07
A_6^{1500}	0.837	0.33-1.91	1.58
A_9^{1500}	0.843	0.37-1.95	1.58
A_{12}^{1500}	0.939	0.41-1.99	1.58
A_{18}^{1500}	4.81	1.03-16.89	15.86
A_{24}^{1500}	4.93	1.30-17.63	16.33
A_{36}^{1500}	4.97	1.33-19.56	18.23
A_3^{1600}	5.35	1.52-21.44	19.92
A_6^{1600}	5.42	2.20-21.82	19.62
A_9^{1600}	5.57	2.73-22.63	19.9
A_{12}^{1600}	6.07	2.80-25.8	23
A_3^{1700}	7.30	2.99-26.39	23.4
A_6^{1700}	13.75	3.25-33.50	30.25
A_9^{1700}	15.46	3.68-40.92	37.24
A_{12}^{1700}	17.11	4.31-41.21	36.9

Table 4.5 shows that the average grain size increases with the increase in the sintering temperature and soaking time period. The grain size range for the samples is low in the sample A_3^{1500}. The lowest and the highest ranges of grain size are 0.22 – 1.29 μm and 4.31 – 41.21 μm for the samples A_3^{1500} and A_{12}^{1700} respectively. The grain size difference of the sintered samples increases with increasing sintering temperature and soaking time periods. The Fig.4.9 (a) shows the grain size increases with increasing soaking time period only upto 18hr and above that the change in grain size is very small. Fig. 4.9 ((b) and (c)) show for the samples sintered at 1600°C and 1700°C respectively, the grain size increases with increasing soaking time period.

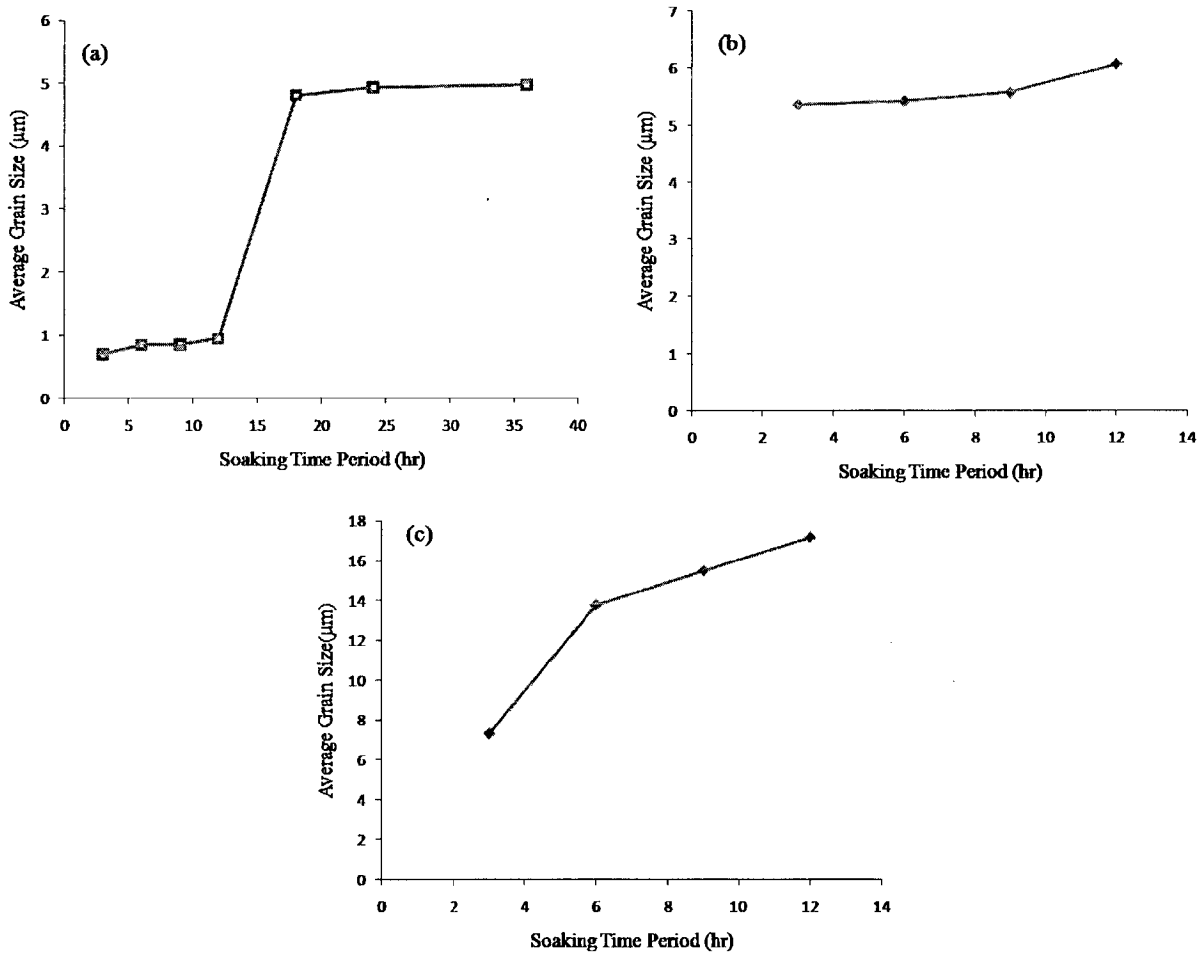

Fig.4.9 Average grain size vs. soaking time period for the samples sintered at (a) 1500°C, (b) 1600°C and (c) 1700°C for different soaking time periods.

4.4.2. Grain size histogram of the sintered Al_2O_3 samples

As the grains in all the samples vary over a range of size rather than preferably having uniform size for a particular sintering schedule, it is appropriate to show the actual size distribution that has been resulted. The measured grain sizes were subdivided into small size intervals and plots were made in the form of histograms to show the grain size distribution. Fig.4.10 presents a few of such histograms for the samples sintered at 1500°C, 1600°C and 1700°C. It can be seen from the Fig. 4.10(a) that though the grains in the sample are of different sizes varying from about 0.3 to about 1.9μm, a large number of grains fall between 0.7 and 1.1μm. However, the grains are significantly smaller in this case (A_9^{1500}) compared to those in other samples shown in the histogram plots. Similarly the Fig. 4.10((b) and (c)) show that though there is a wide variation in the grain size of the samples, a large number of grains fall in the size range of 1 to 4μm according to the Fig.4.10(b) and in 1 to 8μm corresponding to the Fig. 4.10(c). Therefore the grain size distribution in Fig. 4.10((a)-(c)) can approximately be taken as bimodal type. However discontinuities in grain size variation are observed over 6 to 18 μm in Fig. 4.10(b) and 8 to 25 μm in Fig.4.10(c). Whereas, no clusters showing relatively uniform grain size as has been found in Fig. 4.10((a)-(c)), can be observed in Fig. 4.10(d) which implies that the grain size distribution in Fig. 4.10(d) is rather more wide and the distribution can be treated far from bimodal type. The grain size variation in Fig. 4.10(d) is discontinuous across the entire grain size range.

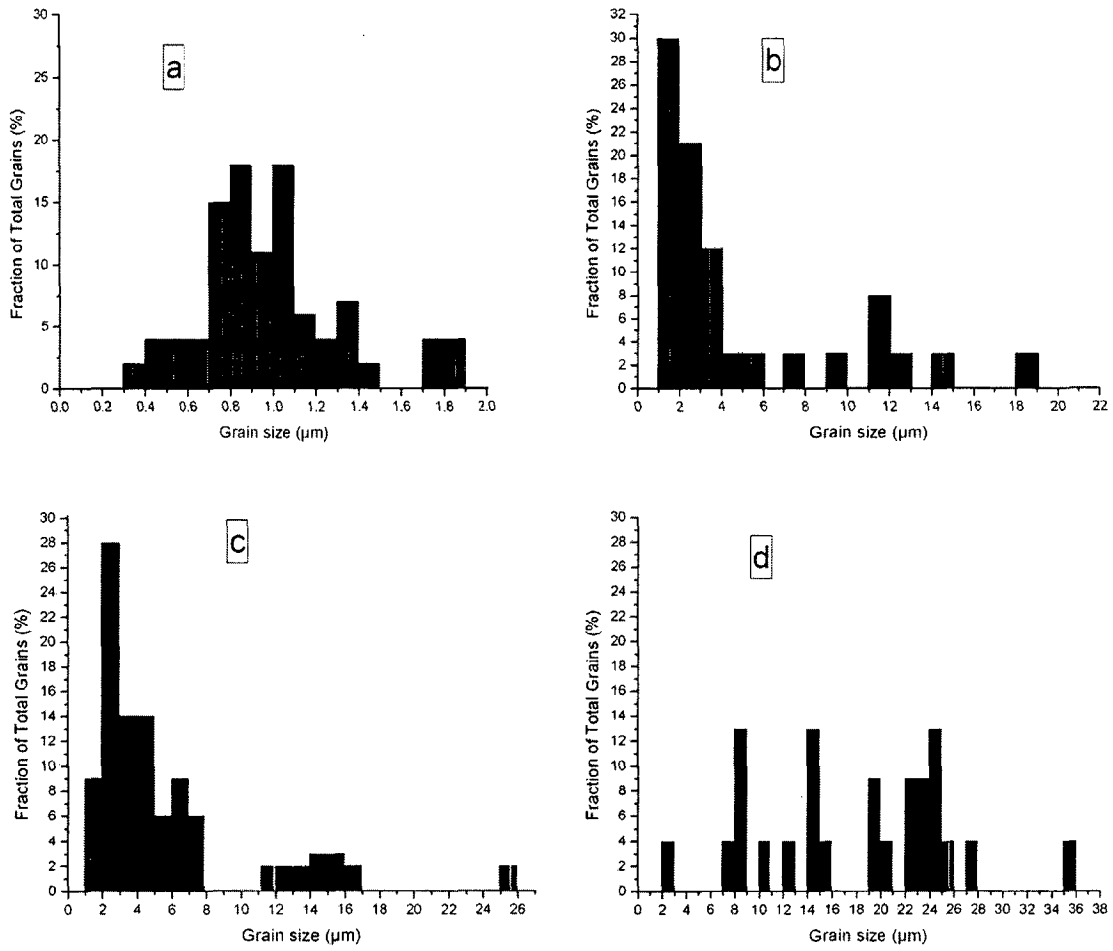

Fig.4.10 Grain size histograms for the samples of (a) A_9^{1500}, (b) A_{18}^{1500}, (c) A_9^{1600}, (d) A_9^{1700}.

4.5 Effect of mechanical properties of Al_2O_3 sintered at different temperatures for different soaking times

4.5.1 Hardness of the sintered Al_2O_3 samples

The influence of sintering temperature and soaking time period on hardness of Al_2O_3 ceramics has been investigated.

4.5.1.1 Effect of soaking time period on hardness

Fig. 4.11((a) – (c)) show the hardness of the samples as a function of soaking time period. Fig.4.11 (a) shows the hardness decreases with increasing soaking time periods and the hardness values of the samples sintered at 1500°C varies from 8.7 to 15.52 GPa. Fig.4.11 (b) shows the hardness of the samples sintered at 1600°C decreases slightly with increasing soaking time period. The hardness of these samples varies from 7.68 to 8.64 GPa. Fig.4.11 (c) also shows the hardness of the samples sintered at 1700°C marginally vary with increasing soaking time period. The hardness of these samples varies from 6.56 to 7.74 GPa.

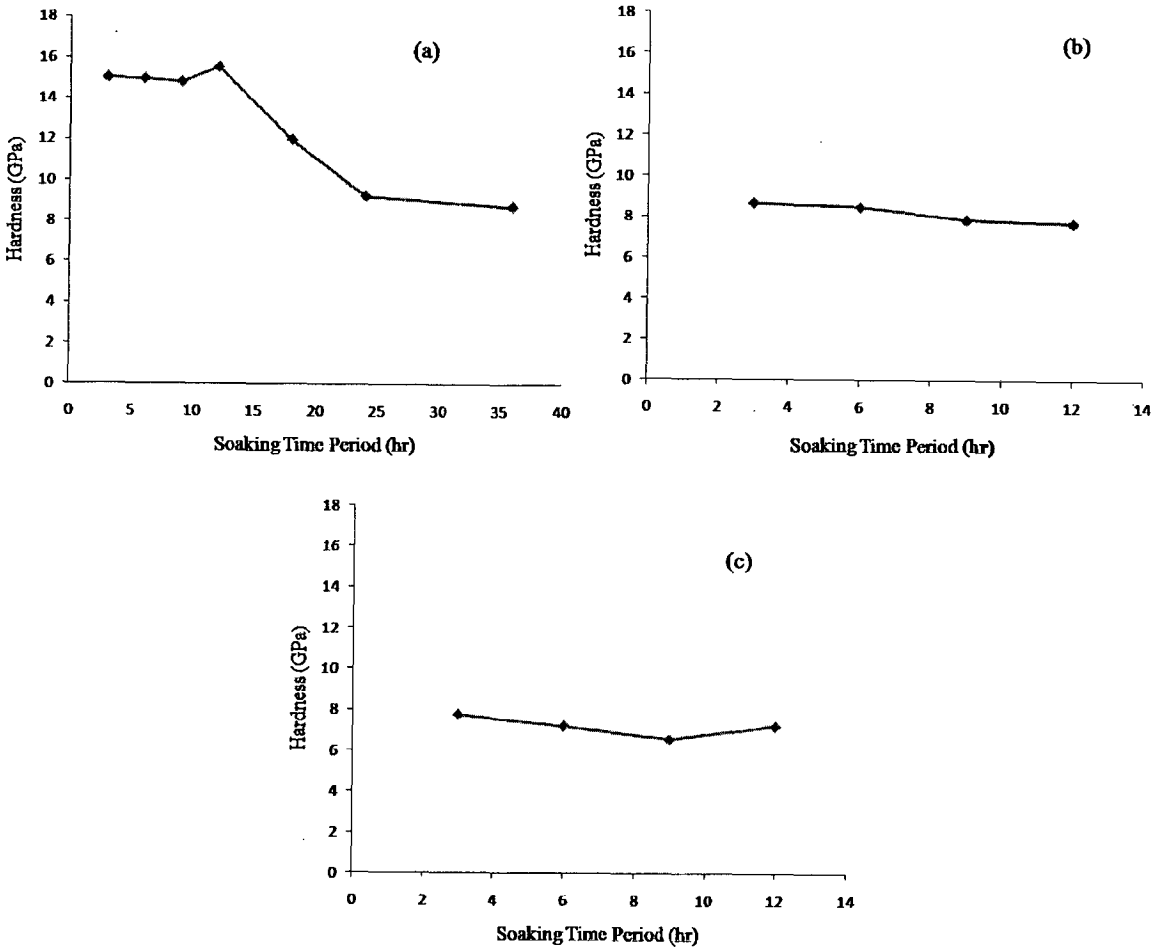

Fig.4.11 Hardness of Al_2O_3 samples sintered at (a) 1500°C, (b) 1600°C and (c) 1700°C as a function of soaking time period.

4.5.1.2 Effect of grain size on hardness

Different parameters like processing condition (in air or inert condition), sintering parameter (sintering temperature and soaking time period) may change the grain size. The grain size affects the dislocation movement and which changes the mechanical properties like hardness. Decreasing the grain size increases the amount of possible pile up of dislocation at grain boundaries, requiring the increased amount of applied stress necessary to move a dislocation across a grain boundary. The theory is that more grain boundaries create more opposition to dislocation movement and in turn strengthens the material. There is a domain in the grain size range under which the theory of grain boundary strengthening is valid (Callister, 1995, Kashyap and Chandrashekar, 2001).

4.5.1.2.1 Fitting the hardness data into Hall Petch type equation

The dependence of hardness on the grain size of the samples has been shown through Hall-Petch type relationship. The plot has been made between the Hardness and $d^{-1/2}$ in the Fig.4.12. The hardness measurements for all the samples were made at different indentation loads varying from 5 to 40 kgs. However, the Hall-Petch plots for all the samples have been made using the hardness data obtained with an indentation load of 5 kg. The hardness value as high as 15.52 GPa for the sample $A_{12}{}^{1500}$ is obtained at an indentation load of 40 Kgs (Tani et al., 1986). The entire hardness data set as can be examined from the Fig.4.12, can be divided into two distinctly different ranges of (i) 9.34 to 12.42 GPa and (ii) 5.2 to 8.4 GPa.

The Hall-Petch type relationship as given by the following equation

$$H_{v,m} = H_{v,0} + k_{v,hp} d^{-1/2} \qquad (4.1)$$

where, $H_{v,m}$ is the measured hardness by Vickers indentation method; $H_{v,0}$, the reference hardness i.e. the hardness of the material in its single crystal form and d, the mean grain size of the material. k_v, a proportionality constant. A smooth linear fitting of the points Fig.4.12 gives two distinct linear graphs marked Line1 and Line2 which can be expressed by mathematical equations (4.2) and (4.3) respectively as given below,

$$H_v = 10.86\, d^{-1/2} + 2.532 \qquad (4.2)$$

$$H_v = 4.337 d^{-1/2} + 7.420 \qquad (4.3)$$

Hall-Petch equation 4.4 given below, describes the effect of grain size on the strength of materials.

$$\sigma_y = \sigma_o + k_y d^{-1/2} \qquad (4.4)$$

where, σ_y is the tensile yield strength; σ_o, the reference strength, k_y, a proportionality constant (Hah et al.,1995, Courtney, 1990, Miyahara et al., 1994).

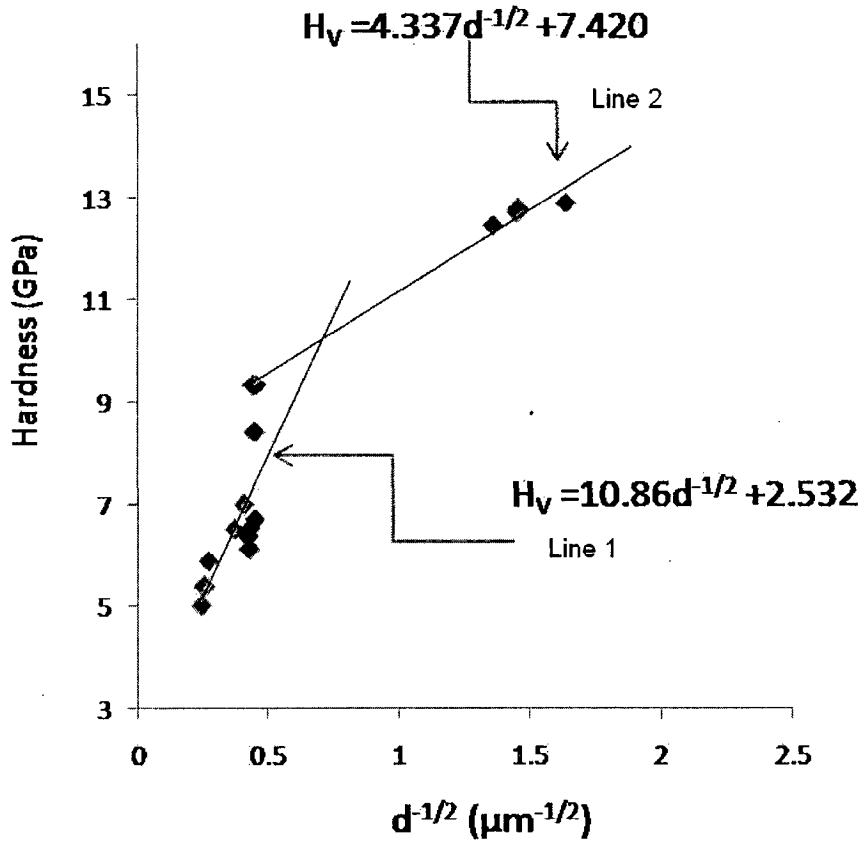

Fig.4.12 Grain size dependent hardness of Al_2O_3 ceramics

It can be seen from the Fig.4.12 that the hardness variation with $d^{-1/2}$ in Line1 (i.e. over one range of data) significantly differ from that in Line2 (i.e. over another data set). The two linear fits give a point of intersection at H_v = 10 GPa and $d^{-1/2}$ = 0.8 $\mu m^{-1/2}$ with d = 1.56 μm. It can be seen that the deviation of hardness data points from the linear fit is more for Line 1 compared to that for Line 2. This signifies that hardness data for the samples having larger grains have more scattering than that of samples having relatively smaller grains.

4.5.1.3 Reverse Indentation Size Effect

The indentation size effect (ISE) is a phenomenon that the hardness is load dependent and the gradual lowering of hardness results in with the increase in indentation load. The usual trend of the ISE is that the microhardness decreases with increase in applied test load. However, the ISE is valid upto a certain maximum load (5 kg) beyond which the reverse indentation size effect (RISE) is observed. RISE refers to the increase in hardness with increase in applied load (Gong et al., 1999).

The hardness measurements for each sample were made at several points on the surface with different indentation loads. The average hardness data of the samples sintered at 1500°C for different soaking time periods of 6hr, 12hr, 18hr and 24hr, taken at different loads have been plotted against the applied load as shown in Fig.4.13. These plots show an overall increase in hardness with increase in indentation load and this behaviour is shown by smooth linear fittings of the data points. It can be seen from the Fig. 4.13 that considerable deviations of the data points exist from the linear fit for the sample A_{24}^{1500}. However, for other three samples i.e. A_3^{1500}, A_{12}^{1500} and A_{18}^{1500} the linear fitting is relatively better.

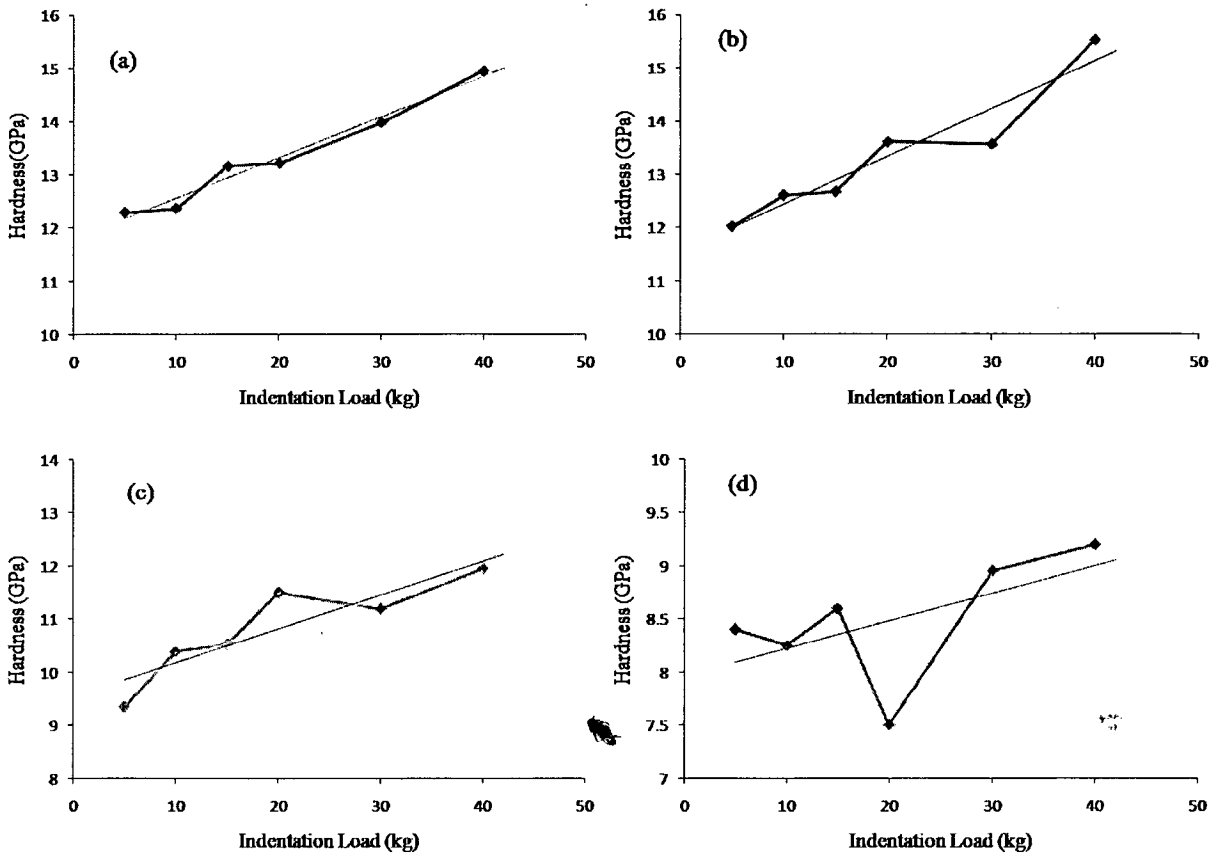

Fig.4.13 Hardness of the Al_2O_3 samples sintered at 1500°C for soaking time of (a) 6hr, (b) 12hr, (c) 18hr and (d) 24hr, as a function of indentation load.

The plots between the hardness and the indentation load for the samples A_3^{1600} and A_{12}^{1600} are shown in Fig.4.14. The RISE behaviour can also be seen for these samples. Wonsiewicz et al. have proposed that the primary slip system alone is not capable of fully accommodating the increased amount of plastic flow to create the larger impression. Then the additional slip system must be active to produce the increased flow of material in the vicinity of the indentation. The presence of the material flow on multiple slip systems contributing the deformation around the indentation was examined by many researchers to reveal the role of dislocations around the indentations (Kaji et al., 2002, Wonsiewicz and Chin, 1973, Ma and Clarke, 1995). Feltham and Banerjee (Feltham and Banerjee, 1992) and Banerjee and Feltham (Banerjee and Feltham, 1974) have suggested that the RISE may be related to the energy loss as a result of specimen chipping surrounding the indentation during

loading. Because of the cracking, a smaller indentation size results and the indentation test yields a higher apparent microhardness for a given applied test load (Li and Bradt, 1996, Dey et al., 2009).

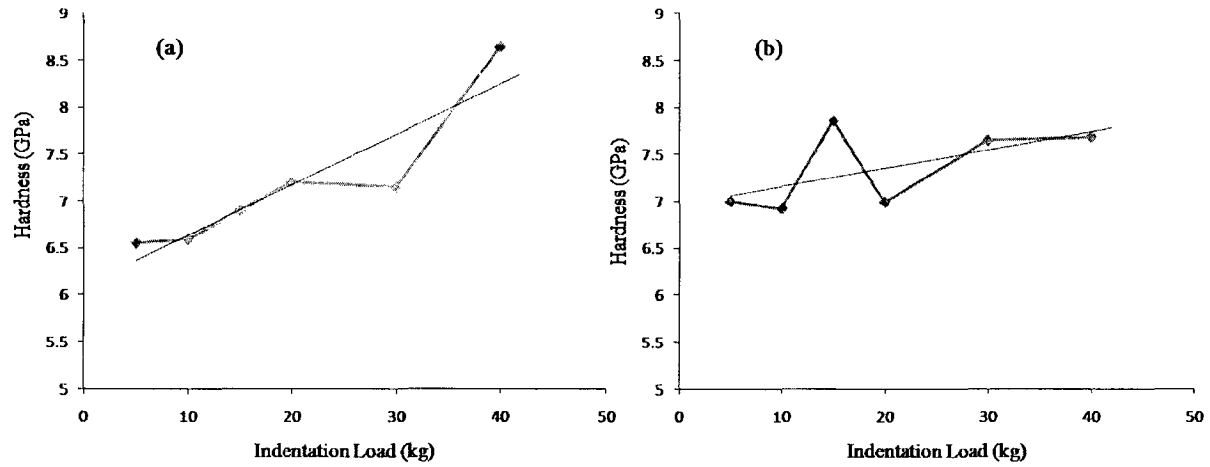

Fig.4.14 Hardness vs. indentation load for the sample sintered at 1600°C for (a) 3hr and (b) 12hr.

In the case of samples sintered at 1700°C (Fig.4.15), the RISE behaviour is observed for A_3^{1700} sample, while the samples A_6^{1700}, A_9^{1700} and A_{12}^{1700} exhibit ISE behaviour. However, for these samples the deviations of the data points from the corresponding linear fittings are larger than that of samples sintered at 1500°C and 1600°C. In ISE, the size of the indentation impression increases because the deformed, or flowed, volume of material surrounding the impression also increases in order to accommodate the larger amount of material flow about the impression. It is expected that the deformation through primary slip system will occur more efficiently in the material having larger grains. The indentation-associated cracking increases with increasing indentation test load (Kaji et al., 2002, Reimanis, 1997). ISE in these samples is therefore attributed to the larger grain size and the smaller value of grain size difference throughout the microstructure.

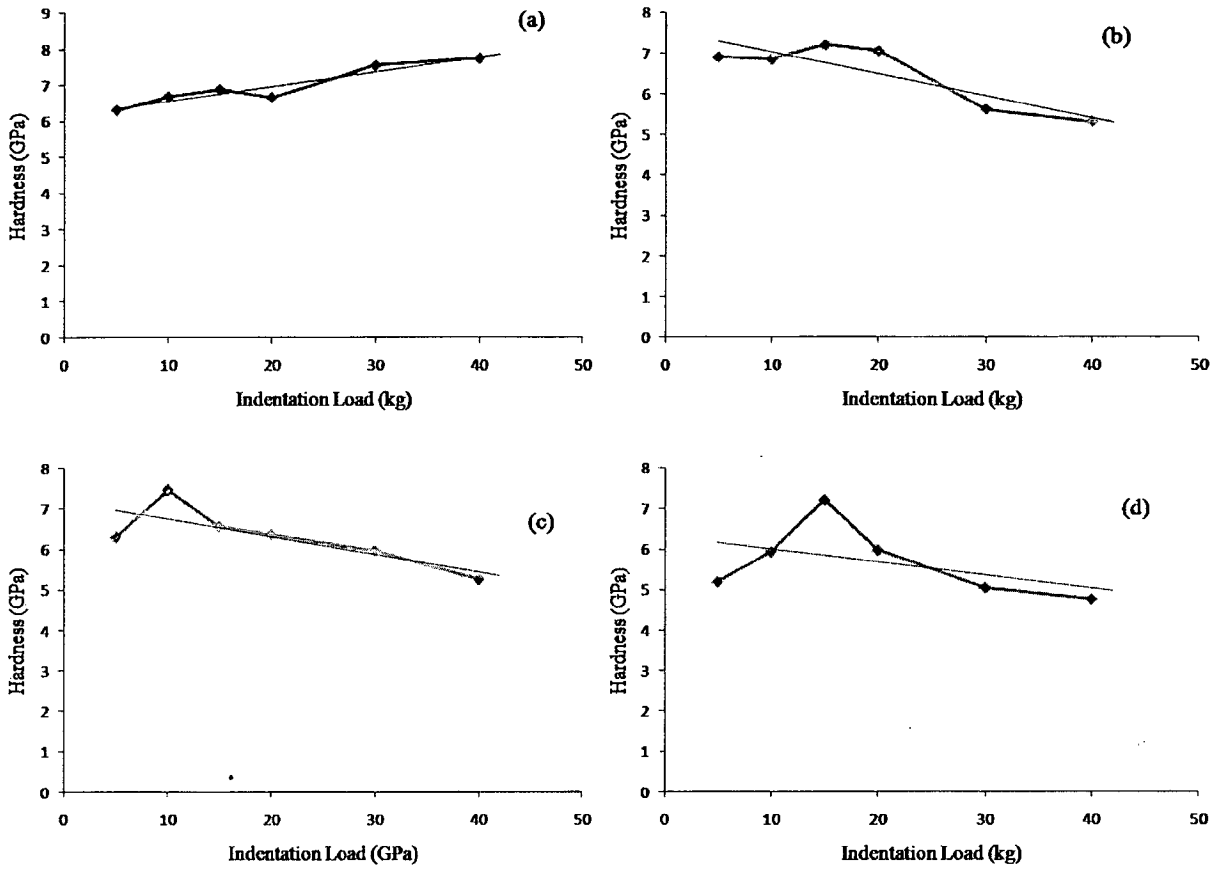

Fig.4.15 Hardness vs. indentation load of sintered sample at 1700°C for (a) 3hr, (b) 6hr, (c) 9hr and (d) 12hr.

4.5.1.4 Proportional Specimen Resistance Model

The ISE can, phenomenologically, be described by the proportional specimen resistance (PSR). According to the PSR model the relation between the applied test load, P and the average length (L) of the diagonals of the indentation is as follows (Li and Bradt, 1993, Michels and Frischat, 1882)

$$P = a_1 L + a_2 L^2 \qquad (4.5)$$

where a_1 (g μm^{-1}) is the coefficient related to the proportional resistance of the test specimen and a_2 (g μm^{-2}) is a constant. Li and Bradt pointed out that the constants a_1 and a_2 of equation (4.5) are related with the elastic and plastic properties of the material, respectively (Li and

Bradt, 1993, Sangwal et al., 2002). The equation (4.5) may be rearranged in the form given below:

$$P/L = a_1 + a_2 L \qquad (4.6)$$

which enables one to determine a_1 and a_2 from the plot of P/L as a function of L.

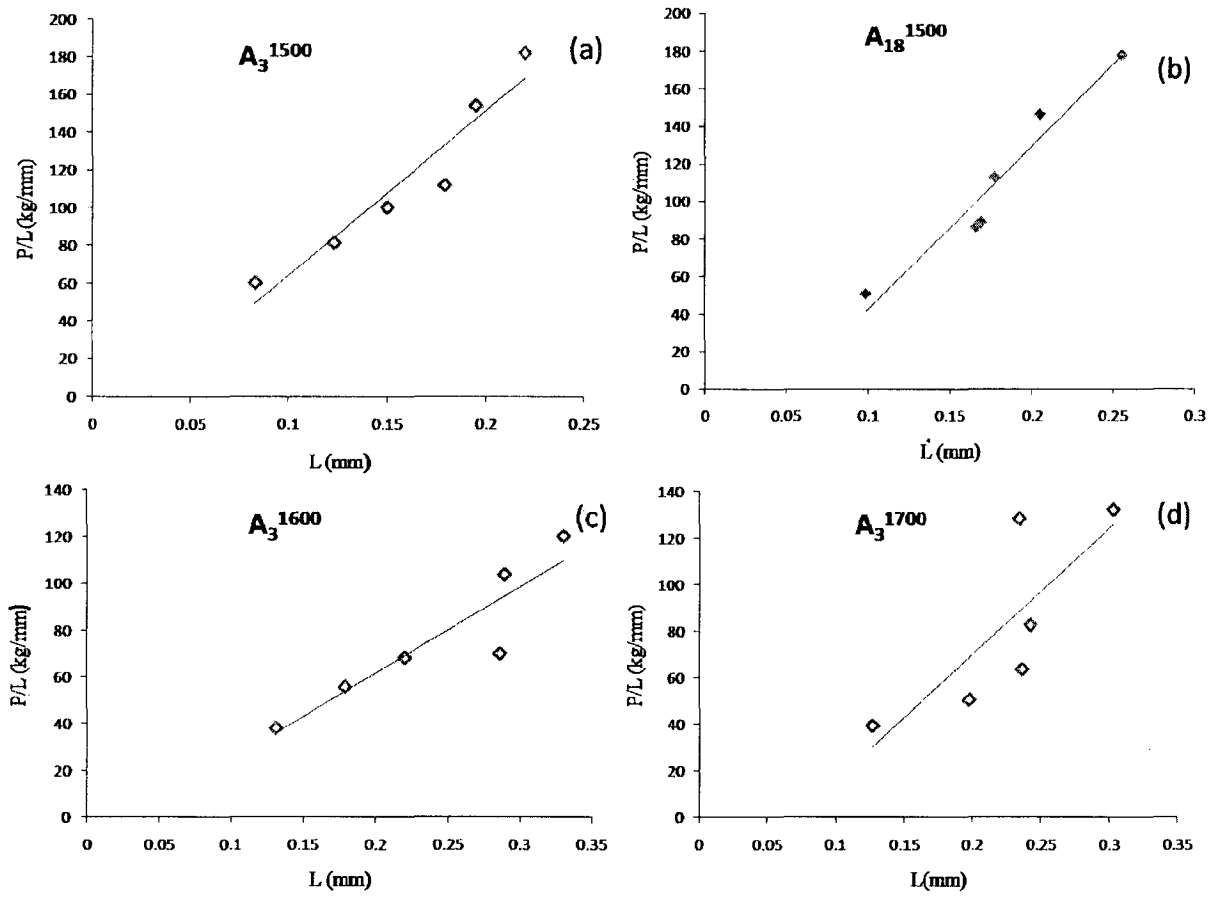

Fig.4.16 P/L vs L plots for the Al_2O_3 ceramic samples sintered at (a)1500°C for 3hr, (b) 1500°C for 18hr, (c) 1600°C for 3hr and (d) 1700°C for 3hr.

The plots of P/L vs L for the different samples are shown in Fig.4.16. This linearized form gives a straight line plot which has an intercept equal to a_1. The slope, a_2, relates to the load-independent hardness as Frischat has discussed (Frischat, 1985). The smooth linear fitting of the data points shows the PSR model is followed. In Fig.4.16, the plots of P/L vs. L, are

almost straight line. The PSR behaviour is witnessed in both the cases of RISE and ISE (Andrejovská and Dusza, 2009).

4.5.2 Fracture toughness of the sintered Al_2O_3 samples

Low fracture toughness of ceramic materials restricts them from using in various applications especially as structural ceramics. In the present study some attempts have been made to improve the fracture toughness in Al_2O_3 ceramics which is as follows.

4.5.2.1 Effect of sintering temperature on the fracture toughness

The change in fracture toughness on the sintering temperature is very important because sintering temperature is the parameter which requires for preparing the ceramic material (Miyahara et al., 1994). The microstructure of single phase ceramic materials generally consists of non-uniform grains. The grain morphology is controlled by the chemical reaction of dopants used with Al_2O_3 ceramic producing liquid phase during sintering (Park, 1996). However, in that section (section 4.5.2.1) an attempt has been made to develop the variability in grain morphology by solid state sintering of pure Al_2O_3 ceramics by changing the sintering temperature and soaking time period.

Table 4.6 Hardness and fracture toughness of Al_2O_3 samples sintered at 1500°C, 1600°C and 1700°C.

Sample	Average grain size (μm)	Hardness (GPa)	Fracture Toughness (MPa $m^{-1/2}$)
A_3^{1500}	0.688	15.01	5.22 ± 0.39
A_6^{1500}	0.837	14.94	5.20 ± 0.19
A_9^{1500}	0.843	14.77	5.38 ± 0.46
A_{12}^{1500}	0.939	15.52	5.37 ± 0.54
A_{18}^{1500}	4.81	11.95	5.27 ± 0.23
A_{24}^{1500}	4.93	9.2	5.28 ±0.18
A_{36}^{1500}	4.97	8.7	5.33 ± 0.41
A_3^{1600}	5.35	8.64	5.44 ± 0.36
A_6^{1600}	5.42	8.46	5.45 ± 0.27
A_9^{1600}	5.57	7.84	5.57 ± 0.52
A_{12}^{1600}	6.07	7.68	5.01 ± 0.42
A_3^{1700}	7.30	7.74	4.56 ± 0.52
A_6^{1700}	13.75	7.2	4.99 ± 0.49
A_9^{1700}	15.46	6.56	4.85 ± 0.27
A_{12}^{1700}	17.11	7.21	5.03 ± 0.59

In the present study it has been tried to establish a link between the ceramic microstructure that develops on sintering and the resulting fracture toughness of the materials prepared. The fracture toughness of the samples reported in the Table 4.6, has been measured by Vickers indentation method. Fracture toughness of the sample sintered at 1500°C varies between 5.20 ± 0.19 and 5.37 ± 0.54 MPa $m^{-1/2}$. For the samples sintered at 1600°C and 1700°C fracture toughness varies in the range of 5.01 ± 0.42 to 5.57 ± 0.52 and 4.56 ± 0.52 to 5.03 ± 0.59 MPa $m^{-1/2}$ respectively. So the fracture toughness at the sintering temperature 1600°C is more than the 1500°C and 1700°C sintered samples. Microstructure of the sample is responsible for the change in fracture toughness of the sample sintered at different temperature. In general microstructural and morphological features play leading roles in the emergence of properties of ceramic materials. For monolithic Al_2O_3, only coarse grains, elongated grains and grains with high aspect ratio, can result in an increased fracture toughness. Such improvement can be attributed to the mechanisms of crack bridging and crack deflection (Xu et al., 2005; Ighodaro and Okoli., 2008). The sintering process resulted in grain shape variation which has been taken into account by calculating aspect ratio (AR) parameter for several grains in the samples sintered at 1500°C, 1600°C and 1700°C for one particular soaking period of 9 hr as an example and the calculated ARs are presented in Table 4.7. The ARs of the grains considering the samples sintered at all the three temperatures, are found to lie between 1.0 and 2.85. These values are further shown (in Table 4.7) subdivided into following three different ranges of (i) 1.0 - 1.30, (ii) 1.31 - 1.80 and (iii) 1.81 - 2.85 for each sample to indicate the degree of deviation of the grain shape from the regular equiaxed nature. The values in the same row correspond to a same range. The Table 4.7 shows the grains having AR ranges of 1.0-1.30 and 1.31-1.80 are nearly comparable in number for the samples sintered at 1500°C,1600°C and 1700°C. However, the grains having AR in the range of 1.81-2.85 are significantly more in number for the samples sintered at 1600°C than the samples sintered at 1500°C and 1700°C. Therefore the contribution of grain bridging effect towards the higher fracture toughness of the samples sintered at 1600°C for a soaking time of 9 hr is perhaps important (Kovar et al., 2000).

The hardness of the samples varies in the range of 6.56 to 15.52 GPa for the samples sintered at 1500°C, 1600°C and 1700°C. The hardness of the material decreases with

increasing sintering temperature. Lu et al. also reported the hardness values of 2.26 and 2.09 GPa for pure Al_2O_3 and composite of Al_2O_3-5wt.% MgB_2 (Lu et al.,2005).

Table 4.7 Aspect Ratio (AR) of the samples sintered at 1500°C, 1600°C and 1700°C for the soaking time periods of 9 hr.

AR of A_9^{1500} samples	AR of A_9^{1600} samples	AR of A_9^{1700} samples
1.01,1.05,1.09,1.11,1.13,1.15, 1.15,1.15,1.16,1.18,1.21,1.21, 1.22,1.23,1.24,1.25, ,1.29,1.29	1,1.02,1.02,1.08,1.11,1.19,1.19 1.23,1.23,1.23,1.25,1.27,1.28 1.28	1.02,1.03,1.06,1.07,1.08,1.09, 1.18,1.18,1.19,1.21,1.21,1.23, 1.24,1.25,1.29
1.31,1.36,1.43,1.44,1.45,1.51, 1.51,1.51,1.52,1.54,1.55,1.58, 1.67,1.69,1.72,1.73,1.79	1.32,1.38,1.38,1.43,1.43,1.47, 1.48,1.51,1.54,1.56,1.56,1.57 1.58,1.61,1.62,1.66,1.67	1.34,1.34,1.35,1.36,1.36,1.39, 1.41,1.44,1.46,1.48,1.48,1.51, 1.55,1.61,1.64,1.64,1.64,1.64
1.91,2.04,2.34	1.84,1.86,1.91,1.95,1.96,2.12, 2.18,2.23,2.5,2.74	1.85,2.02,2.28,2.85

4.5.2.2 Effect of grain size on the fracture toughness

The changes in grain size of the samples with increasing sintering temperature and soaking time periods have been shown in the Table 4.5. Grain size increases with increasing sintering temperature and time. The Table 4.6 show the fracture toughness of the samples increases with increasing grain size. The samples sintered at 1500°C show the fracture toughness increases marginally with increasing grain size. For the samples sintered at 1600°C fracture toughness increases with increasing grain size until 5.57 μm in the sample and further above the fracture toughness decreases. The samples sintered at 1700°C show the lower fracture toughness than the fracture toughness of samples sintered at 1500°C and 1600°C. Miyahara et al. reported the increase in fracture toughness with the increasing grain size due to R-curve behavior (Miyahara et al., 1994). Vekinis et al. also reported that grain size dependence of fracture toughness. They also reported that the crack growth resistance is

responsible for the fracture toughness enhancement following the grain bridging mechanism (Vekinis et al., 1990). But in the present study it has been shown that the upto a certain grain size fracture toughness increases slightly with increasing grain size. Grain bridging may be the one mechanism to cause the increase in the fracture toughness with increasing grain size. The samples sintered at 1600°C have mixed (i.e. smaller and larger) grains facilitating the propagation of the intergranular and transgranular cracks resulting in higher fracture toughness. The dependence of fracture toughness with average grain size has been shown in Fig.4.17.

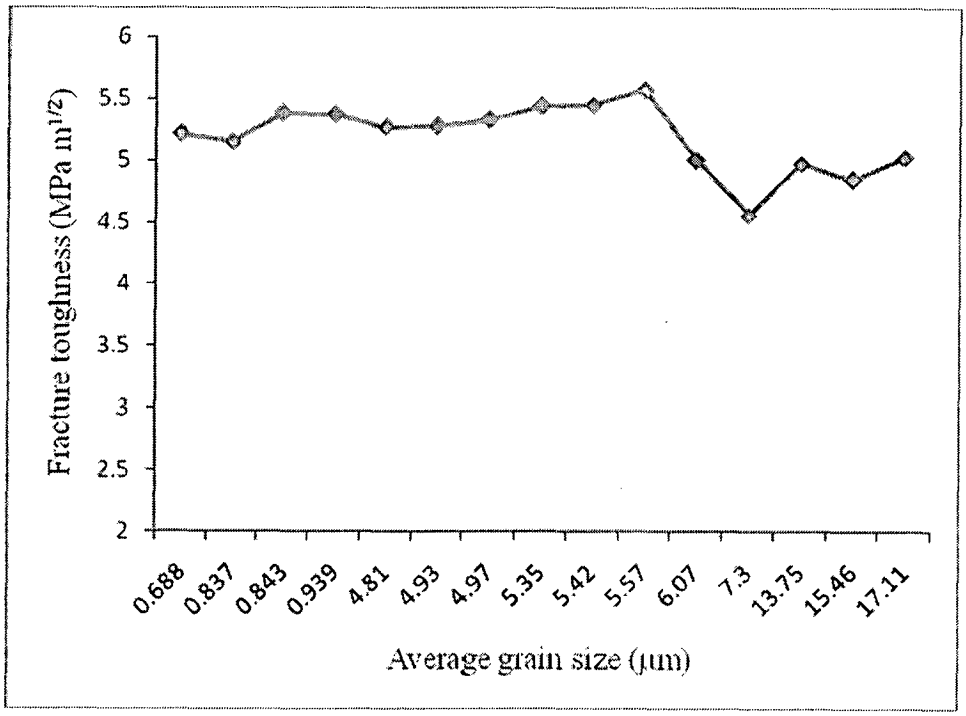

Fig.4.17 Fracture toughness of the Al_2O_3 ceramics sintered at 1500°C ,1600°C and 1700°C as a function of average grain size.

4.5.2.3 Correlation of fracture toughness with mode of crack propagation

Fig.4.18 shows an optical micrograph of the Vickers indentation on the sample showing the cracks emanating out from the corners of the indentation in Al_2O_3 samples sintered at 1600°C for 3hr. An enlarged view of the crack path in one case is shown in an inset of the Fig. 4.18. The zig-zag crack path as can be seen in the inset indicates the crack deflection during the crack propagation.

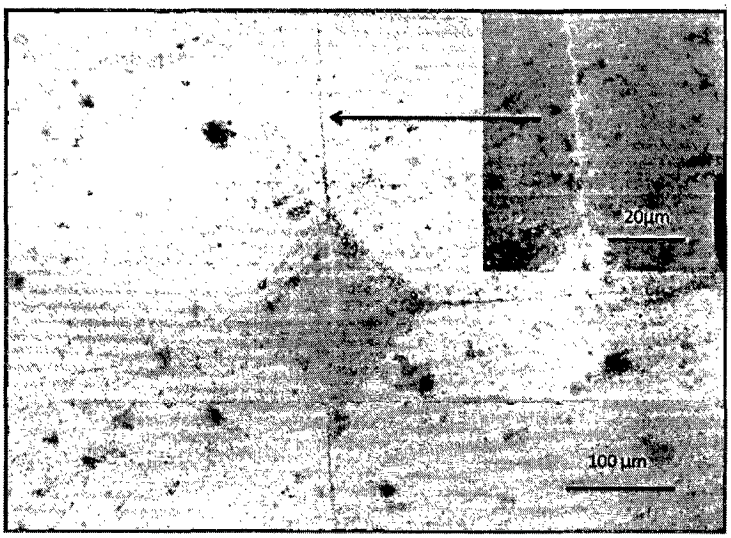

Fig.4.18 Vickers's indentation with crack in the Al_2O_3 samples sintered 1600°C for 3hr.

The mode of the crack propagation has been revealed by showing a partial crack lengths at higher magnification in Fig.4.19, which shows that the crack propagation is mainly intergranular in nature indicating the crack deflection is the predominant mechanism for higher fracture toughness of these samples. The crack deflection in the samples sintered at 1500°C and 1600°C resulted in higher fracture toughness.

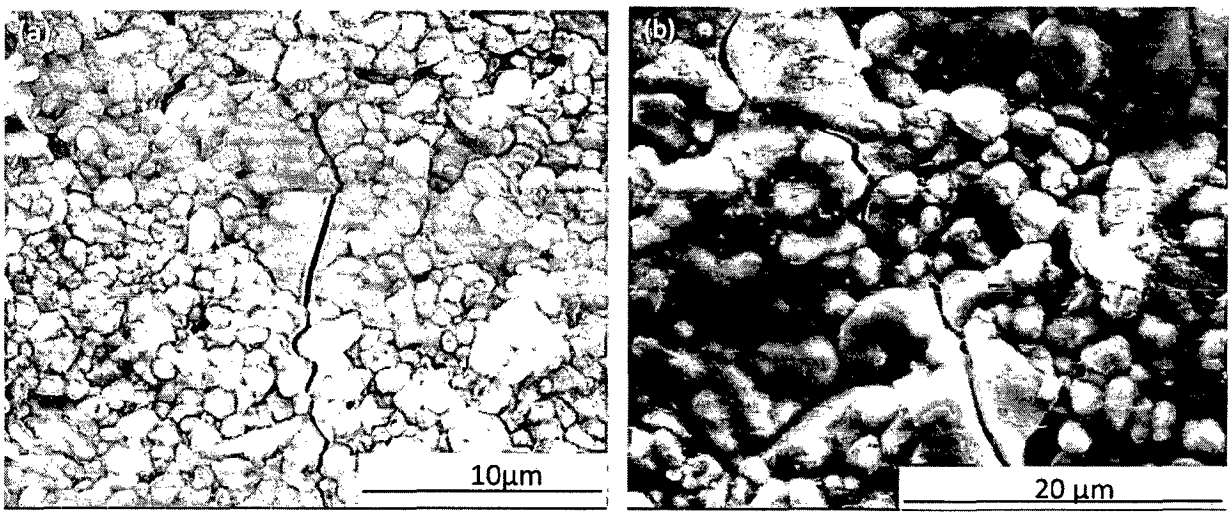

Fig.4.19 SEM micrograph of Al_2O_3 sample sintered at (a)1500°C for 3hr, (b) 1600°C for 3hr.

The micrograph in Fig.4.20 shows the transgrannular fracture in Al_2O_3 samples sintered at 1700°C for 3hr. The transgranular fracture is the consequence to lower facture toughness of the samples sintered at 1700°C for almost all the soaking time periods considered. Micrographs of Fig.4.19 and Fig.4.20 have been taken after the indentation on the sintered samples.

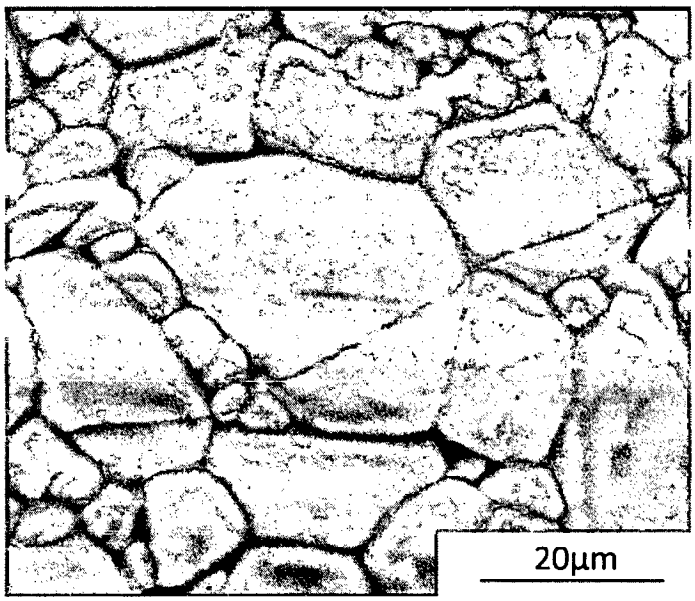

Fig.4.20 SEM micrograph of Al_2O_3 sample sintered at 1700°C for 3hr.

4.5.2.4 Microstructures of the fracture surfaces

To relate the crack propagation mode on the sample surface due to indentation, with the failure mode operative in the bulk of the sample, microstructures of the fracture surfaces of the samples were studies. Micrographs of fracture surfaces of the samples sintered at 1500°C, 1600°C and 1700°C are shown in Fig.4.21. The fracture surfaces were created from these samples by subjecting them three point bend test mode for failure. In Fig. 4.21(a) the presence of smaller grains is clear and the surface topography shows that the fracture has taken place predominantly due to the intergranular mode. It is more clear from Fig. 4.21(b) that the smaller grains remain in almost the same size range as obtained in the case of Fig. 4.21(a), however the larger grains have grown substantially in relation to that in Fig. 4.21(a). This observation matches well with the microstructure of the sample surface as given in Fig. 4.6(c). Further the fracture surface topography confirms that fracture has taken place due to

mixed mode of intergranular and transgranular fracture, with larger proportion of the intergranular mode. The fracture toughnesses of these samples (Fig. 4.21(b) and (c)) show relatively higher toughness as listed in Table 4.6. But in Fig. 4.21(d) the flat surface topography over a considerable region in the micrograph area shows that the fracture has occurred predominantly due to transgranular mode. The lower fracture toughness obtained is the obvious consequence to such fracture surface feature (Deng et al., 2003). Fig.4.21(c) shows that a large portion of microstructure area is occupied by large grains with smaller area portion filled with smaller sized grains. This observation is also consistent with the microstructure given in Fig. 4.7(a). Though the fracture by transgranular type is present, but intergranular fracture mode is clear from the Fig.4.21(c) and also from Fig.4.19(b).

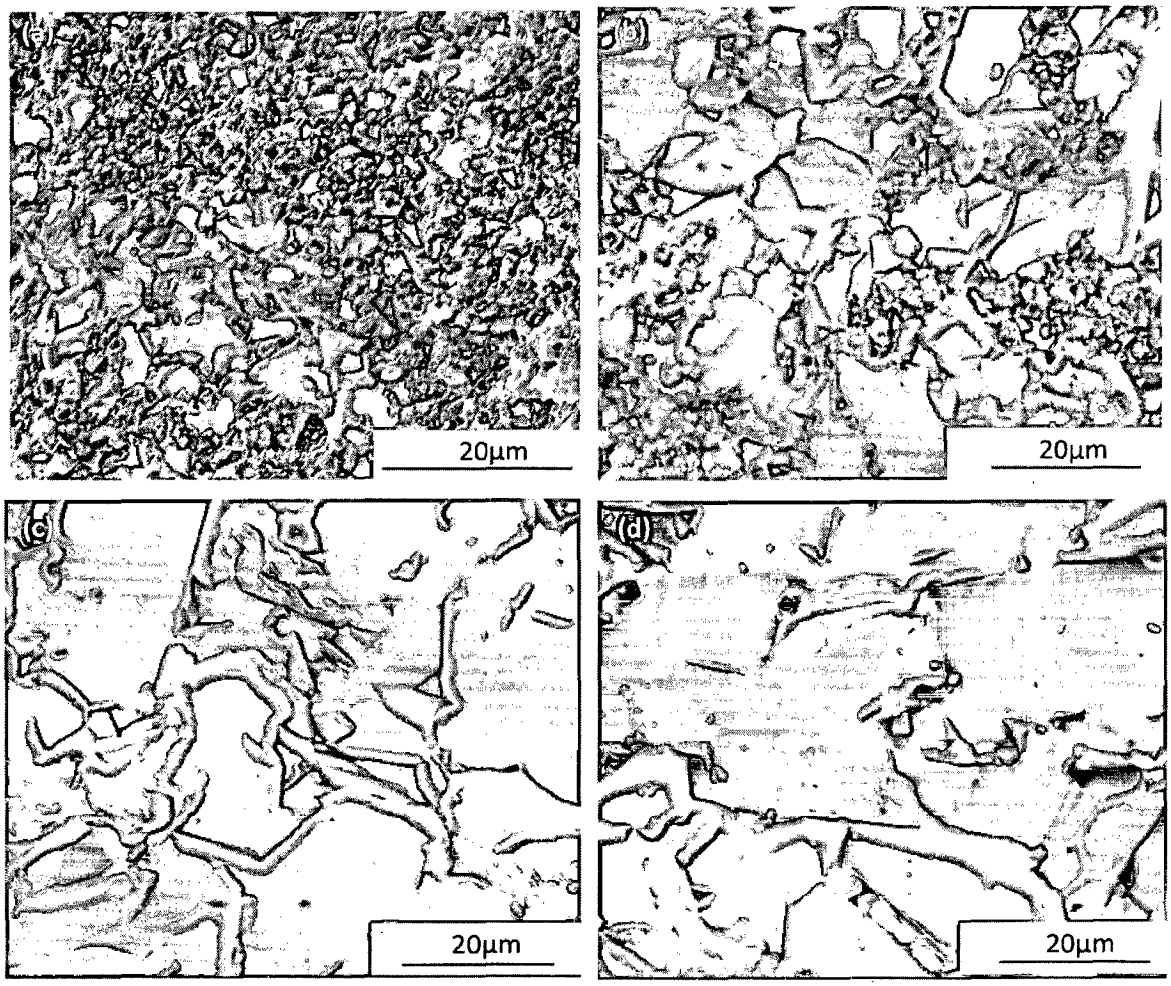

Fig.4.21 SEM micrograph of fracture surface of Al_2O_3 sample sintered at (a) 1500°C for 3hr, (b) 1500°C for 18hr, (c) 1600°C for 3hr and (d) 1700°C for 3hr.

4.5.2.5 Grain size histograms and there correlation with fracture toughness

The internal stress in the samples having larger grains that develops during cooling, generates small cracks which affects the hardness as well as fracture toughness of the materials (Baddi et al., 1986, Evans et al., 1970). As the grains in all the samples vary over a range of size rather than preferably having uniform size for a particular sintering schedule, it is appropriate to show the actual size distribution that has been resulted. The grain size distribution of the samples has shown in the Fig.4.10. The grain size distribution influences the fracture toughness of the materials. The combination of smaller and larger grains improves the fracture toughness. The smaller and larger grains combination has been shown in the Fig.4.7 and materials possessing such combination generally have higher fracture toughness as given in Table 4.6.

4.5.2.6 Correlation of fracture surface roughness with the fracture toughness

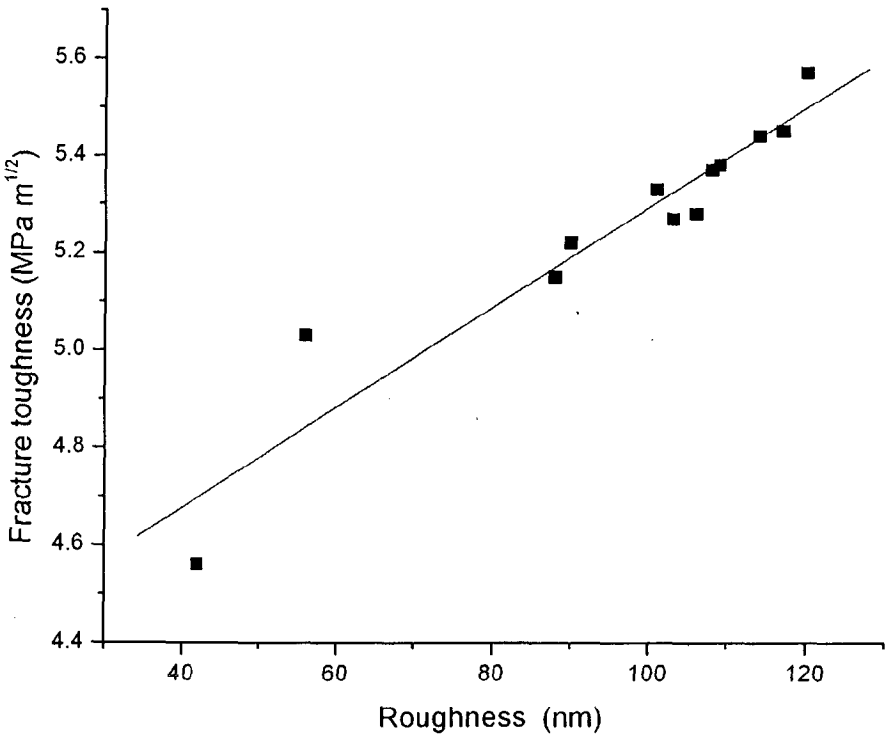

Fig.4.22 Fracture toughness vs fracture surface roughness of the samples sintered at 1500°C, 1600°C and 1700°C.

Fig. 4.22 shows data points plotted between fracture toughness and fracture surface roughness of the samples sintered at 1500°C, 1600°C and 1700°C. A best fit line has been drawn through these data points. It can be seen that the data points in the higher range of fracture toughness fall on or very close to the straight line drawn, whereas the points in the lower fracture toughness region are far apart from the straight line. This means that the samples with lower fracture toughness do not follow the same linear relationship when extended to the lower fracture toughness region. Boccaccini et al. have shown the linear correlation between the fracture toughness and fracture surface roughness which gives rise to the crack deflection as the toughening mechanism in the Al_2O_3 platelet reinforced glass matrix composites (Boccaccini and Winkler, 2002).

4.5.2.7 R- curve behavior of Al_2O_3 samples

The influence of sintering temperature and soaking time period on R-curve behavior of Al_2O_3 samples has been investigated. The increasing fracture resistance with crack extension in ceramics (R-curve behaviour) is highly desirable for their use in structural applications.

Table 4.8 Average crack length and fracture toughness of the samples sintered at 1500°C, 1600°C and 1700°C for the different soaking time periods.

Sample	Average crack length (μm) at different load						Fracture toughness ($MPa\ m^{1/2}$)	Average fracture toughness ($MPa\ m^{1/2}$)
	5kg	10kg	15kg	20kg	30 kg	40 kg		
A_3^{1500}	48.5	94.08	115.52	124.75	173.48	188.25	5.22 ± 0.39	5.28 ±0.08
A_6^{1500}	47	81.25	121.5	135	181.25	222.5	5.20 ± 0.19	
A_9^{1500}	50.7	86.8	100.7	130.72	186.53	227.5	5.38 ± 0.46	
A_{12}^{1500}	53.25	80	113.75	123.3	154.45	218.5	5.37 ± 0.54	
A_{18}^{1500}	-	84.3	98.28	132.79	158.44	230.28	5.27 ± 0.23	
A_{24}^{1500}	-	78.05	129.94	146.72	197	230.01	5.28 ± 0.18	
A_3^{1600}	53.45	93.8	181.57	169.6	182.03	282.01	5.44 ± 0.36	5.37 ±0.25
A_6^{1600}	45.97	82.53	116.03	137	184.89	229.21	5.45 ± 0.27	
A_9^{1600}	-	95.92	147.88	184.6	211.78	239	5.57 ± 0.52	
A_{12}^{1600}	-	100.68	145.76	160.6	216.5	253	5.01 ± 0.42	
A_3^{1700}	-	151	165.86	180	191.55	261.88	4.56 ± 0.52	4.86 ±0.21
A_6^{1700}	-	89.7	107.15	144.63	251.36	301.43	4.99 ± 0.49	
A_9^{1700}	-	94.48	122.45	199.27	286.4	299.51	4.85 ± 0.27	
A_{12}^{1700}	55.63	82.8	166.27	257.23	289.39	305.6	5.03 ± 0.59	

Table 4.8 shows the fracture toughness and crack length in the samples sintered at 1500°C, 1600°C and 1700°C for different soaking time periods. The fracture toughness of the samples sintered at 1500°C varies from 5.20 to 5.38 MPa $m^{1/2}$ and maximum crack length observed was 230.28 μm for the sample sintered for 18 hr and the indentation load was 40 kg. The samples sintered at 1600°C show marginally higher average fracture toughness lying between 5.01 and 5.57 MPa $m^{1/2}$ and maximum crack length of 282.01μm has been observed for the soaking time of 3hr. Fracture toughness of the samples sintered at 1700°C is relatively lower and the value lies between 4.56 and 5.03 $MPam^{1/2}$ and has maximum crack length of 305.6 μm in the sample soaked for 12hr.

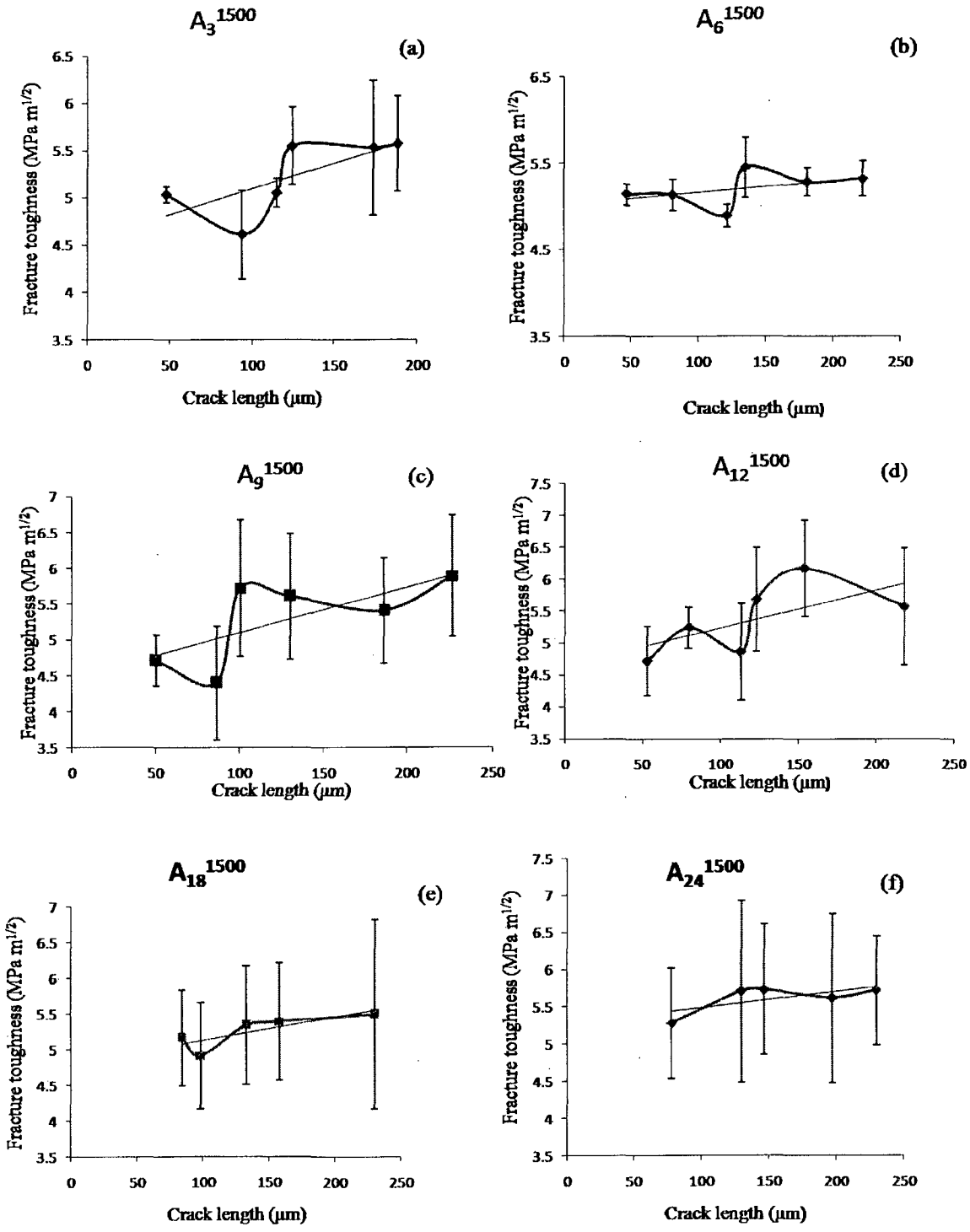

Fig.4.23 Fracture toughness vs. average length of the crack in the Al_2O_3 ceramics sintered at 1500°C for (a) 3hr, (b) 6hr,(c) 9hr,(d) 12hr,(e) 18hr and (f) 24hr.

In Fig.4.23, the measured K_{IC} values are plotted as a function of the crack length for Al_2O_3 ceramics sintered at 1500°C. The variation in the fracture toughness obtained from several indentations at a given load has been represented by error bars in the respective plots. The linear fit of the data points shows an increase in K_{IC} with increase in crack length extension, indicating the R-curve behavior of the sample. The linear fit of average K_{IC} s for each load, shows the increase in K_{IC} with crack length extension. However, the increase is lower for the samples soaked for 18 hr and 24 hr compared to those soaked for 3, 9 and 12 hr.

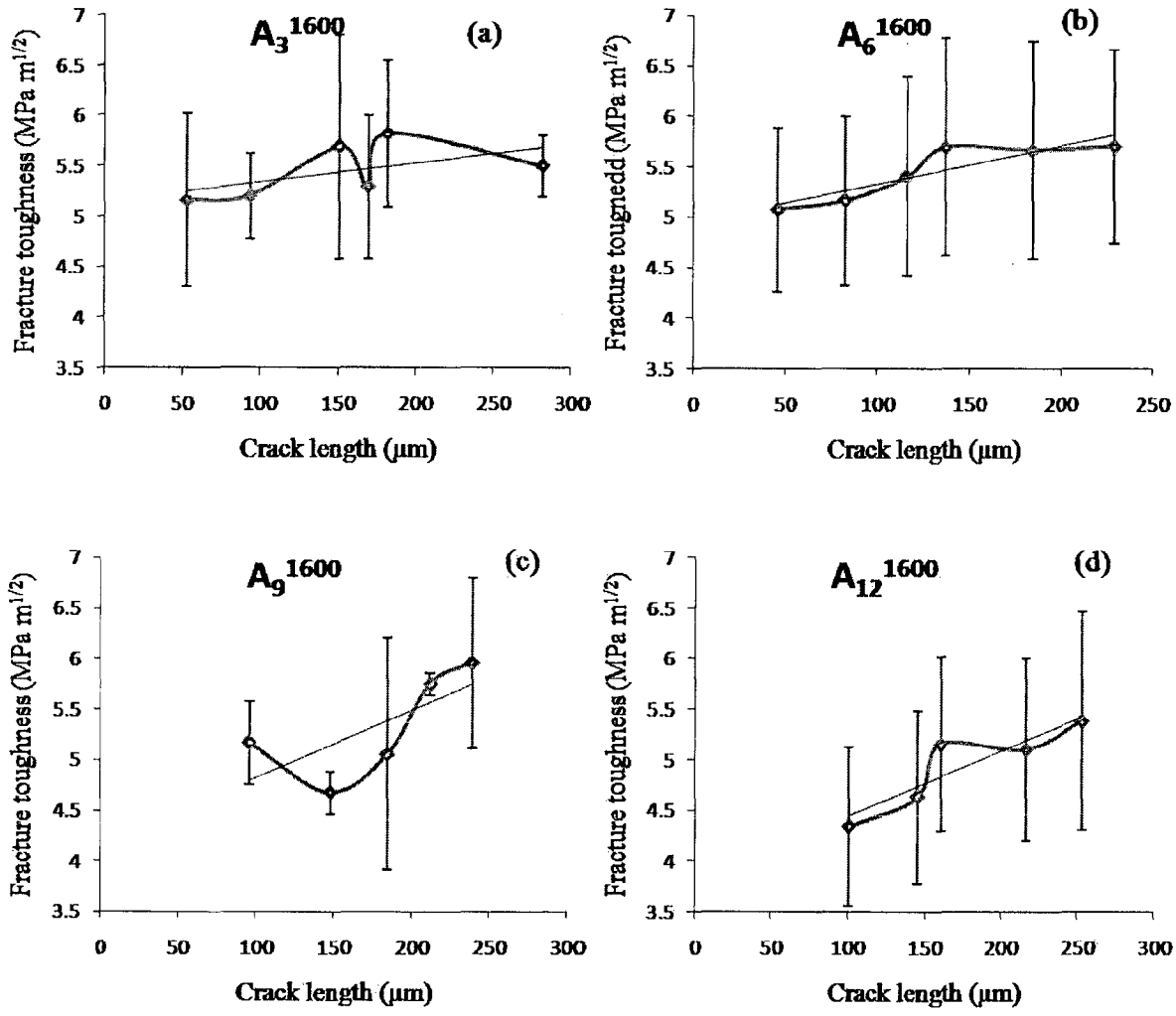

Fig.4.24 Fracture toughness vs. average length of the crack in the Al_2O_3 ceramics sintered at 1600°C for (a) 3hr,(b) 6hr,(c) 9hr and (d) 12hr.

The average linear fit of all the data points in different plots of Fig.4.24 shows that all the samples sintered at 1600°C show the trend for the R-curve behavior. There is an over all increase in K_{IC} with increase in crack extension length. Crack deflection might be the reason to maintain the R-curve in the samples sintered at 1500°C and 1600°C where grain bridging is not the main mechanism behind that for smaller grain size (Tomaszewski et al.,2000a). The linear fit of average K_{IC} s values shows continuous increase in K_{IC} with crack length extension. Therefore the samples sintered at 1600°C obey R-curve behavior.

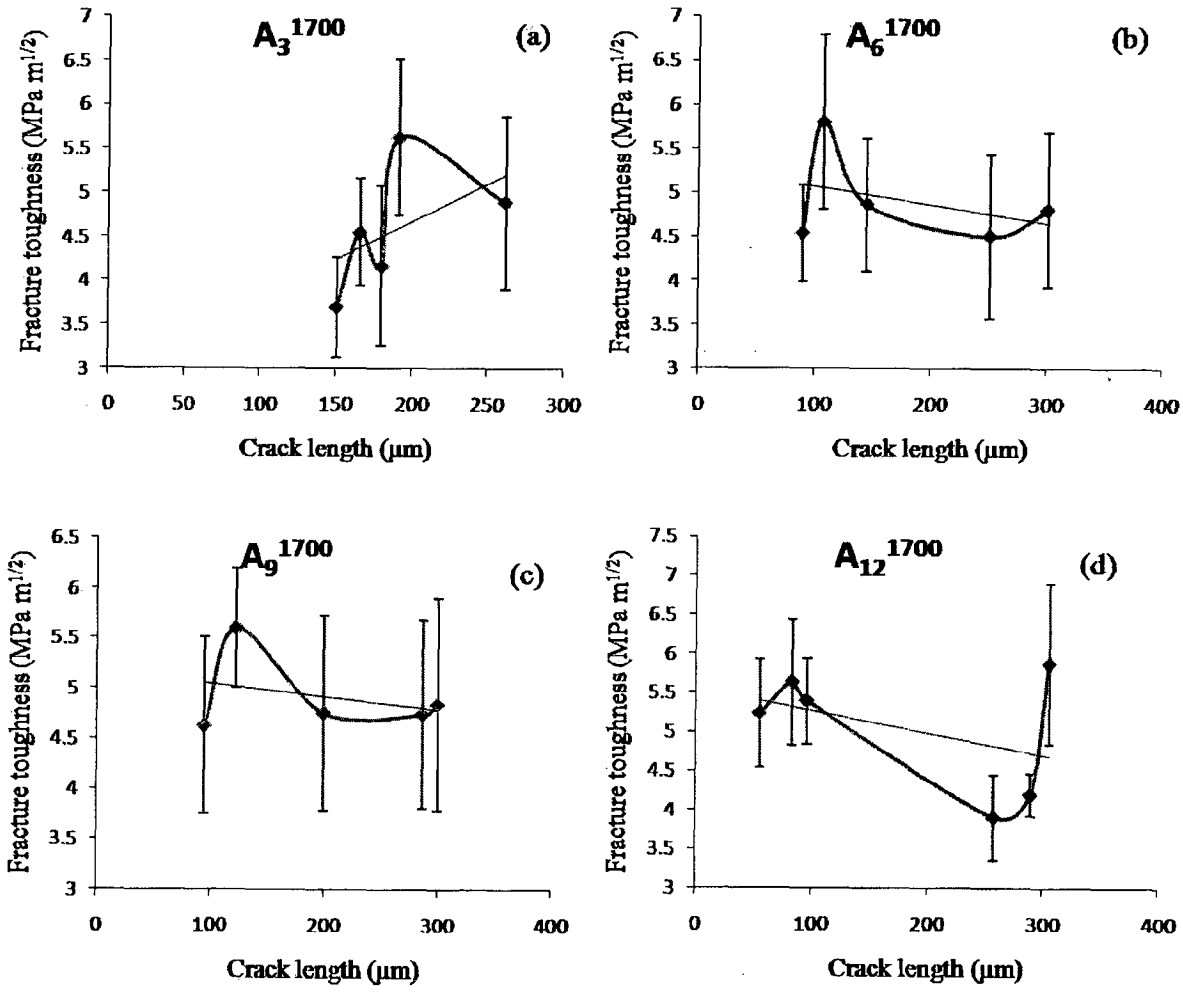

Fig.4.25 Crack extension resistance of Al_2O_3 ceramics sintered at 1700°C for (a) 3hr,(b) 6hr, (c) 9hr and (d) 12hr.

The samples sintered at 1700°C shows different results from that of the samples sintered at 1500°C and 1600°C. Fig. 4.25(a) shows the increase in fracture toughness with increase in the crack length extension has been observed for A_3^{1700} samples. The samples sintered at 1700°C for 6 hr, 9hr and 12hr show decrease in fracture toughness though marginally with crack length extension.

4.5.2.8 Fracture toughness of Al_2O_3 measured by Single-edge precracked beam method

4.5.2.8.1 Comparison of Indentation method and single edge precracked beam (SEPB) method for the calculation of fracture toughness

The fracture toughness of the samples has also been estimated by single edge precracked beam (SEPB) test method using three-point bending test. The comparison of fracture toughness measured by indentation and SEPB method has been given in the Table 4.9. The difference between the fracture toughness values of the samples measured by Indentation method and SEPB method is very low. The relative uncertainty in the fracture toughness values estimated by using Indentation method is more compared to that estimated from the SEPB method. It can be seen from the Table 4.9 that the fracture toughnesses determined by the two methods are almost equal.

Table 4.9 Comparison of fracture toughness measured by Indentation method and SEPB method.

Sample	Fracture toughness estimated by (MPa $m^{1/2}$)	
	Indentation method	SEPB method
A_3^{1500}	5.22 ± 0.39	4.79 ± 0.20
A_6^{1500}	5.25 ± 0.19	5.26 ± 0.14
A_9^{1500}	5.38 ± 0.46	5.19 ± 0.22
A_{12}^{1500}	5.37 ± 0.54	5.25 ± 0.32
A_{18}^{1500}	5.27 ± 0.23	5.02 ± 0.37
A_{24}^{1500}	5.28 ± 0.18	5.10 ± 0.30
A_{36}^{1500}	5.33 ± 0.41	5.12 ± 0.34
A_3^{1600}	5.44 ± 0.36	4.98 ± 0.25
A_6^{1600}	5.45 ± 0.27	5.18 ± 0.02
A_9^{1600}	5.57 ± 0.52	5.28 ± 0.16
A_{12}^{1600}	5.01 ± 0.42	5.20 ± 0.30
A_3^{1700}	4.56 ± 0.52	4.59 ± 0.07
A_6^{1700}	4.99 ± 0.49	5.05 ± 0.37
A_9^{1700}	4.85 ± 0.27	4.96 ± 0.38
A_{12}^{1700}	5.03 ± 0.59	5.15 ± 0.36

4.6 Summary

Microstructural and morphological factors play leading roles in the emergence of properties of ceramic materials. Kovar et al. has reported that for monolithic Al_2O_3, only coarse grains and grains having high aspect ratio can produce an improvement in fracture toughness. This is because only crack bridging and crack deflection mechanisms can be activated; longer and larger particles can bridge and deflect cracks more effectively. Kovar et al. correlated the fracture toughness with grain size distribution and grain shape distribution. They have reported the fracture toughness value of Al_2O_3 is about 5 MPa $m^{1/2}$ (Kovar et al., 2000). In the present work, improvement in fracture toughness of Al_2O_3 has been observed by changing the sintering temperature and soaking time periods. The average grain size of the samples increases with increasing sintering temperature and soaking time periods. A wide range of the grain size variation occurs in the samples sintered at 1700°C. The highest fracture toughness of the sample A_9^{1600} has been reported as 5.57 MPa $m^{1/2}$. Crack deflection and intergranular mode of crack path are the predominant mechanisms for higher fracture toughness of the Al_2O_3 samples. The elongated grains with higher aspect ratio in the sample also contributes enhancing the fracture toughness of the material. While the elongated grains causes the fracture toughness enhancement by mainly grain bridging mechanism, the crack deflection mechanism is effected by the grain size distribution. Therefore the detailed grain size distributions for the Al_2O_3 samples sintered at 1500 °C, 1600 °C and 1700 °C for all the soaking times considered, have been presented by way of grain size histograms. Grain size distribution is an important feature to estimate the applicability of crack deflection mechanism for the fracture toughness enhancement. To the best of the candidate's knowledge, such attempt to analyses fracture toughness results with grain size distribution has not been reported by other researchers. The increase in fracture surface roughness with the increase of fracture toughness is also reported. The samples sintered at 1500°C and 1600°C follow Reverse indentation Size effects (RISE) and R-curve behaviour. But the samples sintered at 1700°C for soaking time period more than 3hr does not follow the R-curve and RISE which has not been reported, so far, by other researchers. The comparison of Indentation method and Single edge precracked beam method for the determination of fracture toughness has been reported.

Chapter 5

Microstructure, hardness and fracture toughness of Y_2O_3 doped Al_2O_3 ceramic composites

---

Chapter 5

Rare earth element doping improves the sinterability of the ceramic materials thereby resulting in better mechanical properties of the ceramics. Dopant yttrium (Y) plays a major role in determining the final microstructure and related properties of sintered Al_2O_3. Y has a very limited solubility of 10 ppm in α -Al_2O_3. Due to the low solubility of Y in bulk α -Al_2O_3, Y is segregated at grain boundary (GB), which leads to significant modification of the mechanical properties of the material viz. fracture toughness, creep resistance etc. (Gulgun et al., 1999, Pogrion et al., 2004, Maiti and Sil, 2006, Rani et al., 2004).

5.1 Effect of sintering temperature and soaking time on physical properties of Al_2O_3 – Y_2O_3 composites

The physical properties viz. relative density, weight loss and linear shrinkage of the Y_2O_3 doped Al_2O_3 samples have been reported.

5.1.1 Relative density

The relative density of the samples varies with soaking time and the chemical composition. The relative density of the Al_2O_3 – Y_2O_3 sample decreases with increasing Y_2O_3. The Y content when is greater than 300 ppm, segregates at the grain boundary and retards the grain growth which decreases the rate of densification. From the Table 5.1 it is clear that the relative density of the sample increases with the increase in soaking time period. The relative density of samples A varies between 96.60 and 98.32%. For the doped sample the relative density decreases with the increase in the doping level. The relative density of the doped samples varies between 93.0 and 97.73%. The sample A15Y sintered for the soaking time period of 3hr shows lowest relative density of 93%. The sample doped with 15000 ppm Y_2O_3 shows lower relative density for all the soaking time periods compared to the other doped samples studied (Chae et al., 1993).

Table 5.1 Relative density of the Al_2O_3 and Y_2O_3 doped Al_2O_3 samples sintered at 1500°C for different soaking time periods.

Sample	Relative density (%) of the sample sintered for different soaking time periods			
	3hr	6hr	9hr	12hr
A	97.73	96.60	98.07	98.32
A1Y	95.47	97.31	97.31	97.73
A3Y	95.16	95.48	95.73	96.25
A5Y	94.29	95.31	95.65	96.11
A10Y	94.46	94.68	95.41	95.99
A15Y	93.00	94.75	95.42	95.14

5.1.2 Weight loss

Table 5.2 Weight loss of the Al_2O_3 and Y_2O_3 doped Al_2O_3 samples sintered at 1500°C for different soaking time periods

Sample	Weight loss (%) of the sample sintered for the soaking time periods			
	3hr	6hr	9hr	12hr
A	4.20	4.51	4.48	4.59
A1Y	4.5	4.31	4.43	4.61
A3Y	4.37	4.39	4.60	4.86
A5Y	4.34	4.62	4.86	4.99
A10Y	4.45	4.85	4.56	6.38
A15Y	6.23	7.31	8.63	8.36

Table 5.2 shows the weight loss of the samples having different compositions and sintered at 1500°C for different soaking time periods. A15Y and A10Y samples show the higher weight loss compared to the other samples and the weight loss for all the doped and undoped samples varies between 4.20 and 8.63 %. The higher weight loss results in the lower density of the samples, which inturn causes poor mechanical properties.

5.1.3 Shrinkage

Table 5.3 Linear shrinkages in the Al_2O_3 and Y_2O_3 doped Al_2O_3 samples sintered at 1500°C for different soaking time periods

Sample	Linear shrinkage (%) of the sample sintered for different soaking time periods			
	3hr	6hr	9hr	12hr
A	14.29	14.41	14.34	14.30
A1Y	13.89	14.19	14.48	14.24
A3Y	13.31	14.12	14.06	14.08
A5Y	13.28	14.15	14.37	14.15
A10Y	12.98	13.75	13.99	13.58
A15Y	12.89	14.11	14.02	14.04

Table 5.3 shows the linear shrinkages in the Al_2O_3 and Y_2O_3 doped samples. The samples sintered for the soaking time period of 3hr show the decrease in linear shrinkage with increasing Y_2O_3 content and the range of linear shrinkage varies between 12.89 and 14.29%. The samples sintered for higher soaking time periods of 6, 9 and 12 hr show very small difference in linear shrinkages. The variation in linear shrinkage is larger for the samples sintered for 3hr compared to the samples soaked for time period larger than 3hr.

5.2 Microstructure analysis

5.2.1 Microstructure of Y_2O_3 doped Al_2O_3 sample

Fig.5.1 shows the SEM micrograph of pure Al_2O_3 and Y_2O_3 doped Al_2O_3 samples both sintered at 1500°C for the soaking time of 6hr. It can be seen from the micrographs that the grain size of the sample decreases with increasing Y_2O_3 content in the sample. Y^{3+} restricts the grain growth in the Al_2O_3 sample which results in lower grain size in the Y_2O_3 doped Al_2O_3 samples.

It can be seen from Fig.5.1 (a) that the grains of the pure Al_2O_3 samples are nearly rounded and polygonal type. Exaggerated grain growth at some places is evident from the micrograph. A few grains are appeared to have joined each other across the interface thereby resulting in non uniform size and irregular shape in a few grains. The average grain size in the sample is 1.58 μm and the grain size varies between 0.33 and 1.91 μm. The morphology of the surface of the sample in Fig. 5.1(b) is different from that of the pure Al_2O_3 samples. The grain size range of 0.29 to 1.44 μm with an average grain size of 0.75 μm results in this sample (Fig. 5.1(b)). The evidence of exaggerated grain growth, however to a limited extent, is also seen only for a fewer grains. There are some columnar grains observed in 1000 ppm Y_2O_3 doped Al_2O_3 composites; this feature is different from pure Al_2O_3 samples. These columnar grains are formed, as reported, due to segregation of Y^{3+} on the grain boundary (Gall et al., 1995). The micrograph in Fig.5.1(c) shows that the grain structure consists of grains having nonuniform size and shape. This is due to the preferential segregation of dopant oxides on the grain boundaries leading to the grain growth control. A tendency to the formation of elongated grains is observed with this doping level.

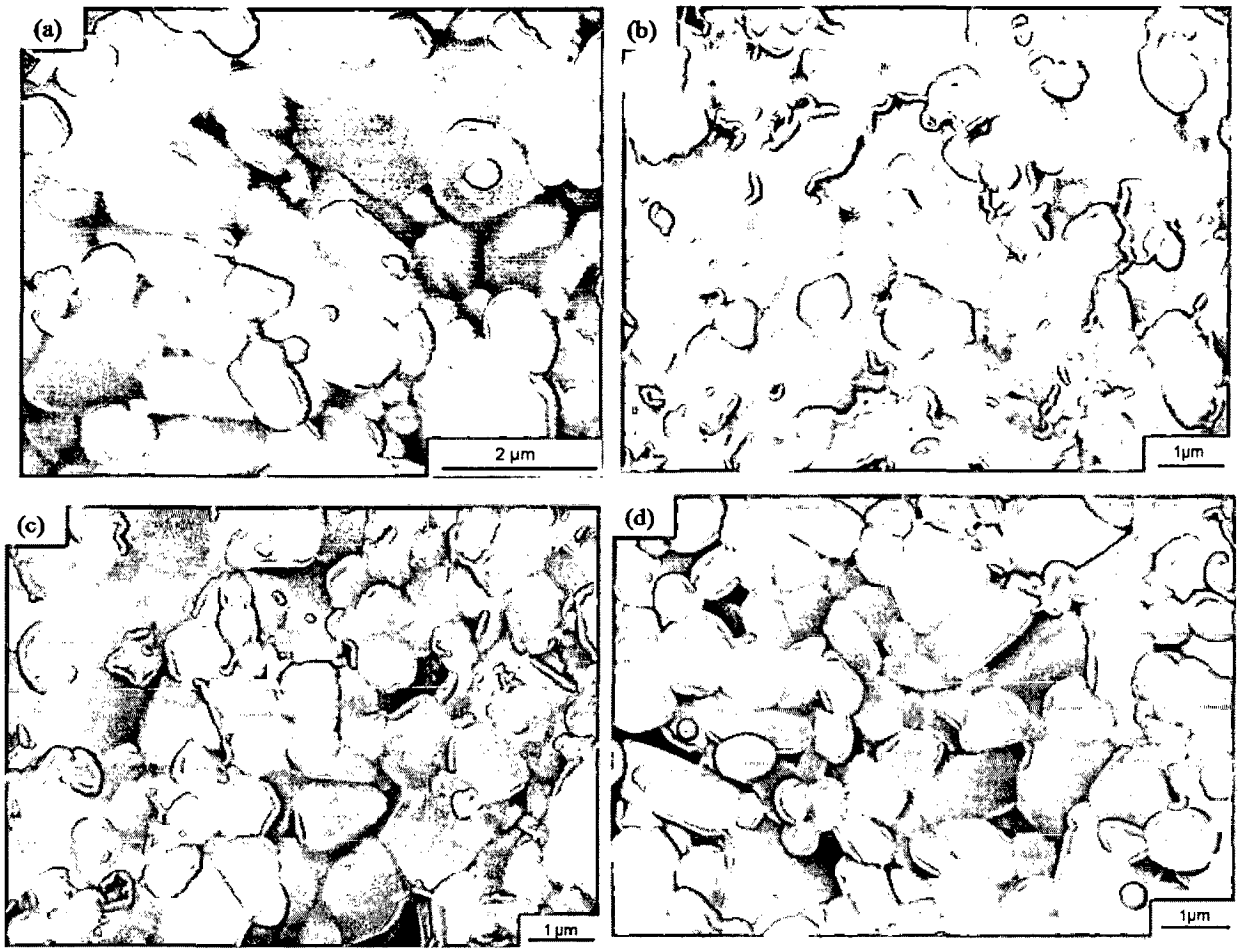

Fig. 5.1 SEM micrograph of (a) A, (b) A1Y, (c) A5Y and (d) A15Y sintered at 1500°C for the soaking time period of 6hr.

This micrograph (Fig. 5.1(d)) shows that the A15Y samples have more columnar type grains than that of A1Y and A5Y samples. The grain structure consists of two different grain shapes which are of nearly equiaxed and elongated types. Therefore the Y_2O_3 dopant has caused anisotropic grain growth in the materials due to sintering and the formation of elongated grains increases with increase in dopant concentration. Such microstructural design is beneficial for the toughness improvement in the samples through the mechanisms of crack bridging and / or crack deflection. The examination of micrograph also shows negligible porosity in the samples. The above Fig. 5.1(d) indicates that the rare earth cations have a strong potential to modify equiaxed Al_2O_3 grains to anisotropic elongated grains. This elongated morphology is believed to be due to preferential segregation of ions in basal planes

(0001) in Al_2O_3 grain boundaries (Altay and Gulgun, 2003). Grain boundaries in the samples A5Y and A15Y are relatively distinct.

The Table 5.4 shows the grain size range and the average grain size of the A and the AY samples. From the Table 5.4 it is clear that the grain size is lower in AY samples compared to that of the sample A. The range of grain size decreases with increasing Y_2O_3 content in the samples. For the sample A average grain size and range of grain size remain same with increasing time periods. The samples A1Y and A3Y show the increase in average grain size and range of grain size with increasing sintering temperature and soaking time periods. For the sample A5Y, A10Y and A15Y, the average grain size and grain size range remain closer for the samples sintered for the soaking time periods of 6, 9 and 12hr.

Table 5.4 Grain size and grain size range of the Al_2O_3 and Y_2O_3 doped Al_2O_3 samples sintered at 1500°C for different soaking time periods.

Sample	Soaking time periods							
	3hr		6hr		9hr		12hr	
	Range of grain size (μm)	Avg. grain size (μm)	Range of grain size (μm)	Avg. grain size (μm)	Range of grain size (μm)	Avg. grain size (μm)	Range of grain size (μm)	Avg. grain size (μm)
A	0.22 – 1.29	1.07	0.33- 1.91	1.58	0.37 – 1.95	1.58	0.41 -1.99	1.58
A1Y	0.34 – 1.57	0.65	0.29 – 1.44	0.75	0.33 – 1.58	0.83	0.32 – 1.71	0.94
A3Y	0.31 – 1.44	0.66	0.30 – 1.43	0.69	0.31 – 1.55	0.74	0.34 – 1.67	0.88
A5Y	0.28 – 1.63	0.72	0.38 – 1.64	0.86	0.40 – 1.63	0.87	0.34- 1.59	0.89
A10Y	0.29 – 1.29	0.66	0.4 – 1.86	0.75	0.27 – 1.47	0.76	0.29 – 1.36	0.74
A15Y	0.30 – 1.25	0.69	0.39 – 1.85	0.84	0.32 – 1.76	0.86	0.26 – 1.82	0.86

5.2.2 Grain size histogram

Fig.5.2 shows the histograms of grain size distribution of the samples A_6^{1500}, $A1Y_6^{1500}$, $A5Y_6^{1500}$, and $A15Y_6^{1500}$. Histograms show that the grain size ranges are not very different for one sample to another. In $A1Y_6^{1500}$ sample the distribution of different sized grains is identical. For $A15Y_6^{1500}$ sample the distribution of different sized grains are random than the others sample.

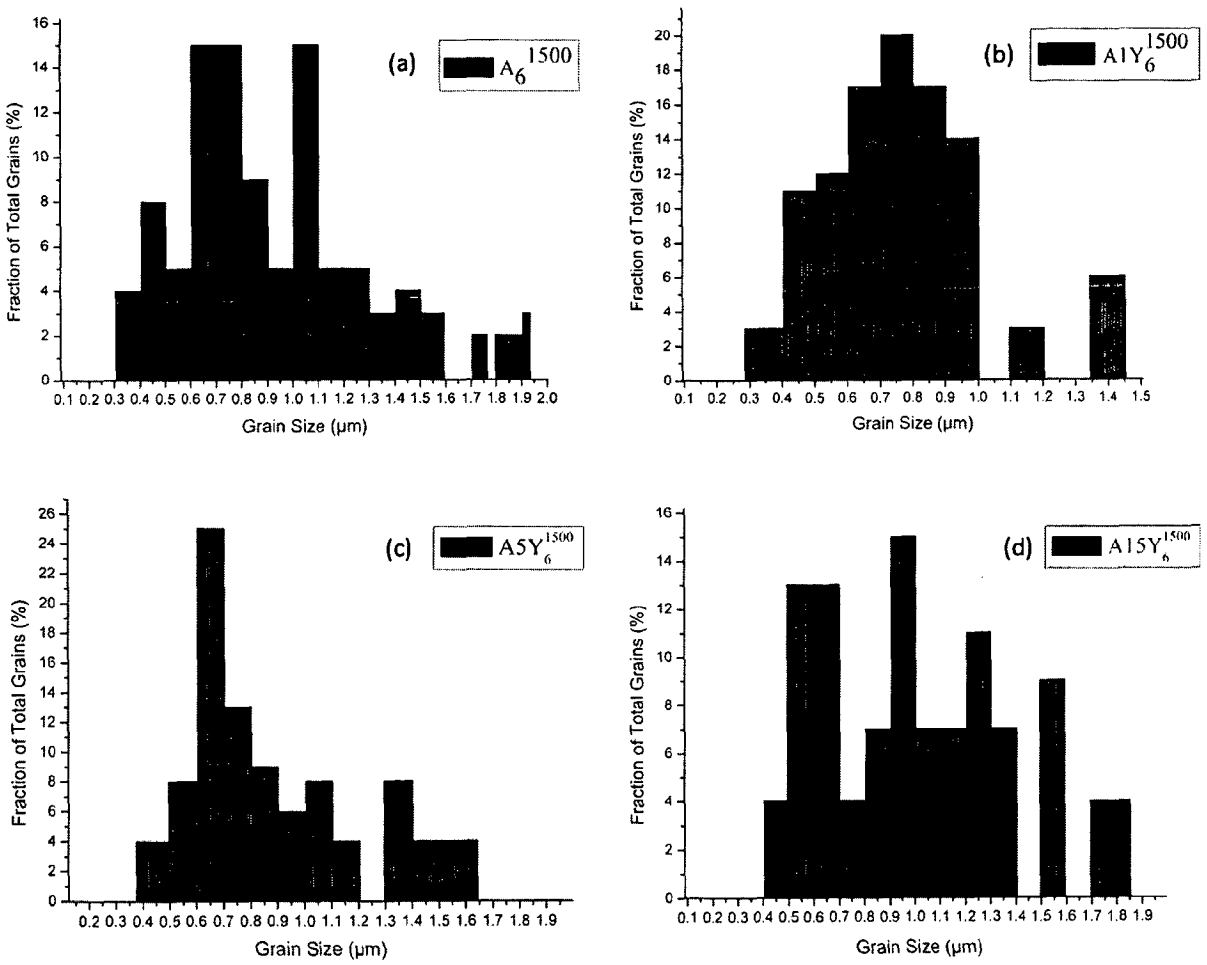

Fig.5.2 Grain size histograms of the samples (a) A_6^{1500}, (b) $A1Y_6^{1500}$, (c) $A5Y_6^{1500}$ and (d) $A15Y_6^{1500}$.

5.3 Effect of mechanical properties of A and AY samples sintered at 1500°C for different soaking time periods

Mechanical properties like hardness and fracture toughness of A and AY sample sintered at 1500°C for different soaking time periods has been studied.

5.3.1 Hardness of the sintered sample

The influence on hardness in the AY samples has been studied for different Y_2O_3 compositions and soaking time periods. The microstructural changes with Y_2O_3 content have been discussed with mechanical properties of the AY sample.

5.3.1.1 Effect of soaking time on hardness

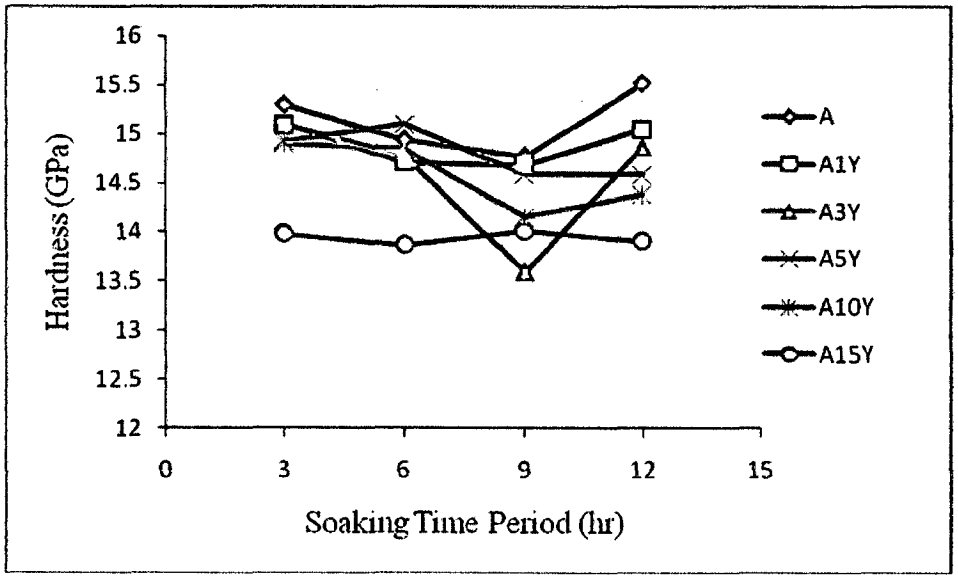

Fig.5.3 Hardness of A and AY samples as a function of soaking time period

Fig.5.3 shows the hardness of the A and AY samples for the different soaking periods. The A samples show the higher hardness than the AY samples. The A15Y samples have lower hardness than the other AY samples. The A1Y samples sintered for the soaking time period of 12 hr result in higher hardness compared to all other AY samples. The range of hardness for the AY samples is 13.59 - 15.1 GPa.

5.3.1.2 Effect of grain size on the hardness of the sample

Table 5.5 Hardness and grain size of the A and AY samples sintered at 1500°C for different soaking time periods.

Sample	Soaking time periods							
	3hr		6hr		9hr		12hr	
	Avg. grain size (μm)	Hardness (GPa)	Avg. grain size (μm)	Hardness (GPa)	Avg. grain size (μm)	Hardness (GPa)	Avg. grain size (μm)	Hardness (GPa)
A	1.07	15.3	1.58	14.94	1.58	14.77	1.58	15.52
A1Y	0.65	15.1	0.75	14.71	0.83	14.68	0.94	15.05
A3Y	0.66	15.09	0.69	14.78	0.74	13.59	0.88	14.87
A5Y	0.72	14.93	0.86	15.1	0.87	14.59	0.89	14.59
A10Y	0.66	14.9	0.75	14.85	0.76	14.15	0.74	14.38
A15Y	0.69	13.98	0.84	13.86	0.86	14.01	0.86	13.90

Table 5.5 shows the hardness of A and AY samples depending on the grain size. The hardness of the sample A varies between 14.77 and 15.52 GPa. The range of hardness of the AY samples is less than that of the sample A. The average grain size difference of the AY samples is not very significant and the variation of hardness of one sample to another sample is not significant. The addition of Y_2O_3 resulted in slight decrease in the hardness (Xu et al., 2006). Although in AY samples the grain size is not found decreased with increasing Y_2O_3 content, implying that the density of the sample has a primary effect on lowering the hardness of the samples.

5.3.2 Fracture toughness of the sample

The fracture toughness of monolithic A samples has been changed with the variation of the Y_2O_3 content and soaking time period of sintering.

5.3.2.1 Effects of soaking time period on fracture toughness of A and AY samples

Table 5.6 The fracture toughness of the A and AY samples sintered 1500°C for the different soaking time periods.

Sample	Fracture toughness(MPa $m^{1/2}$) of the sample sintered for different soaking time period			
	3hr	6hr	9hr	12hr
A	5.22	5.20	5.38	5.37
A1Y	4.99	5.40	5.43	5.69
A3Y	4.77	5.05	5.32	5.31
A5Y	5.02	4.81	5.08	5.23
A10Y	4.75	4.80	4.98	4.99
A15Y	4.48	4.65	4.80	4.90

Table 5.6 shows the fracture toughness of A and AY samples. The A1Y samples show higher fracture toughness compared to other samples. $A1Y_{12}^{1500}$ sample shows the fracture toughness of 5.69 MPa $m^{1/2}$ which is highest among all the values for A and AY samples. The fracture toughness of the undoped sample A varies between 5.20 and 5.38 MPa $m^{1/2}$. The fracture toughness of A10Y and A15Y samples is relatively lower than that of the A3Y and A5Y samples. The lower relative density of A10Y and A15Y samples may be one of the reason for low fracture toughness of the samples. The precipitation of YAG phase decreases

the fracture toughness of the A15Y (Loudjani & Haut, 1996). The formation of YAG phase in the A15Y has been shown in the section of XRD analysis (Section 5.4).

5.3.2.2 Effects of Y_2O_3 on the fracture toughness of A and AY samples

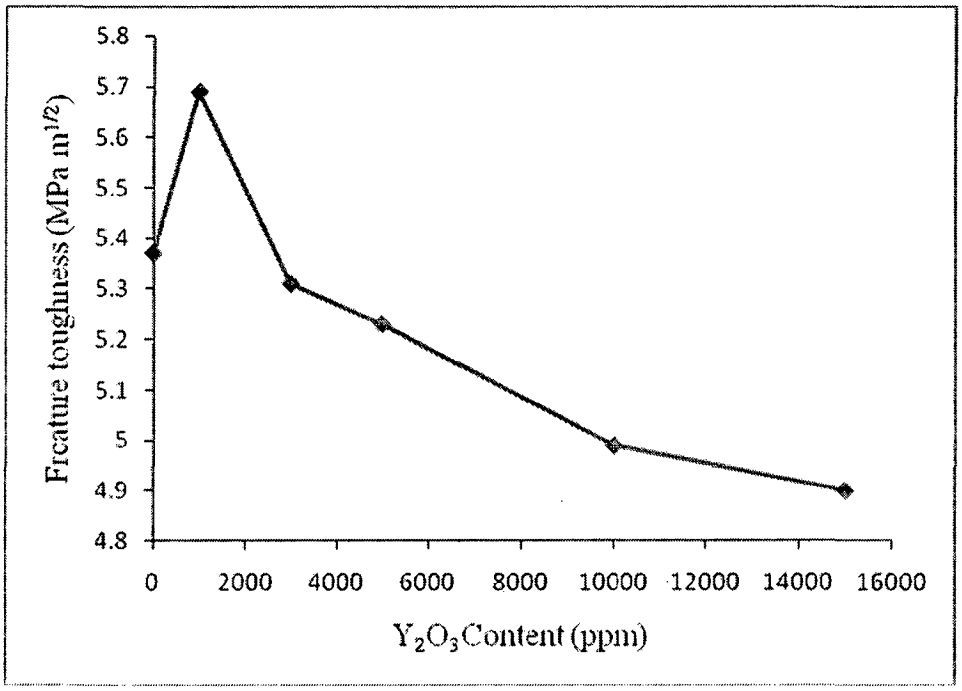

Fig.5.4 Fracture toughness of A and AY samples containing different Y_2O_3 contents sintered at 1500°C for the soaking time period of 12hr.

Fig.5.4 shows that the incorporation of Y_2O_3 in Al_2O_3 can improve the fracture toughness of the sample when its content is less than 1000 ppm. Particularly, for the samples containing 1000 ppm Y_2O_3, the fracture toughness reaches to 5.69 MPa $m^{1/2}$ which is more than that of the undoped Al_2O_3 sample. Weak interface deflects the crack path causes the increase in the fracture toughness. Interfaces between yttrium (Y) and matrix become weak due to segregation of Y. The interfacial bonding strength is consequently decreased which makes it prone for the cracks to extend along the interfaces. However with increase in Y content the proportion of weak interfaces relative to strong interfaces increases. Because of the coexistence of both strong and weak interfaces, toughening mechanism like crack bridging, crack deflection and microcracking results the improvement in fracture toughness of A1Y sample (Xu et al., 2006).

5.3.2.3 Correlation of fracture toughness with mode of crack path

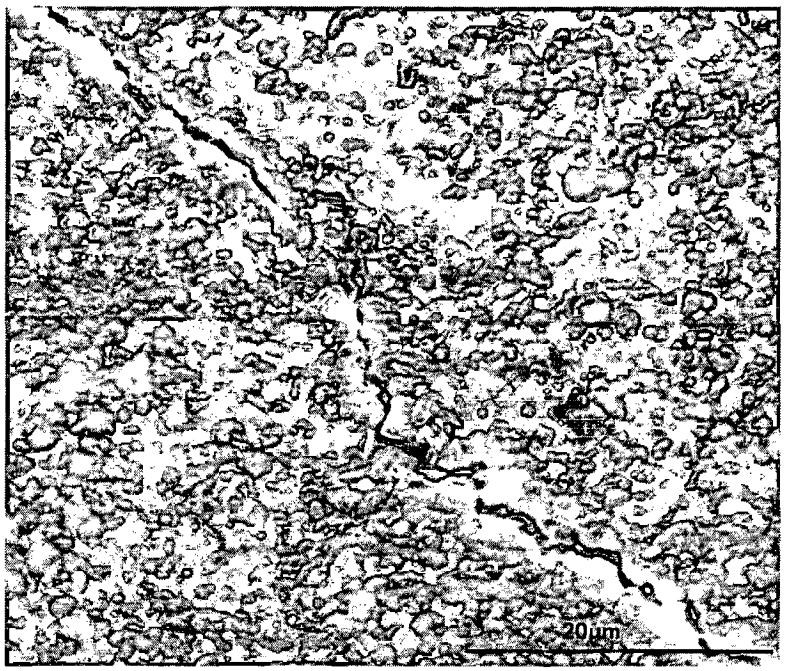

Fig.5.5 SEM micrograph of A1Y sample sintered at 1500°C for 6hr.

The micrograph of the $A1Y_6^{1500}$ sample in Fig.5.5 shows the evidence of crack deflection which perhaps contributed partially to the higher fracture toughness of the sample.

5.4 XRD analysis

Fig. 5.6 shows the XRD patterns of (a) $A1Y_9^{1500}$, (b) $A5Y_9^{1500}$, (c) $A10Y_9^{1500}$ and (d) $A15Y_9^{1500}$ samples. The pattern in Fig.5.6 (a), shows the peaks of Al_2O_3 (ICSD data file No. 01-071-1124) along with that of $Y_3Al_5O_{12}$ (ICSD data file No. 01-088-2048 with second highest intensity peak) (Zakharchenya and Vasilevskaya, 1993). The pattern in Fig.5.6 (b) shows the peaks of Al_2O_3 along with that of $Y_3Al_5O_{12}$ and $YAlO_3$ (Yttrium aluminum perovskite) (ICSD data file NO. 01-087-1288 with highest intensity peak) (Ross, 1996). The pattern in the Fig.5.6 (c) shows the peaks of Al_2O_3 along with $YAlO_3$, $Al_{2.66}O_4$, $Y_3Al_5O_{12}$ (ICSD data file No. of $Al_{2.66}O_4$ is 01-082-0575). The pattern in Fig.5.6 (d) shows the presence of Al_2O_3 along with YAG phase (ICSD data file No. 01-088-2047) (Bagdasarov et al., 1991).

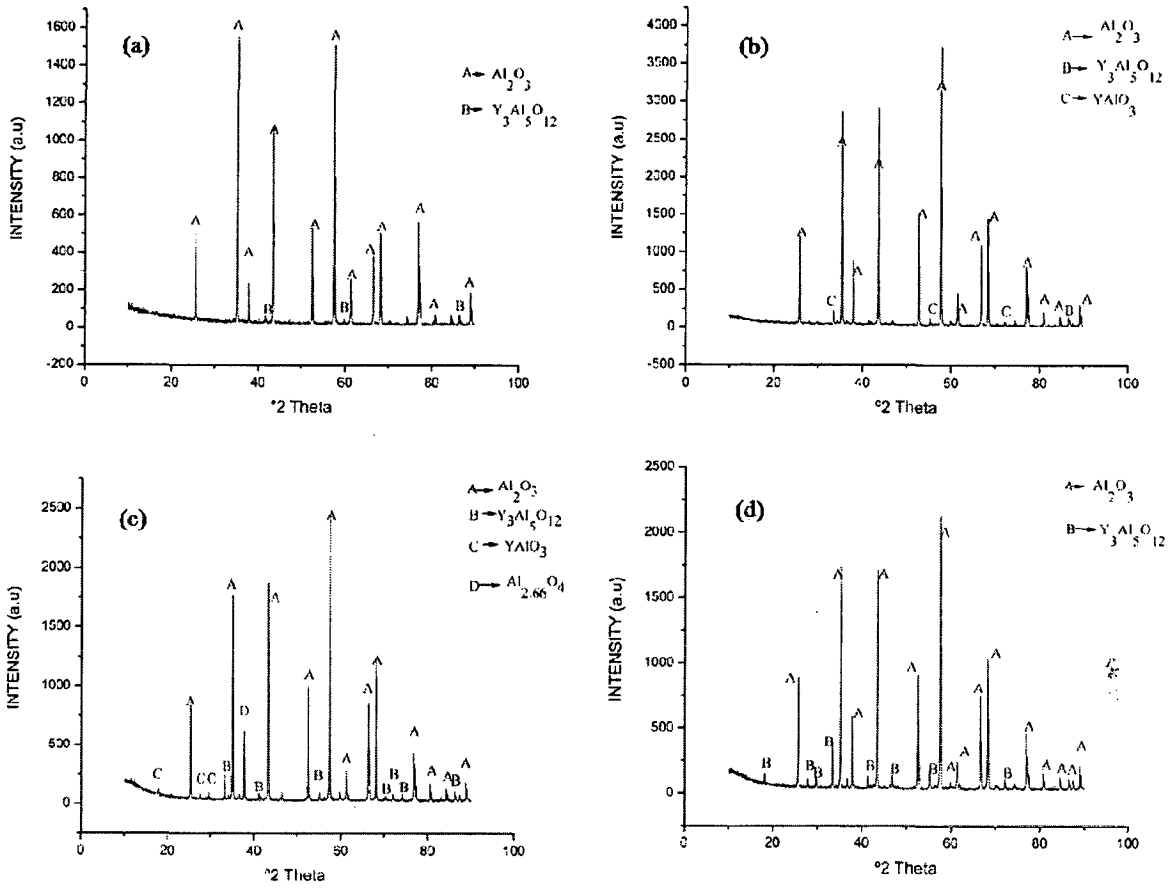

Fig.5.6 X-ray diffraction pattern of (a) $A1Y_9^{1500}$, (b) $A5Y_9^{1500}$, (c) $A10Y_9^{1500}$ and (d) $A15Y_9^{1500}$

Yttrium aluminium garnet (YAG or $Y_3Al_5O_{12}$) has a cubic structure and is of great interest as a high-temperature engineering material, due to its high-temperature strength coupled with low creep rate which indicates that YAG is a suitable reinforcing phase (Wang et al., 2006). Omri et al., reported that in the system ZrB_2 – YAG during sintering between 1000°C and 1600°C, YAG melts and the space between ZrB_2 particles gets filled with the molten material (Omri M., 2000). The fracture toughness of YAG contained ZrB_2 is higher than only Y contained ZrB_2 (Song et al., 2009). Though YAG content in $A15Y_9^{1500}$ sample is more than that in $A1Y_9^{1500}$ sample, the fracture toughness of A15Y is lower than that of A1Y. The interface between Y and Al_2O_3 is more in A15Y than A1Y which decreases the fracture toughness in sample A15Y.

5.5 Comparison of Indentation method (IM) and SEPB method for the calculation of fracture toughness

Table 5.7 Fracture toughness of the A and AY samples measured by SEPB and indentation methods.

Sample	Fracture toughness of the samples sintered at (MPa $m^{1/2}$)							
	3hr		6hr		9hr		12hr	
	SEPB method	IM method	SEPB method	IM method	SEPB method	IM method	SEPB method	IM method
A	4.79	5.22	5.26	5.20	5.19	5.38	5.25	5.37
A1Y	4.70	4.99	5.27	5.40	5.19	5.43	5.62	5.69
A3Y	4.05	4.77	4.65	5.05	4.81	5.32	5.23	5.31
A5Y	3.99	5.02	4.48	4.81	4.55	5.08	4.77	5.23
A10Y	4.25	4.75	4.41	4.80	4.37	4.98	4.53	4.99
A15Y	3.66	4.48	4.15	4.65	4.54	4.80	4.81	4.90

Table 5.7 shows that for the samples the SEPB method yields lower fracture toughness compared to using indentation method.

5.6 Mechanical properties of 1000 ppm Y $(NO_3)_3.6H_2O$ doped Al_2O_3 ceramic composites

Table 5.7 shows the sample $A1Y_{12}{}^{1500}$ has higher fracture toughness than other Y_2O_3 doped and undoped samples. The fracture toughness decreases with increasing Y_2O_3 content greater than 1000 ppm. It has been optimized that for the improvement of fracture toughness in Y_2O_3 doped Al_2O_3, 1000 ppm of Y_2O_3 is suitable. The ionic size of Y is more than that of Al and it has been reported that the Y goes to the grain boundary of Al_2O_3 (Bender et al., 1980). Researchers introduced Y^{3+} in Al_2O_3 by using the raw material $Y(NO_3)_3.6H_2O$.

Segregation or precipitation in grain boundary of Al_2O_3 induces a decrease in the grain size. The grain size influences the fracture toughness of the Al_2O_3 sample (Loudjani et al., 1993). To know the possible locations of the Y in 1000 ppm Y $(NO_3)_3$ $6H_2O$ doped Al_2O_3 sample EDS was carried out. The point scan on the grain boundary reveals the presence of Y as shown in Fig.5.7.

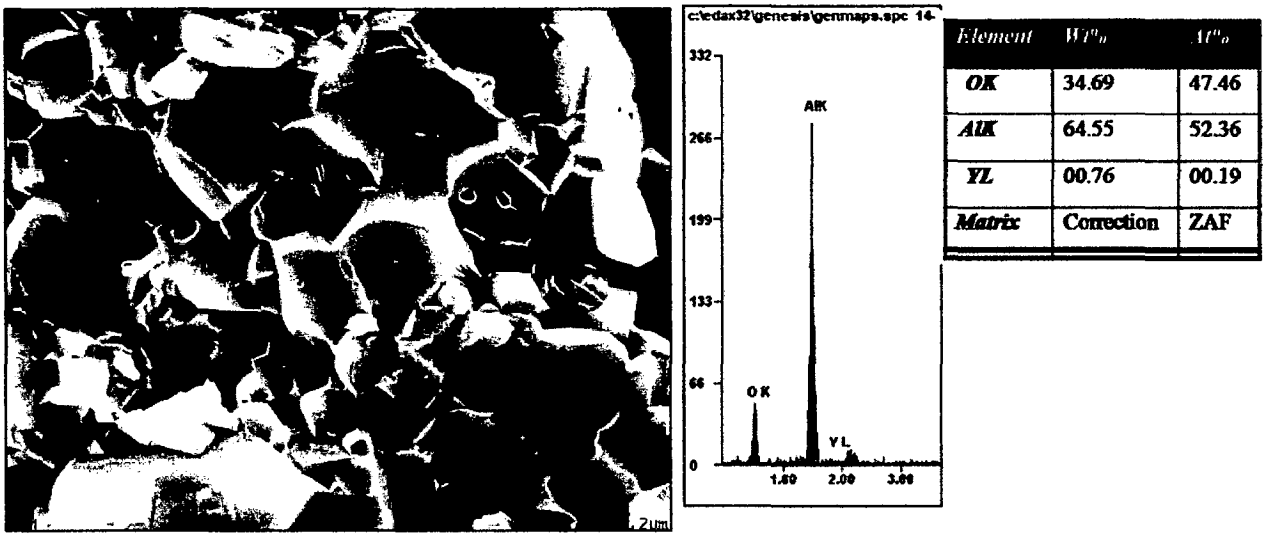

Element	Wt%	At%
OK	34.69	47.46
AlK	64.55	52.36
YL	00.76	00.19
Matrix	Correction	ZAF

Fig.5.7 SEM micrograph of 1000 ppm $Y(NO_3)_3$ $6H_2O$ doped Al_2O_3 ceramic composites sintered at 1500°C for 12hr.

Table 5.8 shows the hardness and fracture toughness of Y $(NO_3)_3$ $6H_2O$ doped Al_2O_3 samples sintered at 1500°C for 12 hr. The fracture toughness of the sample measured by two different methods are given in the Table 5.8. The fracture toughness of this sample is almost identical with the $A1Y_{12}^{1500}$ sample.

Table 5.8 Hardness and fracture toughness of Y $(NO_3)_3$ $6H_2O$ doped Al_2O_3 sample sintered at 1500°C for 12 hr

ample	Hardness (GPa)	Fracture toughness (MPa $m^{1/2}$)	
		SEPB method	VIF method
Al_2O_3 - $Y(NO_3)_3$ $6H_2O$	14.95	5.59	5.66

5.7 Summary

The large grain size helps to improve the fracture toughness by following the grain bridging mechanism. Microcracks, residual stress form with increasing grain size and beyond the critical size of grain the fracture toughness of the sample reduces. The solubility of Y is 10 ppm in Al_2O_3 and the excess amount of Y goes to the grain boundary. Precipitation occurs when grain boundary becomes insufficient to accommodate the Y on its surface (Cawley and Halloran, 1986). The interface between Y and Al_2O_3 is generally weak leading the cracks to travel through that this interface.

So by considering the formation of weak interface between Y and Al_2O_3 and restriction of grain growth, rare earth oxide (Y_2O_3) has been introduced as dopant in Al_2O_3. The sample has been prepared by varying Y_2O_3 content. The doping level of Y_2O_3 has been varied between 1000 ppm and 15,000 ppm. The samples were sintered at 1500°C for four different soaking time periods. It has been observed that the relative density of the doped samples decreases with increasing Y_2O_3 content. Micrographs of the sintered AY samples show the formation of elongated grains in $A15Y_6^{1500}$ sample. The average grain size of the samples decreases with increasing Y_2O_3 content. The A1Y sample shows the highest fracture toughness compared to A and other AY samples. Therefore this study reveals that 1000 ppm Y_2O_3 is optimum to get improved fracture toughness in AY system. The XRD analysis of AY samples shows the presence of YAG, $YAlO_3$ and $Al_{2.66}O_4$ phases along with Al_2O_3. Samples have also been prepared using 1000 ppm $Y(NO_3)_3\ 6H_2O$ as the source of the dopant in Al_2O_3 and the fracture toughness of this sample is found nearly same as that of A1Y. The EDS analysis of the sintered sample shows the presence of Y element in grain boundary of Al_2O_3. To the best of the candidate's knowledge the optimization of doping level by considering different dopant concentrations has not been reported by other researchers. The formation of the secondary phase YAG is evident from the XRD analysis data, which shows that this phase perhaps play a role to give rise to the observed higher fracture toughness of the samples A1Y.

Chapter 6

Microstructural changes with single and double rare earth doped $Al_2O_3 - ZrO_2$ composites and their fracture toughness

Chapter 6

6.1 Introduction

The brittleness and poor damage tolerance have limited the scope of almost all the ceramic materials for their use as advanced engineering materials. The fracture toughness of the ceramic materials is generally low because the dislocation motion in the material is extremely limited due to the nature of the chemical bonds which are ionic and/or covalent. The problem of the low fracture toughness of the ceramics can be overcome by designing and preparing the composite materials reinforced with fibers, whiskers and particulates of the same phase as that of matrix or of any other suitable phase (Tuan et al., 2008, Endo et al., 1994, Wang and Stevens, 1989). The ZrO_2 based ceramics have relatively higher fracture toughness compared to other oxide ceramics (Porter et al., 1979, Shukla et al., 2002, Kosmac et al., 1985). Pure ZrO_2 has three polymorphic forms. At very high temperatures (>2370°C) the crystalline structure is cubic. At intermediate temperatures i.e. between 1170 and 2370°C it exists in tetragonal structure. At temperature below 1170°C the structure is monoclinic.

The addition of ZrO_2 to the Al_2O_3 ceramics increases the fracture toughness of the ceramic composite materials. This effect is due to the tetragonal to monoclinic phase transformation of ZrO_2, with an increase in the specific volume of the material by 3–6%. This volume increase generates a compressive stress in the ceramic matrix near the interface between ZrO_2 and Al_2O_3, which makes the propagation of any crack progressing to the interface difficult (Daguano et al., 2007). This stress-induced phase-transformation toughening and micro-crack toughening are the major toughening mechanisms in Al_2O_3 – ZrO_2 (ZTA) composites (Shin et al., 1999). The material ZTA is used for making metal cutting tools, wear components, bearings and joint implants, etc (Garvie and Swain, 1985, Basu and Sarkar, 2001).

6.2 Physical properties of Al_2O_3–5wt% ZrO_2 composites

The physical properties of Al_2O_3 –5wt% ZrO_2 have been reported. The EDS analysis has also been reported to determine the chemical composition of the powder.

6.2.1 EDS analysis of ZrO_2 powder

The average particle size of the ZrO_2 powder used was 0.4 μm and the purity of the powder was 99%. Chemical composition of raw materials has been determined by using EDS.

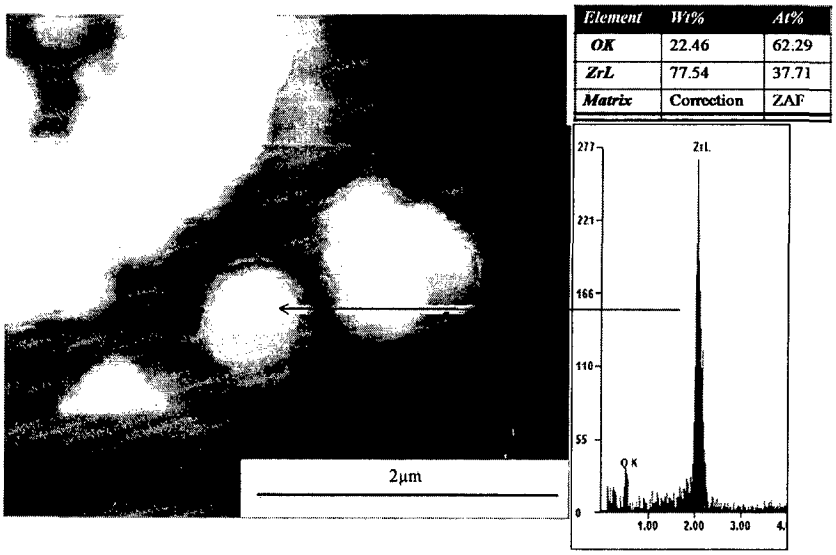

Fig.6.1 EDS spectra of as received ZrO_2 powder

Fig.6.1 shows the EDS spectra of the ZrO_2 powder used. The analysis of the spectra gives the atomic ratio between the Zr and O is (Zr content 37.71 at% and O content 62.29 at %) showing that the powder is nearly stoichiometric compound and having no other elements present as an impurity.

6.2.2 Sintering of ceramics

ZrO_2 powder is mixed with Al_2O_3 to improve the densification and mechanical properties of the monolithic Al_2O_3 (Tuan et al., 2002). The change in the microstructural morphology was induced by following the same strategy for sintering as was used in the case of Al_2O_3. The samples were sintered at 1500°C, 1600°C and 1700°C for 3hr, 6hr, 9hr and 12hr.

6.2.3 Relative density of the AZ samples

Table 6.1 presents relative densities of the Al_2O_3–5wt% ZrO_2 (AZ) composites sintered at 1500°C, 1600°C and 1700°C for the soaking time period of 3hr, 6hr, 9hr and 12hr.

The estimation of these density data is based on the theoretical density of the composite which was calculated following rule of mixtures. The relative densities vary between 97.27% and 98.76%.

Table 6.1 Relative density of AZ samples sintered at 1500°C, 1600°C and 1700°C for different soaking time periods.

Sintering temp. (°C)	1500				1600				1700			
Soaking time (hr)	3	6	9	12	3	6	9	12	3	6	9	12
Relative density (%)	97.27	97.52	98.26	98.26	98.01	98.26	98.51	98.76	98.51	98.01	97.76	97.76

6.2.4 Weight loss

The weight losses for sintering the samples AZ at 1500°C, 1600°C and 1700°C, are shown in Fig.6.2., the sintered sample has denoted as AZ1500, AZ1600 and AZ1700 respectively. The samples sintered at 1700°C (AZ1700) show higher weight loss. Weight loss for the samples sintered at 1500°C and 1600°C are almost identical.

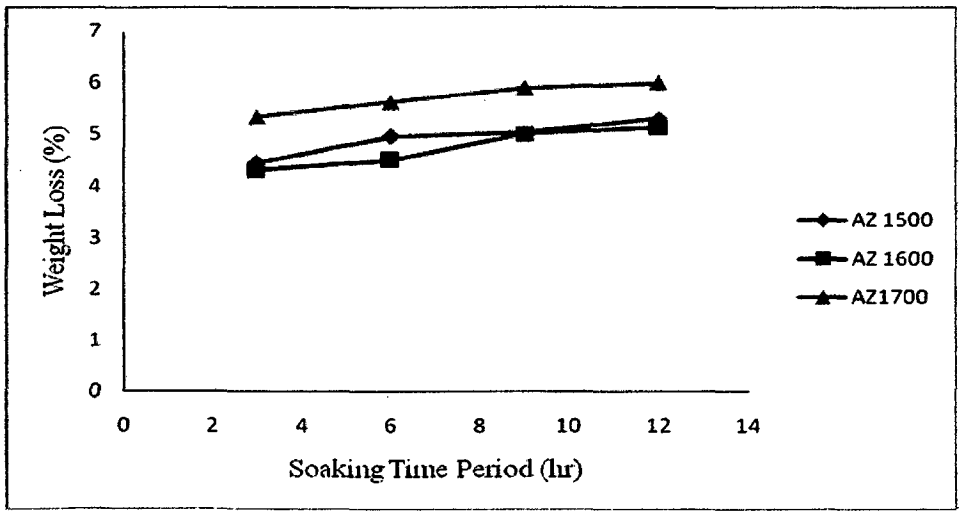

Fig.6.2 Weight loss as a function of soaking time of sintering the AZ samples at 1500°C, 1600°C and 1700°C.

6.2.5 Linear shrinkage

Fig. 6.3(a) shows the linear shrinkage in the samples sintered at 1500°C remains unchanged with increasing the soaking time period. For the samples sintered at 1600°C and 1700°C the degree of the linear shrinkage is almost same and for both these samples the linear shrinkage remains unchanged with increasing soaking time period. The linear shrinkage of AZ_3^{1500} sample is lower than the other samples. The range of linear shrinkage in the samples sintered at 1500°C, 1600°C and 1700°C lies between 12% and 14 %.

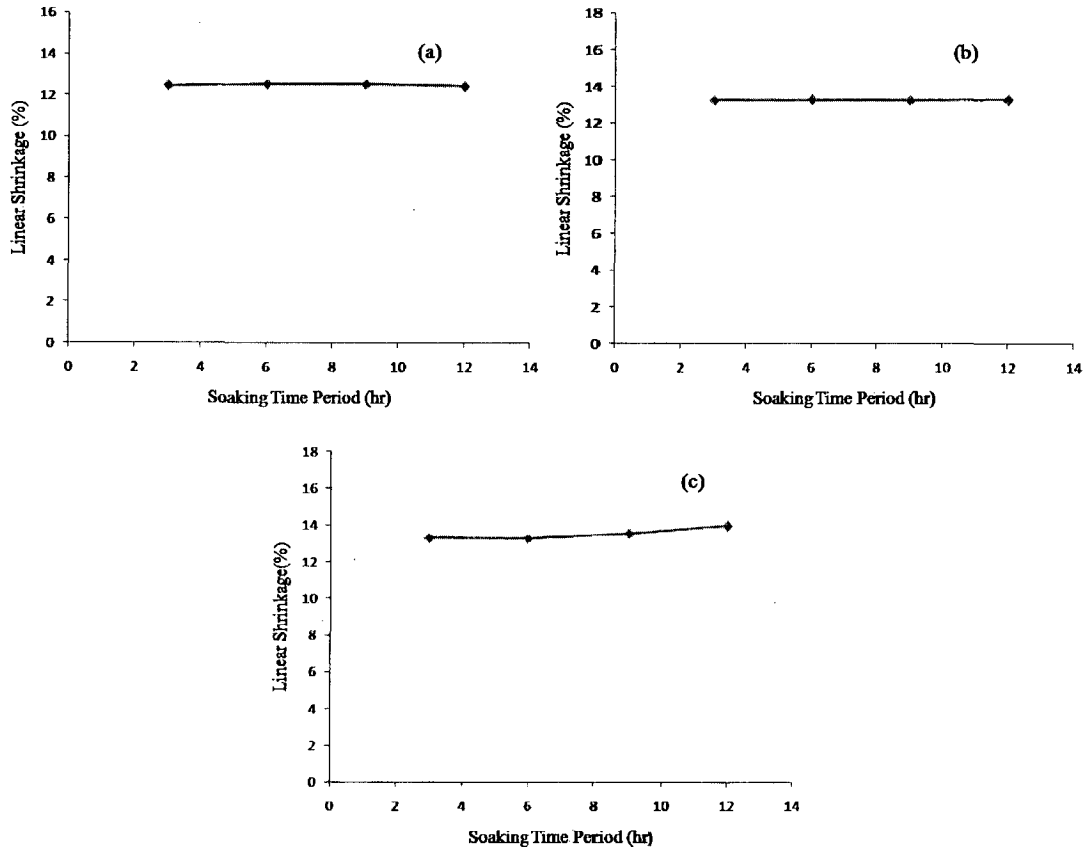

Fig.6.3 Linear shrinkage as a function of soaking time period for the samples sintered at (a) 1500°C, (b) 1600°C and (c) 1700°C.

6.3 Analysis of microstructure of AZ samples

6.3.1 Microstructure of sintered AZ samples

Fig.6.4 shows the SEM micrographs of (a) AZ_3^{1500}, (b) AZ_{12}^{1500} samples. Fig. 6.4(a)

shows the smaller grains are in round shape and larger grains are in irregular shape. It can be observed from the Fig. 6.4(a) that at some locations on the grain morphology a few grains are found to have diffused each other giving rise to apparently larger grains at those locations. Such grains are assumed to have disproportionately larger size than the average size of the remaining individual grains constituting the microstructure. The grain size variation considering all sizes of the grain lies in the range of 0.4 to 4.32 μm with the average grain size of 1.33 μm. Fig. 6.4(b) shows that the average grain size is larger than that in Fig. 6.4(a). In this sample also the smaller grains are in round shape and larger grains have irregular shape. The larger grains are more and smaller grains are less than that in the sample AZ_3^{1500}. The grain size varies between 0.6 and 6.92 μm with the average grain size 1.90 μm. As evident from the phase diagram (Fig. 2.11), the solubiliy of ZrO_2 in Al_2O_3 is as low (~2000ppm), the ZrO_2 and the Al_2O_3 remain as separate phases for the composition used in the present study. This is to mention that a very small quantity of ZrO_2 forms solid solution with Al_2O_3, and this trace amount is not detectable in the micro analysis of the samples. In view of the fact that small quantity of ZrO_2 compared to Al_2O_3, ZrO_2 grain size is limited to very small size and forms preferably at tripple points in the grain structure. In order to know the possible locations of the ZrO_2 particles, microanalysis of one sample AZ_{12}^{1500} as a typical representative of the AZ ceramic composites prepared, was done and the results, along with the micrograph is presented in Fig. 6.4(b).

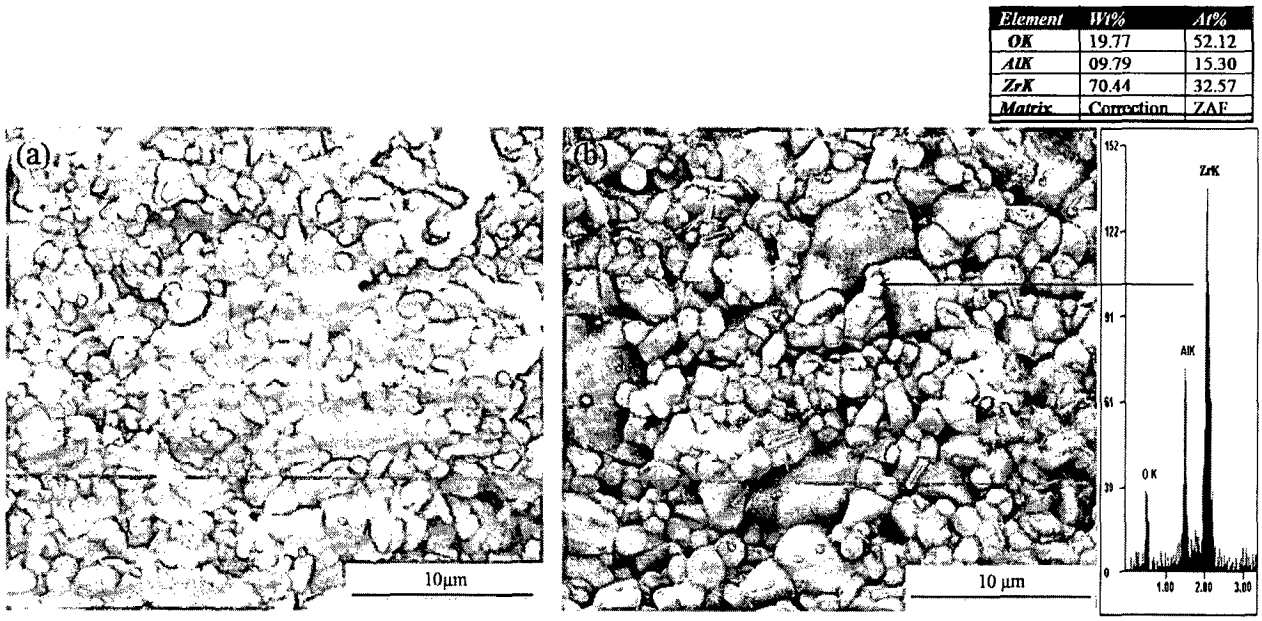

Fig.6.4 SEM micrograph of composite samples (a) AZ_3^{1500}, (b) AZ_{12}^{1500} with EDS spectra.

Fig. 6.5(a) and (b), show the SEM micrographs of AZ_3^{1600} and AZ_{12}^{1600} composite samples respectively, which have compact grain structures compared to those in the samples sintered at 1500°C. It is evident that the samples consist of mixed grain sizes, the smaller grains are of round shape and larger grains have irregular shape (Fig.6.5 (a) and (b)). Fig. 6.5 shows that a few larger grains have grown at the expense of smaller grains and the intergranular regions of such larger grains are occupied by a number of samller grains. Fig.6.5 (a) shows all the grains are larger compared to that in Fig.6.4. The grain size range of the sample AZ_3^{1600} is 1.65-34.55 μm with the average grain size of 7.52 μm. The grain size range of the sample AZ_{12}^{1600} is 2.33-47.22 μm with the average grain size of 9.66 μm.

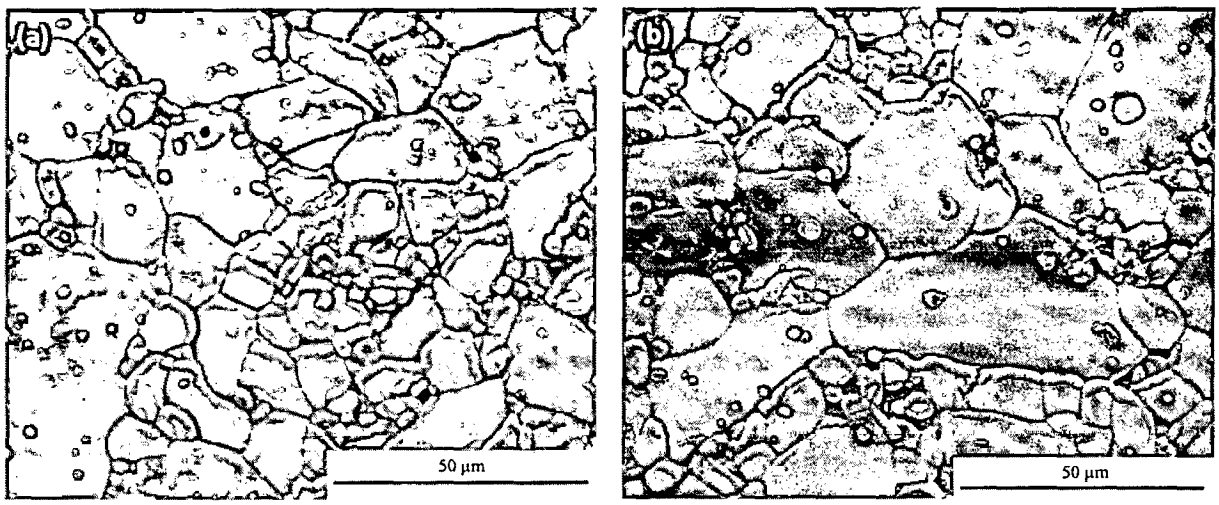

Fig.6.5 SEM micrograph of (a) AZ_3^{1600}, (b) AZ_{12}^{1600} composite samples.

Fig.6.6 (a) and (b), show the SEM micrographs of AZ_3^{1700} and AZ_{12}^{1700} composite samples. The Fig.6.6(b) shows the grains are of round shaped and relatively larger grains are irregular in shape. The grain size ranges of the samples AZ_3^{1700} and AZ_{12}^{1700} are 2.20 – 39.94 µm and 6.23 – 75.01 µm respectively. The average grain size of the samples AZ_3^{1700} and AZ_{12}^{1700} are 13.10µm and 23.20µm respectively.

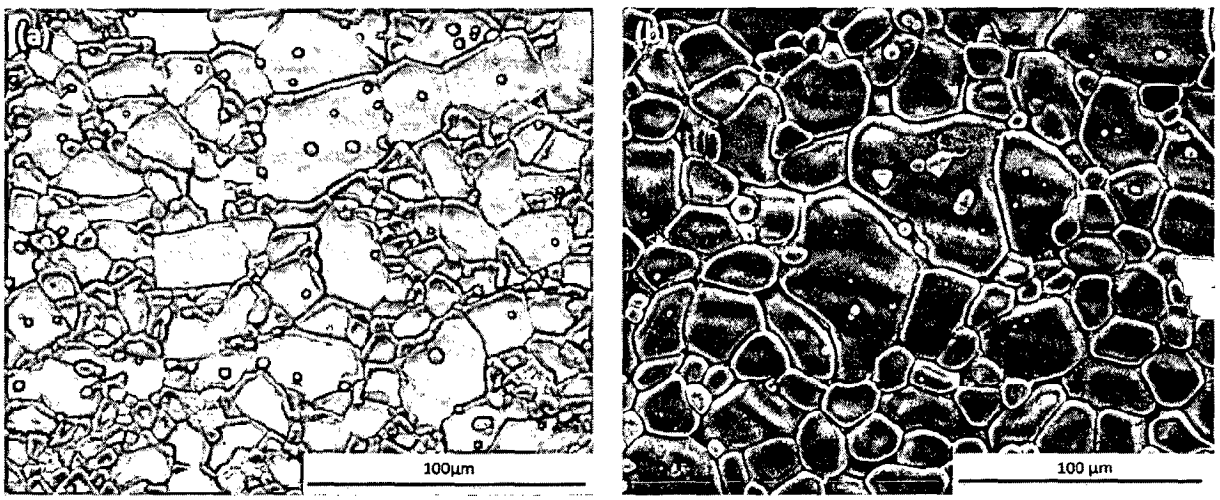

Fig.6.6 SEM micrograph of (a) AZ_3^{1700}, (b) AZ_{12}^{1700} composite samples.

Table.6.2 Average grain size, grain size range and grain size difference of AZ samples sintered at 1500°C, 1600°C and 1700°C for different soaking time periods.

Sample	Average grain size (μm)	Grain size range (μm)	Grain size difference (μm)
AZ_3^{1500}	1.33	0.4-4.32	3.92
AZ_6^{1500}	1.70	0.5-5.05	4.55
AZ_9^{1500}	1.81	0.6-6.8	6.2
AZ_{12}^{1500}	1.90	0.6- 6.92	6.32
AZ_3^{1600}	7.52	1.65-34.55	32.9
AZ_6^{1600}	8.45	1.71- 35.97	34.26
AZ_9^{1600}	8.90	1.75-39.52	37.77
AZ_{12}^{1600}	9.66	2.33-47.22	44.89
AZ_3^{1700}	13.10	2.20-39.94	37.74
AZ_6^{1700}	19.61	4.33-49.8	45.47
AZ_9^{1700}	21.51	5.38-65.45	60.07
AZ_{12}^{1700}	23.20	6.23-75.01	68.78

Table 6.2 shows that the average grain size increases with increasing sintering temperature and soaking time period for a fixed sintering temperature. The average grain size of the samples sintered at 1500°C is low. The average grain size varies between 1.33 and 1.90 μm depending on the soaking time period for the samples sintered at 1500°C. The grain size ranges for the samples sintered at 1600°C and 1700°C are 7.52 - 9.66 μm and 13.10 – 23.20

μm respectively. It can be seen from the Table 6.2 that the grain in the samples sintered at 1600°C and 1700°C are in wider size range compared to the samples sintered at 1500°C.

6.3.2. Grain size histogram plots for the AZ samples

The measured grain size data range for each sample was subdivided into smaller segments and the histogram plots were made to show the grain size distribution. Fig.6.7, Fig.6.8 and Fig.6.9 present a few of such histograms for the samples sintered at 1500°C, 1600°C and 1700°C respectively. This histogram revels that the grain growth occurs with increasing soaking time period. In the Fig. 6.7(a), the grain size varies from 0.4 to about 6 μm and large number of grains fall between 0.4 and 2 μm. In the Fig. 6.7(b), the grain size varies from 0.5 to about 6 μm and large number of grains fall in the range of 2 to 3 μm.

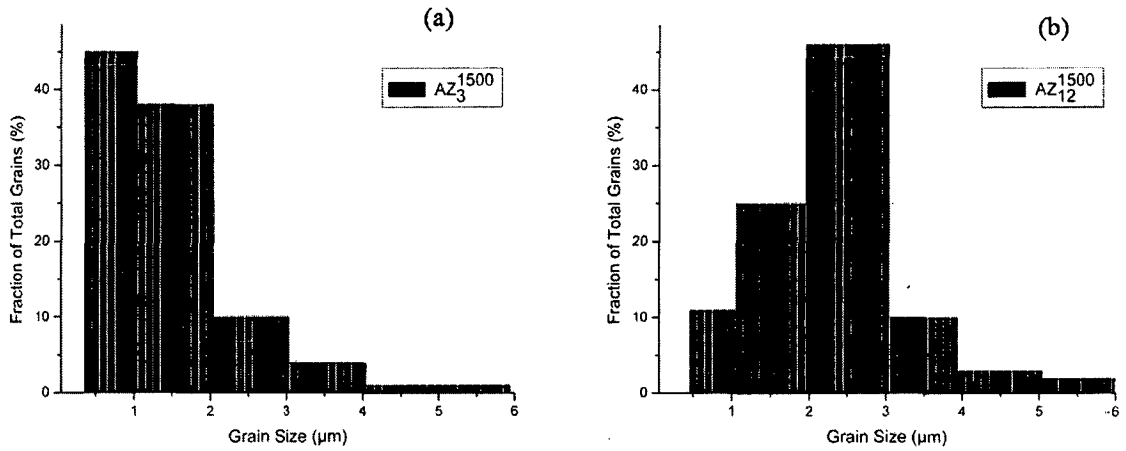

Fig.6.7 Grain size histograms for the samples of (a) AZ_3^{1500}, (b) AZ_{12}^{1500}.

Fig.6.8 (a) and (b) show the grain size histogram of samples AZ_3^{1600} and AZ_{12}^{1600} respectively. Fig.6.8 shows the grain size is more than that in the Fig.6.7. The Fig.6.8 (a,b) shows that there is a wide range in the grain size but the majority of the grains fall in the lower part of the size range.

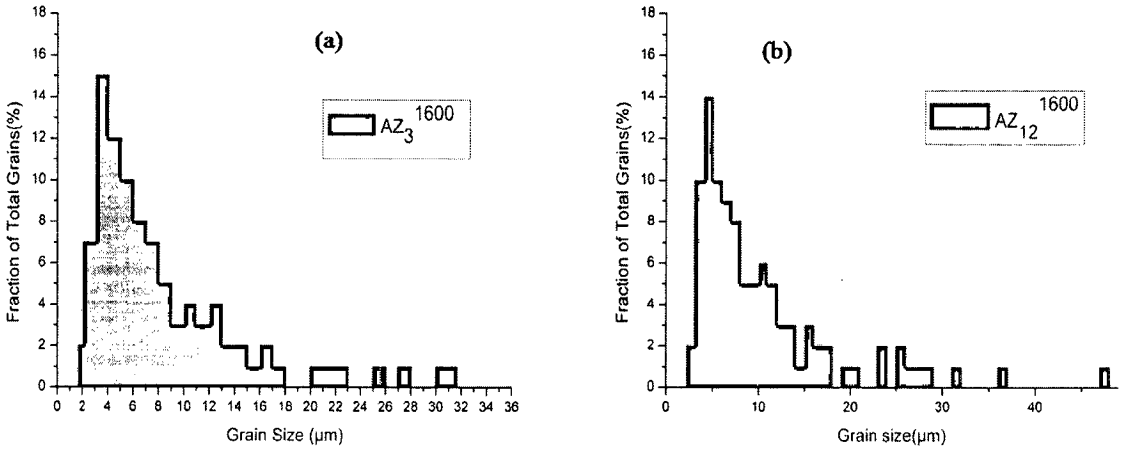

Fig.6.8 Grain size histograms for the samples (a) AZ_3^{1600}, (b) AZ_{12}^{1600}.

Fig. 6.9 (a) and (b) show the grain size histograms of the samples $AZ_3^{1700}$and AZ_{12}^{1700} respectively. The grain size distribution is different in the Fig. 6.9(b) compared to that in Fig.6.7, Fig.6.8 and Fig. 6.9(a). The range of grain size of the sample as shown in the Fig. 6.9 (b) is wider compared to other samples. The grain size distribution is more discrete and the individual grains are relatively larger compared to the other samples.

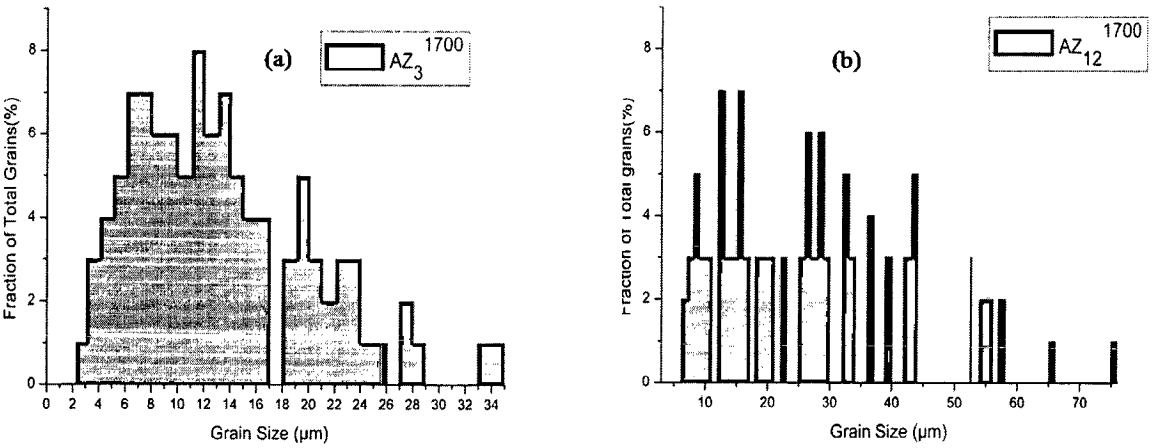

Fig.6.9 Grain size histograms for the samples of (a) AZ_3^{1700}, (b) AZ_{12}^{1700}.

6.4 Effect of mechanical properties of AZ sample sintered at different temperatures for various soaking time periods

6.4.1 Hardness of the sintered AZ samples

The influence of sintering temperature and soaking time period on hardness of AZ ceramic composites has been investigated. The samples were prepared by solid state sintering at 1500°C, 1600°C and 1700°C for different soaking time periods of 3hr, 6hr, 9hr and 12hr under atmospheric pressure.

6.4.1.1 Effect of sintering temperature on hardness of the samples

The effect of sintering temperature on the hardness of the composite materials is presented in Fig.6.10 for the case of samples sintered for soaking time period of 3 hrs.

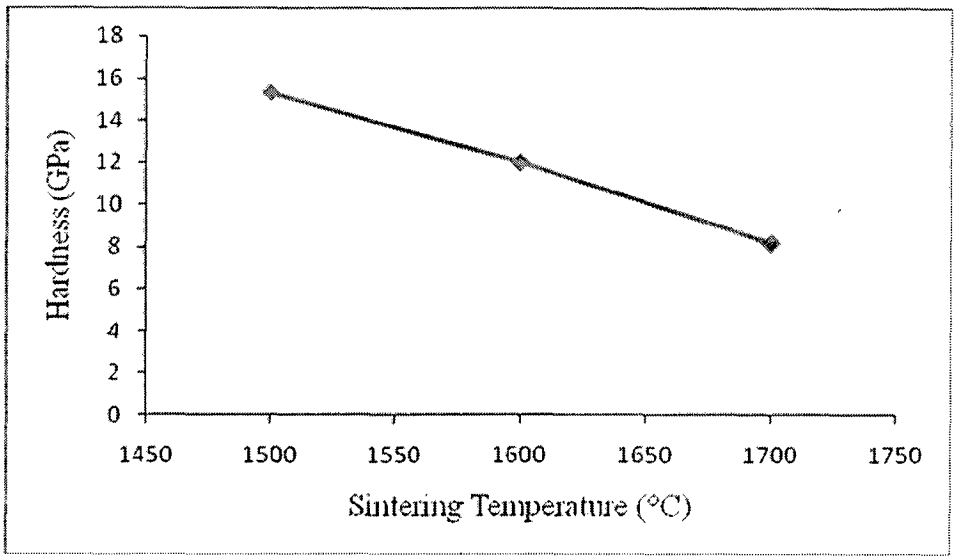

Fig.6.10 Variation of hardness of the AZ samples with sintering temperature for a soaking time period of 3hr

The hardness decreases from 15.3 GPa to 8.19 GPa with a corresponding sintering temperature variation from 1500°C to 1700°C. The hardness variation is attributed to the larger grains developed for sintering at higher temperature.

6.4.1.2 Effect of soaking time period on hardness

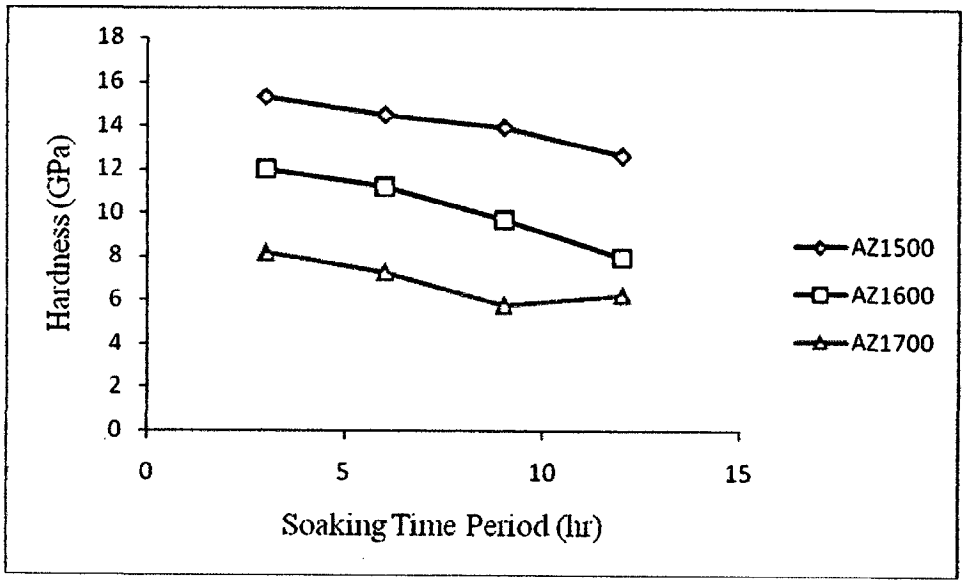

Fig.6.11 Hardness of the AZ samples as a function of soaking time period.

The variation of hardness of the samples sintered at three different temperatures with the soaking time period is shown in Fig 6.11. The decrease of hardness of the samples with increase in soaking time is evident for all the samples. For the samples sintered at 1500°C the hardness of 15.3 GPa corresponding to the soaking time of 3hr is reduced to 12.63 GPa when soaking time was 12hr. The hardness reduces from 12 to 7.94 for the samples sintered at 1600°C when the soaking time was varied from 3 to 12hr respectively. The soaking time variation for the samples sintered at 1700°C has a least influence on the hardness variation. The hardness variation in this case is limited to 6.25 - 8.19 GPa.

6.4.1.3 Effect of grain size on hardness

The grain size variation has been resulted in due to the variation in soaking time period in sintering. The hardness of the samples having different average grain sizes has been determined and presented in Table 6.3.

6.4.1.3.1 The effect of grain size on the hardness through Hall Petch Equation

The measured Hardness values of different samples have been plotted with $d^{-1/2}$ in the

Fig.6.12. The Hall-Petch type relationship between the hardness and the grain size is given by the following equation

$$H_{v,m} = H_{v,0} + k_{v,hp} d^{-1/2} \quad (6.1)$$

where, $H_{v,m}$ is the measured hardness by Vickers indentation method; $H_{v,0}$, the reference hardness and d, the mean grain size of the material. A smooth linear fitting of the points in the plot gives two distinct linear graphs, the equations of which are

$$H_v = 0.172 + 28.617\ d^{-1/2} \quad (6.2)$$

$$H_v = 9.177 + 6.420\ d^{-1/2} \quad (6.3)$$

It can be seen from the Fig.6.12 that the hardness variation with $d^{-1/2}$ in one range significantly differs from that in the other range. The two linear graphs give a point of intersection at H_v= 11.50 GPa and d = 6.25 μm.

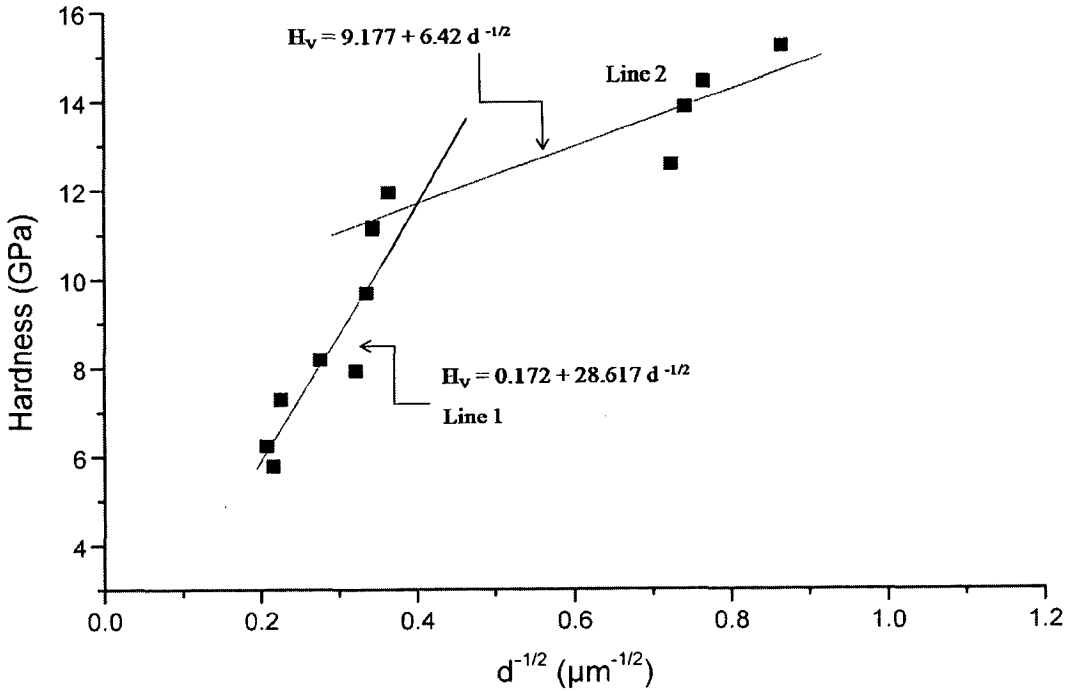

Fig.6.12 Grain size dependent hardness of AZ ceramic composites.

6.4.2 Fracture toughness of the sintered AZ samples

ZrO_2 changes physical and microstructural feature of Al_2O_3 – 5 wt% ZrO_2. This section describes the fracture toughness of Al_2O_3 – 5 wt% ZrO_2. In particulate reinforced composites, the mechanical properties can be improved by way of controlling the microstructure of the matrix (Green, 1982) of the composites.

6.4.2.1 Effect of sintering temperature on the fracture toughness of AZ samples

The addition of small quantities of ZrO_2 into Al_2O_3 enhances the density of the material i.e. AZ samples. Moreover, fracture toughness of a material depends upon its density which is governed by the sintering process. As in the present study essentially two sintering parameters are used sintering temperature and soaking time, are used.

The present section reports the variation of fracture toughness of AZ sample due to the alteration of sintering temperature. The fracture toughness of AZ samples sintered at 1500°C varies in the range of 5.35 – 5.95 MPa $m^{1/2}$. The fracture toughness of AZ samples sintered at 1600°C varies in the range of 5.43 – 6.01 MPa $m^{1/2}$ which is higher than that of the AZ samples sintered at 1500°C. The $AZ_3{}^{1700}$ sample shows the fracture toughness of 5.40 MPa $m^{1/2}$. But the lower fracture toughness varying between 1.86 and 2.28 MPa $m^{1/2}$ is resulted for the samples $AZ_6{}^{1700}$, $AZ_9{}^{1700}$ and $AZ_{12}{}^{1700}$. The microstructural feature having lower grain to grain contact and larger grain size difference of the samples sintered at 1700°C for the soaking time period more than 3hr is perhaps the cause of lower fracture toughness.

Table 6.3 Hardness, fracture toughness and grain size of the AZ samples sintered at 1500°C, 1600°C and 1700°C for different soaking time periods.

Sample	H_V (GPa)	K_{IC} (MPa $m^{1/2}$)	Average grain size (μm)
AZ_3^{1500}	15.3	5.95	1.33
AZ_6^{1500}	14.5	5.92	1.70
AZ_9^{1500}	13.93	5.89	1.81
AZ_{12}^{1500}	12.63	5.35	1.90
AZ_3^{1600}	12	5.95	7.52
AZ_6^{1600}	11.18	6.01	8.45
AZ_9^{1600}	9.69	5.45	8.90
AZ_{12}^{1600}	7.94	5.43	9.66
AZ_3^{1700}	8.19	5.40	13.10
AZ_6^{1700}	7.29	2.28	19.61
AZ_9^{1700}	5.79	1.89	21.51
AZ_{12}^{1700}	6.25	1.86	23.20

6.4.2.2 Effect of grain size on the fracture toughness

Fig.6.13 shows the fracture toughness of the AZ samples as a function of grain size. The samples sintered at 1500°C and 1600°C show higher fracture toughness. The AZ_6^{1600} sample having the average grain size of 8.45 μm, shows the higher fracture toughness of 6.01MPa $m^{1/2}$. The average the grain size of AZ_{12}^{1700} is 23.60 μm and the sample has lower fracture toughness of 1.86 MPa $m^{1/2}$.

6.4.2.4 Microstructures of the fracture surfaces

Micrographs of fracture surfaces of the samples sintered at 1500°C, 1600°C and 1700°C are shown in Fig.6.15. The fracture surfaces were generated by subjecting the samples three point bend test mode for failure. In Fig.6.15 (a) the presence of smaller grains is clear and the surface topography shows that the fracture has taken place in a predominantly intergranular mode. From Fig.6.15 (b)-(d) that the fracture surface topography confirms that fracture has taken place due to the mixed intergranular and transgranular modes, with larger proportion of the intergranular mode. But Fig.6.15 (d) shows that the porosity in the samples affects their fracture toughness, which has been discussed later.

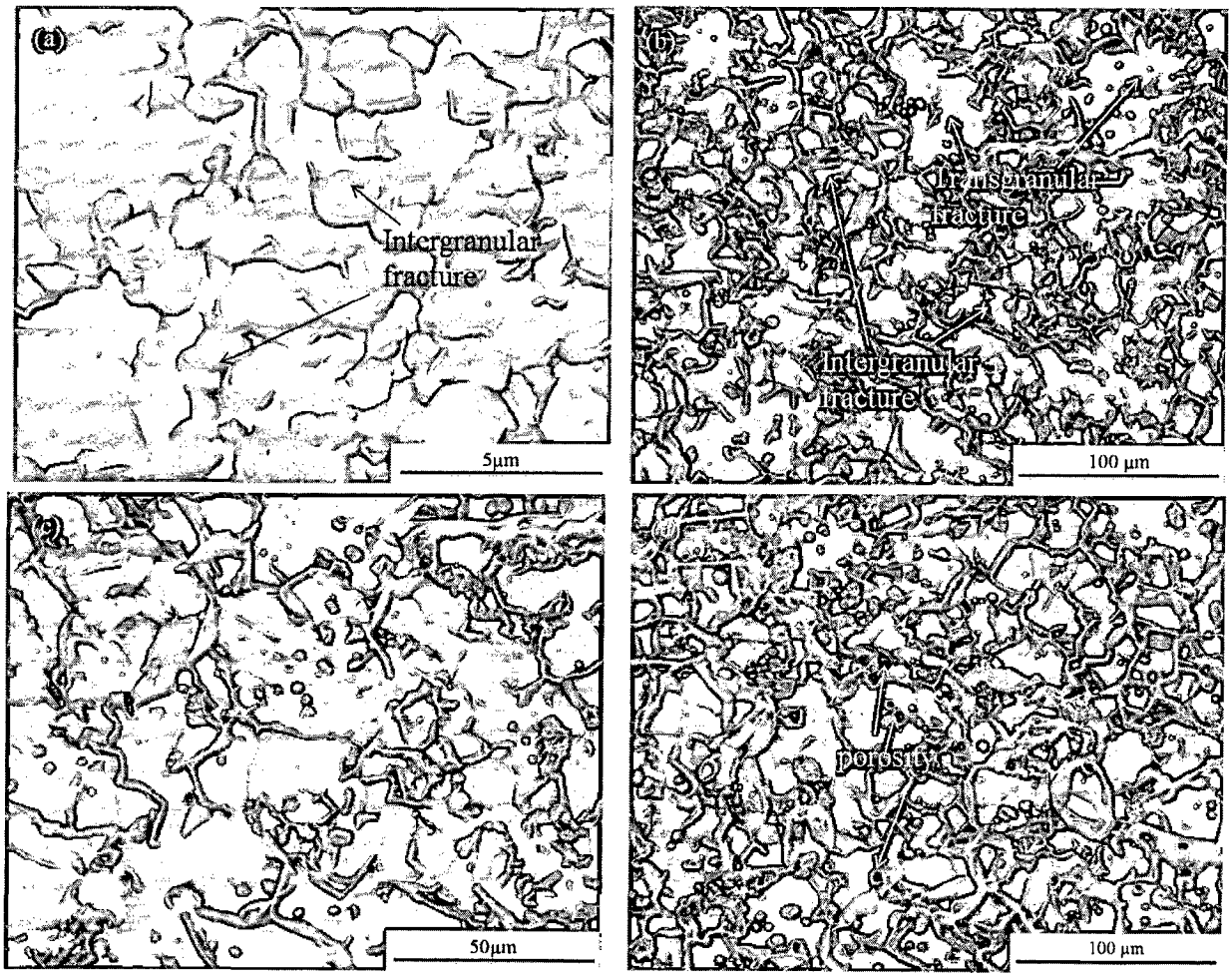

Fig.6.15 SEM micrographs of fracture surface of (a) AZ_3^{1500}, (b) AZ_6^{1600}, (c) AZ_3^{1700} and (d) AZ_{12}^{1700}.

6.4.2.5 Grain size histograms and fracture toughness

The fracture toughness of the AZ samples increases with increasing sintering temperature and soaking time period which are the factors cause to change the grain size and shape of the material. Fig.6.7 and Fig.6.8 show grain size distribution of the samples sintered at 1500°C and 1600°C respectively. It can be seen from the histograms in Fig.6.7 and Fig.6.8 that the grain size distribution is relatively narrow which may be assumed bimodal type whereas in Fig.6.9 (b) the grain size distribution is more wide and is not of the bimodal type. It is evident from the topography of the fracture surfaces that the intergranular fracture is dominated in the samples sintered at 1500°C and 1600°C. Therefore the higher fracture toughness of the samples sintered at 1500°C and 1600°C, is attributed to the bimodal type grain size distribution (Kovar et al., 2000).

6.4.2.6 Comparison of the fracture toughness data obtained by Indentation method and SEPB method

The fracture toughness of the samples determined by indentation method and single edge precracked beam method are given in Table 6.4. The fracture toughness measured by SEPB method varies between 4.87 and 5.29 MPa $m^{1/2}$ which is less compared to the fracture toughness measured by indentation method. The fracture toughness of the samples sintered at 1600°C determined by indentation method varies in the range of 5.43 - 6.01 MPa $m^{1/2}$ while the SEPB method shows almost uniform fracture toughness lying between 5.18 and 5.22 MPa $m^{1/2}$. However, negligible difference between the fracture toughness values obtained by these two different methods for the same type sample sintered at 1700°C is noticed.

Table 6.4 Comparison of the fracture toughness data obtained by Indentation method and SEPB method

Sample	Fracture toughness determined by (MPa $m^{1/2}$)	
	Indentation method	SEPB method
AZ_3^{1500}	5.95	4.87
AZ_6^{1500}	5.92	5.29
AZ_9^{1500}	5.89	5.11
AZ_{12}^{1500}	5.35	5.18
AZ_3^{1600}	5.95	5.21
AZ_6^{1600}	6.01	5.18
AZ_9^{1600}	5.45	5.22
AZ_{12}^{1600}	5.43	5.22
AZ_3^{1700}	5.40	5.21
AZ_6^{1700}	2.28	1.85
AZ_9^{1700}	1.89	1.70
AZ_{12}^{1700}	1.86	1.65

6.5 Al_2O_3 – 5 wt% ZrO_2 composites doped with rare earth elements

Many studies have focused on particulate dispersed Al_2O_3 composites to improve mechanical properties both at room temperature and high temperature (Harmer et al., 1992, Evans, 1990). Basu et al. reported that, in the Al_2O_3 - ZrO_2 base matrix rare earth elements have been introduced to stabilize the ZrO_2 which affects the mechanical properties (Basu et

al., 2004; Tuan et al., 2002). Microstructural control of composites is very important to improve the mechanical properties. The rare earth element controls the morphology of the Al_2O_3 grains which influence the mechanical properties. The needle like grains improve toughening (through the mechanism of deflection) (Jang et al., 1995).

6.5.1 Al_2O_3 – 5 wt % ZrO_2 composites doped with 1000 ppm $Y(NO_3)_3\ 6H_2O$

6.5.1.1 Physical properties of Al_2O_3 – 5wt% ZrO_2 –$Y(NO_3)_3\ 6H_2O$ composites

The physical property of the AZ samples changes with the rare earth doping. The relative densities, weight losses for sintering and linear shrinkages of the samples with sintering temperature and soaking time period have been studied.

6.5.1.1.1 Relative density

The Table 6.5 shows the relative density data of all the samples prepared at different sintering temperatures and for various soaking time periods. It can be seen that all the samples have nearly uniform density within a range of 97.75 to 99.25%.

Table 6.5 Relative densities of AZY samples sintered at 1500°C, 1600°C and 1700°C for different soaking time periods.

Temperature (°C)	1500				1600				1700			
Soaking time (hr)	3	6	9	12	3	6	9	12	3	6	9	12
Relative density (%)	98.0	98.25	98.25	97.75	99.0	99.25	99.25	99.25	99.0	99.0	98.75	98.75

6.5.1.1.2 Weight loss

In Fig.6.16 (a), the weight loss is almost the same for samples sintered at 1500°C and for different soaking time periods. The weight loss is more for the samples sintered at 1600°C for soaking times of 6, 9 and 12 hr compared with the sample prepared for 3 hr

soaking time. The same weight loss has been found with the samples prepared for soaking time periods of 6, 9 and 12 hrs. The samples sintered at 1700°C have the same characteristics as that of the samples sintered at 1600°C. Weight loss of the samples sintered at 1500°C is less than the samples sintered at 1600°C and 1700°C. In the chapter 4 the possible reason for weight loss has been discussed.

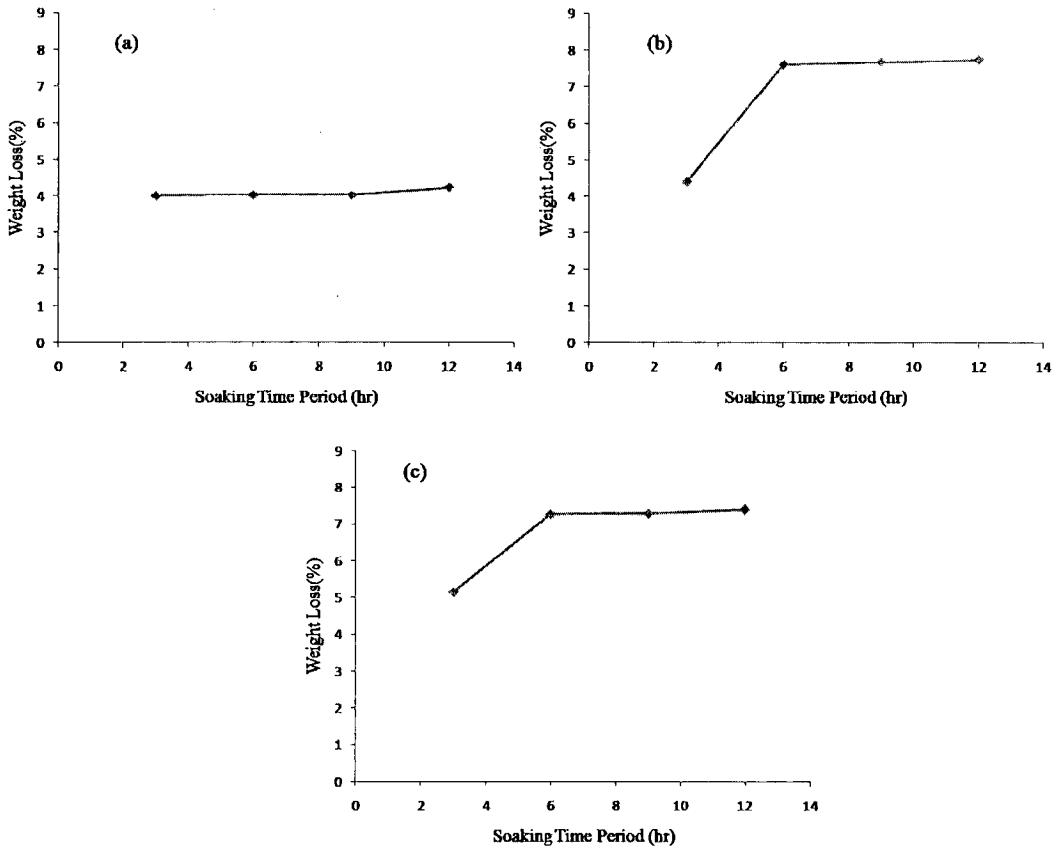

Fig.6.16 Weight loss for sintering of AZY samples sintered at (a) 1500°C, (b) 1600°C and (c) 1700°C for different soaking times.

6.5.1.1.3 Linear shrinkage

The linear shrinkage of the samples sintered at the three different temperatures is nearly same for all the soaking time periods. The range of linear shrinkage varies between 12.97 and 13.41(%). Linear shrinkage is related to the change of volume which is also related to density of the sample.

Table 6.6 Linear shrinkage of AZY samples sintered at 1500°C, 1600°C and 1700°C for different soaking time periods.

Temperature (°C)	1500°C				1600°C				1700°C			
Soaking Time (hr)	3hr	6hr	9hr	12hr	3hr	6hr	9hr	12hr	3hr	6hr	9hr	12hr
Linear Shrinkage (%)	13.05	13.19	13.36	13.41	13.41	13.2	13.3	13.41	13.16	13.41	12.97	13.14

6.5.1.2 Analysis of microstructure of AZY samples

6.5.1.2.1 Microstructure of sintered AZY samples

Fig. 6.17(a) shows the micrograph of the sample AZY_6^{1500} which has the grain size ranging between 0.39 and 2.9μm with an average grain size of 1.03 μm. There is a substantial change in the grain structure developed in the samples AZY_6^{1600}, AZY_3^{1700} and AZY_6^{1700} as shown in Fig. 6.17(b)-(d) respectively, compared to that of the sample AZY_6^{1500} (Fig. 6.17(a)). The range of grain size for the samples AZY_6^{1600}, AZY_3^{1700} and AZY_6^{1700} are 1.75- 27.69 μm, 2.44- 29.92 μm and 2.76- 32.96 μm respectively. The average grain size of the samples AZY_6^{1600}, AZY_3^{1700} and AZY_6^{1700} are 6.89 μm, 10.86 μm and 10.92 μm respectively. So the average grain size in the samples sintered at 1600°C and 1700°C is more than that of the samples sintered at 1500°C. Fig.6.17(c) shows the EDS of the samples, which shows that the triple junctions are occupied by tiny bright particles of ZrO_2. This has already been established by the microanalysis of one sample and the spectrum is given in Fig. 6.4(b). The microanalysis of the sample AZY_3^{1700} shows Y content (0.26 at%) is higher at the grain boundary compared to that (0.00 at%) in the grain interior. The EDS spectra show the presence of Al, O and trace amount of Zr both at the grain interior and near the grain boundary.

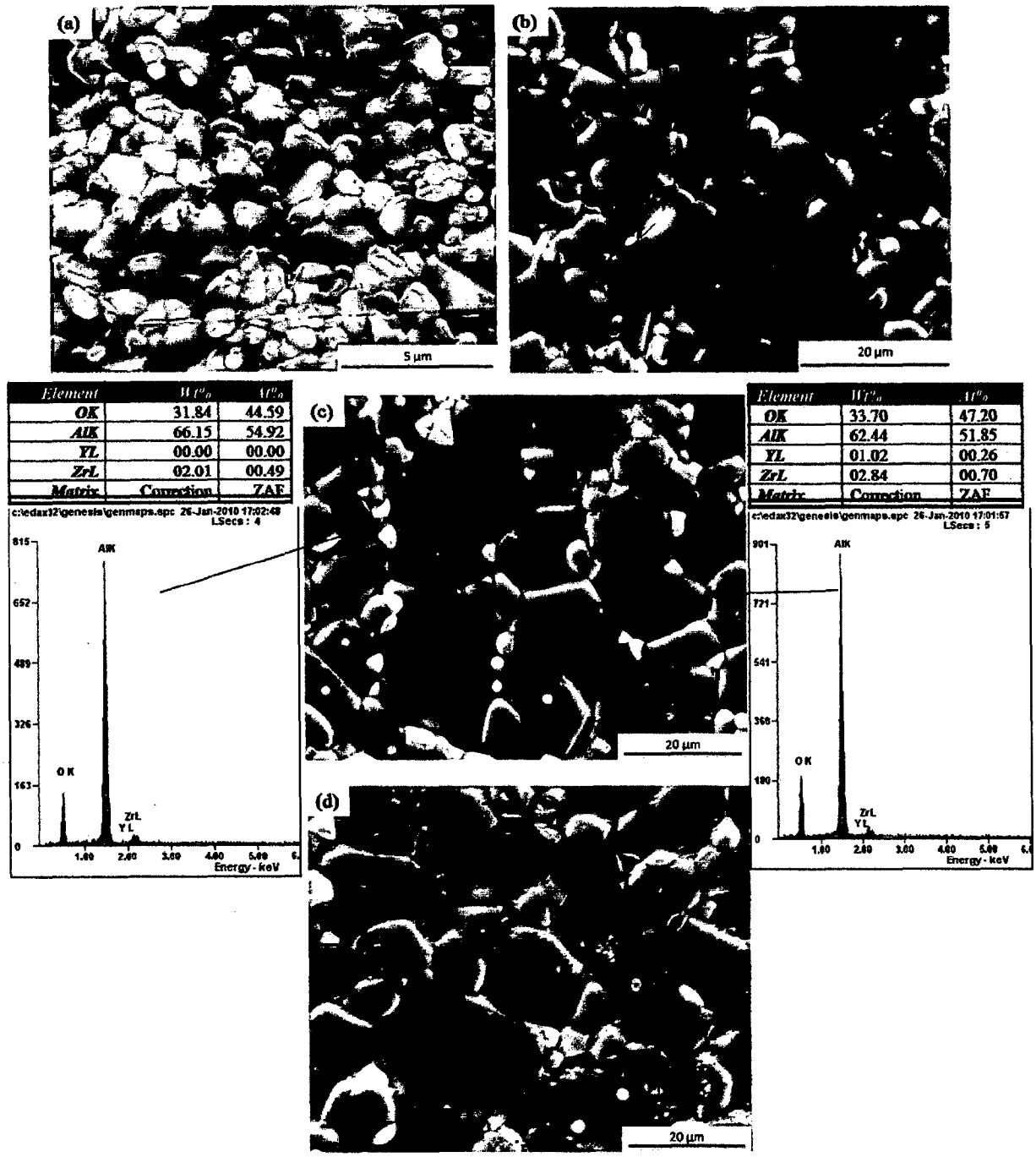

Fig.6.17 SEM micrographs of the samples (a) AZY_6^{1500}, (b) AZY_6^{1600} ,(c) AZY_3^{1700} with EDS and (d) AZY_6^{1700}.

6.5.1.2.2 Grain size histogram of the sintered AZY samples

Fig.6.18 shows the histogram of the AZY samples sintered at 1500°C, 1600°C and

1700°C for the different soaking time periods. The grain size distribution in the form of histograms is shown in Fig.6.18.

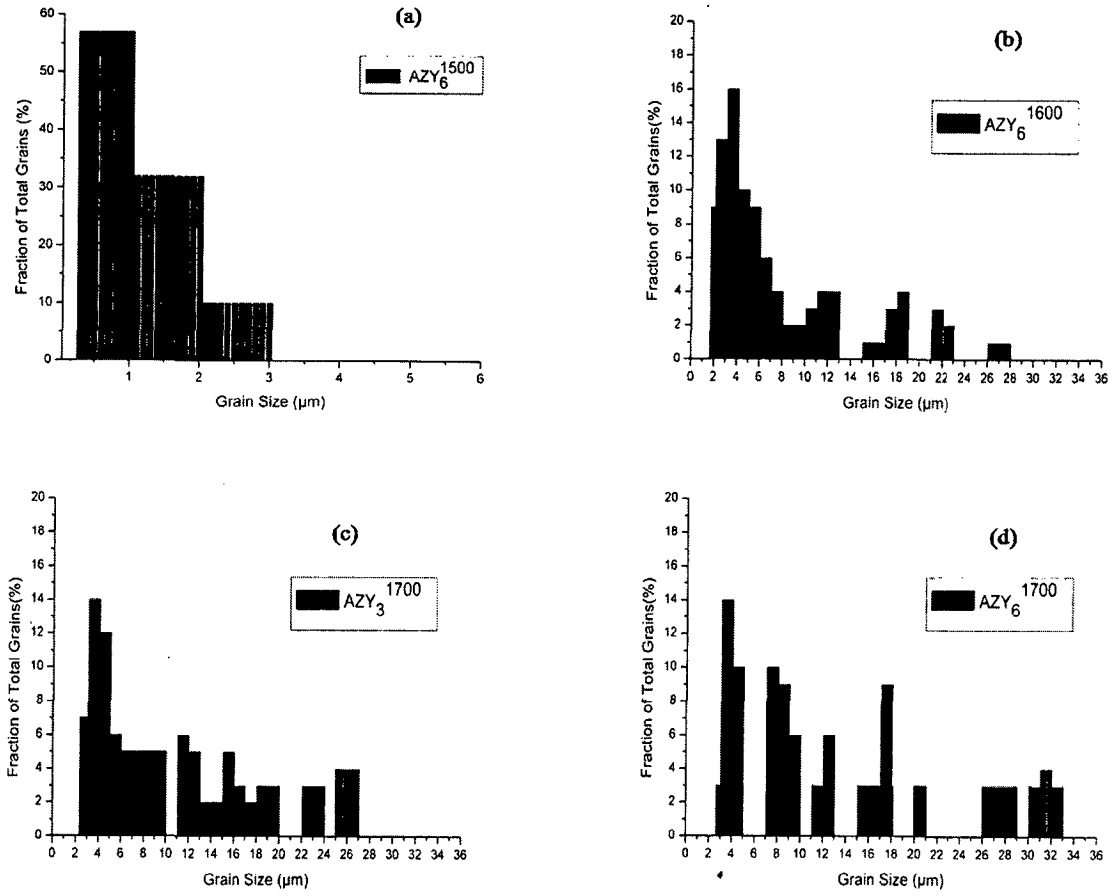

Fig.6.18 Grain size histograms of the sample (a) AZY_6^{1500}, (b) AZY_6^{1600}, (c) AZY_3^{1700} and (d) AZY_6^{1700}.

It can be seen from the Fig.6.18 (a) that the grain size is smaller than that of the other samples. The Fig.6.18 (b,c) show that there is a wide variation in the grain size but majority of the grains fall in the lower part of the size range. The grain size variation shown in Fig.6.18 (d) is larger than that of the other samples. The grain size variation over the entire size range is discrete compared to other histograms shown in Fig.6.18 (a, b, c).

6.5.1.3 Effect of mechanical properties of AZY sample sintered at different temperatures for various soaking time periods

6.5.1.3.1 Hardness of the AZY samples

The influence of rare earth in the AZ samples has been studied with varying sintering temperature and soaking time period.

6.5.1.3.1.1 Effect of sintering temperature on hardness

Fig.6.19 shows the hardness of the AZY samples as a function of sintering temperature. Fig.6.19 shows that the samples sintered at higher temperature have lower hardness. The sample sintered at 1500°C has the hardness of 15.2 GPa which is higher than that of the samples sintered at 1600°C whose hardness is 10.3 GPa. Lower hardness is attributed to the larger grain size of the samples sintered at 1600°C and 1700°C compared to the samples sintered at 1500°C (Hah et al., 1995).

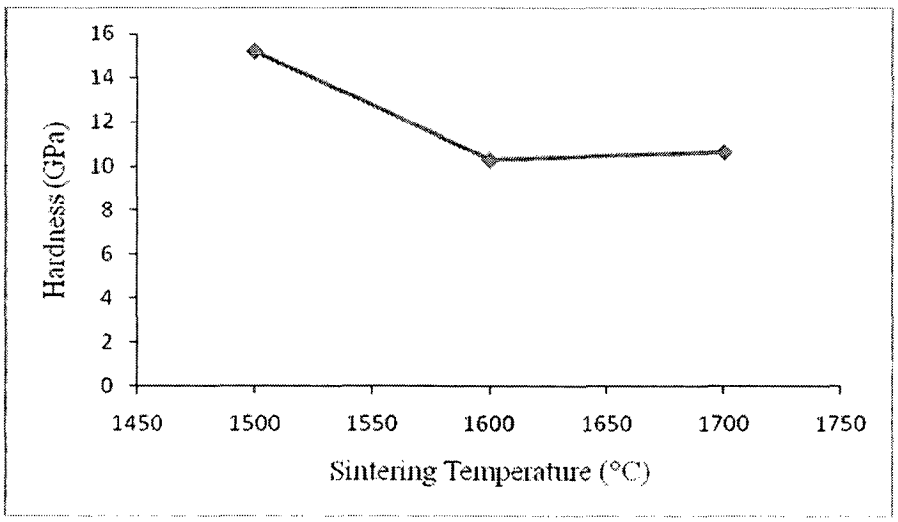

Fig.6.19 Variation of hardness of the AZY samples with sintering temperature for a soaking time period of 3hr

6.5.1.3.1.2 Effect of soaking time period on hardness

Fig.6.20 shows the hardness of AZY samples sintered at different temperatures for different soaking time periods. It is evident from the Fig.6.20 that the hardness decreases

with increasing soaking time period. The hardness of the samples sintered at 1500°C is higher than that of the samples sintered at 1600°C and 1700°C.

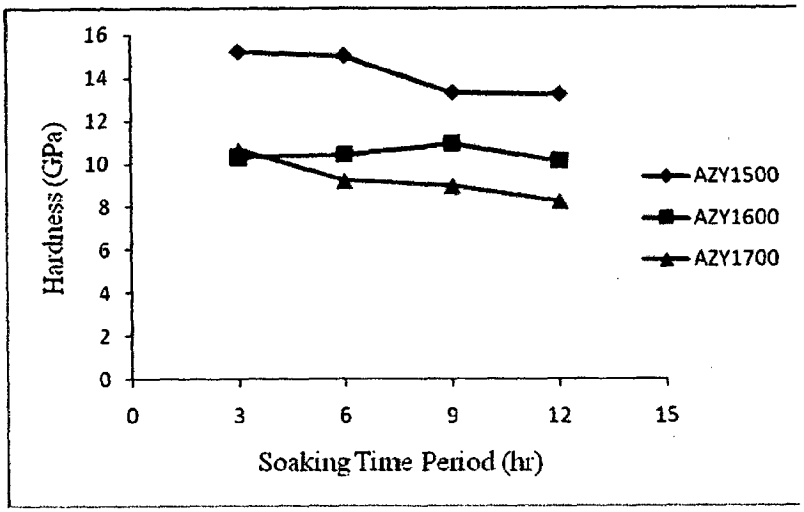

Fig.6.20 Variation of the hardness of AZY samples sintered at 1500°C, 1600°C and 1700°C with soaking time period.

6.5.1.3.1.3 The effect of grain size on the hardness through Hall Petch Equation

The Fig.6.21 shows the plot of hardness vs. $d^{-1/2}$. The entire hardness data set as can be examined from the Table 6.7. The dependence of hardness on the grain size of the AZY samples is shown through Hall-Petch relationship given in the equation 6.1.

The plot in the Fig.6.21 has been made between the hardness and $d^{-1/2}$ and smooth linear fitting of the points gives rise to two distinct linear graphs which can be expressed by mathematical expressions given by (6.4) and (6.5).

$$H_v = 14.29\, d^{-1/2} + 5.25 \qquad (6.4)$$

$$H_v = 8.73\, d^{-1/2} + 5.74 \qquad (6.5)$$

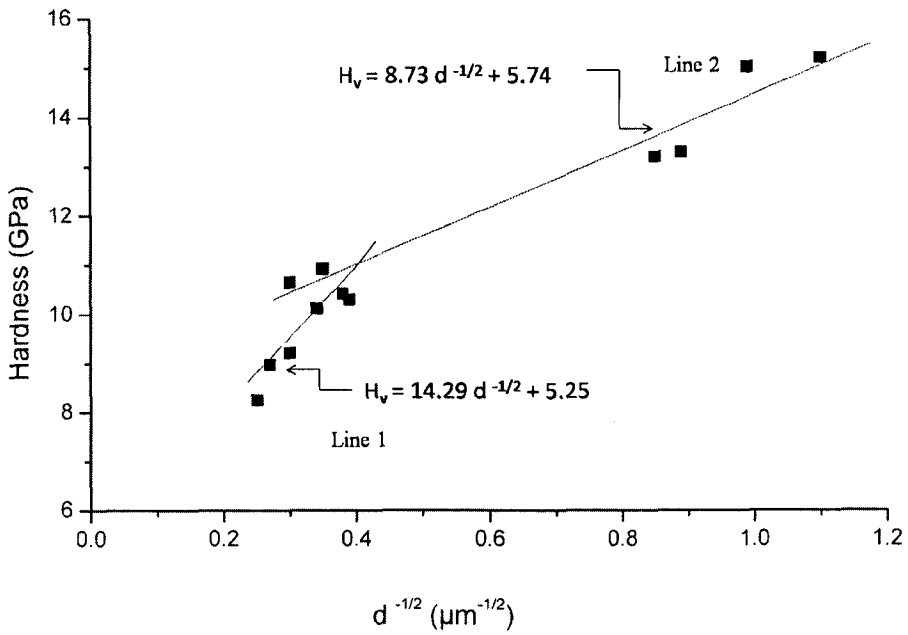

Fig.6.21 Variation of hardness with $d^{-1/2}$ for AZY samples

6.5.1.3.2 Fracture toughness of the sintered AZY samples

6.5.1.3.2.1 Effect of sintering temperature on the fracture toughness

The fracture toughness of the AZY samples sintered at 1500°C is found to increase with increasing soaking time period. The range of fracture toughness of these samples is 5.20 - 6.02 MPa $m^{1/2}$. The range of fracture toughness for the samples sintered at 1600°C and 1700°C are 4.93 – 5.32 MPa $m^{1/2}$ and 4.99 – 5.37 MPa $m^{1/2}$ respectively.

Table 6.7 Grain size, hardness and fracture toughness of AZY samples sintered at 1500°C, 1600°C and 1700°C

Sample	Average grain size (μm)	Grain size range (μm)	Grain size difference (μm)	Hardness (GPa)	Fracture toughness (MPa $m^{1/2}$)
AZY_3^{1500}	0.82	0.35- 2.75	2.40	15.20	5.20
AZY_6^{1500}	1.03	0.39-2.9	2.51	15.01	6.02
AZY_9^{1500}	1.26	0.53-4.14	3.61	13.30	5.31
AZY_{12}^{1500}	1.38	0.59- 4.40	3.81	13.20	5.42
AZY_3^{1600}	6.53	1.7-27.16	25.46	10.30	5.32
AZY_6^{1600}	6.89	1.75- 27.69	25.94	10.42	5.01
AZY_9^{1600}	8.38	1.83- 31.49	29.66	10.94	4.93
AZY_{12}^{1600}	8.82	2.26- 32.9	30.64	10.12	5.22
AZY_3^{1700}	10.86	2.44- 29.92	27.48	10.65	5.37
AZY_6^{1700}	10.92	2.76- 32.96	30.2	9.21	4.99
AZY_9^{1700}	14.18	3.18- 33.38	30.2	8.97	5.29
AZY_{12}^{1700}	16.59	4.85- 37.98	33.13	8.25	5.06

5.5.1.3.2.2 Effect of grain size on the fracture toughness

The average grain size and the size ranges of the samples sintered at different temperatures and for various soaking times are given in the Table 6.7 which shows that higher fracture toughness results in the samples having smaller grain size. The samples sintered at 1500°C have higher fracture toughness than that of the samples sintered at 1600°C

and 1700°C. A plot between fracture toughness vs. the grain size of the AZY samples has been made in Fig.6.22.

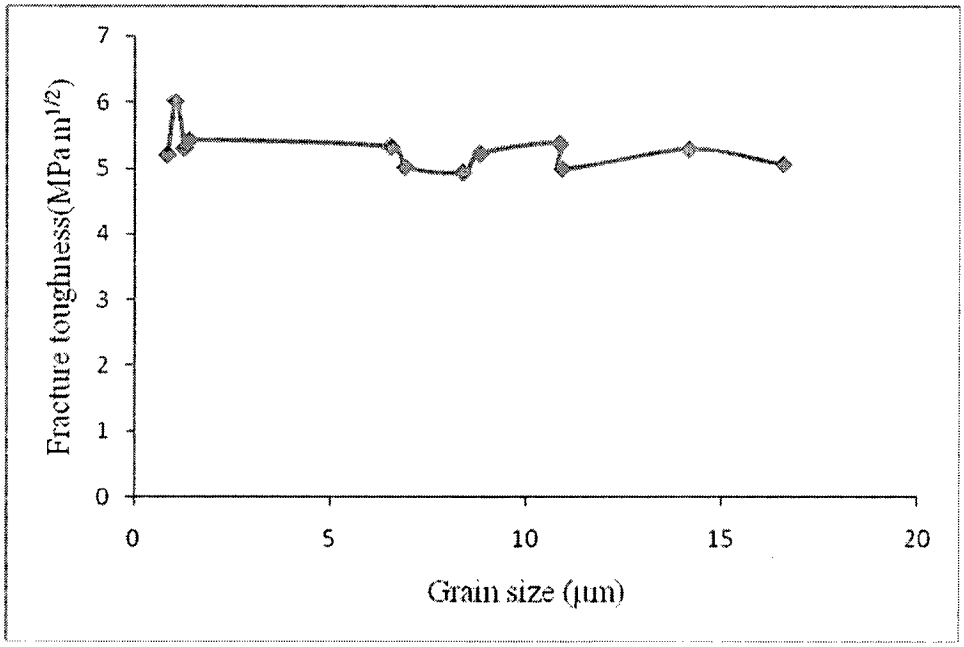

Fig.6.22 Plot of fracture toughness with grain size of the AZY samples.

6.5.1.3.2.3 Correlation of fracture toughness with mode of crack propagation

Fig.6.23 shows the SEM micrographs of the indented AZY_9^{1600} and AZY_9^{1700} without having any surface polishing further. The Fig. 6.23(a) depicts the crack deflection along the grain boundaries on the sample surface resulting in enhanced the fracture toughness in AZY_9^{1600} sample. The Fig. 6.23(b) shows the formation of more cracks (microcracks) instead of one crack in the sample. Microcracks formation is one of the toughening mechanisms in ceramics materials (Evans, 1976).

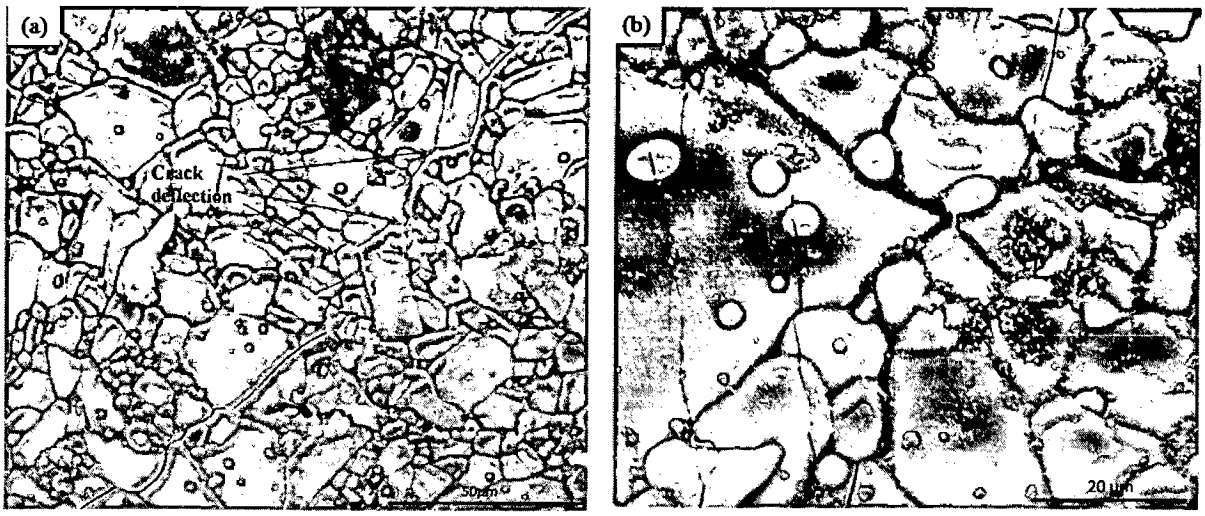

Fig.6.23 SEM micrograph of (a) AZY_9^{1600} and (b) AZY_9^{1700}

6.5.1.3.2.4 Comparison of fracture toughness data obtained by Indentation method and SEPB method

For the valid results of fracture toughness the different technique has been tried. Indentation method is very simple method to measure the fracture toughness but there might be some manual error to measure the crack length. So to check the accuracy of results, two different methods has been done.

Table 6.8 Comparison of fracture toughness determined by Indentation method and SEPB method

Sample	Fracture toughness (MPa $m^{1/2}$) estimated by	
	Indentation method	SEPB method
AZY_3^{1500}	5.20	4.45
AZY_6^{1500}	6.02	4.66
AZY_9^{1500}	5.31	4.73
AZY_{12}^{1500}	5.42	4.88
AZY_3^{1600}	5.32	4.97
AZY_6^{1600}	5.01	4.66
AZY_9^{1600}	4.93	4.68
AZY_{12}^{1600}	5.22	4.90
AZY_3^{1700}	5.37	5.26
AZY_6^{1700}	4.99	4.96
AZY_9^{1700}	5.29	5.22
AZY_{12}^{1700}	5.06	4.52

The difference in fracture toughness determined by these two methods for each sample is not very significant, however, the indentation method yields consistently higher values for all the samples.

6.5.2 Al_2O_3 – 5wt% ZrO_2 composites doped with 1000 ppm $La(NO_3)_3.6H_2O$

6.5.2.1 Physical properties of Al_2O_3 – 5 wt% ZrO_2 – La $(NO_3)_3.6H_2O$ composites

6.5.2.1.1 Relative density of AZL samples

Table 6.9 shows the relative density of the AZL samples sintered at 1500°C, 1600°C and 1700°C for different soaking time periods. The relative density vary between 97.02 and 98.75%. The AZL_3^{1500} shows the lower relative density compared to the other sintered AZL samples.

Table 6.9 Density of AZL samples sintered at 1500°C, 1600°C and 1700°C for different soaking time periods.

Temperature (°C)	1500				1600				1700			
Soaking Time (hr)	3hr	6hr	9hr	12hr	3hr	6hr	9hr	12hr	3hr	6hr	9hr	12hr
Relative density (%)	97.02	97.27	97.77	98.01	98.51	98.75	98.26	98.51	98.26	98.01	98.01	97.77

6.5.2.1.2 Weight loss

Fig. 6.24 shows the weight loss of the AZL samples increases with increasing sintering temperature. The weight loss due to sintering at 1600 °C and 1700 °C are almost same at the corresponding soaking time periods. Lower weight loss has occurred for the samples sintered at 1500 °C. However, the weight loss increases marginally with increasing soaking time period.

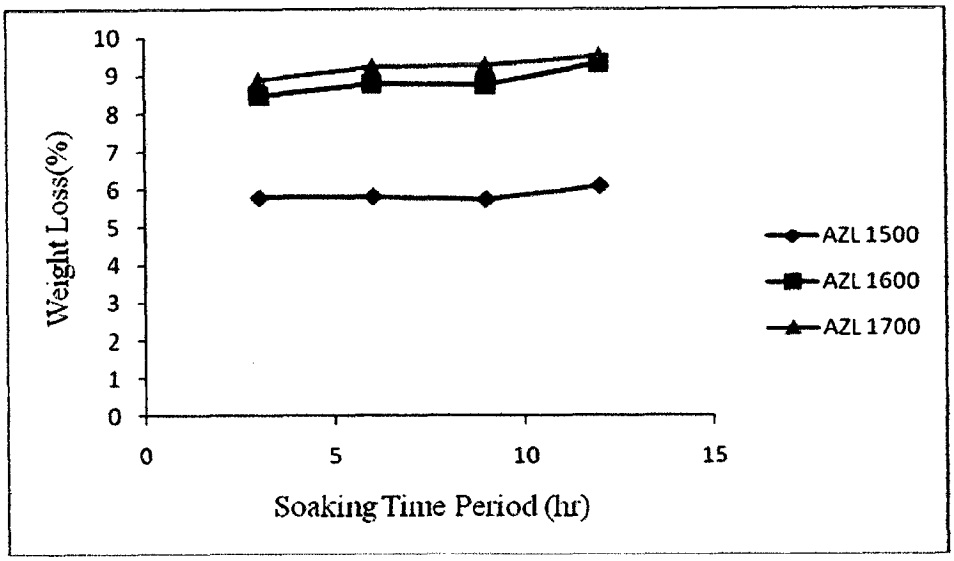

Fig.6.24 Weight loss as a function of soaking time of the samples sintered at 1500°C, 1600°C and 1700°C.

6.5.2.1.3 Linear shrinkage

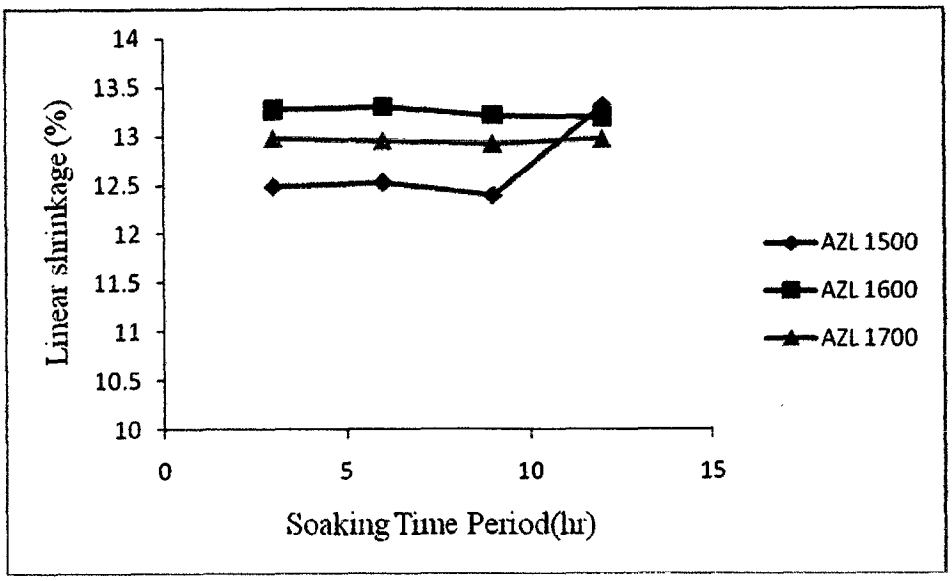

Fig.6.25 Linear shrinkage of the AZL samples sintered at 1500°C, 1600°C and 1700°C for different soaking time periods.

Fig. 6.25 shows the linear shrinkage is not significantly different from each other for the samples sintered at the three different temperatures. However, relatively higher shrinkage has

been found for the samples sintered at 1600°C. Moreover, variation in soaking time has also least influence on the shrinkage variation.

6.5.2.2 Analysis of microstructure of AZL samples

6.5.2.2.1 Microstructure of sintered AZL samples

In Fig. 6.26(a) the grains are approximately round in shape and the grain size varies from 0.40 to 3.10 μm. However, an extensive grain growth is observed for the sample AZL_6^{1600}, whose grain size range is 2.01 – 36.11μm giving an average grain size of 9.23 μm. In Fig.6.26(c) the number of larger grains is more than that of the sample AZL_6^{1600} (Fig.6.26 (b)). Fig.6.26(c) shows the FESEM micrograph along with microanalysis (EDS) of the sample AZL_3^{1700}. The grain size of this sample varies between 2.4 and 39.1 μm with the average grain size of 11.70μm. The EDS spectra from the grain interior surface and grain boundary regions show the presence of La along with other major elements such as Al, Zr and O. However, the rare earth (La) content at or near the grain boundary region is less (0.11 at%) compared to that (0.25 at%) in the grain interior. The microstructures in Fig. 6.26(a)-(c) show that the grains are densely packed compared to that in the sample whose micrograph is shown in Fig. 6.26(d). The grain size range of the sample AZL_6^{1700} varies between 3.9 and 46.48μm with the average grain size of 17.49 μm.

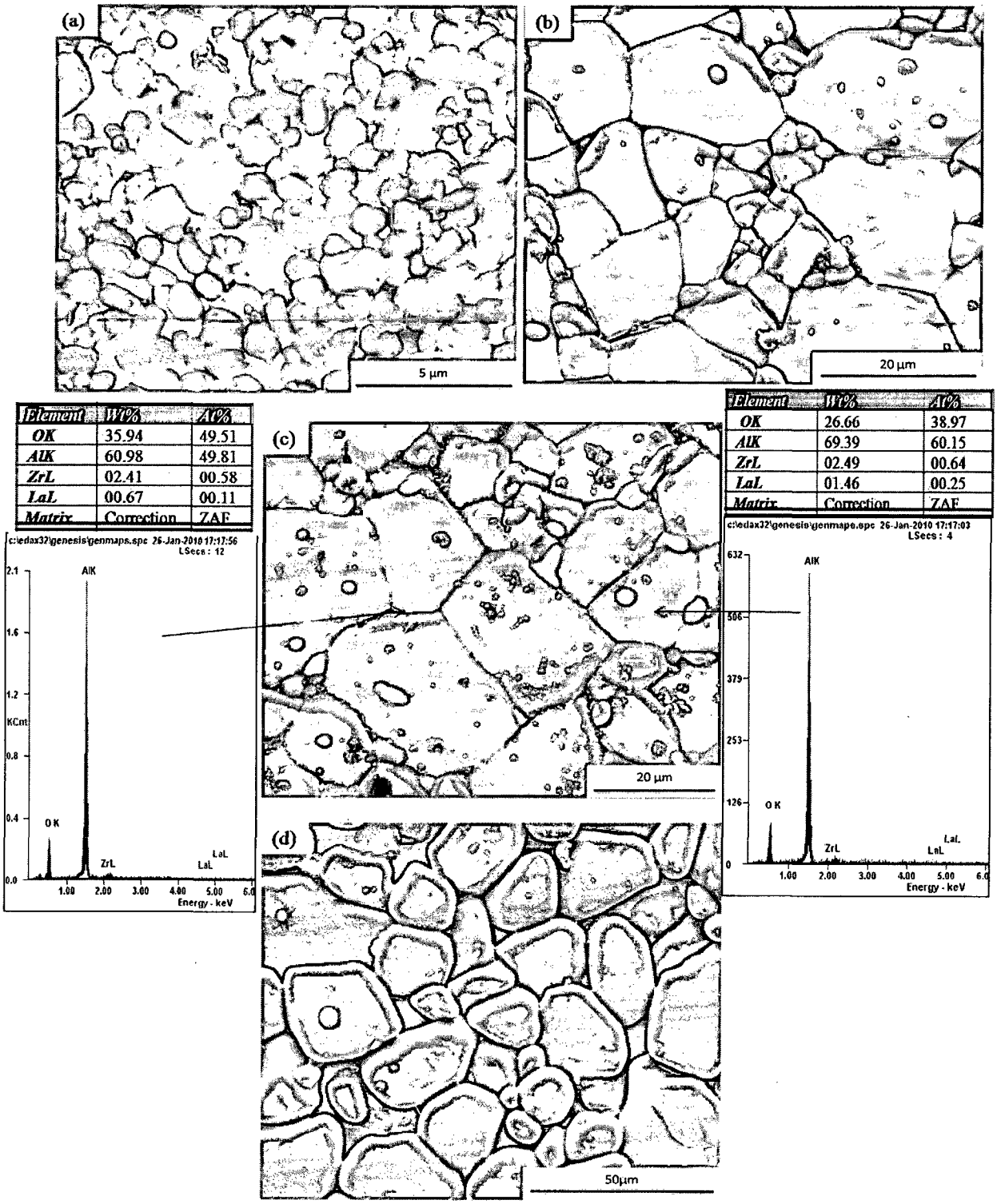

Fig.6.26 SEM micrographs of the samples (a) AZL_6^{1500}, (b) AZL_6^{1600} ,(c) AZL_3^{1700} with EDS analysis and (d) AZL_6^{1700}

6.5.2.2.2 Grain size histogram of the sintered AZL samples

The grain size distribution of the samples is shown in the Fig.6.27. The Fig. 6.27(a) shows the histogram of grain size distribution in the sample AZL_6^{1500}. This sample shows the bimodal type grain size distribution in the materials. The grain size distribution in the samples AZL_6^{1600} and AZL_3^{1700} is approximately bimodal type. A wide distribution of the grain size is observed in the sample AZL_6^{1700}.

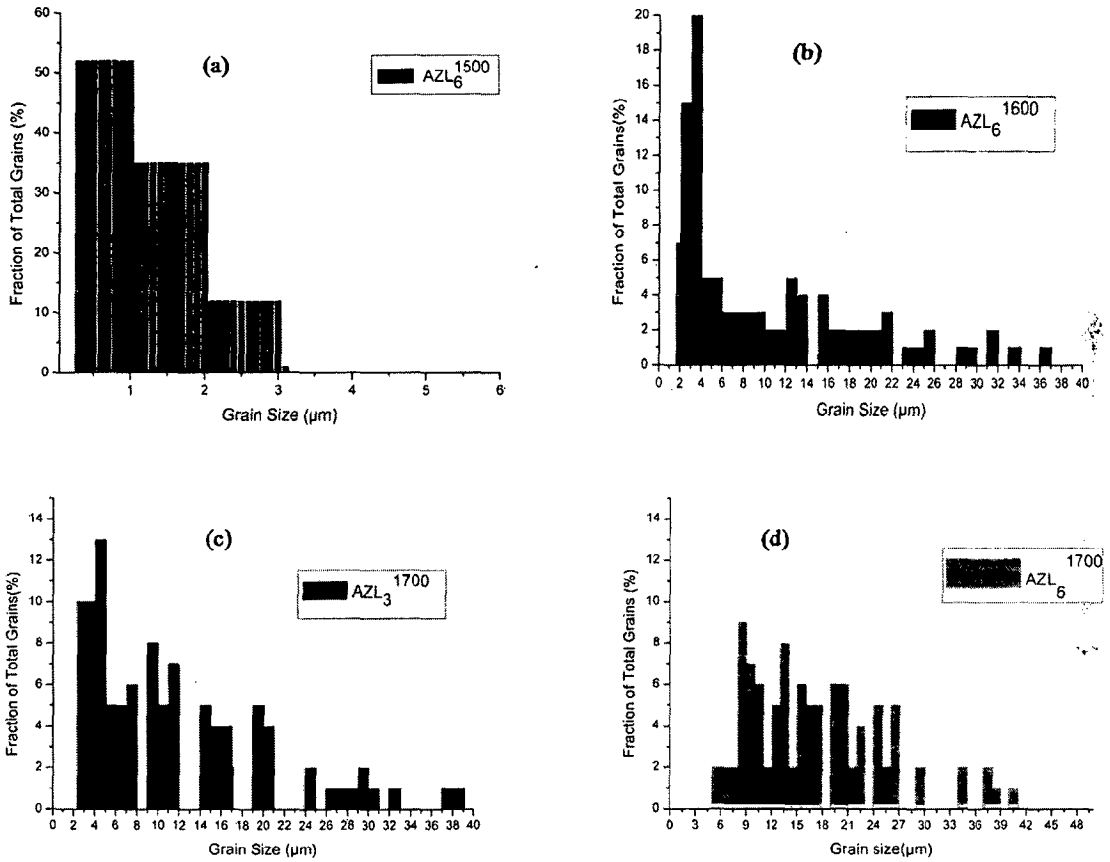

Fig.6.27 Histograms of the grain size in the samples (a) AZL_6^{1500}, (b) AZL_6^{1600}, (c) AZL_3^{1700}, (d) AZL_6^{1700}.

6.5.2.3 Effect of mechanical properties of AZL samples sintered at different temperature for various soaking time periods

6.5.2.3.1 Hardness of the AZL samples

6.5.2.3.1.1 Effect of sintering temperature on hardness

The hardness of the samples is found to decrease with the increase in sintering temperature and Fig.6.28 depicts such variation. The samples sintered at 1700°C have lower hardness compared to the samples sintered at 1500°C and 1600°C. The hardness of the sample AZL_3^{1500} is 14.80 GPa, while the hardness of AZL_3^{1700} is 4.03 GPa.

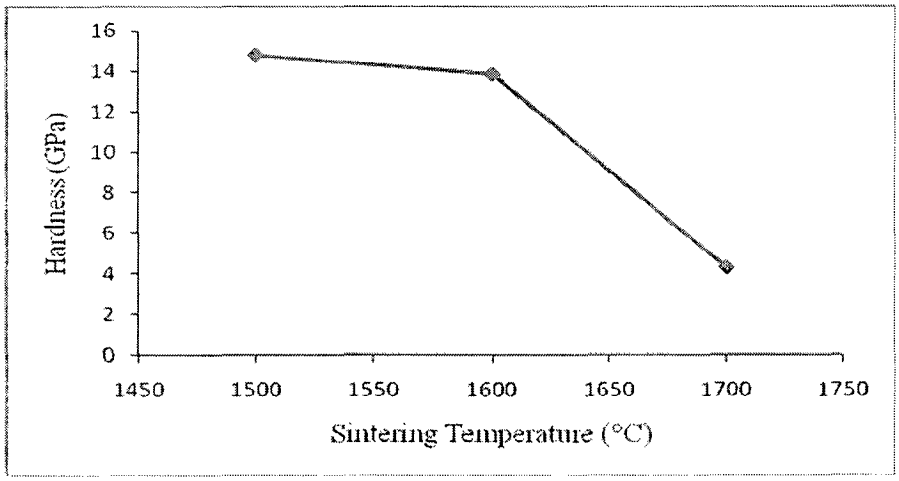

Fig.6.28 Variation of hardness of the AZL samples with sintering temperature for a soaking time period of 3hr.

6.5.2.3.1.2 Effect of soaking time period on hardness of the sample

Fig. 6.29 shows the variation of hardness of the samples with soaking time period for sintering temperature of 1500°C. The range of hardness of the samples is 12.97 to 14.80 GPa. The hardness for the samples sintered at 1600°C varies between 11.69 and 13.86 GPa. However, the samples sintered at 1700°C have lower hardness and the range of which is 4.03 - 4.30 GPa.

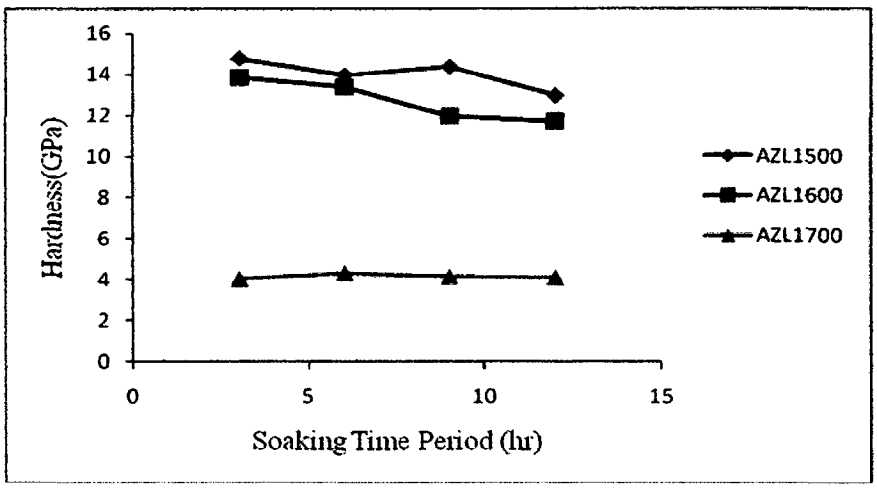

Fig.6.29 Hardness of AZL samples sintered at (a) 1500°C, (b) 1600°C and (c) 1700°C for different soaking time periods.

6.5.2.3.1.3 The effect of grain size on the hardness through Hall Petch Equation

The dependence of hardness on the grain size of the samples has been shown through Hall-Petch relationship. The plot has been made between the Hardness and $d^{-1/2}$ in the Fig.6.30.

Smooth linear fit of the data points yields two distinct linear graphs which can be expressed by mathematical equations (6.6) and (6.7).

$$H_v = 53.60\ d^{-1/2} - 8.238 \qquad (6.6)$$

$$H_v = 2.534\ d^{-1/2} + 11.782 \qquad (6.7)$$

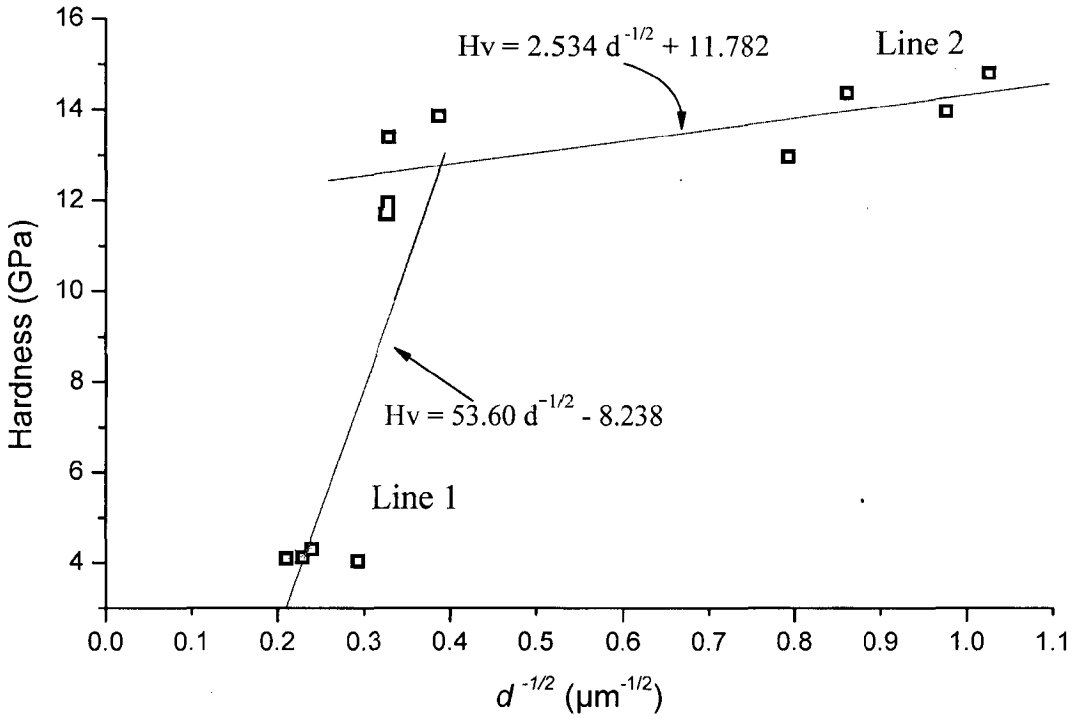

Fig.6. 30 Grain size dependent hardness of AZL samples

6.5.2.3.2 Fracture toughness of the sintered AZL samples

6.5.2.3.2.1 Effect of sintering temperature on the fracture toughness

The fracture toughness of the samples depends on preparative parameters viz. sintering temperature and soaking time period. The microstructure of the AZL samples influences the fracture toughness of the samples. The AZL samples sintered at 1700°C show the decrease in fracture toughness with increasing soaking time periods. The fracture toughness of the AZL samples varies between 1.84 and 5.45 MPa $m^{1/2}$. The hardness and fracture toughness of the sample sintered at 1700°C are lower compared to those of the samples sintered at 1500°C and 1600°C.

Table 6.10 Hardness and fracture toughness of the AZL samples sintered at different temperatures.

Sample	Average grain size (μm)	Grain size range (μm)	Grain size difference (μm)	Hardness (GPa)	Fracture toughness (MPa $m^{1/2}$)
AZL_3^{1500}	0.95	0.38- 2.98	2.6	14.80	4.89
AZL_6^{1500}	1.05	0.40- 3.10	2.7	13.96	5.24
AZL_9^{1500}	1.35	0.5- 5.05	4.55	14.37	5.21
AZL_{12}^{1500}	1.59	0.56-5.98	5.42	12.97	5.45
AZL_3^{1600}	6.67	1.9- 32.33	30.43	13.86	5.18
AZL_6^{1600}	9.23	2.01- 36.11	34.1	13.40	5.32
AZL_9^{1600}	9.30	2.02- 38.01	35.99	11.95	4.89
AZL_{12}^{1600}	9.44	2.19- 38.54	36.35	11.69	4.92
AZL_3^{1700}	11.70	2.4- 39.1	36.7	4.03	5.30
AZL_6^{1700}	17.49	3.9- 46.48	42.58	4.30	2.19
AZL_9^{1700}	19.19	5.06-60.89	55.83	4.12	1.97
AZL_{12}^{1700}	22.72	6.12- 66.79	60.67	4.09	1.84

6.5.2.3.2.2 Effect of grain size on the fracture toughness

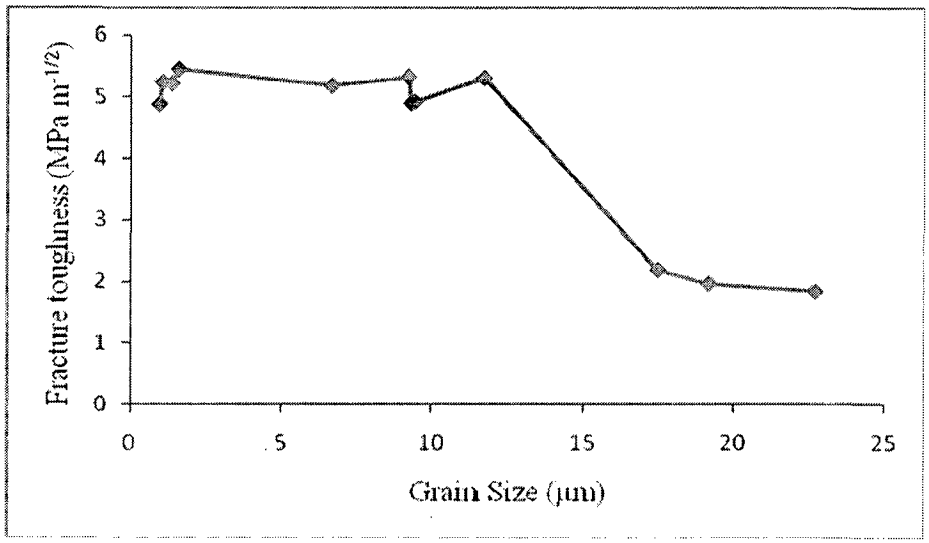

Fig.6.31 Plot of fracture toughness with grain size of the AZL samples

Fig.6.31 shows variation of the fracture toughness of the AZL samples with the grain size. The fracture toughness of the AZL samples increases with increasing the grain size upto the grain size of 1.59 μm. The fracture toughness of the sample remains in the range of 4.89 to 5.45 MPam$^{-1/2}$ upto the grain size of 11.70 μm. The fracture toughness of the materials having an average grain size of more than 11.70 μm decreases with increasing grain size. The lower fracture toughness falls in the range 1.84 - 2.19 MPa m$^{-1/2}$. The microstructure of the sample (AZL_6^{1700}) shown in Fig. 6.26 (d) reveals that perhaps the porosity in the sample is responsible for the lower fracture toughness.

6.5.2.3.2.3 Fracture toughness with mode of crack propagation and fracture surface

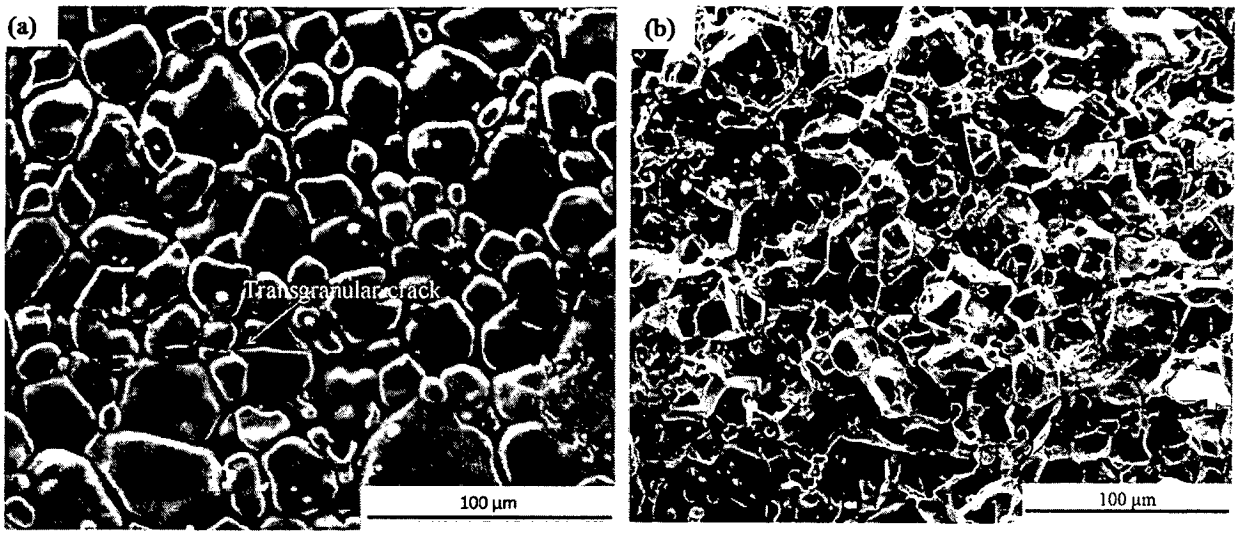

Fig.6.32 SEM micrograph of (a) AZL_6^{1700} and (b) fracture surface of AZL_6^{1700}.

Mode of crack propagation has been shown in the Fig. 6.32(a). The crack path is mainly transgrannular which may also cause lower the fracture toughness in the AZL_6^{1700} sample. The Fig.6.32 (b) shows the SEM micrograph of fracture surface of the sample AZL_6^{1700}. Fig.6.32 shows the porosity on the fracture surface as shown in the Fig. 6.15(d) may results in the lower fracture toughness of the samples sintered at higher temperature.

6.5.2.3.2.4 Comparison of fracture toughness data obtained by Indentation method and SEPB method.

Table 6.11 shows the comparison of the fracture toughness of the samples AZL sintered at different temperatures for different soaking time periods. Fracture toughness of the samples sintered at 1500°C was measured using indentation method, which varies between 4.89 and 5.45 MPa $m^{1/2}$. Whereas the fracture toughness of the samples sintered at 1500 °C determined by SEPB method is found to lie in the range of 4.21- 4.57 MPa $m^{1/2}$. The samples sintered at higher temperatures have lower fracture toughness determined using both the methods.

Table 6.11 Comparison of fracture toughness determined using Indentation method and SEPB method.

Sample	Fracture toughness (MPa $m^{1/2}$) measured using	
	Indentation method	SEPB method
AZL_3^{1500}	4.89	4.21
AZL_6^{1500}	5.24	4.33
AZL_9^{1500}	5.21	4.46
AZL_{12}^{1500}	5.45	4.57
AZL_3^{1600}	5.18	4.67
AZL_6^{1600}	5.32	4.92
AZL_9^{1600}	4.89	4.70
AZL_{12}^{1600}	4.92	4.72
AZL_3^{1700}	5.30	5.28
AZL_6^{1700}	2.19	2.12
AZL_9^{1700}	1.97	1.81
AZL_{12}^{1700}	1.84	1.80

6.5.3 Al_2O_3 – 5wt% ZrO_2 composites doped with 1000 ppm $Y(NO_3)_3.6H_2O$ –1000 ppm La $(NO_3)_3.6H_2O$

The studies on the single rare earth doped AZ samples have been presented in the earlier sections. The Y doped AZ composite shows higher fracture toughness than the La doped AZ samples.

6.5.3.1 Physical properties of Al_2O_3 – 5 wt% ZrO_2 –1000 ppm $Y(NO_3)_3.6H_2O$ – 1000 ppm La $(NO_3)_3.6H_2O$ composites

6.5.3.1.1 Relative density

Table 6.12 shows relative densities of the AZYL samples sintered at different temperatures for different soaking time periods. The densities lie in the range 97.50 - 99.25 %.

Table 6.12 Relative densities of Al_2O_3 samples sintered at 1500°C, 1600°C and 1700°C for different soaking time periods.

Temperature (°C)	1500°C				1600°C				1700°C			
Soaking Time (hr)	3hr	6hr	9hr	12hr	3hr	6hr	9hr	12hr	3hr	6hr	9hr	12hr
Relative density (%)	97.5	97.75	98.0	98.5	98.5	99.0	99.25	99.25	98.5	99.0	98.5	99.0

6.5.3.1.2 Weight loss for sinter

The weight losses of the AZYL samples sintered at 1500°C, 1600°C and 1700°C for different soaking time periods are shown in Fig.6.33. The samples sintered at 1500°C undergoes a weight loss of about 5 %, however the weight losses for the samples sintered at 1600°C and 1700°C are about 8-9 %. The samples sintered at 1600°C have marginally higher weight loss than those sintered at 1700°C.

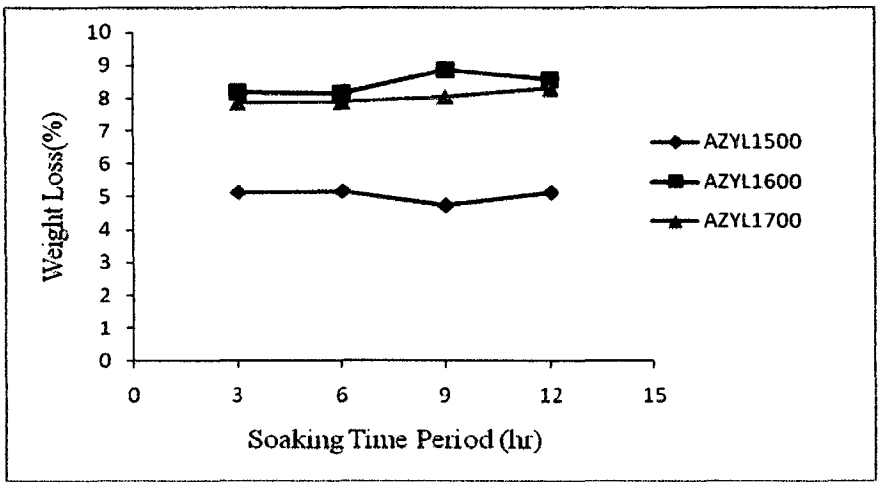

Fig.6.33 Variation of weight loss of the AZYL samples sintered at 1500°C, 1600°C and 1700°C for different soaking times

6.5.3.1.3 Linear shrinkage

Fig.6.34 shows the linear shrinkage of the AZYL samples sintered at 1500°C, 1600°C and 1700°C for different soaking time periods. The samples sintered at 1500°C experience lower shrinkage compared to the samples sintered at 1600 and 1700°C.

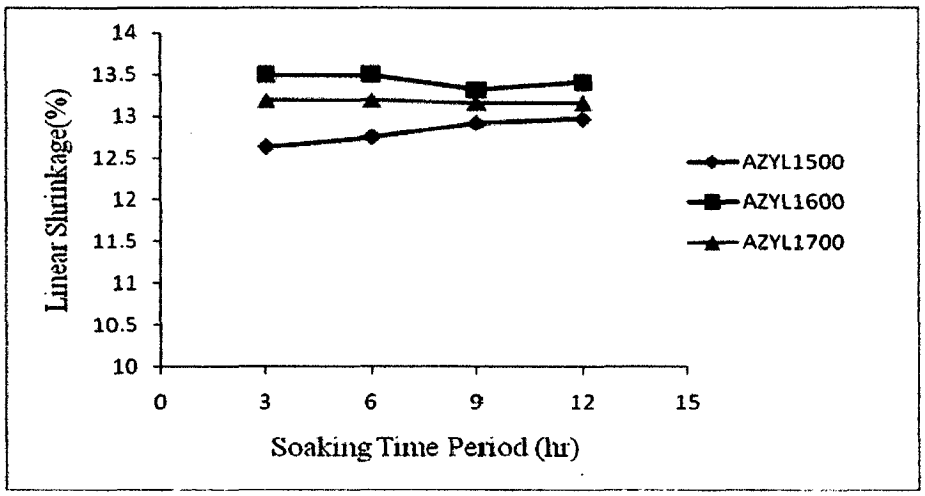

Fig.6.34 Linear shrinkage of the AZYL samples sintered at 1500°C, 1600°C and 1700°C for different soaking time periods.

6.5.3.2 Analysis of microstructure of AZYL samples

6.5.3.2.1 Microstructure of sintered AZYL samples

Fig. 6.35(a) shows the microstructure of $AZYL_6^{1500}$ sample which consists of smaller grains which are round in shape and a few larger grains of largely elongated type. The grain size in the sample $AZYL_6^{1500}$ varies between 0.39 and 3.07 μm with the average grain size 1.07μm. In Fig. 6.35(b), the range of grain size of the sample $AZYL_6^{1600}$ is 1.61 – 26.35 μm and the average grain size is 6.63μm. In Fig. 6.35(b)-(d), the larger grains are of Al_2O_3 and smaller grains which appear bright are of ZrO_2. The ranges of grain size in the samples $AZYL_3^{1700}$ and $AZYL_6^{1700}$ are 2.39 – 31.86 μm and 4.48 – 33.36 μm respectively. The EDS spectra obtained from a ZrO_2 grain situated at the grain boundary region of Al_2O_3 is shown in Fig.6.35(c) which shows besides the major elements Al, Zr, O, the presence of both Y and La with Y larger in proportion than La.

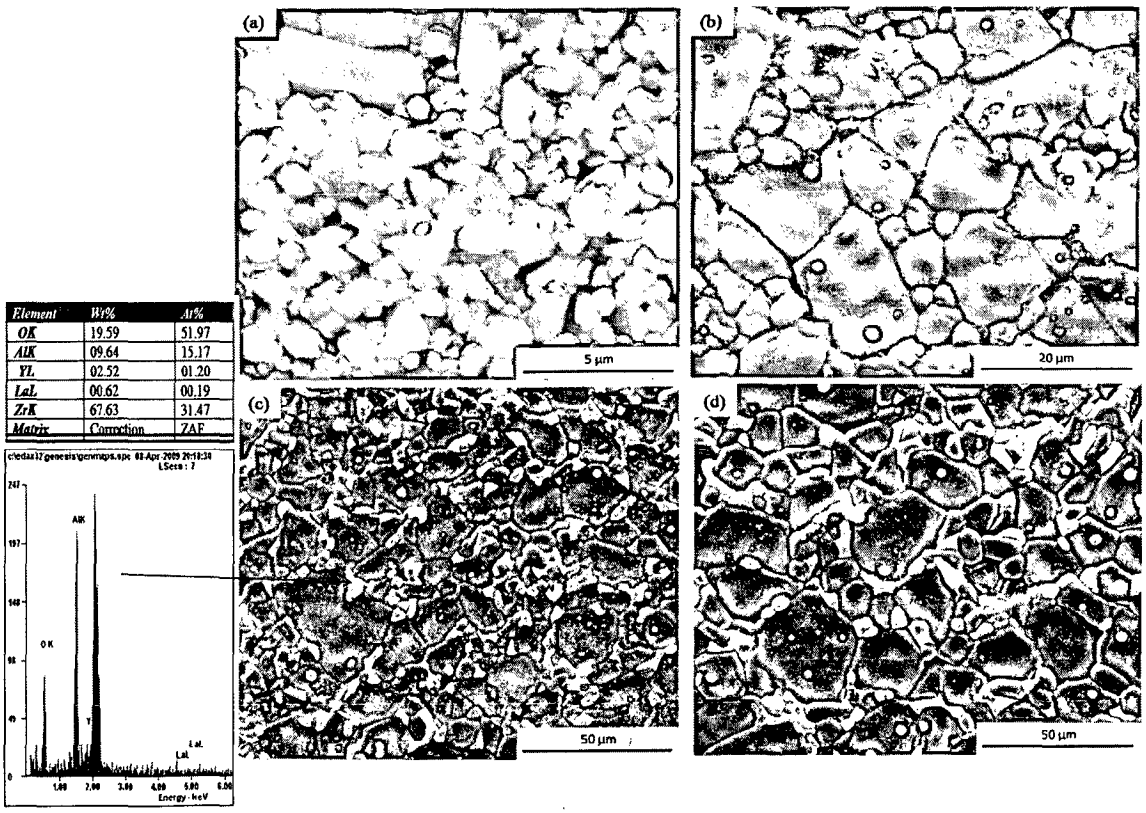

Fig.6.35 SEM micrographs of the samples (a) $AZYL_6^{1500}$, (b) $AZYL_6^{1600}$,(c) $AZYL_3^{1700}$ with EDS result and (d) $AZYL_6^{1700}$

Average grain size of the samples $AZYL_3^{1700}$ and $AZYL_6^{1700}$ are 11.02 μm and 14.21μm respectively. The grain size of the AZYL samples increases with increasing both sintering temperature and soaking time period. The average grain size of the samples sintered at 1500°C is very small lying between 1.01 and 1.42 μm. The grains in the samples sintered at 1600°C are larger (6.44 to 9.27 μm).

6.5.3.2.2 Histograms of grain size data of the sintered AZYL samples

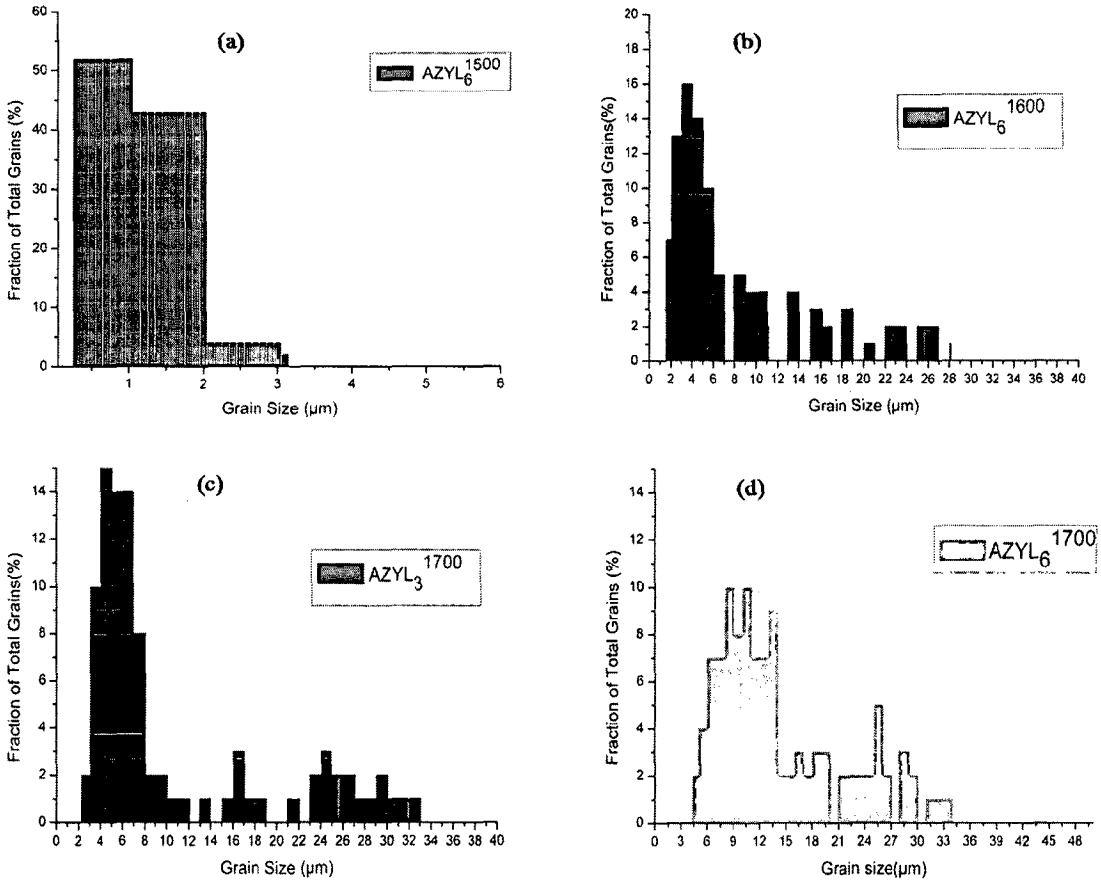

Fig.6.36 Grain size histograms of the samples (a) $AZYL_6^{1500}$, (b) $AZYL_6^{1600}$, (c) $AZYL_3^{1700}$, (d) $AZYL_6^{1700}$.

Fig.6.36 show the grain size histograms of AZYL samples sintered at different temperatures for different soaking time periods. Fig.6.36 (a) shows the grain size distribution is of bimodal

type. The wide distributions in grain size of the samples $AZYL_6^{1600}$, $AZYL_3^{1700}$, $AZYL_6^{1700}$ are found.

6.5.3.3 Effect of mechanical properties of AZYL samples sintered at different temperatures for various soaking time periods

6.5.3.3.1 Hardness of the AZYL samples

The influence of variation in sintering temperature and soaking time period on hardness of AZYL samples has been investigated.

6.5.3.3.1.1 Effect of sintering temperature on hardness

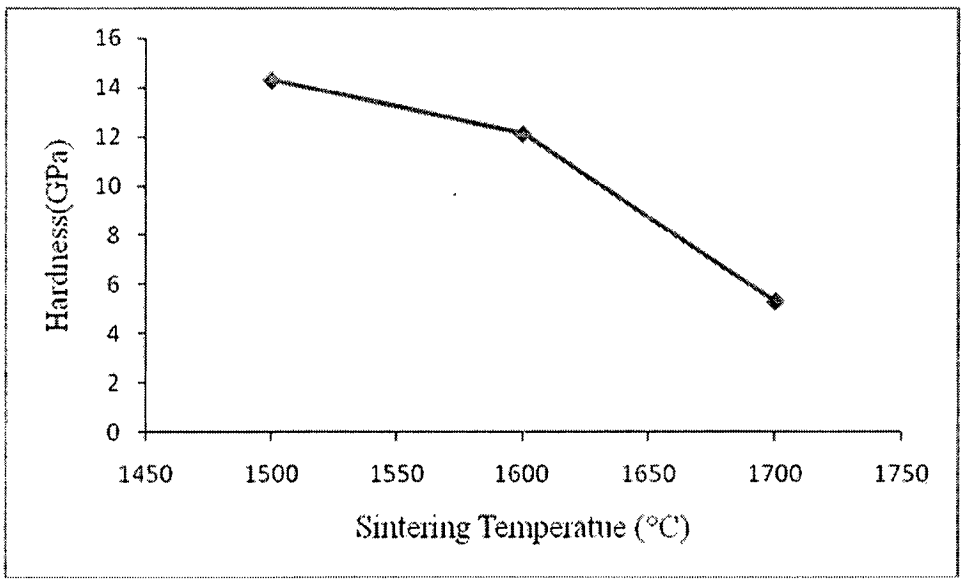

Fig.6.37 Variation of hardness of the AZL samples with sintering temperature for a soaking time period of 3hr

Fig.6.37 shows the hardness of the sample AZYL decreases with increasing sintering temperature. The plot shows the point to point joining of the hardness data at three different temperatures. These samples were sintered for a fixed soaking time period of 3h.

6.5.3.3.1.2 Effect of soaking time period on hardness

Fig.6.38 shows the variation of the hardness of the samples AZYL with soaking time period. It is evident from the Fig.6.38 that the hardness remains unchanged with increasing

soaking time period. The hardness of the samples sintered at 1500°C is higher than that of the samples sintered at 1600°C the hardness values of which are greater than that of the samples sintered at 1700°C.

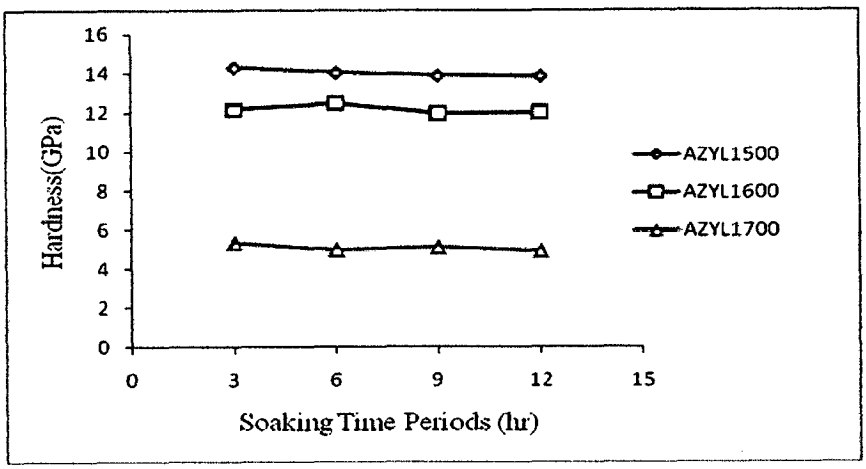

Fig.6.38 Hardness of AZYL samples sintered at 1500°C, 1600°C and 1700°C for different soaking time periods.

6.5.3.3.1.3 The effect of grain size on the hardness through Hall Petch Equation

The dependence of hardness on the grain size of the AZYL samples is shown through Hall-Petch relationship given in the equation 6.1.

The plot in the Fig.6.39 has been made between the hardness and $d^{-1/2}$ and smooth linear fitting of the points gives rise to two distinct linear graphs which can be expressed by mathematical expressions given by equation (6.8) and (6.9).

$$H_v = 66.24\, d^{-1/2} - 11.981 \qquad (6.8)$$

$$H_v = 3.32\, d^{-1/2} + 10.95 \qquad (6.9)$$

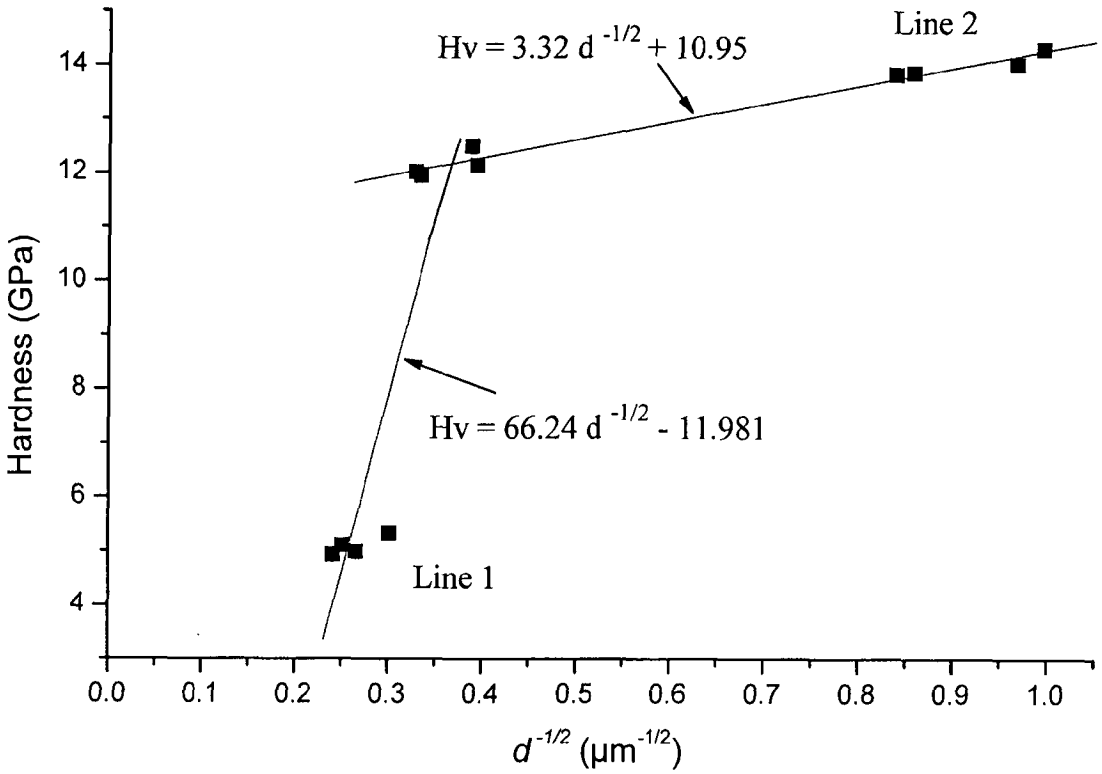

Fig.6.39 Grain size dependent hardness of AZYL ceramics composites.

6.5.3.3.2 Fracture toughness of the sintered AZYL samples

6.5.3.3.2.1 Effect of sintering temperature on the fracture toughness

Table 6.13 shows the hardness decreases with increasing average grain size of the samples. For the samples sintered at 1600°C the hardness varies between 12.02 and 12.14 GPa. The fracture toughness of the samples AZYL varies between 4.93 and 5.69 MPa $m^{-1/2}$. The hardness and fracture toughness of the samples sintered at 1700°C are low compared to the samples sintered at other two temperatures.

Table 6.13 Hardness, fracture toughness and grain size of AZYL samples sintered at 1500°C, 1600°C and 1700°C.

Sample	Average grain size (μm)	Grain size range (μm)	Grain size difference (μm)	Hardness (GPa)	Fracture toughness (MPa $m^{1/2}$)
$AZYL_3^{1500}$	1.01	0.39- 2.92	2.53	14.29	4.99
$AZYL_6^{1500}$	1.07	0.39- 3.07	2.68	14.02	5.42
$AZYL_9^{1500}$	1.36	0.47- 5.1	4.63	13.86	5.19
$AZYL_{12}^{1500}$	1.42	0.50-5.98	5.48	13.83	5.46
$AZYL_3^{1600}$	6.44	1.4- 25.51	24.11	12.14	5.28
$AZYL_6^{1600}$	6.63	1.61- 26.35	24.74	12.49	5.27
$AZYL_9^{1600}$	8.98	1.78-30.12	28.34	11.95	5.21
$AZYL_{12}^{1600}$	9.27	1.97-30.5	28.53	12.02	5.09
$AZYL_3^{1700}$	11.02	2.39- 31.86	29.47	5.33	5.69
$AZYL_6^{1700}$	14.21	4.48- 33.36	28.88	4.99	5.09
$AZYL_9^{1700}$	15.85	5.20- 36.81	31.61	5.11	5.05
$AZYL_{12}^{1700}$	17.25	5.9- 41.6	35.7	4.93	4.93

6.5.3.3.2.2 Effect of grain size on the fracture toughness

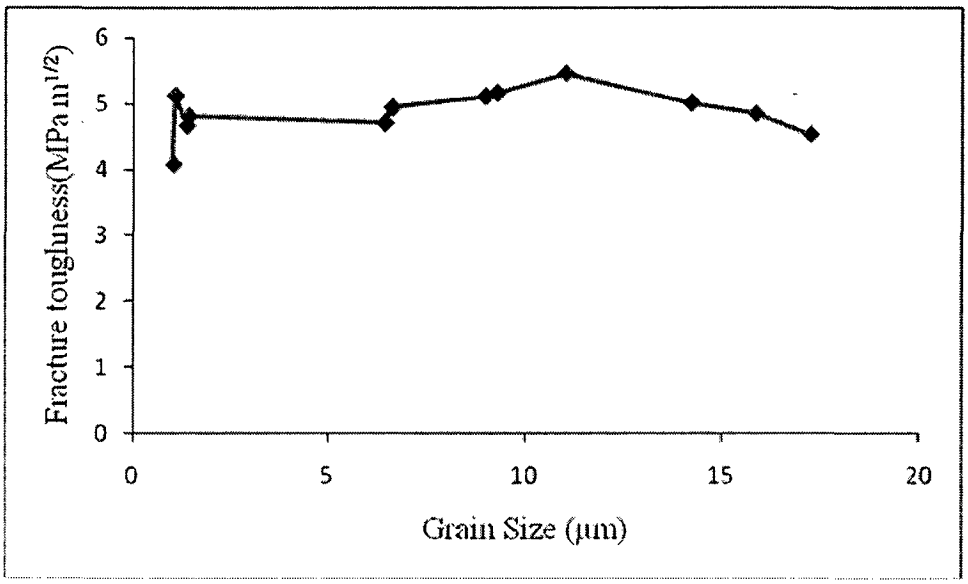

Fig.6.40 Plot of fracture toughness with grain size of the AZYL samples

Fig.6.40 shows the fracture toughness of the samples AZYL for different grain sizes. It can be seen from the Fig.6.40 that the fracture toughness of the sample AZYL increases marginally with increasing the average grain size upto the 11.02μm and decreases thereafter.

6.5.3.3.2.3 Correlation of fracture toughness with mode of crack propagation

Fig.6.41 shows an optical micrograph of the $AZYL_3^{1500}$ sample surface with Vickers indentation on it showing the cracks are emanating from the vertices of the indentation impression. An enlarged view of a crack path is shown in the inset of the Fig. 6.41. The zig-zag nature of the crack path (Fig 6.41) signifies the occurrence of the crack deflection.

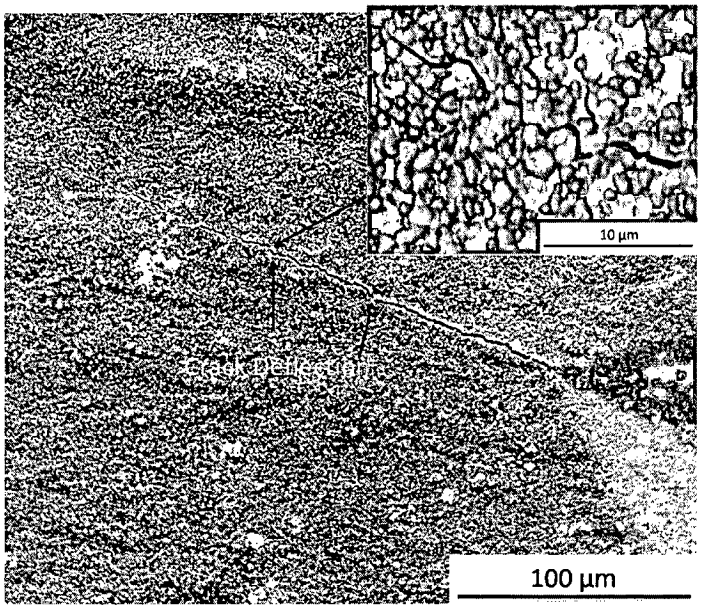

Fig.6.41 SEM micrograph of $AZYL_3^{1500}$ sample surface showing the crack path induced by Vickers indentation.

6.5.3.3.2.4 Microstructure of the fracture surfaces

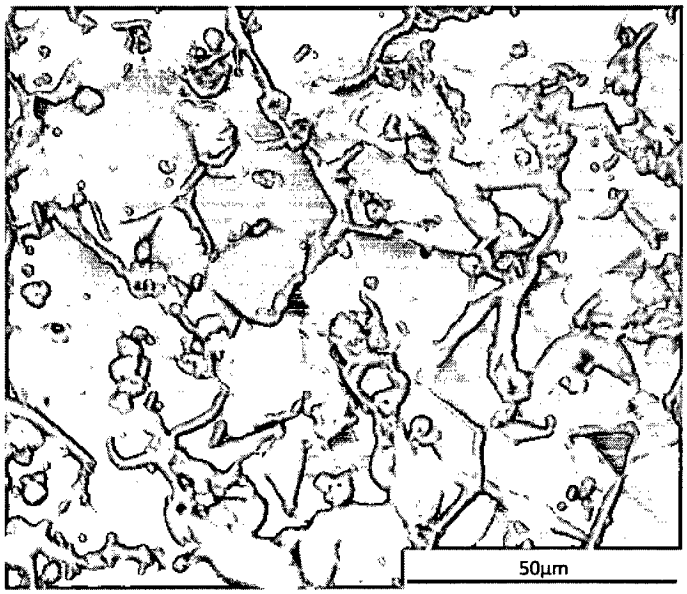

Fig.6.42 SEM micrograph of fracture surface of $AZYL_6^{1700}$

The fracture surface of the $AZYL_6^{1700}$ is shown in Fig. 6.42, the topography of the fracture surface reveals that fracture is caused by the mixed modes of intergranular and transgranular fractures.

6.5.3.3.2.5 Comparison of fracture toughness data obtained by Indentation method and SEPB method

Table 6.11 shows the comparison of the fracture toughness of the samples AZYL sintered at different temperatures for different soaking time periods. The samples sintered at 1500°C show the fracture toughness ranges between 4.99 and 5.46 MPa $m^{1/2}$ measured by indentation method where as three point bend test method shows the fracture toughness range of 4.08 – 5.12 MPa $m^{1/2}$.

Fracture toughness of the samples sintered at 1500°C was measured using indentation method, which varies between 4.93 and 5.42 MPa $m^{1/2}$. Whereas the fracture toughness of the samples sintered at 1500 °C determined by SEPB method is found to lie in the range of 4.21- 4.57 MPa $m^{1/2}$. The samples sintered at higher temperatures have lower fracture toughness determined using both the methods. The samples sintered at 1600°C and 1700°C has the range of fracture toughness of 4.93 – 5.69 MPa $m^{1/2}$ and 4.53 – 5.45 MPa $m^{1/2}$ measured by indentation method and SEPB method respectively.

Table 6.14 Comparison of fracture toughness measured by Indentation method and SEPB method.

Sample	Fracture toughness measured by (MPa $m^{1/2}$)	
	Indentation method	SEPB method
$AZYL_3^{1500}$	4.99	4.08
$AZYL_6^{1500}$	5.42	5.12
$AZYL_9^{1500}$	5.19	4.67
$AZYL_{12}^{1500}$	5.46	4.81
$AZYL_3^{1600}$	5.28	4.71
$AZYL_6^{1600}$	5.27	4.94
$AZYL_9^{1600}$	5.21	5.11
$AZYL_{12}^{1600}$	5.09	5.16
$AZYL_3^{1700}$	5.69	5.45
$AZYL_6^{1700}$	5.09	5.01
$AZYL_9^{1700}$	5.05	4.85
$AZYL_{12}^{1700}$	4.93	4.53

6.6 Comparison of physical properties and mechanical properties of A, AZ, AZY, AZL and AZYL samples

6.6.1 Physical properties

By the above sintering process, the compound formation and the elimination of the

porosity in the powder compacts were achieved (Haldar et al., 2002). The relative density of all the samples varies from 96.72 to 99.25 %. The relative density of the sample A_3^{1500} is lower compared to the other samples. The AZ samples sintered at 1700°C show lower relative density than the samples sintered at 1500°C and 1600°C. The samples A, AZY and AZYL show higher relative density than the samples of AZ and AZL sintered at higher temperatures (Boutz et al., 1994, Chae et al., 1993).

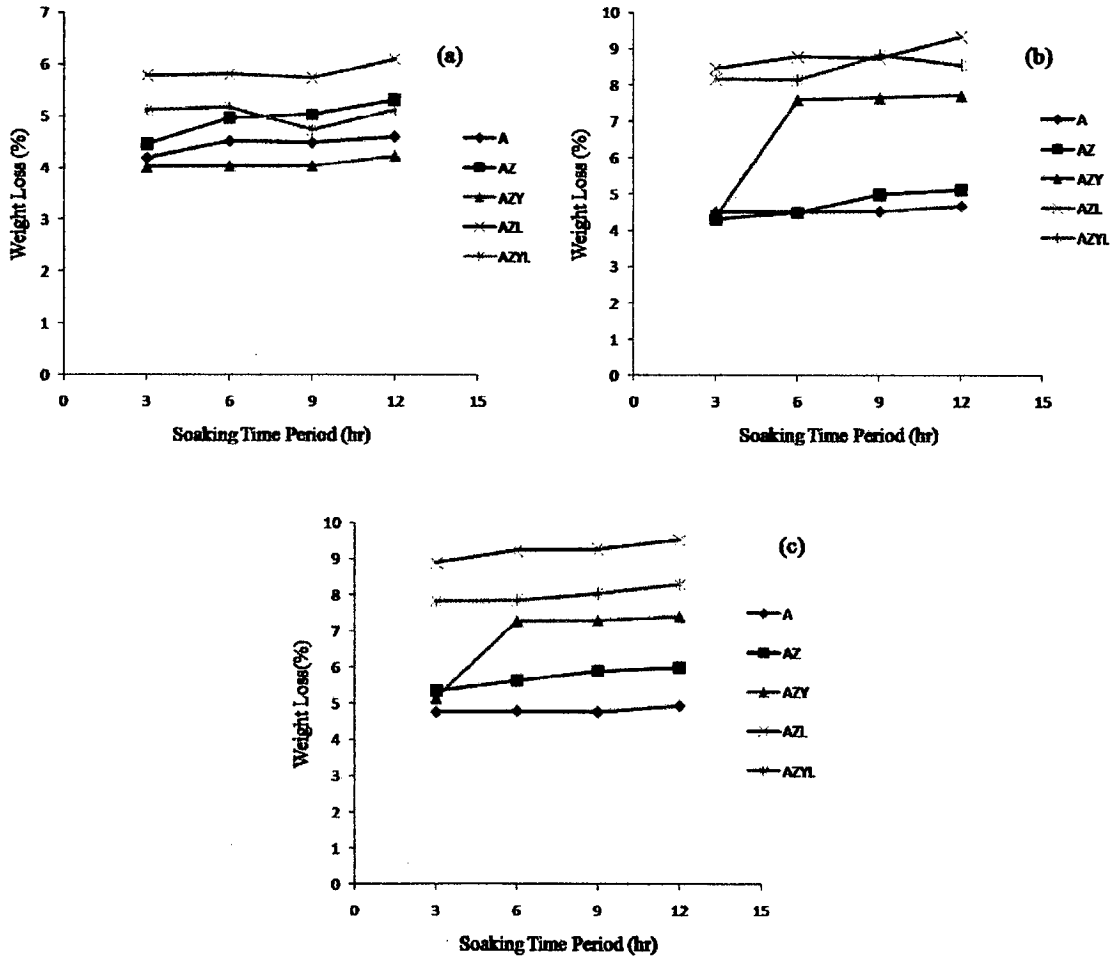

Fig.6.43 Weight loss as a function of sintering time of the samples sintered at (a) 1500°C, (b) 1600°C and (c) 1700°C.

The weight loss (i.e. the difference in weights of the green compact and the sintered sample) of the samples A, AZ, AZY, AZL and AZYL for sintering at 1500°C, 1600°C and 1700°C are shown in Fig. 6.43. For the sample AZ sintered at 1500°C weight loss as shown in Fig.

6.43(a), is more than the AZY and AZYL. But weight loss is less in the sample AZ sintered at 1600°C and 1700°C than AZY, AZL and AZYL. The AZL sintered at 1500°C, 1600°C and 1700°C shows the higher weight loss signifying the formation of more volatile matter thereby leading to lower densification (Haldar et al., 2002). Chemical reaction or formation of compound may promote the weight loss (Hue et al., 1997). Therefore the porosity development in the samples is also more in these samples which consequently reduces the density of these materials. This causes lower fracture toughness, as given in Table 6.15, of the samples AZL sintered at 1700°C.

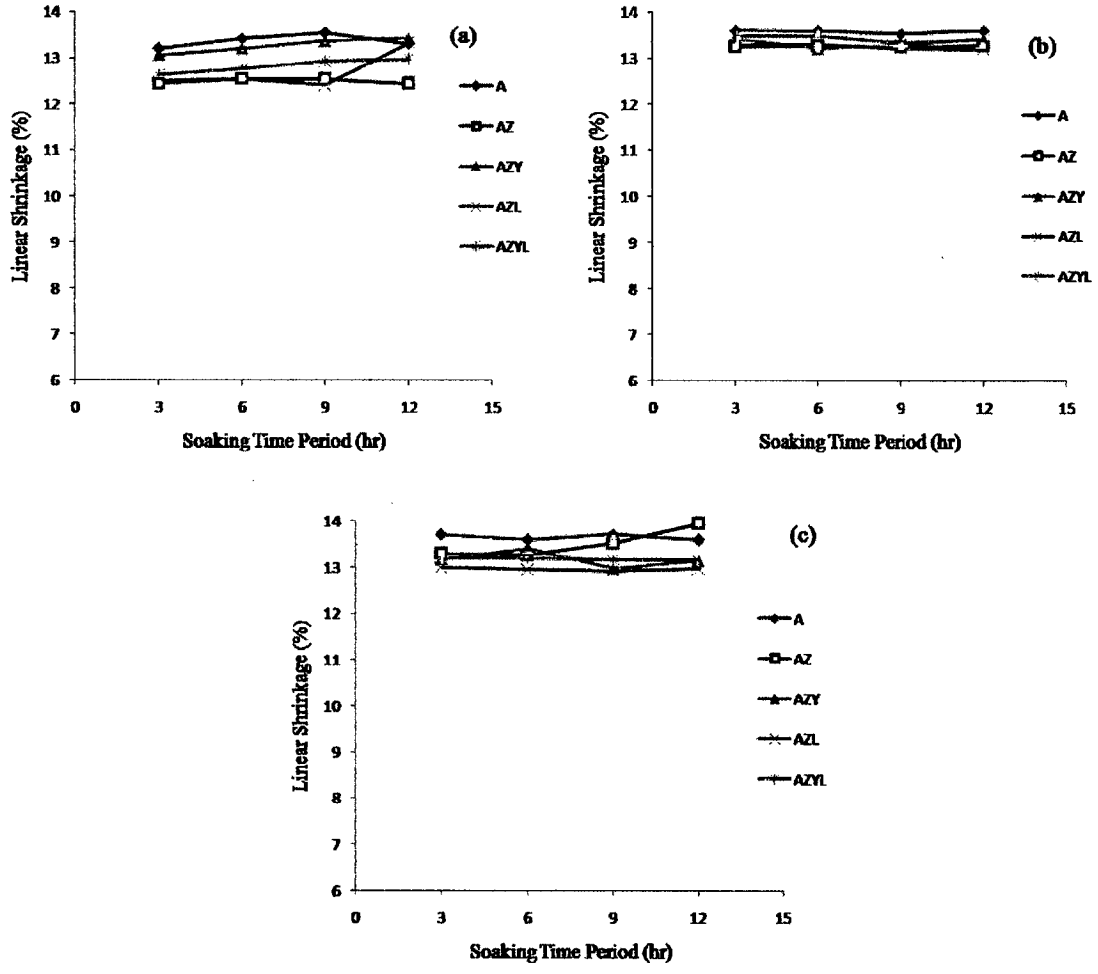

Fig.6.44 Linear shrinkage for the samples sintered at (a) 1500°C, (b) 1600°C and (c) 1700°C for different soaking time periods

Fig.6.44 shows the plots of linear shrinkage in the samples sintered at different temperature for different soaking time periods. Linear shrinkage is high with the sample A sintered at the 1500°C. The linear shrinkages in the samples sintered at 1600 °C and 1700 °C are higher and the shrinkages are the same for all the samples is almost same.

6.6.2 XRD patterns

Fig. 6.45 shows the XRD patterns of the samples AZ_6^{1700} and A_6^{1700} While all the peaks in the pattern for A_6^{1700} sample belongs to Al_2O_3 (ICSD file No. 01-071-1124), the pattern for the sample AZ_6^{1700} consists the phases of Al_2O_3, $Al_{0.18}Zr_{0.82}O_{1.91}$ and ZrO_2 (ICSD file Nos.01-071-1124, 00-053-0572 and 01-074-1201 respectively).

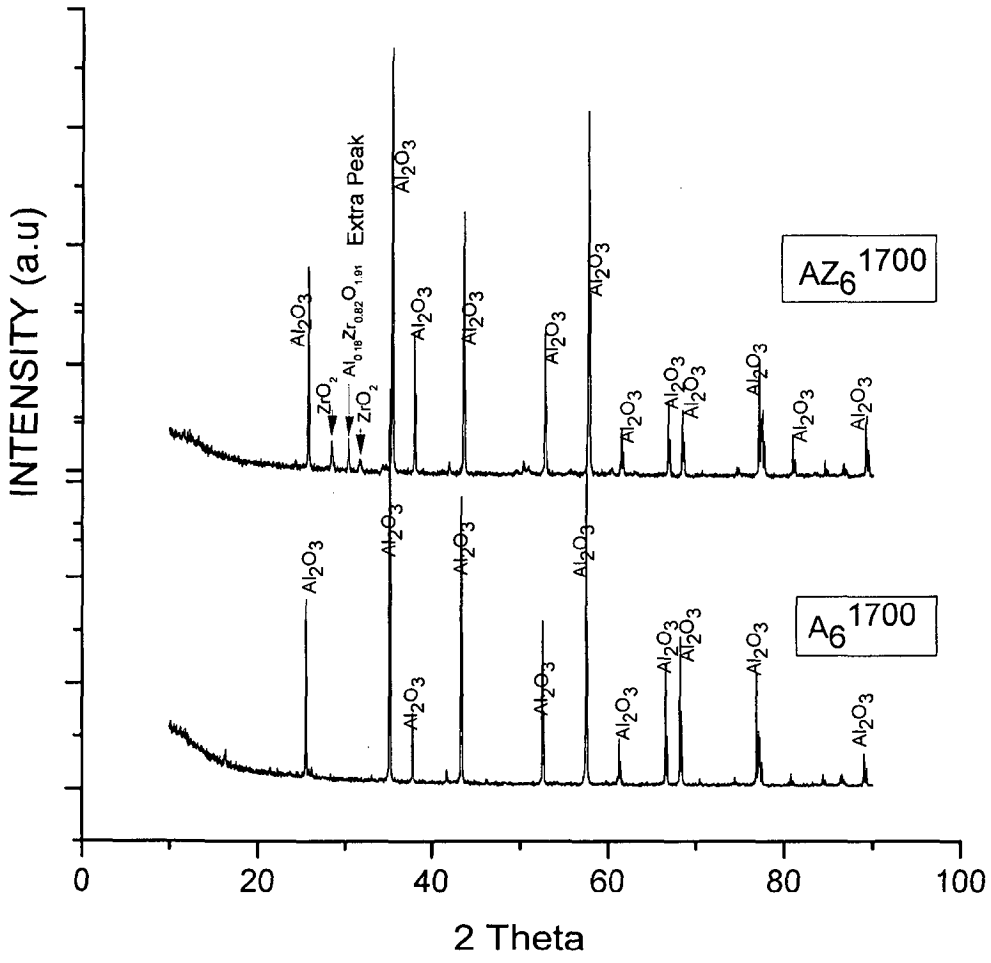

Fig.6.45 X-ray diffraction patterns of A_6^{1700} and AZ_6^{1700} samples

The patterns over the angular range of 2θ between 22° and 36° are shown separately in Fig.6.46. The appearance of the peaks for AZ_6^{1700} over this angular range was also reported by other researchers (Shukla et al., 2002, Li et al., 1992, Rajendran et al., 1989). The XRD pattern of AZY_6^{1700} composite is shown in Fig. 6.46(c), which shows the phase of $Zr_{0.88}Y_{0.12}O_{1.94}$ (ICSD data file No. 01-082-1242 with highest intensity peak) is present along with ZrO_2 and Al_2O_3 phases (Biswas and Choudhuri, 1999). The XRD pattern of AZL_6^{1700} composite in Fig. 6.46(d), shows the phases of $Al_{0.01}Zr_{0.99}O_{1.99}$ (ICDD data file No. 00-053-0548), $La_{0.9}Al_{11.76}O_{19}$ along with ZrO_2 and Al_2O_3 are present. The height of 100% intensity peak of the compound $Al_{0.01}Zr_{0.99}O_{1.99}$ is negligibly small. XRD analysis of the co-doped (with Y+La) material was carried out for one sample of $AZYL_6^{1700}$.

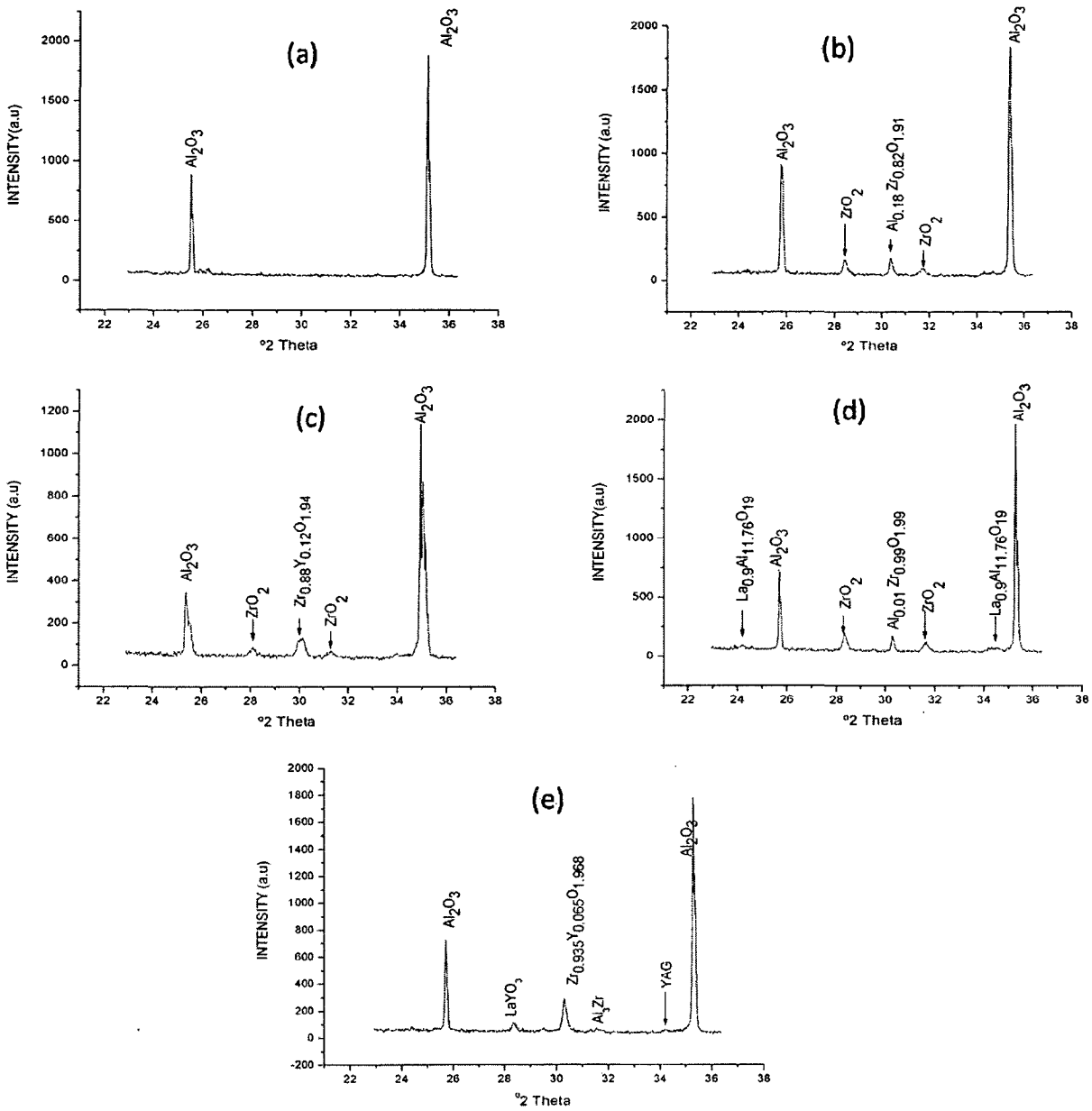

Fig.6.46 X-ray diffraction pattern of (a) A_6^{1700}, (b) AZ_6^{1700},(c)AZY_6^{1700},(d) AZL_6^{1700} and (e) $AZYL_6^{1700}$.

The XRD pattern (Fig.6.46(e)) of $AZYL_6^{1700}$ composite shows the formation of $Zr_{0.935}Y_{0.065}O_{1.968}$ phase (ICSD file No. 01-078-1808) along with of $LaYO_3$, Al_3Zr and ZrO_2 phases.

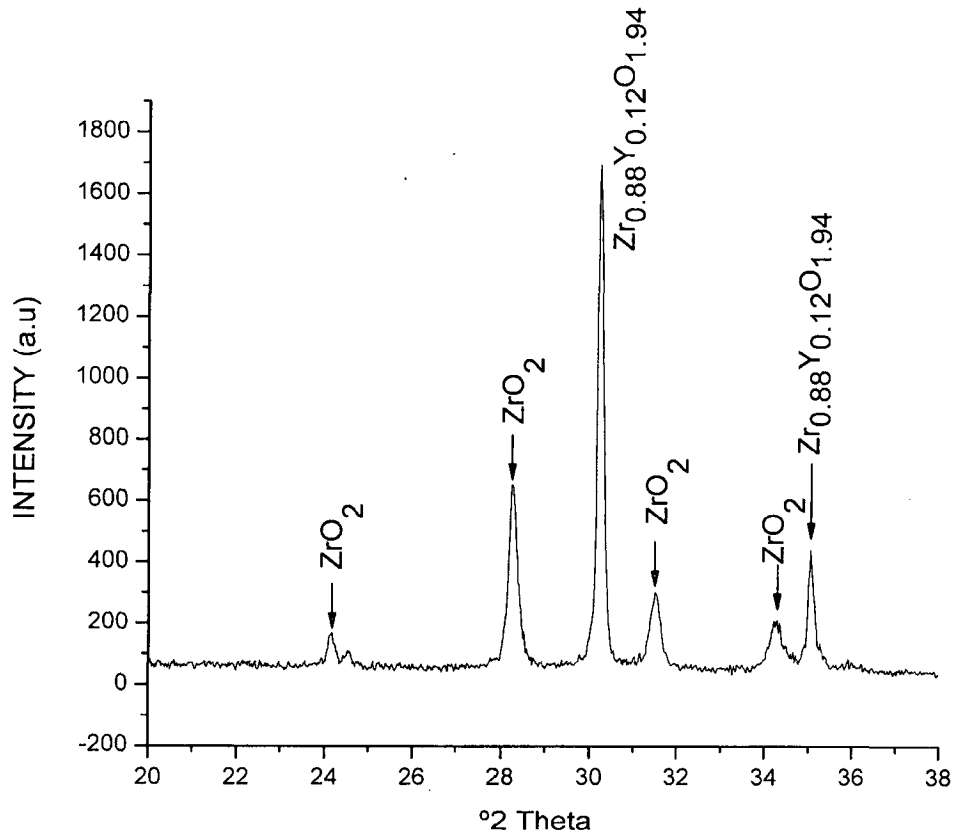

Fig.6.47 X-ray diffraction patterns of ZrO_2 and $Y(NO_3)_3.6H_2O$ composite sintered at 1500°C for the soaking period of 6hr.

The compound $Zr_{0.88}\ Y_{0.12}O_{1.94}$ is present in the interfacial region in the AZY material in very minute proportion compared to the bulk Al_2O_3. Therefore the relative intensity of the XRD peaks of this phase $Zr_{0.88}Y_{0.12}O_{1.94}$ in the pattern is very low which consequently poses difficulty to predict the presence of such phases. In order to establish the predictability of the phases the compound $Zr_{0.88}Y_{0.12}O_{1.94}$ was separately synthesized by the method of mixing of the raw materials ZrO_2 and $Y(NO_3)_3.6H_2O$ powders in the proportion of 0.88 ZrO_2 : $0.12Y(NO_3)_3.6H_2O$ followed by calcination at 1500°C for 6hr. The calcined powder was characterized by X-ray diffractometry. The XRD pattern is shown in Fig.6.47 which shows the evidence of the formation of chemical compound $Zr_{0.88}\ Y_{0.12}O_{1.94}$. This control experiment thus confirms the formation of the stated phase in the intergranular region of AZY material.

6.6.3 Mechanical properties

Fracture toughness and hardness of the samples are listed in Table 6.15. The hardness of the samples A sintered at 1500°C varies between 14.77 and 15.52 GPa and for the samples sintered at 1600°C and 1700°C the hardness varies between 6.56 and 8.64 GPa. The lowering of the hardness is attributed to the larger grain sizes for the samples sintered at 1700°C and 1600°C compared to the samples sintered at 1500°C. The doped samples sintered at 1600°C shows higher hardness compared to undoped samples. The AZ, AZY, AZL and AZYL samples sintered at 1500°C and 1600°C show higher hardness compared to the 1700°C sintered samples. Sintered at 1700°C, the samples A, AZ and AZY show higher hardness than that of the La doped samples AZL and AZYL. Lower hardnesses were also observed by other researcher. Lu et al. reported the hardness values of 2.26 and 2.09 GPa for pure Al_2O_3 and composite of Al_2O_3–5wt% MgB_2 respectively (Lu et al., 2005).

The fracture toughness of the samples A, AZY and AZYL sintered at 1700°C for all the soaking periods studied are moderately high. However the fracture toughness of AZ, AZL samples sintered at 1700°C for soaking times of 6hr, 9hr and 12hr is relatively lower.

The XRD analysis has shown the formation of the phases $Al_{0.18}Zr_{0.82}O_{1.91}$ and $Al_{0.01}Zr_{0.99}O_{1.99}$ in AZ_6^{1700} and AZL_6^{1700} respectively. The lower fracture toughness of these samples may be attributed to the combined effect of larger grain size (Daguano et al., 2007) and the intergranular phases formed. The lower fracture toughness in the sample AZ_6^{1700} and AZL_6^{1700} can be attributed primarily to the microstructure of non densified grain structure (Rice, 2000, Rajendran and Rossell, 1991). On the other hand the compounds $Zr_{0.88}Y_{0.12}O_{1.94}$ and $Zr_{0.935}Y_{0.065}O_{1.968}$ in the samples AZY_6^{1700} and $AZYL_6^{1700}$ respectively seem to play an important role in enhancing fracture toughness (Biswas Choudhuri, 1999, Howard et al., 1988). This observation has not been reported so far.

Table 6.15 Fracture toughness and hardness of the A, AZ, AZY, AZL and AZYL samples sintered at different temperatures and soaking time periods

Temp (°C)	Time (hr)	A		AZ		AZY		AZL		AZYL	
		H_V (GPa)	K_{IC} (MPa $m^{1/2}$)	H_V (GPa)	K_{IC} (MPa $m^{1/2}$)	H (GPa)	K_{IC} (MPa $m^{1/2}$)	H_V (GPa)	K_{IC} (MPa $m^{1/2}$)	H_V (GPa)	K_{IC} (MPa $m^{1/2}$)
1500°C	3hr	15.01	4.01	15.3	4.87	15.20	4.45	14.80	4.21	14.29	4.08
	6hr	14.94	5.26	14.5	5.29	15.01	4.66	13.96	4.33	14.02	5.12
	9hr	12.77	4.97	13.93	5.11	13.30	4.73	14.37	4.46	13.86	4.67
	12hr	15.52	5.25	12.63	5.18	13.20	4.88	12.97	4.57	13.83	4.81
1600°C	3hr	6.56	4.92	7.94	5.21	10.30	4.97	13.86	4.67	12.14	4.71
	6hr	7.20	4.98	9.69	5.18	10.42	4.66	13.40	4.92	12.49	4.94
	9hr	7.84	5.14	11.18	5.22	10.94	4.68	11.95	4.70	11.95	5.11
	12hr	7.68	5.20	12	5.22	10.12	4.90	11.69	4.72	12.02	5.16
1700°C	3hr	7.74	4.51	8.19	5.21	10.65	5.26	4.03	5.28	5.33	5.45
	6hr	8.64	4.55	7.29	1.85	9.21	4.96	4.30	2.12	4.99	5.01
	9hr	8.46	4.95	5.79	1.70	8.97	5.22	4.12	1.81	5.11	4.85
	12hr	7.21	5.15	6.25	1.65	8.25	4.52	4.09	1.80	4.93	4.53

6.7 Nano size ZrO_2 dispersed Al_2O_3 ceramic

The effect of particle size on physical and mechanical properties of Al_2O_3 has been studied. The main objective of the present work is to investigate the effects of nano and micron sized ZrO_2 particle dispersion in Al_2O_3 matrix on hardness and fracture toughness in Al_2O_3-ZrO_2 composites. The change in microstructure and grain size distribution improves

the mechanical properties. Al_2O_3– ZrO_2 ceramic composites were prepared with 1vol% micron-sized and 1vol% nano-sized ZrO_2 particles by uniaxial pressing and sintered at 1500°C for soaking time period of 3hr, 6hr and 9hr. The following nomenclatures AMZ and ANZ have been used to represent the composites Al_2O_3 -1vol% micron-sized ZrO_2, Al_2O_3 - 1vol% nano-sized ZrO_2 respectively.

6.7.1 Physical properties

Table 6.16 shows that the density of ANZ is marginally higher compared to A and AMZ samples. This can be attributed to the higher packing density resulted in the green compact of ANZ due to nano-sized ZrO_2 particles, which occupies part of the voids among Al_2O_3 particles (Guimaraes et al., 2009). Linear shrinkages of the samples are nearly equal in all three types systems A, AMZ and ANZ. Nearly same amount of weight loss is observed in ANZ and AMZ samples, which is less than that of A.

Table 6.16 Density, shrinkage and grain size of A, AMZ and ANZ sintered at 1500°C for 3 hr, 6hr and 9hr.

Sample	Soaking Time (hr)	Sintered density (gm/cc)	Relative density (%)	Linear shrinkage (%)	Weight loss (%)	Average grain size (μm)
A	3	3.83	96.23	14.19	6.42	0.59
	6	3.90	97.99	14.25	6.44	0.83
	9	3.92	98.49	14.54	6.53	0.85
AMZ	3	3.87	96.75	13.91	6.07	0.69
	6	3.90	97.50	13.85	6.02	1.19
	9	3.89	97.25	14.07	6.09	1.27
ANZ	3	3.90	97.50	14.16	6.04	0.81
	6	3.92	97.99	13.95	6.11	1.32
	9	3.91	98.25	14.25	6.14	1.40

6.7.2 Microstructural analysis

6.7.2.1 Effect of micron and nano sized ZrO_2 powder dispersion on microstructure of Al_2O_3-ZrO_2 samples

Fig.6.48 shows that the average grain size is more in the AMZ and ANZ samples compared to that in the sample A. The grain size data are given in Table 6.16. The grain size in ANZ is maximum. The ZrO_2 phase is shown by arrows in the micrographs (Fig.6.48). Microstucture in Fig. 6.48(b) reveals that micron-sized ZrO_2 is present as separated particles as well as in the form of agglomeration, at the grain boundaries and grain junctions. In ANZ the nano ZrO_2 particles, are largely situated at the grain boundaries and within the grains also.

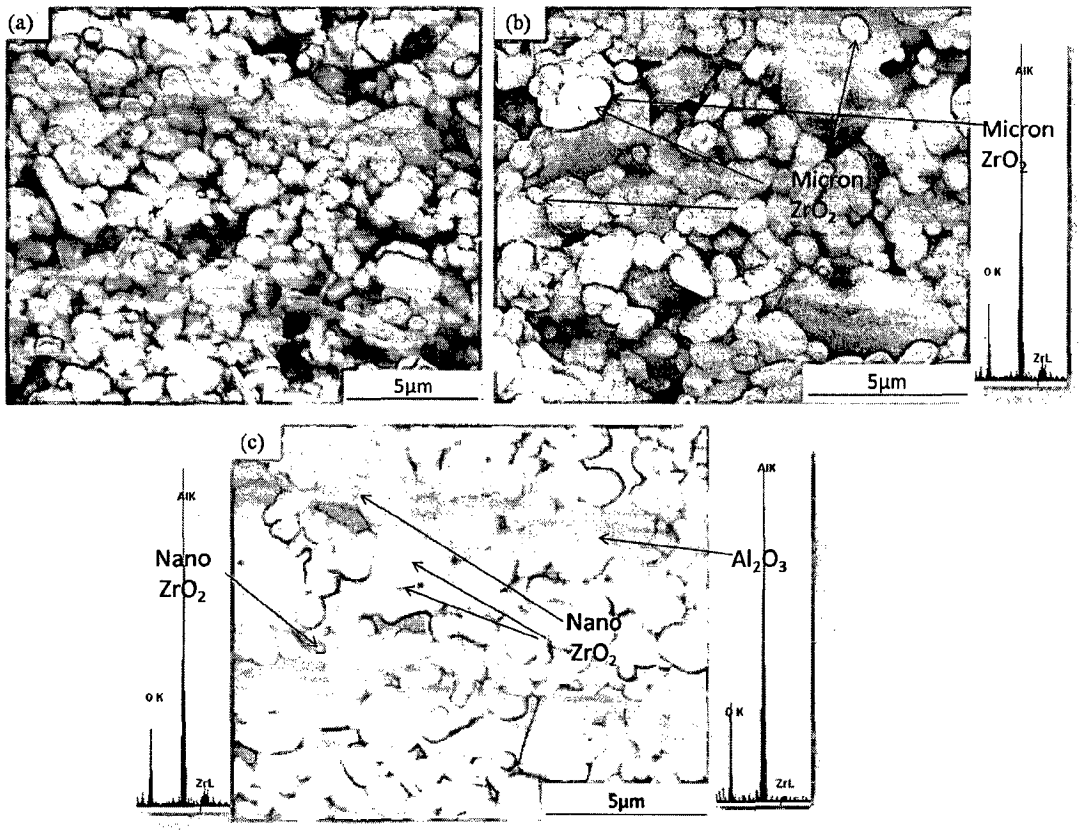

Fig.6.48 SEM micrograph of (a) A, (b) AMZ and (c) ANZ composites sintered at 1500°C for 6 hr.

6.7.2.2 Grain size histogram of Al_2O_3 and Al_2O_3- ZrO_2

As the grains in all the samples vary over a range of size rather than preferably having uniform size for a particular sintering schedule, it is appropriate to show the actual size distribution that has been resulted due to sintering. The measured grain sizes were subdivided into small size intervals and plots were made in the form of histograms to show the grain size distribution. Fig.6.49 presents such histograms for the samples sintered at A_6^{1500}, AMZ_6^{1500} and ANZ_6^{1500}. It can be seen from the Fig. 6.49 (a) that though the grains in the sample A are of different sizes varying from about 0.3 to about 1.9μm, a large number of grains fall in the lower size sub range of 0.4 - 0.6μm. The grain size ranges of the samples AMZ and ANZ as shown in Fig. 6.49 (b) and (c) are larger than that of the sample A. The size ranges are 0.3 – 4.5 μm and 0.3 – 6.0 μm respectively for AMZ and ANZ.

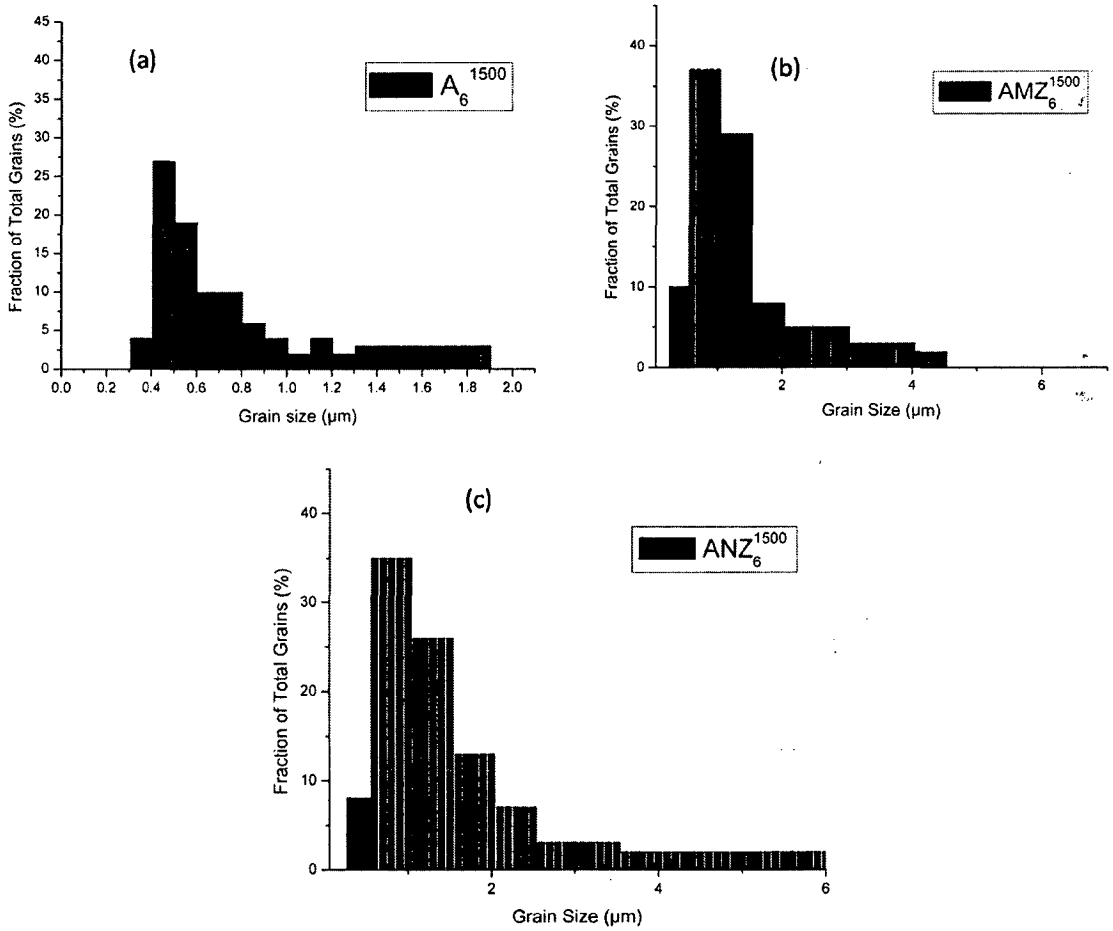

Fig.6.49 Grain size histograms for the samples (a) A_6^{1500}, (b) AMZ_6^{1500} and (c) ANZ_6^{1500}.

6.7.3 Mechanical properties

Table 6.17 shows the mechanical properties of the samples A, AMZ and ANZ sintered at 1500°C for different soaking time periods. The hardness for each type of sample decreases marginally with the increase in soaking period. Such gradual lowering of the hardness is attributed to the increase in grain size with the increase in soaking time for each type of samples (Lu et al., 2005). The range of fracture toughness of the sample ANZ is 5.24 – 5.76 $MPam^{1/2}$ which is higher compared to the sample AMZ and A for which the ranges are 5.05 – 5.35 $MPam^{1/2}$ and 4.79 – 5.26 $MPam^{1/2}$ respectively.

Table 6.17. Fracture toughness and hardness of A, AMZ and ANZ samples sintered at 1500°C for 3 ,6 and 9hr.

Sample	A			AMZ			ANZ		
Soaking time period (hr)	3	6	9	3	6	9	3	6	9
Fracture toughness (MPa $m^{1/2}$)	4.79	5.26	5.19	5.05	5.35	5.28	5.54	5.76	5.24
Hardness (GPa)	15.01	14.94	14.77	14.82	14.68	14.73	14.95	14.93	14.79

6.7.4 Microstructure of fracture surface

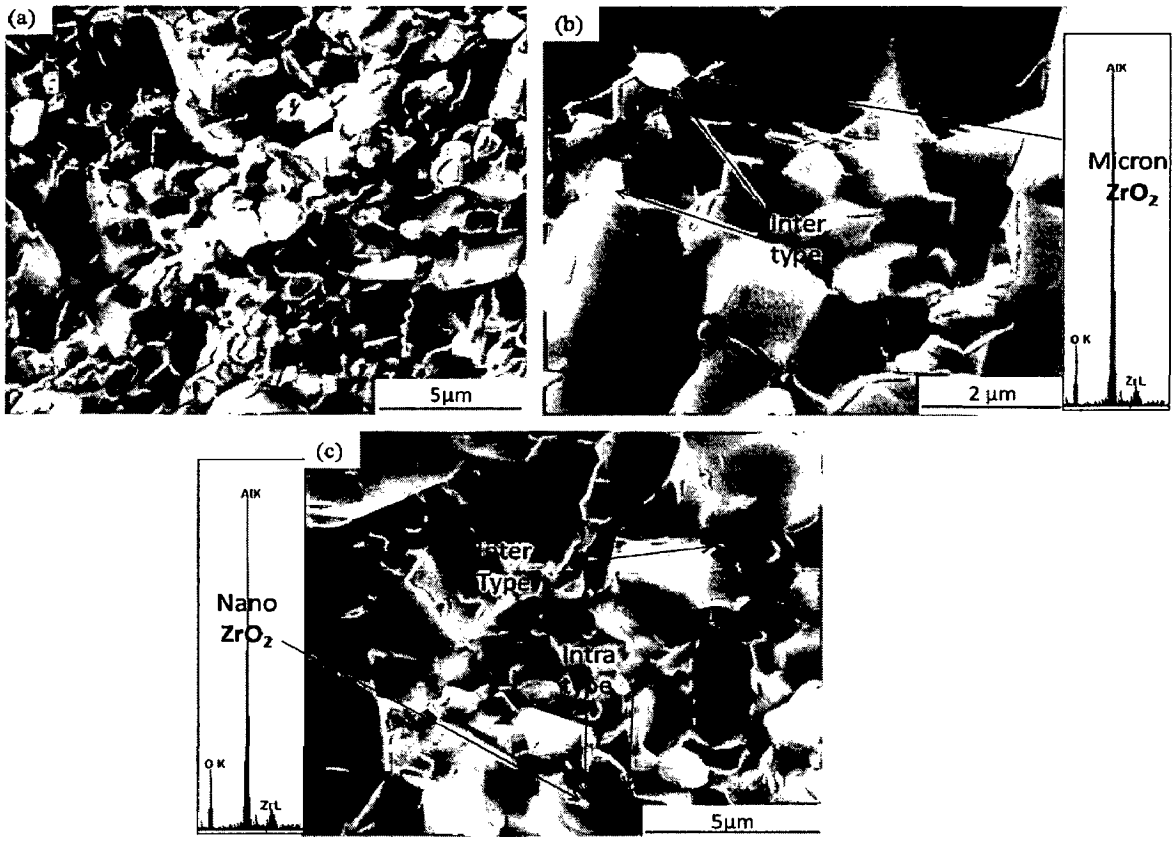

Fig.6.50 SEM micrographs of fracture surfaces of (a) A, (b) AMZ and (c) ANZ composites sintered at 1500°C for 6 hr.

Fig. 6.50 (a) shows the fracture surface of A sample in which the fracture has taken place predominantly by the intergranular mode. Fig.6.50 (b) also shows predominantly intergranular fracture mode but the presence of the ZrO_2 particles in the triple point is evident. Thermal expansion coefficient mismatch between Al_2O_3 and ZrO_2 creates thermal stress. The thermal stress increases the fracture toughness by deflecting the crack path (Ekstrom, 1993). Fig.6.50 (c) shows the fracture surface of ANZ where fracture has taken place due to mixed mode of intergranular and transgranular fracture (Chou et al., 2009). The fracture toughnesses of these samples (Fig. 6.50(c)) show relatively higher toughness as listed in Table 6.17.

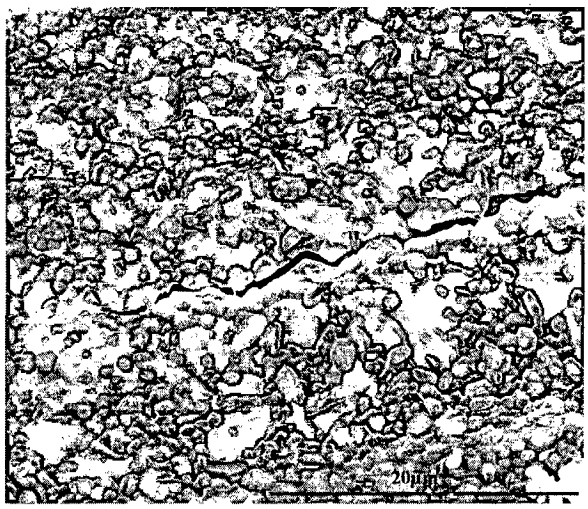

Fig.6.51 SEM micrograph of ANZ_6^{1500}

Crack path shown in Fig.6.51 reveals that the crack propagation is mainly of an intergranular nature showing the crack deflection is the predominant mechanism for toughness enhancement.

6.8 Summary

Rare earth elements (Y and La) doped (both singly and simultaneously) ZrO_2 dispersed Al_2O_3 composites have been prepared following ultrasonic slurry dispersion method. The effect of doping with rare earth elements on ceramic composites has been studied by considering the composite as Al_2O_3 – 5 wt% ZrO_2, as it reported in the literature that the densification characteristics of this composite is superior. The microstructural change and morphological variation of the grains, which play crucial role for fracture toughness and hardness of the materials, have been realized by preparing the samples at different sintering temperatures of 1500°, 1600° and 1700°C for various soaking time periods of 3, 6, 9 and 12hr. Researchers reported the rare earth element doping in oxide ceramics causes grain boundary segregation resulting in altering the cohesive property of the grain boundary of the material, which in turn influences the mode of crack propagation. The XRD analyses of one sample in each system studied show the evidence of compounds formation for sintering. The EDS analyses have indicated that these compounds especially the major secondary phases develop in the grain boundary region.

XRD analyses were done for all the samples sintered at 1700°C for soaking time of 6 hr. The XRD patterns of AZ_6^{1700} and AZL_6^{1700} show the major secondary phases formed in the materials are $Al_{0.18}Zr_{0.82}O_{1.91}$ and $Al_{0.01}Zr_{0.99}O_{1.99}$ respectively. However for AZL_6^{1700} sample a trace amount of the phase $La_{0.9}Al_{11.76}O_{19}$ is also present in the material. Whereas in the samples AZY_6^{1700} and $AZYL_6^{1700}$, the compounds $Zr_{0.88}Y_{0.12}O_{1.94}$ and $Zr_{0.935}Y_{0.065}O_{1.968}$ respectively are the major secondary phases. The low values of fracture toughness of the samples AZ_6^{1700}, AZ_9^{1700}, AZ_{12}^{1700}, AZL_6^{1700}, AZL_9^{1700} and AZL_{12}^{1700} may be attributed to the role of $Al_{0.18}Zr_{0.82}O_{1.91}$ for AZ and $Al_{0.01}Zr_{0.99}O_{1.99}$ for AZL samples. However, the fracture toughnesses of AZY and AZYL samples sintered at 1700°C for 6, 9 and 12 hr are consistantly larger compared to AZ and AZL samples sintered at 1700°C for corresponding soaking times.

Therefore the secondary phases $Zr_{0.88}Y_{0.12}O_{1.94}$ and $Zr_{0.935}Y_{0.065}O_{1.968}$ perhaps play an important role for higher fracture toughness in the samples AZY and AZYL. The basis of such interpretation to relate the role of the secondary phases with the fracture tougness is further justified in view of the fact that the fracture toughness which is low for AZL_6^{1700} has been restored to the value as good as found in other samples in simultaniously doped $AZYL_6^{1700}$ sample. To the best of the candidate's knowledge, the dependence of mechanical properties (such as fracture toughness in the present study) on possible secondary phase (s) formation in the material for application of structural ceramics has not been reported, so far, by other researchers.

Chapter 7

Conclusions and suggestions for future work

Chapter 7

Microstructural characterization and fracture toughness behaviour of oxide dispersed ceramic composites have been addressed in the present thesis by preparing 5 wt % ZrO_2 dispersed Al_2O_3 ceramic composites doped with rare earth elements (Y and La) and investigating microstructural developments in all types of the samples prepared and correlating the morphological features of the sintered samples with their mechanical properties viz. fracture toughness and hardness. The studies have been made on six different types of samples prepared. As the studies have been demonstrated on the Al_2O_3 based ceramic composites, samples of only Al_2O_3 have been investigated initially. Al_2O_3-5 wt% ZrO_2 has been studied separately for the sake of comparison of the effect of doping with Y and La elements individually and simultaneously. Grain size and shape variations have been achieved by controlling the sintering parameters i.e. temperature and soaking time. Y_2O_3 doped Al_2O_3 systems have also been investigated to determine the optimum level of the dopant.

The following are the broad conclusions of the present study.

7.1 Studies on the Al_2O_3 ceramics

1. The average size of the grains of the Al_2O_3 samples prepared by solid state sintering at 1500°, 1600° and 1700 °C for various soaking times of 3, 6, 9 and 12hr. The smallest size of the sample sintered at 1500°C for 3hr, whereas the sample sintered at 1700°C for 12hr yields largest grains.

2. The green and sintered densities of powder compacts made in uniaxial press by applying a load between 15 x 10 and 22.5 x 10 kN are not significantly different from those when powder compacts were made isostatically with a load 150 MPa.

3. Fracture toughness of the samples sintered at 1500°C for soaking times of 3, 6, 9, 12, 18, 24 and 36hr lie in the range of 5.20 - 5.38 MPa $m^{1/2}$ with an average value of 5.28 ± 0.08 MPa $m^{1/2}$. Fracture toughness of the samples sintered at 1600°C lies in the range of 5.01 - 5.57 MPa $m^{1/2}$ having an average of 5.37 ± 0.25 MPa $m^{1/2}$

which is slightly higher than that of the samples sintered at 1500°C. The range of fracture toughness of the samples sintered at 1700°C is 4.56 - 5.03 MPa $m^{1/2}$ giving an average of 4.86 ± 0.21 MPa $m^{1/2}$, which is lower than that of the samples sintered at 1500°C and 1600°C.

4. The analysis of fracture surface of the samples sintered at 1500°C and 1600°C reveals that fracture has occurred due to both intergranular and transgranular modes with larger proportion of former type. Such observation leads one to conclude that crack deflection mechanism is primarily give rise to the higher fracture toughness in these samples. However, calculation of aspect ratios of grains shows that grains having larger aspect ratio in the samples sintered at 1600°C and 1500°C are more compared to the samples sintered at 1700°C. Therefore the effect of grain shape giving rise to grain bridging mechanism can also be taken as contributing factor for higher fracture toughness of these samples.

5. Transgranular fracture is a predominant mode for the samples sintered at 1700°C for soaking time of 3hr. This is evident from the microstructural observation on fracture surface of the sample.

6. The linear relationship between the fracture surface roughness and the fracture toughness is well represented for the samples having higher fracture toughness.

7. The variation of hardness of the samples with their average grain size following Hall Petch equation give rise to two linear graphs described mathematically by the following equations :

   $H_v = 10.86\, d^{-1/2} + 2.532$

   and

   $H_v = 4.337 d^{-1/2} + 7.420$

   where, H_v is hardness and d is average grain size of the sample.

8. The hardness determination of the samples by indentation method depends critically on applied load for indentation. Indentation Size effect (ISE) is observed for the samples having average grain size greater than 7.3 μm. Whereas the samples having average grain size less than 7.3 μm experience Reverse indentation size effect (RISE). To the best of the candidate's knowledge the finding of such critical grain size of Al_2O_3 sample showing the alteration of the size effect, has not been reported by other researchers.

9. R-curve behaviour of samples having an average grain size upto 7.3 μm is revealed in the present study. For the samples having an average grain size above 7.3 μm, the crack length extension does not follow the R-curve behaviour. The finding of the critical grain size of Al_2O_3 sample showing R-curve behaviour, has not been reported so far.

7.2 Studies on Y_2O_3 doped Al_2O_3 materials

10. Relative density of the Y_2O_3 doped Al_2O_3 sample decreases with increasing Y_2O_3 content.

11. The investigation on using different doping levels of Y_2O_3 (1000, 2000, 3000, 5000, 10000 and 15000 ppm) in Al_2O_3 shows the sample containing 1000 ppm Y_2O_3 has higher fracture toughness. Highest fracture toughness of 5.69 MPa $m^{1/2}$ is found with the sample $A1Y_{12}{}^{1500}$. The fracture toughness of the samples for all other doping levels is lower. The Y goes to the grain boundary of the Al_2O_3. Though, with higher Y_2O_3 doping levels elongated grains are resulted in the samples but lower relative density causes lower fracture toughness for these samples.

7.3 Studies on Al_2O_3 – 5 wt% ZrO_2, Y, La doped (singly and simultaneously) Al_2O_3 - 5 wt % ZrO_2

12. 5 wt% ZrO_2 dispersed Al_2O_3 has been prepared and investigated to develop ceramic composite having improved densification characteristics to be used further for doping with rare earth elements.

13. The segregation of the ZrO_2 at the triple junctions and the intergranular regions of the Al_2O_3 grains is observed from the micrographs of the samples AZ.

14. The fracture toughness of the AZ samples sintered at 1600°C varies in the range of 5.43 - 6.01 MPa $m^{1/2}$ which is highest among all the values for AZ samples.

15. The tendency for Y segregation at the intergranular region is more compared to La. This is evident from the XRD analysis and EDS that (Zr-Y-O) compound forms at intergranular region.

16. The major second phase compounds that form in AZ, AZY, AZL and AZYL samples are $Al_{0.18}Zr_{0.82}O_{1.91}$, $Zr_{0.88}Y_{0.12}O_{1.94}$, $Al_{0.01}Zr_{0.99}O_{1.99}$ and $Zr_{0.935}Y_{0.065}O_{1.968}$ respectively.

17. The fracture toughness of the samples sintered at 1500°C and 1600°C for undoped and rare earth doped are nearly same. However, the samples sintered at 1700°C show lower fracture toughness for AZ and AZL samples sintered for soaking times of 6, 9 and 12 hr. There is no decrease in fracture toughness for the samples AZY and AZYL sintered at 1700°C for any of the soaking time periods used. The fracture toughness is marginally higher for AZY and AZYL samples compared to other systems studied.

18. The higher fracture toughness of the samples AZY_6^{1700}, AZY_9^{1700}, AZY_{12}^{1700}, $AZYL_6^{1700}$, $AZYL_9^{1700}$ and $AZYL_{12}^{1700}$ is attributed to the formation of the secondary Zr-Y-O phases which play an important role.

19. The low values of fracture toughness of the samples AZ_6^{1700}, AZ_9^{1700}, AZ_{12}^{1700}, AZL_6^{1700}, AZL_9^{1700} and AZL_{12}^{1700} may be attributed to the secondary Al-Zr-O phases.

20. Hardness of the AMZ and ANZ samples sintered at 1500°C for soaking times of 3, 6 and 9 hr determined by Vickers indentation method lies between 14.68 and 14.95 GPa.

21. The fracture toughness of the ANZ is found higher than that of AMZ as well as A. The sample ANZ_6^{1500} has highest fracture toughness of 5.76 MPa $m^{1/2}$.

22. The fracture in the ANZ is caused by mixed mode of intergranular and transgranular types.

7.4 Suggestions for future work

1. Interfacial property of the rare earth doped Al_2O_3 based ceramic composites can be studied using advanced characterization techniques e.g. Electron energy loss spectroscopy (EELS), X-ray photoelectron spectroscopy (XPS) and (Scanning) transmission electron microscopy (TEM/STEM) etc.

2. The present study in the thesis has revealed that the fracture toughness enhancement of the ceramic composites mainly in Y and simultaneously (Y + La) doped is due to combined effect of several mechanisms such as intergranular mode of crack propagation, crack deflection and crack bridging. Effort can be made using several characterization methods to quantify the role of each mechanism in giving rise to the fracture toughness enhancement.

3. Such studies will lead to the development of ceramics with higher fracture toughness for promising candidates of structural ceramics.

4. One can further study the characterizations of all the second phases that form during sintering and relate their effect on other mechanical properties such as strength characteristics.

5. Theoretical modeling can be developed for fracture toughness by considering the parameters such as chemical composition of powder mixture, particle size of the powder, load for powder compaction, sintering temperature and soaking time period.

References

1 *Acchar, W., Greil, P., Martinelli, A. E.,Vieira, F. A., Bressiani, A. H. A., Bressiani, J. C., "Effect of Y_2O_3 addition on the densification and mechanical properties of alumina -niobium carbide composites", Ceram. Int., 27 (2001) 225.*

2 *Agrawal, D. C., Gopalakrishnan, R., Chakravorty, D., "Phases and microstructures in zirconia-calcia-titania multiphase ceramics", J. Am. Ceram. Soc., 72 (1989) 912*

3 *Altay, A. and Gulgun, M. A., "Microstructure evolution of ceramic doped α –alumina", J. Am. Ceram. Soc., 86 (2003) 623.*

4 *Andrejovská, J., Dusza, J., "Hardness and indentation load/size effect in silicon based ceramics", NANOCON 2009, Rožnov pod Radhoštěm, Česká Republika.*

5 *Anstis, G. R., Chantikul, P., Lawn, B. R., and Marshall, D. B., "A critical evaluation of indentation techniques for measuring fracture toughness: I, direct crack measurements", J. Am. Ceram. Soc., 64 (1981) 533.*

6 *Anthony, C. J., Helen, C. A., Paul, R. C., Richard, J. P., Kaupo, K., Antti, R., Mikko, R., Markku, L., "Recent developments in the MOCVD and ALD of rare earth oxides and silicates", J. Mat. Sci. Eng. B, 118 (2005) 97.*

7 *Arato, P., Besenyel, E., Kele, A., Weber, F., "Mechanical properties in the initial stage of sintering", J. Mat. Sci., 30 (1995) 1863.*

8 *Auerkari, P., Research notes, VTT Manufacturing Technology, Finland,1996*

9 *Awaji, H., Choi, S. M., Yagi, E., "Mechanisms of toughening and strengthening in ceramic-based nanocomposites", Mech. Mater., 34 (2002) 411.*

10 *ASTM C-1421, Standard Test Methods for Determination of Fracture Toughness of Advanced Ceramics at Ambient Temperature, 2007.*

11 *ASTM 1327-03 Standard Test Method for Vickers Indentation Hardness of Advanced Ceramics, 2005.*

12 *Baddi, R., Crampon, J., Duclos, R., "Temperature and porosity effects on the fracture of fine grain size MgO", J. Mater. Sci., 21 (1986) 1145.*

13 *Bae, I. J. and Baik, S., "Densification of critical concentration of silica and/or calcia for abnormal grain growth", J. Am. Ceram., 76 (1993) 1065.*

14 *Bagdasarov, K. S., Bolotina, N. B., Kalinin, V. I., Karyagin, V. F., Kuz'min, B. V., Muradyan, L. A., Ryadnov, S. N., Uyukin, E. M., Chernaya, T. S., Fedorov, E. A., Chudakov, V. S., Simonov, V. I., Kristallografiya, 36 (1991) 715.*

15 *Baik, S., Fowler, D. E., Blakely, J. M. & Raj, R., "Segregation of Mg to the (0001) surface of doped sapphire", J. Am. Ceram. Soc., 68 (1985) 281.*

16 *Baik, S., & White, C. L., "Anisotropic calcium segregation to the surface of Al_2O_3", J. Am. Ceram. Soc., 70 (1987) 682.*

17 *Banerjee, R., Feltham, P., "Deformation and fracture of germanium single crystals", J. Mater. Sci., 9 (1974) 1478.*

18 *Baron, B., Kumar, C. S., Gonidec, G.L. and Hampshire, S., "Comparison of different alumina powders for the aqueous processing and pressureless sintering of Al_2O_3–SiC nanocomposites", J. Eur. Ceram. Soc., 22 (2002) 1453.*

19 *Barsoum, M. W., Fundamentals of Ceramics, McGraw Hill, Singapore, 1997.*

20 *Basu, D., and Sarkar, B. K., "Effect of zirconia addition on the fatigue behaviour of fine grained alumina", Bull. Mater. Sci., 24 (2001) 101.*

21 *Basu, B., Vleugels, J., Biest, O.V.D., "ZrO_2–Al_2O_3 composites with tailored toughness", J. Alloys Compd., 372 (2004) 278.*

22 *Becher, P. F., Hsueh, C. H., Angelini, P. and Tiegs, T. N., "Toughening behavior in whisker-reinforced ceramic matrix composites", J. Am. Ceram. Soc., 71 (1988) 1050.*

23 *Becher, P. F., Fuller Jr, E. J. and Angelini, P., "Journal. matrix-grain-bridging contributions to the toughness of whisker-reinforced ceramics", J. Am. Ceram. Soc., 74 (1991) 2131.*

24 *Becher, P. F., "Microstructural design of toughed ceramics", J. Am. Ceram. Soc., 74 (1991) 255.*

25 *Bender, B., Williams, D. B. and Notis, M. R., "Investigation of grain–boundary segregation in ceramic oxides by analytical scanning transmission microscopy", J. Am. Ceram. Soc., 63 (1980) 542.*

26 *Bennison, S. J. and Lawn, B. R., "Role of interfacial grain-bridging sliding friction in the crack-resistance and strength properties of nontransforming ceramics", Acta Metall., 37 (1989) 2659.*

27 *Biswas, N. C., Choudhuri, S. P., "Comparative study of zirconia – mullite and alumina-zirconia composites", Bull. Mater. Sci., 22 (1999) 37.*

28 *Boccaccini, A. R., Winkler V., "Fracture surface roughness of Al_2O_3–plateler reinforced glass matrix composites", Composites: Part A, 33 (2002) 125.*

29 *Boch, P., Niepce, J. C., "Ceramic materials processes, properties and applications", USA, 2007.*

30 *Boutz, M. M. R., Winnubst, A. J. A., Hartgers, F., Burggaaf, A. F., "Effect of additives on densification and deformation of tetragonal zirconia", J. Mater. Sci., 29 (1994) 5374.*

31 *Boutz, M. M. R., Winnubst, A. J. A., Langerak, B. V., Oldescholtenhuis, R. J. M., Kreuwel, K., Burggraaf, A. J., "The effect of ceria co-doping on chemical stability and fracture toughness of Y-TZP", J. Mat .Sci., 30 (1995) 1854.*

32 *Bowman, K., Mechanical behavior of materials, John Wiley and Sons, 2004.*

33 *Buban , J. P., Matsunaga, K., Chen, J., Shibata, N., Ching, W. Y., Yamamoto, T., Ikuhara, Y., "Grain boundary strengthening in alumina by rare earth impurities", Science, 311 (2006) 212.*

34 *Cahnoon, H. P., Christensen, C. J., "Sintering and grain growth of alpha-alumina", J. Am. Ceram. Soc., 39 (1956) 377.*

35 *Callister, W. D., Fundamentals of Materials Science and Engineering, 2nd ed. Wiley & Sons., (1995) 252.*

36 *Campbell, G. H., M. Ruhle, M., Dalgleish, B. J. and Evans, A. G., "Whisker toughening: a comparison between aluminum oxide and silicon nitride toughened with silicon carbide", J. Am. Ceram. Soc., 73 (1990) 521.*

37 *Carty, W. M. and Senapati, U., "Porcelain—raw materials, processing, phase evolution, and mechanical behavior", J. Amer. Ceram. Soc., 81 (1998) 3.*

38 *Castel, A., Les alumines et leurs applications, Nathan, 1990.*

39 *Cawley, J. D. and Halloran, J. W., "Dopant distribution in nominally yttrium-doped sapphire", J. Am. Ceram. Soc., 69 (1986) 195.*

40 *Chae, K. W., Kim, D. Y., Kim, B. C., Kim, K. B., "Effect of Y_2O_3 additions on the densification of an Al_2O_3 - TiC composite", J .Am. Ceram. Soc., 76 (1993) 1857.*

41 *Chantikul, P., Bennison, S. J. and Lawn, B. R., "Role of grain size in the strength and R-*

curve properties of alumina", J. Am. Ceram. Soc., 73 (1990) 2419.

42 *Chen, P. L. and Chen, I. W., "In situ alumina/aluminate platelet composites", J. Am. Ceram. Soc., 75 (1992) 2610.*

43 *Ching, W. Y., Xu, Y .N. and Ru¨hle, M., "Ab-initio calculation of yttrium substitutional impurities in α-Al_2O_3", J. Am. Ceram. Soc., 80 (1997) 3199.*

44 *Cho, J., Wang, C. M., Chan, H. M., Rickman, J. M., Harame, M. P., "A study of grain boundary structure in rare-earth doped aluminas using an EBSD technique", J. Mat. Sci., 37 (2002) 59.*

45 *Cho, J., Rickman, J. M., Chan, H. M. and Harmer, M. P., "Modeling of grain boundary segregation behavior in aluminum oxide", J. Am. Ceram. Soc., 83 (2000) 344.*

46 *Cho, J., Harmer, M. P., Chan, H. M., Rickman, J. M. and Hompson, A. M., "Effect of yttrium and lanthanum on the tensile creep behavior of aluminum oxide", J. Am. Ceram. Soc., 80 (1997) 1013.*

47 *Chonghai, X., "Study on microstructure of alumina based rare earth ceramic composite, J. Rare Earths, 24 (2006) 217.*

48 *Chonghai X., "Effects of processing technology on the property and microstructure of rare earth containing ceramic composite", J. Rare Earths, 22 (2004) 146.*

49 *Chou, S. N., Lu, H. H., Lii, D. F., Huang, J. L., "Investigation of residual stress effects in an alloy reinforced ceramic/metal composite", J. Alloys Compd., 470 (2009) 117.*

50 *Claussen, N., "Fracture toughness of Al_2O_3 with an unstabilized ZrO_2 dispersed phase", J. Am. Ceram. Soc., 59 (1976) 49.*

51 *Clinton, D. J. and Morrell, R., "Hardness testing of ceramic materials", Mat. Chem. Phy., 17 (1987) 46l.*

52 *Coble, R. L., "Sintering crystalline solids: I. Intermediate and final stage diffusion models", J. Appl. Phys., 32 (1961) 787.*

53 *Cocks, A. C. F., "The structure of constitutive laws for the sintering of fine grained materials", Acta Metall. Mater., 42 (1994) 2191.*

54 *Cook, R. F. and Schrott, A. G., "Calcium segregation to grain boundary in alumina", J. Am. Ceram. Soc., 71 (1988) 50.*

55 *Courtney, T. H., Mechanical Behavior of Materials, McGraw-Hill, New York, (1990) 170.*

56 *Daguano, J. K. M. F., Santos, C., Souza, R. C., Balestra, R. M., Strecker, K. and Elias, C. N., "Properties of $ZrO_2 - Al_2O_3$ composite as a function of isothermal holding time", Int. J. Refract. Metals Hard Mater., 25 (2007) 374.*

57 *Daniel, C., Adrian, F., Luis, L., Marc, A., "Fracture toughness and mechanical strength of Y-TZP/PSZ ceramics", Scripta Mater., 45 (2001) 213.*

58 *Davidge, R.W. and Green, T.J., "The strength of two-phase ceramic/glass materials", J. Mater. Sci., 3 (1968) 629.*

59 *Delaunay, D., Huntz, A.M. and Lacombe, P., "The influence of yttrium on the sintering of alumina", J. Less-Common Metals, 70 (1980) 115.*

60 *Deng, Z. Y., Zhou, Y., Brito, M. E., Yang, J. F. and Ohji, T., "Fracture-mode change in alumina-silicon carbide composites doped with rare earth impurities", J. Am. Ceram. Soc., 86 (2003) 1789.*

61 *Deng, Z. Y., Zhou, Y., Brito, M. E., Yang, J. F. and Ohji, T., "Effects of rare earth dopants on grain boundary bonding in alumina–silicon carbide composites", J. Eur. Ceram. Soc., 24 (2004) 511.*

62 *Dey, A., Mukhopadhyay, A. K., Gangadharan, S., Sinha, M. K., Basu, D., Bandyopadhyay, N. R., "Nanoindentation study of microplasma sprayed hydroxyapatite coating", Ceram. Int., 35 (2009) 2295*

63 *Dhas, N. A., Patil, K. C., "Combustion synthesis and properties of zirconia---alumina powders", Ceram. Int., 20 (1994) 57.*

64 *Dieter, G. E., Mechanical metallurgy. Singapore: McGraw-Hill Book Company (SI Metric Edition); 1988.*

65 *Dorre, E., Hubner, H., "Alumina: Processing, Properties, and Applications", Springer: Berlin, 1984.*

66 *Dudkin, B. N., Bugaeva, A. Y., Zainullin, G. G. and Filippov, V. N., "The effect of tttrium oxide on the microstructure and properties of ceramics based on lanthanum hexaaluminate synthesized by the sil- gel method", Refrcator. Industr. Ceram., 45 (2004) 31.*

67 *Duk, H. Y., Shik, C. H., Rag, D. Y., "The optical properties of $(Y_{1-x}\ Gd_x)_{3-z}\ (A_{1-y}\ Ga_y)_5\ O_{12}$ $:Ce_z$ phosphors for white LED", Bull. Korean. Chem. Soc., 23 (2002) 1435.*

68 *Durrani, S. K., Akhtar, J., Ahmad, M., Hussain, M. A., "Synthesis and characterization of*

low density calcia stabilized zirconia ceramic for high temperature furnace application", Mat. Chem. Phy., 100 (2006) 324.

69 *Dutta, S., "Fracture toughness and reliability in high-temperature structural ceramics and composites: prospects and challenges for the 21st Century", Bull. Mater. Sci,. 24 (2001) 117.*

70 *Endo, T., Miyagawa, N., Takizawa, H., Shimada, M., "Multiphase composites of tetragonal zirconia agglomerate dispersed into alumina and alumina-zirconia matrices", J. Mat. Sci., 29 (1994) 2395.*

71 *Ekstrom, T., "Alumina ceramics with particle inclusions", J.Eur.Ceram.Soc.11, 487 (1993).*

72 *Evans, A. G., "On the formation of a crack tip microcrack zone", Scripta Metall., 10 (1976) 93.*

73 *Evans A. G. and Faber, K. T., "Toughening of ceramics by circumferential microcracking", J. Am. Ceram. Soc., 64 (1981) 394.*

74 *Evans, A. G. and McMeeking, R. M., "On the toughening of ceramics by strong reinforcements", Acta Metall., 34 (1986) 2435.*

75 *Evans, A. G., "Perspective on the development of high-toughness ceramics", J. Am. Ceram. Soc., 73 (1990) 187.*

76 *Evans, A. G. and Cannon, R. M., "Toughening of brittle solids by martensitic transformation", Acta Metall., 34 (1986) 761.*

77 *Evans, A. G., Gilling, D., Davidge, R. W., "The temperature-dependence of the strength of polycrystalline MgO", J. Mater. Sci., 5 (1970) 187.*

78 *Evans, A. G. and Charles, E. A., "Fracture toughness determinations by indentation", J. Am Ceram. Soc., 59 (1976) 371.*

79 *Faber, K. T. and Evans, A. G., "Crack deflection processes-I. Theory" Acta Metall., 31 (1983) 565.*

80 *Faber, K. T. and Evans, A. G., "Crack deflection processes-II. Experiment", Acta Metall., 31 (1983a) 577.*

81 *Fang, J., Thompson, A. M., Harmer, M. P. and Chan, H. M., "Effect of yttrium and lanthanum on the final-stage sintering of ultrahigh-purity alumina", J. Am. Ceram. Soc., 80 (1997) 2005.*

82 *Feltham, P., Banerjee, R., "Theory and application of microindentation in studies of glide and cracking in single crystals of elemental and compound semiconductors", J. Mate., Sci., 27 (1992) 1626.*

83 *Flinn, B., Bordia, R., Zimmermann, A. and Rodel, J., "Evolution of defect size and strength of porous alumina during sintering", J. Eur. Ceram. Soc., 20 (2000) 2561.*

84 *Feret, F. R. , Roy, D., Boulanger, C., "Determination of alpha and beta alumina in ceramic alumina by X-ray diffraction", Spectrochim. Acta Part B, 55 (2000) 1051.*

85 *Fett, T. and Munz, D., "Subcritical crack growth of macrocracks in alumina with R-curve behavior", J. Am. Ceram. Soc., 75 (1992) 958.*

86 *Frischat, G. H., "Load-independent microhardnesses of glasses" in Strength of Inorganic Glass. Edited by C. R. Kurkjian. Plenum Publishing Co., New York, 1985.*

87 *Gall, M. L., Huntz, A. M. and Lesage, B., "Self-diffusion in α-alumina and growth rate of alumina scales formed by oxidation: effect of Y_2O_3 doping", J. Mater. Sci., 30 (1995) 201.*

88 *Garive, R. C., Hannink, R. H. J. and Pascoe, R. T., Ceramic Steel?, Nature (London) 258 (1975) 703.*

89 *Garvie, R. C., Swain, M. V., "Thermodynamics of the tetragonal to monoclinic phase transformation in constrained zirconia microcrystals", J. Mater. Sci., 20 (1985) 1193.*

90 *Glandus, J. C., Rouxel, T., and Tai, Q., "Study of the Y-TZP toughness by an indentation method", Ceram. Int., 17 (1991) 129.*

91 *Gong, J., "Determining indentation toughness by incorporating true hardness into fracture mechanics equations", J. Eur. Ceram. Soc., 19 (1999) 1585.*

92 *Gong, J., Wu, J. and Guan, Z., "Examination of the indentation size effect in low-load Vickers hardness testing of ceramics", J. Eur. Ceram. Soc., 19 (1999) 2625.*

93 *Gong, J., Wang, J., and Guan, Z., "A comparison between Knoop and Vickers hardness of silicon nitride ceramics", Mater Lett., 56 (2002) 941.*

94 *Green, D. J., Hannink, R. H. J. and Swain, M. V., "Transformation toughening of ceramics", CRC Press Inc., Boca Raton, FL. 1989.*

95 *Green, D. J., "Critical microstructures for microcracking in Al_2O_3-ZrO_2 composites", J. Am. Ceram. Soc., 65 (1982) 610.*

96 *Gruffel, P. and Carry, C., "Effect of grain size on yttrium grain boundary segregation in*

fine-grained alumina", J. Eur. Ceram. Soc., 11 (1993) 189.

97 *Guanming, Q., Xikun, L., Tai, Q., Haitao, Z., Honghao, Y., Ruiting, M., "Application of rare earths in advanced ceramic materials", J. Rare Earths, 25 (2007) 281.*

98 *Guimaraes, F. A. T., Silva, K. L., Trombini ,V., Pierri, J. J., Rodrigues, J. A., Tomasi, R., Pallone, E. M. J. A., "Correlation between microstructure and mechanical properties of Al_2O_3/ZrO_2 nanocomposites", Ceram.Int., 35 (2009) 741.*

99 *Gulgun, M. A., Putlayev, V. and Ruhle, M., "Effects of Yttrium doping a-Alumina: I, microst-ructure and microchemistry", J. Am. Ceram. Soc., 82 (1999) 1849.*

100 *Hah, S. R., Fisher, T. E., Gruffel, P., Carry, C., "Effect of grain boundary dopants and mean grain size on tribological behavior of highly purified α – alumina in the mild wear regime", Wear, 181 (1995) 165.*

101 *Haldar, M. K., Pal, T. K., Banerjee, G.,"Preparation and properties of Y_2O_3 containing zirconia–mullite composites derived from sillimanite beach sand",Ceram.Int.,28 (2002) 311.*

102 *Han, L. X., Warren, R. and Suresh, S., "An experimental study of toughening and degradation due to microcracking in a ceramic composite", Acta Metall. Mater., 40 (1992) 259.*

103 *Hardy, D. and Green, D., "Mechanical properties of a partially sintered alumina", J. Eur. Ceram. Soc., 15 (1995) 769.*

104 *Harmer, M. P., Chan, H. M. and Miller, G. A., "Unique opportunities for microstructural eng- ineering with duplex and laminar ceramic composites", J.Am.Ceram.Soc.,75 (1992) 1715.*

105 *Hashimoto, M., Ishida, Y., Yamamoto, R. & Doyama, M., "Atomic studies of grain boundary segregation in Fe-P and Fe-B alloys--I. Atomic structure and stress distribution", Acta Metall., 32 (1984) 1.*

106 *He, Z., Ma, J., "Densification and grain growth during interface reaction controlled sintering of alumina ceramics", Ceram. Int., 27 (2001) 261.*

107 *Heuer, A. H. and Hobbs, L. W. (edts.) "Science and Technology of Zirconia," Advances in Ceramics Vol. 3, The American Ceramic Society, Columbus, OH. (1981).*

108 *Hondros, E. D. & Seah, M. P., "The theory of grain boundary segregation in terms of surface adsorption analogues", Met. Trans. A, 8A (1977) 1363.*

109 *Hongzhi, W., Lian, G., Zhijian, S., Mats, N., "Mechanical properties and microstructures of Al_2O_3 –5 vol.% YAG composites", J. Eur. Ceram. Soc., 21 (2001) 779.*

110 *Hooker J. D., Kilbride I. P., Randle V., Properties of rare earth oxide doped translucent polycrystalline alumina, J. Mat. Proc. Tech., 118 (2001) 256.*

111 *Hottaa, T., Abeb, H., Naitob, M., Takahashic, M., Uematsud, K. and Kato, Z., "Effect of coarse particles on the strength of alumina made by slip casting", Powder Technol., 149 (2005) 106.*

112 *Howard, J., Hill, R. J., Reichert, B. E., "Structure of the ZrO_2 polymorphs at room temperature by high resulation neutron powder diffraction,Acta Cryst., Sec. B: Structural Science, 44, (1988), 116.*

113 *Hue,F., Jorand, Y., Dubois, J. & Fantozzi, G., "Analysis of the weight loss during sintering of silicon-carbide whisker-reinforced alumina composites", J .Eur. Ceram. Soc., 17 (1997) 557.*

114 *Hutchinson, J. W., "Crack tip shielding by micro-cracking in brittle solids", Acta Metall., 35 (1987) 1605.*

115 *Ighodaro, O. L. and Okoli, O. I., "Fracture toughness enhancement for alumina systems: A Review", Int. J. Appl. Ceram. Technol., 5 (2008) 313.*

116 *Ishizawa, N., Miyata, T., Minato, I., Marumo, F. and Iwai, S., "A structural investigation of α-Al_2O_3 at 2170 K", Acta Cryst. Sec. B. 36 (1980) 228.*

117 *Janbey, A., Pati, R. K., Tahir, S., Pramanik, P., "A new chemical route for the synthesis of nano-crystalline alpha-Al_2O_3 Powder", J. Eur. Ceram. Soc., 21 (2001) 2285.*

118 *Jang, B. K., Enoki, M., Kishi, T. and Oh, H. K., "Effect of second phase on mechanical properties and toughened of Al_2O_3 based ceramic composites", Composites Engineering, 5 (1995) 1275.*

119 *Ji, Y., Yeomans, J. A., "Processing and mechanical properties of Al_2O_3–5 vol.% Cr nanocomposites", J. Eur. Ceram. Soc., 22 (2002) 1927.*

120 *Johnson, S. and Rowcliffe, D. J., SRI International Report to EPRI, "Ceramics for electric power-generating systems", 1986.*

121 *Kaji, M., Stevenson, M. E. and Bradt, R. C., "Knoop microhardness anisotropy and the indentation size effect on the basal plane of single-crystal alumina (sapphire)", J. Am.*

Ceram. Soc., 85 (2002) 415.

122 *Kaplyanski, A. A., Kulinkin, A. B., Kutsenko, A. B., Feofilov, S. P., Zakharchenya, R. I. and Vasilevskaya, T. N., "Optical spectra of triply-charged rare-earth ions in polycrystalline corundum", Phys. Solid State, 40 (1998) 1310.*

123 *Kashyap, K. T. and Chandrashekar, T., "Effects and mechanisms of grain refinement in aluminum alloys", Bull. Mater. Sci., 24 (2001) 345.*

124 *Katz, R. N., "Applications of high performance ceramics in heat engine design", Mat. Sci. Engg., 71 (1985) 227.*

125 *Kim, H. E., Moorhead, A. J, Sang, H. K, "Strengthening of alumina by formation of a mullite/glass layer on the surface", J. Am. Ceram. Soc., 80 (1997) 1877.*

126 *Kingery, W. D., Bowen, H. K., Uhlmann, D. R., Introduction to ceramics, John Wiley & Sons, USA, 1960.*

127 *Kinsman, K. M., McKittrick, J., Sluzky, E., Hesse, K., "Phase development and luminescence in chromium-doped yttrium aluminum garnet (YAG:Cr) phosphors", J. Am. Ceram. Soc., 77 (1994) 2866.*

128 *Kobayashi, K. and Kaneno, M., "Utilzing mixtures of yttria, magnesia, and lanthanium oxide in manufacture of transparent alumina", US Patent No.3, 792, 142, February 12 1974.*

129 *Kobayashi, K. and Kameno, M., "Translucent alumina containing magnesia yttria and lanthium oxide", US Patent No. 3,905,845, September 16 1975.*

130 *Korinek, S. L., Carry, C., Priester, L., "Multiscale aspects of the influence of yttrium on microstructure,sintering and creep of alumina", J. Eur. Ceram. Soc., 22 (2002) 1525.*

131 *Kosmac, T., Swain, M. V.,Claussen, N.,"The role of tetragonal and monoclinic ZrO_2 particles in the fracture toughness of Al_2O_3-ZrO_2 composites", Mater. Sci. Eng. A, 71 (1985) 57.*

132 *Kovar, D., Bennison, S. J. and Readey, M. J., "Crack stability and strength variability in alumina ceramics with rising toughness-curve behavior", Acta Mater., 48 (2000) 565.*

133 *Koyama, T., Nishiyama, A., Nihara, K., "Effect of grain morphology and grain size on the mechanical properties of Al_2O_3 ceramics", J. Mat. Sci., 29 (1994) 3949.*

134 *Kronberg, M. L., "Plastic deformation of single crystals of sapphire: Basal slip and twinning", Acta Metall., 5 (1957) 507.*

135 *Kumar, A. S., Durai,A. R., Sornakumar, T., "Development of yttria and ceria toughened alumina composite for cutting tool application", Int. J. Refract. Metals Hard Mater., 25 (2007) 214.*

136 *Kumar, D., Pennycook, S. J., Lupini, A., Duscher, G., Tiwari, A., Narayan, J., "Synthesis and atomic-level characterization of Ni nanoparticles in Al_2O_3 matrix", Applied Physics letters, 81(2002) 4204.*

137 *Lagrange, M. H., Huntz, A. M. and Laval, J. Y., "Effect of yttrium on the microstructure and diffusion properties of α-alumina", Ann. Chim. Fr., 12 (1987) 9.*

138 *Lange, F. F., "Sinterability of agglomerated powders", J. Am. Ceram. Soc., 67 (1984) 83.*

139 *Lange, F. F., "The interaction of a crack front with a second-phase dispersion", Phil. Mag., 22 (1970) 983.*

140 *Lawn, B. R. and Marshall, D. B. "Hardness, toughness, and brittleness: An indentation analysis", J. Am. Ceram. Soc., 62 (1979) 347.*

141 *Lee, M., and Brun, M. K., "Fracture toughness measurement by microindentation and three-point bend methods", Mat. Sci. Engg. A, 105 (1988) 369.*

142 *Levin, E. M. and McMurdie, H. F., Fig.4378 in Phase Diagrams for Ceramists, Vol.3. Edited by M. K. Reser. American Ceramic Society, Westerville, OH, 1975.*

143 *Li, Y., Qiao, G., Jin, Z., "Machinable Al_2O_3/BN composite ceramics with strong mechanical properties", Mat. Res. Bull., 37 (2002) 1401.*

144 *Li, G., Jiang, Z., Jiang, A. and Zhang, L., "Strengthening of porous Al_2O_3 ceramics through nanoparticle addition", NanoStruct. Mater., 8 (1991) 749.*

145 *Li, C. W. and Kingery, W. D., "Solute segregation at grain boundaries in polycrystalline Al_2O_3", In Advances in Ceramics, Vol.10, ed. W. D. Kingery. Am. Ceram. Soc., Columbus OH, (1985) 368.*

146 *Li, H., Bradt, R. C., "The effect of indentation-induced cracking on the apparent microhardness", J. Mater. Sci., 31 (1996) 1065.*

147 *Li, H., Bradt, R. C., "The microhardness indentation load/size effect in rutile and cassiterite single crystals", J. Mat. Sci., 28 (1993) 917.*

148 *Li, Y.O., Xu, J., Qiu, T., He, X.C., Sheng, X.M., "Alumina effect on the phase transformation in vibration ball-milling zirconia (yttria) powders", J. Mater. Sci. Lett.,11 (1992) 669.*

149 *Lie, F., Master Thesis, Lulea University of Technology, Kiruna, 2005.*

150 *Lin, J. D., Duh, J. G., "Fracture toughness and hardness of ceria- ad yttria- doped tetragonal zirconia ceramics", Mat. Chem. Phy., 78 (2002) 253.*

151 *Lo, J. R., Tseng, T. Y., Phase development and activation energy of the $Y_2O_3 - Al_2O_3$ system by a modified sol – gel process", Mat. Chem. Phy., 56 (1998) 56.*

152 *Loudjani, M. K., Huntz, A. M. & Cortts, R., "Influence of yttrium on microstructure and point defect in α-Al_2O_3 in relation with oxidation", J. Mater. Sci., 28 (1993) 6466.*

153 *Loudjani, M. K. & Haut, C., "Influence of the oxygen pressure on the chemical state of yttrium in polycrystalline α - alumina. Relation with microstructure and mechanical toughness", J. Eur. Ceram. Soc., 16 (1996) 1099.*

154 *Louet, N., Reveron, H., Fantozzi, G., "Sintering behaviour and microstructural evolution of ultrapure α-alumina containing low amounts of SiO_2", J. Eur. Ceram. Soc., 28 (2008) 205.*

155 *Lu, H. X., Sun, H. W., Li, G. X., Chen, C. P., Yang, D. L., Hu, X., "Microstructure and mechanical properties of Al_2O_3 –MgB_2 composites", Ceram. Int., 31(2005)105.*

156 *Ma, Q. and Clarke, D. R., "Size dependent hardness of silver single crystals", J. Mater. Res., 10 (1995) 853.*

157 *Ma, J., Constitutive modeling of the densification of porous ceramic components, PhD thesis, University of Cambridge, 1997.*

158 *Maiti, K. and Sil, A., "Preparation of rare earth doped alumina ceramics, their hardness and fracture toughness determinations", Ind. J. Engg. Mat. Sci., 13 (2006) 443.*

159 *Majumdar, S., Kupperman, D., Sing J., "Determinations of residual thermal stresses in a SiC- Al_2O_3 composite using neutron diffraction", J. Am. Ceram. Soc., 71 (1988) 858.*

160 *Majumdar, R., Gilbart, E. and Brook, R. J., "Kinetics of densification of alumina–zirconia ceramics", Br. Ceram. Trans. J., 85 (1993) 156.*

161 *Mackrodt, W. C. & Tasker, P. W., "Segregation isotherms at the surfaces of oxides", J. Am. Ceram. Soc., 72 (1989) 1576.*

162 *Mason, J. and McLean, A. F., "Ceramics for gas turbine engines", Mater. Soc., 8 (1984) 201.*

163 *Meguid, S. A., "Mechanics and mechanism of toughening of advanced ceramics", J. Mater. Process. Technol., 56 (1996) 978.*

164 *McCune, R. C., Donlon, W. T. & Ku, R. C., "Yttrium segregation and YAG precipitation at the surfaces of yttrium-doped α-Al_2O_3", J. Am. Ceram. Soc., 69 (1986) 196.*

165 *Miller, J. H., Liaw, P. K., "Fracture toughness of ceramics and ceramic matrix composites", The University of Tennessee, Knoxville, 2000.*

166 *Miyahara, N., Yamaishi, K., Mutoh, Y., Uematsu, K. and Inoue, M, "Effect of grain size on strength and fracture toughness in alumina", Japan Soc. Mech. Eng., 37 (1994) 231.*

167 *Michels, B. D., Frischat, G. H., "Microhardness of chalcogenide glasses of the system Se-Ge-As", J. Mat. Sci., 17 (1982) 329.*

168 *Monceau, D., Petot, C., Petot-Ervas, G., Fraser, J. W., Fraser, M. J., Graham, M. J. and Sproule, G. L., "Surface segregation and morphology of Mg-doped α-alumina powders". J. Eur. Ceram. Soc., 15 (1995) 851.*

169 *Moraes, M. C., Eilias, C. L., Filho, J. D., Oliveira, L. G., "Mechanical properties of alumina- zirconia composites for ceramic abutments", Mat. Res., 7 (2004) 643.*

170 *Moreno, J. M. C., Yoshimura, M., "$Y_3Al_5O_{12}$(YAG)–ZrO_2 Binary eutectic composites obtained by melt quenching", J. Mat. Sci. Eng., A, 375 (2004) 1250.*

171 *Muchtar, A. and Lim, L. C., "Indentation fracture toughness of high purity submicron alumina", Acta Mater., 46 (1998) 1683.*

172 *Mula, S., Padhi, P., Panigrahi, S. C., Pabi, S. K., Ghosh, S., "On structure and mechanical properties of ultrasonically cast Al–2% Al_2O_3 nanocomposite", Mater. Res. Bull., 44 (2009) 1154.*

173 *Nanni, P., Stoddart, C.T.H. and Hondros, E. D., "Grain boundary segregation and sintering in alumina", Materials Chemistry, 1 (1976) 297.*

174 *Nowoski, T., Joud, J. C. & Biscondi, M., "A thermodynamical model of grain boundary segregation for atomistic calculations", Colloque de Physique, les editions de physique (F) Colloque C1, Supplkment au n° 1, 51 (1990) 293.*

175 *Ohji, T., Jeong, Y. K, Choa, Y. H, Niihara, K., "Strengthening and toughening mechanisms of ceramic nanocomposites", J. Am. Ceram. Soc., 81 (1998) 1453.*

176 *Olszyna, A. P., Marchlewski, P. & Kurzydlowski, K. J., "Sintering of high- density, high-purity alumina ceramics", Ceram. Int., 23 (1997) 322.*

177 *Omri, M., Sintering, consolidation, reaction and crystal growth by the spark plasma system*

(SPS), Mater. Sci. Engg. A, 287 (2000) 183.

178 *Palmqvist, S., Energy causing cracks at corners of Vickers indentations as measure of toughness of hard metals; Rissbildungsarbeit bei Vickers-Eindruecken als Mass fuer die Zaehigkeit von Hartmetallen. Archiv fuer das Eisenhuettenwesen, 33 (1962) 629.*

179 *Park, S. Y., "Influence of a liquid phase on the microstructure development of Al_2O_3", J. Mater. Sci. Lett., 15 (1996) 878.*

180 *Park, C. W. and Yoon, D. Y., "Abnormal grain growth in alumina with anorthite liquid and the effect of MgO addition", J. Am. Ceram. Soc., 85 (2002) 1585.*

181 *Pasotti, M. R. R., Bressiani, A. H. A., Bressiani, J. C., "Sintering of alumina - niobium carbide composite", Int. J. Ref. Met. & Hard Mater., 16 (1998) 423.*

182 *Pezzotti, G., "On the actual contribution of crack deflection in toughening platelet reinforced brittle-matrix composites", Acta Metall. Mater., 41 (1993) 1825.*

183 *Peras, A, Y. and Dauknis, V. I., "The effects of small porosity on the strength of brittle ceramic materials", Probl. Prochnosti, 8 (1971) 38.*

184 *Pillai, S. K. C., Baron, B., Pomeroy, M. J. and Hampshire, S., "Effect of oxide dopants on densification,microstructure and mechanical properties of alumina–silicon carbide nano-composite ceramics prepared by pressureless sintering", J. Eur. Ceram. Soc., 24 (2004) 3317.*

185 *Pogrion, N. P., Bercia, R., Tirnovan, M., "Packing models of yttrium doped $\alpha - Al_2O_3$: study of porosity", J. Optoelectron. Adv. Mater., 6 (2004) 1071.*

186 *Porter, D. L., Evans A. G. and Heuer, A. H., "Transformation-toughening in partially-stabilized zirconia (PSZ)", Acta Metall., 27 (1979) 1649.*

187 *Powers, J. D. and Glaeser, A. M., "Grain boundary migration in ceramics interface", Science, 6 (1998) 23.*

188 *Quinn, J. B., Sundar, V., Lioyd, I. K., "Influence of microstructure on the fracture toughness of dental ceramics", Dental Mat., 19 (2003) 603.*

189 *Quantum Precision Group, USA, 2007 (http://www.spsspindle.com/quantum/Ceramic_steel.php)*

190 *Rajendran, S., Rossell, H. J., "Co-Precipitation-derived mullite and mullite-zirconia composites", J. Mater. Sci., 26 (1991) 5815.*

191 *Rajendran, S., Rossell, H. J., Sanders, J. V., "Preparation and characterization of precursor powders for yttria-doped tetragonal zirconia polycrystals (Y-TZP) and Y-TZP-Al_2O_3 composites", J. Mater. Sci., 24 (1989) 1195.*

192 *Rani, D. A., Yoshizawa, Y., Hirao, K. and Yamauchi, Y., "Effect of rare-earth dopants on mechanical properties of alumina", J. Am.Ceram. Soc., 87 (2004) 289.*

193 *Rao, P., Iwasa, M., Kondoh, I., "Properties of low-temperature-sintered high purity α - alumina ceramics", J. Mat. Sci. Lett., 19 (2000) 543.*

194 *Ray, J. C., Pati, R. K. and Pramanik, P., "Chemical synthesis and structural characterization of nanocrystalline powders of pure zirconia and yttria stabilized zirconia (YSZ)", J. Eur. Ceram. Soc., 20, (2000) 1289.*

195 *Reimanis, I. E., "A review of issues in the fracture of interfacial ceramics and ceramic composites", Mater. Sci. Eng. A, 237 (1997) 159.*

196 *Richerson, D. W., "Modern Ceramic Engineering", CRC press (2005)*

197 *Rice, R. W., "Mechanisms of toughening in ceramic matrix composites", Ceram. Engg. Sci. Proc., 2 (1981) 661.*

198 *Rice, R. W., "Mechanical properties of ceramics and composites: grain and particle effects," Marcel Dekker, New York, 2000.*

199 *Riu, D. H., Kong, Y. M., Kim, H. E., "Effect of Cr_2O_3 addition on microstructural evolution and mechanical properties of Al_2O_3", J. Eur. Ceram. Soc., 20 (2000) 1475.*

200 *Rodel, J., Fuller, E. R. and Lawn, B. R., "In situ observations of toughening processes in alumina reinforced with silicon carbide whiskers", J. Am. Ceram. Soc., 74 (1991) 3154.*

201 *Rödel, J., Kounga, A. B.,Eibl, M. W., Koch, D., Bierwisch, A., Rossner, W., Hoffmann, M. J., Danzer, R.,Schneider, G., "Development of a roadmap for advanced ceramics: 2010–2025", J. Eur. Ceram. Soc., 29 (2009) 1549.*

202 *Ross, N. L., "Distortion of $GdFeO_3$-type perovskites with pressure: A study of $YAlO_3$ to 5 GPa", Phase Transitions, 58 (1996) 27.*

203 *Ruhle, M., Dalgleish, B. J. and Evans, A. G., "On the toughening of ceramics by whiskers", Scripta. Metall., 21 (1987) 681.*

204 *Sanyal, M. K., Datta, A. and Hazra, S., "Morphology of nanostructure materials", Pure Appl. Chem., 74 (2002) 1553.*

205 *Sato, E. and Carry, C., "Yttria doping and sintering of sub-micron grained α-alumina", J. Am. Ceram. Soc., 79 (1996) 2156.*

206 *Sangwal, K., Surowskab, B., Błaziak, P., "Analysis of the indentation size effect in the micr-ohardness measurement of some cobalt-based alloys", Mat. Chem. and Phy., 77 (2002) 511.*

207 *Scott, H. G., "Phase relationships in the zirconia- yttria system", J.Mater.Sci.,10 (1975) 1527*

208 *Shackelford, J. F., Introduction to materials science for engineers., Prentice Hall, New Jersey, 2005.*

209 *Sharma, S. C., "Equation for the density of particle-reinforced metal matrix composites: a new approach", J. Mat. Eng. Perform., 12 (2003) 324.*

210 *Shaw, N. J., "Densification and coarsening during solid state sintering of ceramics: a review of the models-III. coarsening, powder", Metall. Int., 21 (1989) 25.*

211 *Shin, Y. S., Rhee, Y. W. and Kang, S. J. L., "Experimental evaluation of toughening mechanism in alumina- zirconia composites", J. Am. Ceram. Soc., 82 (1999) 1229.*

212 *Shukla, S., Seal, S., Vij, R., Bandyopadhyay, S. and Rahman, Z., "Effect of nanocrystallite morphology on the metastable tetragonal phase stabilization in zirconia", Nano Letters, 2 (2002) 989.*

213 *Sickafuss, K. E. & Sass, S. L., "Grain boundary structural transformation induced by solute segregation", Acta Metall., 35 (1987) 69.*

214 *Silva, S. R. P., Knowles, K. M., Amaratunga, G. A. J. and Putnis, A. "The microstructure of inclusions in nanocrystalline carbon films deposited at low temperature", Diamond and Related Materials, 3 (1994) 1048.*

215 *Smallman, R.E., Bishop, R.J., "Modern physical metallurgy & materials engineering", Butterworth Heinemann, Oxford, 2002.*

216 *Song, G. M., Zhou, Y., Sun, Y., "Modeling of fiber toughening in fiber-reinforced ceramic composites", Ceram. Int., 25 (1999) 257.*

217 *Song, J. G., Ji, G. C., Li, S. B., Li, Y. L., Du, D. M., Ju, Y. Y. and Zhang, L. M., "Preparation and properties of ZrB_2 -YAG-Al_2O_3 ceramics", J.Ceram.Proc.Res.,10 (2009) 428.*

218 *Sutton, A.P. & Vitek, V., "An atomistic study of tilt grain boundaries with substitutional impurities", Acta Metall., 30 (1982) 2011.*

219 *Swanson, P. L., Fairbanks C. J., Lawn, B. R., Mai, Y. W., Hockey, B. J., "Crack interface grain bridging as a fracture resistance I, mechanism in ceramics: I, experimental study on alumina", J. Am. Ceram. Soc., 70 (1987) 279.*

220 *Tani, T., Miyamoto, Y., Koizumi, M., "Grain size dependences of Vickers microhardness and in Al_2O_3 and Y_2O_3 ceramics", Ceram Int., 12 (1986) 33.*

221 *Taya, M., Hayashi, S., Kobayashi, A. S., Yoon H. S., "Toughening of a particulate-reinforced ceramic-matrix composite by thermal residual stress", J. Am. Ceram. Soc., 73 (1990) 1382.*

222 *Taylor, R. I., Coad, J. P., Hughes, A. E., "Grain-boundary segregation in MgO-doped Al_2O_3", J. Am. Ceram. Soc., 59 (1976) 374.*

223 *Teng, X., Liu, H. and Huang, C., "Effect of Al_2O_3 particle size on the mechanical properties of alumina-based ceramics", Mater. Sci. Eng. A, 452 (2007) 545.*

224 *Thouless, M. D. and Evans, A. G., "Effects of pull-out on the mechanical properties of ceramic-matrix composites", Acta Metall., 36 (1988) 517.*

225 *Tomaszewski H., Boniecki M., Weglarz H., "Effect of grain size on R-curve behaviour of alumina ceramics" J. Eur. Ceram. Soc., 20 (2000a) 2569.*

226 *Tomaszewski, H., Strzeszewski, J. and Gebicki, W., "The role of residual stresses in layered composites of Y - ZrO_2 and Al_2O_3", J. Eur. Ceram. Soc., 19 (1999) 255.*

227 *Tomaszewski, H., Weglarz, H., Bonniecki, M., Recko, W. M., "Effect of barrier layer thickness and composition on fracture toughness of layered zirconia/alumina composites", J. Mat. Sci., 35 (2000) 4165.*

228 *Tuan, W. H., Chen, R. Z., Wang, T. C., Cheng, C. H., Kuo, P. S., "Mechanical properties of Al_2O_3/ZrO_2 composites", J. Eur. Ceram. Soc., 22 (2002) 2827.*

229 *Tuan, W. H., Chen, J. R., Ho, C. J., "Critical zirconia amount to enhance the strength of alumina", Ceram. Int., 34 (2008) 2129.*

230 *Vekinis, G., Ashby, M. F. and Beaumont, P. W. R., "R-curve behaviour of Al_2O_3 ceramics", Acta Metall. Mater., 38 (1990) 1151.*

231 *Voytovych, R., MacLaren I., Gulgun, M. A., Cannon, R. M., Ruhle, M., "The effect of yttrium on densification and grain growth in α- alumina", Acta Mater., 50 (2002) 3453.*

232 *Wang, L., Shi, J. L., Hua, Z. L., Gao, J. H. and Yan, D. S., "The influence of addition of WC*

pa- rticles on mechanical properties of alumina–matrix composite", Mater. Lett., 50 (2001) 179.

233 *Wang, S. J., Xua Y. B., Lua, P. X., Xu, C.F. and W. Cao, Synthesis of yttrium aluminum garnet (YAG) from an ethylenediaminetetraacetic acid precursor, Mater.Sci. Eng. B 127 (2006) 203.*

234 *Wang, J., Lim, S. J., Ng, S. C., Chew, C. H. and Gan, L. M., "Dramatic Effect of a small amount of MgO addition on the sintering of Al_2O_3 ~ 01% SiC", Nanocomp Mater. Lett., 33 (1988) 273.*

235 *Wang, C. M., Cargill, G. S., Harmer, M. P., Chan, H. M. and Cho, J., "Atomic structural environment of grain boundary segregated Y and Zr in creep resistant alumina from EXAFS", Acta Mater., 47 (1999) 3411.*

236 *Wang, J., Stevens, R., "Review zirconia-toughened alumina (ZTA) ceramics, J. Mat. Science, 24 (1989) 3421.*

237 *Warshaw, I, Roy, R., "Stable and Metastable Equilibria in the Systems Y_2O_2-Al_2O_3, and Gd_2O_3-Fe_2O_3", 42 (1959) 434.*

238 *Wei, G. C. and Becher, P. F., "Improvements in mechanical properties in SiC by the addition of TiC particles", J. Amer. Ceram. Soc., 67 (1984) 571.*

239 *West, A. R., "Solid State Chemistry and its Applications", Wiley Int., 1984*

240 *West, G. D., Perkins J. M., Lewis M. H., "The effect of rare earth dopants on grain boundary cohesion in alumina", J. Eur. Ceram. Soc., 27 (2007) 1913.*

241 *West, G. D., Perkins, J. M., Lewis, M. H., "Characterisation of fine-grained oxide ceramics", J. Mat. Sci., 39 (2004) 6687.*

242 *Wonsiewicz, B .C. and Chin, B. Y., "A theory of knoop hardness anisotropy, in the science of Hardness Testing and Its Research Applications. Edited by Westbrook, J., Shaw, J. and Conrad, H., American Society for Materials-International, Materials Park, OH, (1973) 167.*

243 *Wolkodoff, V. E. and Weaver, R. E., Alumina Ceramic, US Patent No. 3,377,176, April 9 1968.*

244 *Wu, Y.,Zhang, Y., Huang, X. and Guo, J., "Microstructural development and mechanical properties of self-reinforced alumina with CAS addition", J. Eur. Ceram. Soc., 21 (2001) 581.*

245 *Wu, Y., "Study on brittle-ductile transition and surface integrity of ceramic micro-nano composites in the two-dimensional ultrasonic grinding", [A Dissertation for Doctoral Degree]. Shanghai: Shanghai Jiaotong University, 2006.*

246 *Xia, K. and Langdon, T. G., "Review: The toughening and strengthening of ceramic materials through discontinuous reinforcement", J. Mater. Sci., 29 (1994) 5219.*

247 *Xihua, Z., Changxia, L., Musen, L., Jianhua, Z., "Research on toughening mechanisms of alumina matrix ceramic composite materials improved by rare earth additive", J. Rare Earths, 26 (2008) 367.*

248 *Xu, C., Huang, C., Ai, X., "Toughening and strengthening of advanced ceramics with rare earth additives", Ceram. Int., 32 (2006) 423.*

249 *Xu C. H., "Design and simulation of composite ceramic tool materials and their application". Dissertation Jinan: Shandong University of Technology, 1998.*

250 *Xu, L., Xie, Z., Gao, L., Wang, X., Lian, F., Liu, T., Li, W., "Synthesis, evaluation and characterization of alumina ceramics with elongated grains", Ceram. Int., 31 (2005) 953.*

251 *Yan, M. F., Cannon, R. M. & Bowen, H. K., "Space charge elastic field and dipole contributions to equilibrium solute segregation at interfaces", J. Appl. Phys., 54 (1983) 764.*

252 *Yang, Y., Wang, Y., Tian, W., Wang, Z.Q., Zhao, Y., Wang, L., Bian, H.M., "Reinforcing and toughening alumina/titania ceramic composites with nano dopants from nanostructured composite powders", Mat. Sci. Eng. A, 508 (2009) 161.*

253 *Yang, Y., Wang, Y., Wang, Z., Liu, G., Tian, W., "Preparation and sintering behaviour of nanostructured alumina/titania composite powders modified with nano-dopants", Mat. Sci.Eng. A, 490 (2008) 457.*

254 *Yount, H. J., PHD thesis, University of Wisconsin-Madison, 2006.*

255 *Zakharchenya, R., Vasilevskaya, T., Russ. J. Appl. Chem. (Engl. transl.), 65 (1993) 2249.*

256 *Zhao, B., Du, B. Y. and Duan, T.L., "Research on toughening mechanics of zirconia toughened alumina composite ceramics", Advanced Design and Manufactre to gain a competitive edge, Spinger, London, 2008.*

257 *Zhao, Z., Zhang, L., Song, Y., Wang, W. and Wu, J., "Microstructures and properties of rapidly solidified Y_2O_3 doped Al_2O_3/ZrO_2 composites prepared by combustion synthesis", Scripta Mater., 55 (2006) 819.*

258 *Zhao, Z., Zhang, L., Zheng, J., Bai, H., Zhang, S., Xu, B., "Microstructures and mechanical properties of Al_2O_3/ZrO_2 composite produced by combustion synthesis", Scripta Mater., 53 (2005) 995.*

259 *Zhou, G., Lee, S.W., Li, Y., "Preparation and microstructural characterization of Al_2O_3/ZrO_2 nanocomposites to use in the femoral head of hip replacement", International Conference on BioMedical Engineering and Informatics, (2008) 760.*

260 *Zhou, Y., Lei, T. C. & Lu, Y. X., "Grain growth and phase separation of $ZrO_2 - Y_2O_3$ ceramics annealed at high temperature", Ceram. Int., 18 (1992) 237.*

261 *Zhou, X., Shukla, V., Cannon, W. R. and Kear, B. H., "Metastable phase formation in plasma- sprayed ZrO_2 (Y_2O_3) – Al_2O_3", J. Am. Ceram. Soc., 86 (2003) 1415.*